The role of 5-HT dynamics in cortical population activity throughout mammalian life

Gabriel Ocaña Santero

St John's college

University of Oxford

A thesis submitted for the degree of

Doctor of Philosophy

Michaelmas 2024

For my parents, Teresa and Carlos.

Abstract

Cortical serotonin (5-HT) plays critical roles in neurodevelopment and adult behaviour, with 5-HT alterations being associated with neurodevelopmental and neuropsychiatric disorders. Despite all the research conducted on 5-HT, we have identified three major gaps: firstly, a characterization, with high temporal and spatial resolution, of cortical 5-HT dynamics is missing; secondly, the effects of 5-HT in dictating cortical population activity in development and adulthood are not well understood; and thirdly how cortical 5-HT through its effects in cortical activity shapes behaviour is unclear. To address these gaps, we use two-photon imaging of calcium and 5-HT sensors in the barrel field cortex (S1BF) of developing and adult mice, upon genetic, pharmacological and optogenetic manipulation of 5-HT dynamics. Our results show that 5-HT fluctuates with sensation, saliency, reward, and novelty in the adult S1BF. While in the developing S1BF, we observe 5-HT buffering through transient SERT overexpression. Blocking this developmental 5-HT buffering system (SERT-KO or SSRI exposure) can result in early hypoactivity, alterations in interneuron subpopulations (i.e., VIP and Nkx2-1 interneurons) and subsequent hyperexcitability. In the adult cortex of wildtype mice, we observe that 5-HT inhibits bottom-up inputs in layer 4 of S1BF, while producing a mixture of excitation and inhibition in layer 2/3. Optogenetically increasing 5-HT in S1BF can decrease learning from misleading trials during an air puff discrimination task, illustrating that 5-HT gating of bottom-up inputs decreases learning. Pharmacologically decreasing cortical 5-HT with psilocin correlates with increases in learning rate during a reversal learning task. Finally, we capture all these results in a theoretical model using a gated deep neural network. Thus, this project identifies cortical 5-HT as a critical regulator of bottom-up and top-down activity, to control neuroplasticity throughout mammalian life, with consequences for translationally relevant contexts (i.e., developmental SSRI dosing and adult psychedelic exposure).

Acknowledgments

First of all, I would like to acknowledge the unparalleled supervision of my three mentors. Trevor for giving me the opportunity of pursuing this project and guiding me through the complex world of 5-HT neurophysiology, co-transmission and psychedelics. Adam, for teaching me the insights of the optical imaging world, while imprinting on me his “all the things all the time” hard-work discipline. And, finally, Simon for the constant stimulating discussions about the emergence of perception that time and again remind me of the joy of science. I would also like to acknowledge the 5 students that worked with me along my Dphil: Veronica, Christopher, Caius, Abhishek, and Lawrence, with whom I greatly enjoyed discussing the intricacies of the 5-HT system.

Next, I would like to thank the fantastic three-lab (Butt/Packer/Lak lab) environment in DPAG, as well as the Sharp lab in the Pharmacology department, that provided along these years an incredibly fun environment in which to do science, including in no particular order: Ivan, Marko, Sam, Blake, Antara, Andrew, Heather, Hamish, Chiara, Caitlin, Michael, Huriye, Flippo, Anna, Thijs, Sarah, Rob, Hannah, Aurelija, Jess, Helen, Cheryl, Sophie, David, and Zenia. As well as DPAG’s first floor friends Andrada, Candice and Isabella. Thanks to Stefano and Andrew for introducing me to the wonders of theoretical neuroscience, and to the Saxe lab in general for providing a friendly environment for my DPhil secondment.

I want to particularly thank the European network Serotonin & Beyond for providing me with the opportunity and resources to perform this project, as well as St John’s college of Oxford for providing a welcoming student environment and affordable housing throughout my DPhil.

A particular mention to Elba, who has been a constant source of support, and has kept me from disappearing on my work throughout my PhD, and my sister who has taken care of me since the day I was born. Finally, my father, who is directly responsible for my passion for science; and my mother, without a doubt my greatest source of support throughout my whole life.

Summary of contributions

I declare that this thesis is my own and that attribution has been given where information was derived from other sources. Aside from the exceptions outlined below,

I conceptualised the project, designed and performed the experiments, analysed the data and constructed all figures. However, the project has key contributions from others. Throughout the thesis, I employ the pronoun ‘we’ indicating myself and the team below.

Lawrence Tatiqaj (FHS 2022): histological processing of retrograde tracing experiments for chapter 2 (under supervision from myself). Veronica Munday, Caius Gibeily and Christopher Hemingway (all 2023 MSc students): contributed to the collection of developmental two-photon imaging data for chapters 3 and 4 (under supervision from myself). Abhishek Saha (FHS 2023): histological processing of SERT-KO tissue for interneuron quantification (under supervision from myself). Hannah Warming and Heather A. Mackay: slice electrophysiology experiments in SERT-KO mice (appendix 3). Stefano Sarao-Mannelli: theoretical model conceptualization, analytical solution of model differential equations and experimental design, in collaboration with myself (chapter 5 and 6). Andrew Saxe: theoretical model conceptualization and experimental testing interpretation (chapter 5 and 6). Simon Butt, Trevor Sharp and Adam Packer: Conceptualization and supervision throughout.

Funding

The work described in this thesis was funded by the Marie Skłodowska-Curie Action “Serotonin and Beyond”.

Table of contents

List of figures

List of supplementary figures

List of abbreviations

5-HT . . . . .5-hydroxytryptamine or serotonin
AAV . . . . . Adeno-associated virus
AS. . . . . .Active sleep
ANOVA . . . .Analysis of variance
CGE. . . . . Caudal ganglionic eminence
CNS . . . . .Central nervous system
CTB . . . . .Cholera toxin subunit B
DRN . . . . .Dorsal raphe nucleus
E . . . . . .Embryonic day
EC. . . . . .Entorhinal cortex
eYFP . . . . . Enhanced yellow fluorescent protein
EP. . . . . Endopiriform cortex
fMRI . . . . . Functional magnetic imaging
GABA . . . . .γ-Aminobutyric acid
GW . . . . . .Gestational week
H-event . . . High synchronicity event
Het . . . . . .Heterozygous
hSyn . . . . . .human synapsin
i.i.d . . . . . .Independent and identically distributed
i.p. . . . . Intraperitoneal
KO. . . . . .Knockout
L . . . . . .Layer
L-event . . . .Low synchronicity event
LSD . . . . . Lysergic acid diethylamide
MDMA 3,4-Methylenedioxymethamphetamine
MDD. . . . . Major depressive disorder
MGE . . . . . Medial ganglionic eminence
NREM. . . . .Non-rapid eye movement
OCD. . . . . .Obsessive compulsive disorder
OE. . . . . Over-expression
oSGD. . . . .Online stochastic gradient descent
P . . . . . .Postnatal day
PBS . . . . . .Phosphate-buffered saline
PFA . . . . . .Paraformaldehyde
PFC . . . . . .Prefrontal cortex
PTSD. . . . .Post-traumatic stress disorder
PV. . . . . Parvalbumin
QS. . . . . . .Quiet sleep
RSA . . . . . Representational similarity analysis
REM. . . . . Rapid eye movement sleep
S1BF. . . . . Primary somatosensory barrel field
SEM . . . . . Standard error of the mean
S1FL. . . . . Primary somatosensory forelimb cortex
SERT . . . . 5-HT transporter
S2. . . . . . Secondary somatosensory cortex
SSRI. . . . . Selective 5-HT reuptake inhibitor
SST. . . . . Somatostatin
TPH1. . . . .Tryptophan hydroxylase 1
TPH2 . . . . Tryptophan hydroxylase 2
V1 . . . . . .Primary visual cortex
VGLUT3 . . Vesicular glutamate transporter 3
VIP . . . . . Vasoactive intestinal peptide
VTA. . . . . Ventral tegmental area
WT . . . . . Wildtype

1. General introduction

Scope

Our understanding of neuromodulation over the lifetime is incomplete. In particular, how neuromodulatory dynamics shape the activity of excitatory-inhibitory cortical microcircuits fine tuning information transfer from early ages is poorly understood. Out of the variety of neuromodulators, the monoamine 5-hydroxytryptamine (5-HT/serotonin) is of particular interest given its developmental (Ogelman et al., 2024; Sinclair-Wilson et al., 2023; Toda et al., 2013), pathological (Daly et al., 2019; Lin et al., 2014; Pourhamzeh et al., 2022), clinical (Cipriani et al., 2018; Luo et al., 2020) and behavioural (Grossman et al., 2022; Wert-Carvajal et al., 2022) relevance. Thus, this thesis has three major aims: firstly to characterise 5-HT dynamics in the adult and developing mammalian cortex; secondly to study how these 5-HT dynamics influence cortical population activity; thirdly to find a computational justification that reconciles 5-HT dynamics and their effects in cortical activity with the subsequent modulation of mammalian behaviour, i.e., elucidating the role of cortical 5-HT.

1.1 5-HT in cortical circuits

1.1.1 5-HT cortical dynamics

While the dynamics of extracellular 5-HT in cortical circuits remain poorly understood, a number of studies have characterised the firing of 5-HT neurons in the raphe nuclei and associated 5-HT dynamics to different behaviours (Paquelet et al., 2022; Ranade & Mainen, 2009). 5-HT neurons exhibit both phasic and tonic firing (Allers & Sharp, 2003; Hajós et al., 1995; Ranade & Mainen, 2009). The phasic firing of 5-HT neurons has been described time-locked to movement

(Jacobs & Fornal, 1997; Ranade & Mainen, 2009; Veasey et al., 1995), reward (J. Y. Cohen et al., 2015.; Y. Li et al., 2016; Ranade & Mainen, 2009, 2009), aversive experience (J. Y. Cohen et al., 2015; Paquelet et al., 2022; Ren et al., 2018), uncertainty (Grossman et al., 2022), and emotionally salient behaviours (Paquelet et al., 2022). The tonic firing of 5-HT neurons oscillates with the sleep-wake cycle (Kato et al., 2022; Sakai, 2011), with 5-HT firing rate reaching its highest level during wakefulness, decreasing during non-rapid eye movement (NREM) sleep and dropping during rapid eye movement (REM) sleep (Deng et al., 2024; Wan et al., 2021). A recent study has suggested that predictive value could reconcile some of the observed firing dynamics of 5-HT neurons, namely they present a theoretical model that captures the firing of 5-HT neurons during reward, predicted punishment and uncertainty (Harkin et al., 2023). However, this theory fails to capture some observations such as the firing of neurons upon unpredicted aversive experience (J. Y. Cohen et al., 2015). Moreover, to date most studies of 5-HT dynamics are based on neurophysiological recordings from 5-HT neurons (J. Y. Cohen et al., 2015; Hajós et al., 1995; Kato et al., 2022; Y. Li et al., 2016; Paquelet et al., 2022; Ranade & Mainen, 2009; Veasey et al., 1995) rather than measuring 5-HT release (Deng et al., 2024; Kubitschke et al., 2022; Unger et al., 2020; Wan et al., 2021). How the firing of 5-HT neurons relates to 5-HT release is hard to predict given the ability of these neurons to release other neurotransmitters (e.g., glutamate (Sengupta et al., 2017; H.-L. Wang et al., 2019)) as well as to exhibit diverse types of neurotransmission (i.e., synaptic and volumetric (Descarries et al., 1975)). Moreover, given the hodological diversity of 5-HT neurons (Okaty et al., 2019), it is likely that 5-HT dynamics differ across the wide range of postsynaptic targets in the central nervous system. A characterization of extracellular 5-HT fluctuations in anatomically confined cortical regions during animal behaviour is necessary to understand cortical 5-HT dynamics.

1.1.2 5-HT effects in cortical activity

5-HT is a neuromodulator that has a pleiotropic effect on cortical cells (Azimi et al., 2020; Hamada et al., 2022; Lottem et al., 2016; Puig & Gener, 2015; Tian et al., 2017). Part of this complexity arises from the heterogeneity of its receptors, with seven different families (5-HT_{1-7}) many of which have low abundance (Barnes et al., 2021). Among these, the most expressed are 5-HT_1R, which is hyperpolarizing, and 5-HT_2R, which is depolarizing (Barnes et al., 2021). All 5-HT receptor families are metabotropic G protein-coupled receptors (GPCRs) except for 5-HT_3R, which is ionotropic and depolarizing (Barnes et al., 2021). The different families and subtypes of 5-HT receptors exhibit high variability in terms of anatomical localization (Barnes et al., 2021; Salvan et al., 2023), pharmacology (Barnes et al., 2021; Y. Wang et al., 2019) and function (Barnes et al., 2021; Klempin et al., 2010; Salvan et al., 2023).

The diversity of 5-HT receptors extends to their intracellular signalling mechanisms, which influence not only membrane potential but also a range of cellular processes. GPCR-linked pathways include inhibition of adenylate cyclase via Gi proteins (5-HT_1R and 5-HT_5R), activation of phospholipase C via Gq proteins (5-HT_2R), and stimulation of adenylate cyclase via Gs proteins (5-HT_4R, 5-HT_6R and 5-HT_7R) (Barnes et al., 2021). These pathways regulate intracellular calcium levels, phosphoinositide metabolism, and kinase cascades, ultimately affecting gene expression, synaptic plasticity, and neurotrophic responses (Barnes et al., 2021). This functional complexity underscores the intricate role of 5-HT signalling in modulating cortical neurophysiology.

To understand the direct effects of 5-HT in sensory cortical circuits it is important to consider the cortical architecture and the distribution of 5-HT receptors. The canonical connectivity in sensory cortices is that bottom-up thalamic activity accesses the cortex through layer (L) 4, from where it

is relayed into L2/3 (Miller, 2003) and progresses into L5, the primary output layer (Moberg & Takahashi, 2022), on the other hand intracortical activity inputs this circuit in a top-down manner through L1 (Huang et al., 2024, p. 1; Schuman et al., 2021, p. 1). Albeit over simplistic, this flow of information is important to consider given the asymmetric distribution of the 5-HT receptor subtypes across the cortical column. For example, the highest expression of 5-HT_{2A} receptors, the most abundant excitatory receptor, is found in L5, the output layer, across cortex (Andrade & Weber, 2010), albeit L5 pyramidal neurons also express inhibitory 5-HT_{1A} receptors (Azmitia et al., 1996; Saitow et al., 2020). Indeed 5-HT_{1A} show a broad expression pattern in the cortex (Barnes et al., 2021). The expression of 5-HT_{3A}R, an excitatory ionotropic receptor, in cortex is characteristic of a subtype of interneurons that populate the upper layers of cortex and have been ascribed a disinhibitory role (S. Lee et al., 2013). On the basis of this 5-HT receptor distribution, 5-HT could be predominantly inhibitory in input bottom-up layers, while promoting top-down and output layers. The distribution across cortical layers of other 5-HT receptors is less well characterised, albeit all of them have expression in cortical structures (Barnes et al., 2021). Recordings of the effects of manipulations of 5-HT in confined cortical layers are necessary to fully understand the effects of 5-HT in cortical microcircuitry.

Upon 5-HT release, *in vivo* studies in rodents suggest that the effects on cortical circuits are predominantly inhibitory with a minority of neurons being excited (Azimi et al., 2020; Lottem et al., 2016; Puig & Gener, 2015; Schmitz et al., 1998; Tian et al., 2017; Waterhouse et al., 1986), although there is some conflicting literature (Hamada et al., 2024). The diversity of results is mainly driven by the heterogeneity of postsynaptic 5-HT receptors (Barnes et al., 2021). Additional compounding factors are glutamatergic and GABAergic co-transmission (H. Li et al., 2024; Z. Liu et al., 2014; Ren et al., 2019; Sengupta et al., 2017; H.-L. Wang et al., 2019), polysynaptic effects involving other brain regions (Hamada et al., 2024; H.-L. Wang et al., 2019) and 5-HT receptor heterogeneity across development (Morton et al., 2015; Sargin et al., 2019)

and regions (Salvan et al., 2023). All these confounding variables make it hard to interpret the isolated effects of 5-HT in cortical circuits. For example, a recent MRI study has claimed a mostly excitatory role of 5-HT across reward-related brain areas upon optogenetic stimulation of the DRN in awake mice (Hamada et al., 2024). However, due to the temporal resolution of MRI it is difficult to rule out that the observed cortical excitation is being mediated directly by other subcortical areas such as the ventral tegmental area (VTA) (Z. Liu et al., 2014; H.-L. Wang et al., 2019). Indeed, the latter results show an increased blood-oxygen-level-dependent (BOLD) signal in VTA upon DRN stimulation (Hamada et al., 2024). *In vivo* studies in animal models report that DRN optogenetic stimulation decreases spontaneous activity in sensory cortices, while decreasing the gain of evoked activity. These observations have been made in sensory cortices of both anaesthetised (mice) (Lottem et al., 2016) and awake animals (mice and primate) (Azimi et al., 2020; Seillier et al., 2017, p. 1), suggesting a predominantly inhibitory role of 5-HT in sensory cortices.

Altogether, the complexity of results suggests that future studies should perform more spatially controlled 5-HT manipulations within cortical circuits to fully understand the effects of 5-HT on cortical activity.

1.1.3 5-HT effects in behaviour and learning

How 5-HT dynamics in cortex shape behaviour also remains a matter of debate. 5-HT has been associated with a plethora of behavioural effects including thresholding mechano-sensory perception (Dugué et al., 2014), anxiety (Ren et al., 2018), coping (Ren et al., 2018), persistence (K. Miyazaki et al., 2011), social interactions (L. Li et al., 2021; Zou et al., 2020), aggressivity (Audero et al., 2013; da Cunha-Bang & Knudsen, 2021), and fear (Bocchio et al., 2016; Marcinkiewcz et al., 2016). Of particular interest to this thesis is the role of 5-HT in

learning. During learning paradigms, some studies suggest that enhanced 5-HT levels correlate with increased learning (Grossman et al., 2022) while others report a decrease in learning (Kanen et al., 2021). A recent electrophysiological and optogenetic study suggested that increased 5-HT levels upregulate learning rate as a function of unexpected uncertainty, while 5-HT decreases downregulate it during expected uncertainty (Grossman et al., 2022). Conversely, studies of the effects of 5-HT depletion report potentiation of pavlovian associations suggesting that 5-HT decreases learning rate (Kanen et al., 2021). Characterization of animal models with alterations in genes involved in 5-HT transmission (i.e., 5-HT transporter (SERT)-KO), have also shown differences in learning dynamics, such as increases in fear conditioning (Lima et al., 2019) and decreases in learning generalisation (C. C.-G. Guo et al., 2021). The complex role of 5-HT in learning is further highlighted by results illustrating that 5-HT effects on learning are dependent on inter-stimulus interval duration (Iigaya et al., 2018), type of learning (e.g., associative vs reversal learning) (Kanen et al., 2021), and trial outcome (i.e., reward vs punishment) (Michely et al., 2022). This complexity likely arises from the diversity of 5-HT neurons (Okaty et al., 2019), and the large number of postsynaptic targets (Barnes et al., 2021). Indeed some behavioural studies have shown distinct roles of 5-HT neurons with hodological-specificity (Ren et al., 2018). Namely, a recent study has shown that amygdala-projecting 5-HT neurons promote anxiety-like behaviour, while frontal cortex-projecting 5-HT neurons promote active coping (Ren et al., 2018). Thus, future studies on the role of cortical 5-HT should investigate the effects of 5-HT in behaviour and learning using more targeted manipulations of 5-HT.

1.1.4 5-HT clinical relevance

5-HT has a high clinical relevance across neuropsychiatric and neurodevelopmental disorders, both from an etiological (Daly et al., 2019; Pourhamzeh et al., 2022) and a therapeutic perspective (Luo et al., 2020). A range of neuropsychiatric conditions have been associated with alterations in 5-HT (Pourhamzeh et al., 2022). For example, major depressive disorder (MDD) was initially thought to be driven by low levels of 5-HT, known as the 5-HT theory of depression (Coppen, 1967). A recent systematic review suggested that this hypothesis might lack evidence (Moncrieff et al., 2022), however this claim met criticism from the larger research community (Jauhar, Arnone, et al., 2023). Indeed, the etiological involvement of 5-HT in MDD is supported by numerous studies (Jauhar, Cowen, et al., 2023). These studies include associations of MDD with 5-HT-related gene polymorphisms (Murphy & Lesch, 2008), metabolic changes (Correia & Vale, 2022), and the therapeutic effectiveness of 5-HT drugs, particularly selective 5-HT reuptake inhibitors (SSRIs) (Luo et al., 2020). Additionally, several other neuropsychiatric disorders have been associated with alterations in the 5-HT system including post-traumatic stress disorder (PTSD) (Davis et al., 1997; Krystal & Neumeister, 2009), obsessive compulsive disorder (OCD) (Hesse et al., 2011; Nicolini, 2010) and addiction(Y. Li et al., 2021), all of which are also treated with SSRIs (Hidalgo & Davidson, 2000; Kellner, 2010; Torrens et al., 2005; Williams et al., 2022).

Several neurodevelopmental disorders have also been associated with developmental alterations in 5-HT dynamics (Daly et al., 2019; Montgomery et al., 2018; Muller et al., 2016). Clinical studies have identified polymorphisms in the SERT gene (Murphy & Lesch, 2008; Veenstra-VanderWeele et al., 2012) and SSRI exposure during pregnancy (Koc et al., 2023; Morales et al., 2018) as risk factors for disorders such as autism spectrum disorder (ASD) and attention deficit hyperactivity disorder (ADHD), albeit there is some conflicting literature (Ames

et al., 2021; Suarez et al., 2022). The association between these alterations and neurodevelopmental disorders has been reported to interact with exposure to traumatic experiences during critical developmental periods (Brown et al., 2013; Delli Colli et al., 2022). Despite these findings there remains a poor mechanistic understanding of how these developmental 5-HT alterations can lead to neurodevelopmental disorders. Particularly little studied is how 5-HT disruptions impact on early cortical activity to subsequently disrupt the activity-dependent maturation of neural circuits.

Another clinically-relevant aspect of 5-HT is psychedelic drugs (e.g., lysergic acid diethylamide (LSD), psilocin) which typically are 5-HT agonists with high affinity for the 5-HT_{2A} as well as other 5-HT receptors (Holze et al., 2024). Over the last few years, the strong neuroplastic effect of these drugs has raised strong interest in their potential for the treatment of a range of neuropsychiatric conditions such as MDD or addiction (de Vos et al., 2021; Tupper et al., 2015). However, the precise mechanism driving the therapeutic effect of psychedelics remains poorly understood. It remains a matter of discussion which receptor is responsible for the hallucinogenic and therapeutic effect, with several studies suggesting a critical role of 5-HTR_{2A} (Cameron, Patel, et al., 2023; Vargas et al., 2023) despite some conflicting literature (Cameron, Benetatos, et al., 2023; Sekssaoui et al., 2024). It is also unclear whether the therapeutic and hallucinogenic effect can be mechanistically disentangled or whether they are both a consequence of the same signalling pathway (Cameron, Benetatos, et al., 2023; Wallach et al., 2023). A recent study has suggested an instrumental role of the TrKβ-BDNF signalling pathway. Namely the study proposes that psychedelics bind TrKβ directly, stabilising an active conformation which in turn promotes plasticity (Moliner et al., 2023). A new line of research has also suggested that signalling through internalised intracellular 5-HT_{2A} receptors might be a key mediator of the neuroplastic effect (Vargas et al., 2023). Despite the intensive study of psychedelics, little is known of how they affect 5-HT dynamics and whether this plays a role in

their effects. A number of studies from 50 years ago showed that a range of psychedelics suppress the tonic firing of 5-HT neurons in the DRN (Foote et al., 1969; Trulson et al., 1981; Trulson & Jacobs, 1979). Given that non-hallucinogenic analogs (e.g., lisuride) also trigger this decrease in 5-HT firing rate, it is unlikely to be a driver of the hallucinogenic effect of these drugs (Rogawski & Aghajanian, 1979). However, lisuride has also been reported to have antidepressant effects (Qu et al., 2023) suggesting a neuroplastic role. Altogether how this decrease in DRN activity affects cortical 5-HT dynamics and whether this relates to the therapeutic effects of psychedelics remains uncertain.

1.1.5 Theories on the role of 5-HT in CNS function

In contrast to dopamine and the reward prediction error framework (Schultz, 2016), there is not an agreed comprehensive theory of the role of 5-HT in the central nervous system. Some theories of particular roles of 5-HT in the CNS are impulse control (Desrochers et al., 2022), behavioural inhibition (Faulkner & Deakin, 2014) or emotional learning (Meneses & Liy-Salmeron, 2012) among others. A major attempt to provide a comprehensive framework was the opponency theory in which 5-HT would be compensating the behavioural effects of other neuromodulators, particularly dopamine, and thereby stabilising behaviour (Boureau & Dayan, 2011). More recently, another theory based on the role of 5-HT in the gastrointestinal tract hypothesised that 5-HT might be controlling cognitive flux in the brain as a function of how cognitively demanding tasks are (Shine et al., 2022). While these theories were supported by behavioural results and provided a cognitive interpretation of the role of 5-HT, they lacked a detailed mechanistic explanation grounded in the biology of the 5-HT system (Boureau & Dayan, 2011; Okaty et al., 2019; Shine et al., 2022). Last year a more mechanistic theory suggested that 5-HT encodes a metric known as state value (i.e, predicted value), based on the

firing patterns of 5-HT neurons in behaving rodents (Harkin et al., 2023). While this framework made great progress in advancing our understanding of 5-HT dynamics, it failed to account for the postsynaptic effects that 5-HT release would have across its broad spectrum of projection targets and how this would subsequently influence behaviour (Barnes et al., 2021; Puig & Gener, 2015; Salvan et al., 2023). Thus a comprehensive framework of the role of 5-HT in the brain remains elusive.

1.2 Activity-dependent development of excitatory and inhibitory cortical microcircuits

The early development of the cortex is a highly orchestrated process involving the generation, migration, and differentiation of neurons within the ventricular and subventricular zones of the embryonic brain (Bystron et al., 2008). Neurogenesis begins with the proliferation of radial glial cells which act as both neural progenitors and scaffolding for migrating neurons (Bystron et al., 2008). Excitatory pyramidal neurons born from these progenitors migrate radially to form the cortical plate. This establishes the layered structure of the cortex through an inside out gradient where deeper layers form first followed by more superficial ones (Bystron et al., 2008). GABAergic interneurons, generated in the ganglionic eminences, undertake a tangential migration to integrate into the cortical plate (Lim et al., 2018). These interneurons diversify into subtypes, each characterised by distinct morphological and functional properties, and are essential for modulating cortical excitatory-inhibitory balance (Lim et al., 2018).

Activity-dependent mechanisms are instrumental in the maturation of these cortical circuitry through processes such as neuronal survival and synaptic pruning that regulate the connectivity patterns of cortex (Wu et al., 2024). All this highlights the importance of understanding the early patterns of cortical activity.

1.2.1 Early cortical activity

The patterns of cortical activity in the developing brain are drastically different to those in adulthood (Wu et al., 2024). Calcium recordings in the developing cortex of awake head-fixed mice have shown synchronised patterns of cortical activity in the first week of postnatal development (Golshani et al., 2009; Leighton et al., 2021; Martini et al., 2021; Mòdol et al., 2024; Siegel et al., 2012). In the visual cortex these events have been characterised as being either low-synchronicity events (L-events) that recruit 20-80% of cells or high-synchronicity events (H-events) that recruit more than 80% of cells within the recorded area, with only the former depending on retinal activity (Leighton et al., 2021; Siegel et al., 2012). The electrophysiological correlates of these calcium events are not clear but the frequency and retinal-dependency of L-events has led to speculation that they might represent spindle bursts (Siegel et al., 2012). Highly synchronous activity is present until postnatal day 10 at which point cortical activity decorrelates through the onset of cortical inhibition, a process involving parvalbumin (PV) interneuron maturation but regulated by somatostatin (SST) interneurons (Mòdol et al., 2024). This decorrelation is followed by a ~2 day period of low activity or quiescence that precedes the onset of active whisking and eye opening (Domínguez et al., 2021). Thereafter, the sparse neural code characteristic of adult cortical circuitry emerges. While the role of this early synchronised activity is not fully understood, computational modelling studies suggest that H-events regulate connection strength while L-events are responsible for the regulation of connection selectivity (Wosniack et al., 2021). Moreover, a recent study has shown that pre-training artificial neural networks with these early patterns of cortical activity leads to superior performance in motion prediction of natural scenes (May & Gjorgjieva, 2024). So while the mechanistic role of these synchronous events remains unclear, evidence suggests a prominent role in the emergence of functional cortical circuits. Finally, recent methodological advances have allowed the recording of the embryonic cortex during *in vivo* settings which

provide evidence of active circuitry before birth (Munz et al., 2023). These recent results suggest that activity-dependent mechanisms are also crucial for embryonic neurodevelopment. Thus, it is clear that the early patterns of cortical activity dictate the emergence of adult cortical circuitry, a process particularly well characterised in sensory cortices.

1.2.2 Cortical interneurons in neurodevelopment

Cortical interneurons exhibit a large molecular, morphological and functional diversity (Lim et al., 2018). From their embryonic source these interneurons are classified as originating in either the medial or caudal ganglionic eminence (MGE and CGE respectively) (Lim et al., 2018). Interneurons from both sources have been shown to play prominent, but different, roles in cortical development (Che et al., 2018; Mòdol et al., 2024). MGE-interneurons are sub-classified by their expression of either PV or SST (Lim et al., 2018). PV interneurons are the primary source of inhibition, and the onset of their inhibitory role leads to cortical decorrelation (Mòdol et al., 2024). However, it is SST interneurons that orchestrate this developmental emergence of inhibition, controlling the timing of decorrelation through the regulation of the maturation of PV interneurons (Mòdol et al., 2024). Moreover, thalamically driven SST interneurons in L5b show transient circuits in early postnatal murine development providing transient translaminar inhibitory input to L4 (Anastasiades et al., 2016; Marques-Smith et al., 2016). In turn, this thalamic-driven SST activation inhibits ascending sensory input to L4, thereby restricting L-events (Leighton et al., 2021).

CGE-interneurons have also been ascribed a key role in activity-dependent cortical development. The early activity of these interneurons is driven by thalamic projections, leading to the restriction of pyramidal activation which constrains the size of sensory maps (e.g., barrel

formation) (Che et al., 2018). Altogether, the diverse subtypes of cortical interneurons play critical and distinct roles in shaping cortical development.

The development of these GABAergic circuits relies strongly on activity-dependent mechanisms. A seminal study in the rodent S1BF showed that the survival of interneurons emerging from the MGE depends on the activity of pyramidal cells (Wong et al., 2018). The latter study proved that the levels of cortical inhibition develop to match the levels of excitation. Several studies have further characterised how cortical dynamics shape the emergence of cortical inhibition (Che et al., 2018; Che & De Marco García, 2021; De Marco García et al., 2015; Duan et al., 2020; Modol et al., 2020). For example, such studies characterise the early activity patterns of GABAergic neurons (Che & De Marco García, 2021; Modol et al., 2020) or show the instrumental role of immature MGE interneurons in the regulation of their own apoptosis by early interactions with pyramidal neurons (Duan et al., 2020). Of particular interest to this thesis is a study showing that a subpopulation of CGE interneurons (bipolar 5-HT_{3A}R expressing cells) matures as a function of 5-HT, and not glutamate, input (Wong et al., 2022). Thus, evidence suggests that cortical dynamics influenced by neuromodulation mandate the emergence of inhibitory circuitry.

1.2.3 Interneuron alterations in neurodevelopmental and neuropsychiatric conditions

The criticality of cortical interneuron development is highlighted by a large body of literature suggesting that alterations in the development of inhibitory circuits lead to neurodevelopmental disorders such as ASD (Contractor et al., 2021) or ADHD (Edden et al., 2012). Of particular interest for this thesis are studies that have linked these disruptions to activity-dependent processes in the murine developing cortex (Babij et al., 2023; Kourdougli et al., 2023). For

example, a recent study has shown that Gabrb3, a gene associated with ASD and Angelman Syndrome, is essential for inhibitory function and that its ablation leads to decreased GABAergic synapses, increased network synchrony, and heightened neonatal cortical response to tactile stimulation (Babij et al., 2023). Moreover the latter study reported correlations between the spatial distribution of GABRB3 and atypical connectivity observed in human ASD subjects (Babij et al., 2023). Another study has shown in a fragile X syndrome (FXS) model that PV interneurons are hypoactive and disconnected from excitatory neurons, leading to increased apoptosis (Kourdougli et al., 2023). It is reported that pharmacogenetic enhancement of PV activity in neonatal mice improves PV interneuron density but not circuit function. However, using an allosteric modulator of Kv3.1 channels - a voltage-gated potassium channel that enables PV interneuron fast-spiking properties - allowed to increase their activity post-critical period rescuing circuit dynamics and reducing tactile defensiveness. These findings support PV interneurons as a therapeutic target for FXS and similar disorders (Kourdougli et al., 2023). All these results suggest a critical role of interneuron development in the aetiology of a number of neurodevelopmental and neuropsychiatric disorders.

1.2.4 5-HT in neurodevelopment

While the activity-dependent development of cortex has been explored by many studies, how neuromodulation shapes early cortical activity with consequences for circuit maturation remains poorly understood. 5-HT is of particular interest given the large literature relating this neurotransmitter system with neurodevelopmental disorders (Daly et al., 2019).

Evidence suggests that 5-HT dynamics vary through development. Anatomical studies in mice show that cortical structures are innervated by 5-HT neurons during the first postnatal week, followed by a pruning stage (Maddaloni et al., 2017). Electrophysiological studies in the dorsal

raphe nucleus in developing mice suggest that 5-HT neurons have different neurophysiological profiles early compared to later development (Morton et al., 2015). Moreover, a steep drop in 5-HT levels at birth is thought to be instrumental for the development of sensory cortical maps (Toda et al., 2013). These developmental 5-HT dynamics at birth are also critical for the development of thalamocortical projections to sensory cortices (Sinclair-Wilson et al., 2023). The differential regulation of 5-HT dynamics in development is further evidenced by the altered pattern of expression of genes related to 5-HT transmission. For example, while SERT expression is confined to 5-HT neurons in the adult CNS, it presents a broader pattern of expression in the developing brain (embryonic day (E) 15 to postnatal day (P) 10 in mice (X. Chen et al., 2016; De Gregorio et al., 2020) and gestational weeks (GW) 12-13 in humans (Verney et al., 2002)) Thus, SERT is transiently expressed in pyramidal neurons in association cortices, hippocampus and thalamocortical projections to sensory cortices (Narboux-Nême et al., 2008). The role of this transient expression remains a matter of debate, with the two prevailing hypotheses being that it either allows 5-HT release by non-5-HT neurons (Lebrand et al., 1996) or that it mediates a necessary developmental decrease in 5-HT signalling (De Gregorio et al., 2020). Altogether a large body of literature suggests that 5-HT dynamics in early development are likely to be different compared to the adult. However the evolution of 5-HT dynamics during brain development remains uncharacterised.

Evidence suggests that the effects of 5-HT on cortical neuronal activity are also different in the developing brain. For example, the expression of 5-HT receptors changes across development with reported transient expression of 5-HT_{1B}R in thalamocortical projections to the S1BF cortex during early postnatal development (Bennett-Clarke et al., 1993; Laurent et al., 2002; Leslie et al., 1992; Salichon et al., 2001). The 5-HT receptome in cortex has also been suggested to change through development (Sargin et al., 2019), implying differential effects of 5-HT in cortical

activity across development. However, the evolution of cortical responses to 5-HT across development have not been characterised.

5-HT plays a prominent role in neurodevelopment regulating processes from cell division to synaptic connectivity (Daly et al., 2019; Lesch & Waider, 2012). Of particular interest to this thesis is the role of 5-HT in the migration and maturation of interneuron subpopulations (De Gregorio et al., 2020; Frazer et al., 2015; Miceli et al., 2017; Murthy et al., 2014; Wong et al., 2022). A recent publication has shown a role for 5-HT in the regulation of vasointestinal peptide (*VIP*) expressing bipolar cells survival (Wong et al., 2022). Another study has shown alterations in VIP interneuron migration upon developmental SERT disruption (Frazer et al., 2015), and a role of 5-HTR_{3A} in this effect (Murthy et al., 2014). 5-HT also plays a role in the developmental survival of SST interneurons as well as the maturation of their dendritic structure, as evidenced by alterations in SST survival and dendritogenesis observed in SERT-KO mice (De Gregorio et al., 2020). While the role of 5-HT in interneuron development is well established, the extent to which this is mediated by changes in cortical activity remains to be explored.

Thus, despite the numerous studies of the developmental role of 5-HT, how alterations in 5-HT dynamics mandate the balancing of cortical excitatory and inhibitory circuits from an activity-dependent perspective remains unclear.

1.3 5-HT/glutamate co-transmission

A number of studies have defied Dale's principle by characterising neuronal subpopulations with the ability to co-release more than one type of neurotransmitter (e.g., dopamine-GABA (Melani & Tritsch, 2022) or glutamate-GABA (Ajibola et al., 2021)). Indeed, subtypes of 5-HT neurons have been shown to co-release glutamate (H. Li et al., 2024; Sengupta et al., 2017; H.-L. Wang

et al., 2019) or GABA (H. Li et al., 2024; Ren et al., 2019). Glutamatergic co-transmission, particularly to the VTA, has been associated with a role in reward (Z. Liu et al., 2014; H.-L. Wang et al., 2019). The mechanism balancing the release of one neurotransmitter versus the other remains unclear, but a study has shown that these 5-HT neurons preferentially release glutamate during periods of low firing rate whereas 5-HT is preferentially released at higher firing rates (Sengupta et al., 2017). Moreover, a recent study suggests that neurons are able to change the neurotransmitter they co-release as a function of behavioural stressors, a process known as neurotransmitter switching (H. Li et al., 2020, 2024; Spitzer, 2017). In 5-HT neurons, a switch from glutamatergic to GABAergic co-transmission has been observed during a fear association paradigm (H. Li et al., 2024). Interestingly, evidence suggests that perinatal exposure to SSRIs disrupts glutamatergic co-transmission from 5-HT neurons to the VTA triggering motor disruptions (Cunha et al., 2021). Whether 5-HT neurons co-release other neurotransmitters into cortical circuits to alter the emergence of cortical population activity remains unstudied.

1.4 Two-photon imaging of calcium and 5-HT in awake adult and developing rodents

1.4.1 Longitudinal two-photon imaging in rodents

Two-photon microscopy allows the excitation of fluorophores through the simultaneous abortion of two photons with higher wavelength, which only occurs within the micrometre region of focus (Benninger & Piston, 2013). This provides a high optical sectioning, which when combined with the lower scattering of higher wavelengths, allows imaging in deep biological tissues (up to 1 mm) (Benninger & Piston, 2013). The application of this technology in rodents implanted with head-fixing plates and cranial windows, has allowed the monitoring of fluorescence molecules in the cortex of living awake rodents (Holtmaat et al., 2009). For example, calcium indicators such

as GCaMP6s allow the tracking of calcium dynamics, as a proxy of neuronal firing (T.-W. Chen et al., 2013). Recent studies have optimised these surgical procedures in developing postnatal mice (Che & De Marco García, 2021; He et al., 2018), and alive mouse embryos (Munz et al., 2023). This opens the door to monitor cortical neurophysiology with fluorescent indicators during key periods of murine brain development.

1.4.2 Imaging 5-HT using fluorescence biosensors

A major challenge for understanding how 5-HT influences cortical population activity has been the difficulty of tracking 5-HT dynamics *in vivo*. The recent development of neurotransmitter-sensitive fluorescence sensors generated from genes encoding receptors, when combined with multiphoton microscopy, has opened the door to monitoring 5-HT dynamics *in vivo* with high spatial and temporal resolution (Ocana-Santero et al., 2024). In the past five years, a number of 5-HT fluorescence biosensors have been developed (Deng et al., 2024; Dong et al., 2021; Kubitschke et al., 2022; Unger et al., 2020; Wan et al., 2021). These tools have been validated *in vitro*, and studies to date suggest promise for monitoring 5-HT dynamics *in vivo*. Thus, changes in 5-HT signalling dynamics have been detected in cortical regions (Kubitschke et al., 2022; Unger et al., 2020; Wan et al., 2021) in response to alterations in the sleep–wake cycle (Deng et al., 2024; Unger et al., 2020; Wan et al., 2021) and whole body movement (Kubitschke et al., 2022). However, to date, few *in vivo* multiphoton imaging studies of 5-HT biosensors have controlled for the influence on the optical signals of confounding factors such as hemodynamic changes or other potential sources of optical noise. These factors might limit selectivity of the signal and thus the sensitivity to the desired readout.

It is evident from previous calcium- and voltage-sensitive imaging studies that in settings where the changes of fluorescence are small (e.g., widefield imaging or use of sensors with a small dynamic range), activity-dependent optical signals can be a major source of noise (Grinvald et

al., 1982; Valley et al., 2020). Such confounding intrinsic optical signals may arise from many sources including changes in blood flow (e.g., blood vessel dilation) (Grinvald et al., 1986; Morone et al., 2017), differences in haemoglobin and oxygenation state (Morone et al., 2017), and alterations in local cellular activity (L. B. Cohen et al., 1968; Grinvald et al., 1982; Hill & Keynes, 1949; Lipton, 1973; Salzberg et al., 1985; Tasaki et al., 1968). All of these factors might alter the light absorption properties of the tissue imaged, in wavelengths overlapping with the emission spectra of the most common 5-HT sensors (Deng et al., 2024; Kubitschke et al., 2022; Unger et al., 2020; Wan et al., 2021). Given their inherent activity-dependent nature (Ma et al., 2016), all these factors represent challenging confounds to overcome.

A preferred control to account for this source of noise would be to use a second imaging laser tuned to the isosbestic point, the imaging wavelength at which the absorbance, and subsequent emission, of a sensor will not change independently of its conformation (i.e., bound or not to 5-HT). Thus, changes in fluorescence at this wavelength can be attributed to noise rather than changes in 5-HT binding. Simultaneous imaging with one laser tuned to the isosbestic wavelength and another tuned to the peak in fluorophore excitation allows intrinsic artefacts to be subtracted, thereby revealing the true biosensor signal. This control is commonly implemented in fibre photometry (Lerner et al., 2015) but not often with multiphoton microscopy due to the technical complexity of aligning two raster-scanning systems in time and space. Nevertheless, multiphoton imaging presents advantages over fibre photometry that merit its use in biosensor imaging. Namely, it provides a higher spatial resolution with a readout of signal over space, including at depth within the tissue, thanks to its accurate optical sectioning (Benninger & Piston, 2013). Cranial windows also represent a less invasive alternative to fibre implants, albeit at the expense of lack of access to deep brain structures (Holtmaat et al., 2009). Altogether this warrants the testing and optimization of 5-HT biosensors in multiphoton imaging *in vivo*.

Thus, the recent emergence of these tools is a promising prospect for the characterization of *in vivo* 5-HT dynamics in rodents with high spatial-resolution, but their implementation with two-photon microscopy requires the development of appropriate controls to avoid confounding sources of noise such as intrinsic optical signals.

1.5 NeuroAI: Deep neural networks to model the brain

The recent emergence of the field of neuroAI opens the door to understand neuronal processes by modelling them with biologically-inspired architectures, allowing for an analytical understanding of their second order effects (Kriegeskorte & Golan, 2019). Several studies have used deep neural networks to model neuronal and cognitive processes, particularly to characterise the role of neuromodulators like dopamine (Garcia et al., 2023). However, such studies tend to model the effect of neuromodulators directly by changing the learning rule, rather than having a direct effect in the activation of the neurons, as it occurs in the brain. In this sense, gated neural networks – in which the activation of the neurons is modulated by a gate – provide a naturalistic implementation of neuromodulation whereby the effects on learning are second order effects of the change in neuronal activation (Saxe et al., 2022).

Within NeuroAI, the advent of analytical connectionism employs techniques from statistical mechanics to find exact solutions to the evolution of the network parameters during training (Mannelli et al., 2024). This provides an analytical understanding of the network dynamics and mathematically describes the effect a parameter has on the activation and learning dynamics of a network. Despite the promising potential of these modelling tools they remain unused in many fields of neuroscience research due to their novelty. Of particular interest to this thesis is their use to model the role of the 5-HT system.

1.6 Summary

While significant advances have been made in our understanding of 5-HT and cortical population dynamics throughout mammalian life, a number of questions remain unanswered. Firstly, 5-HT dynamics in the adult and developing mammalian cortex during behaviour remain uncharacterized. Secondly, it is unclear how 5-HT dynamics dictate population activity in cortical excitatory-inhibitory microcircuits, both in adulthood and development. Thirdly, how the combination of 5-HT dynamics and its effects in cortical activity shape the emergence of mammalian behaviour is not well understood. The recent development of optical tools to monitor 5-HT dynamics and cortical activity in rodents, as well as the advent of theoretical methods to make sense of the complex datasets these tools generate, provide a unique opportunity to shed light on these three questions.

1.7 Aims

In light of these gaps in the literature, the aims of this thesis and the respective experiments to address them are the following:

In chapter 2, we aim to characterise 5-HT dynamics in both the developing and adult S1BF. For this purpose, we have validated the use of a fluorescence 5-HT biosensor (g5-HT3.0) in the S1BF to monitor 5-HT dynamics through a cranial window in head-fixed mice using two-photon microscopy. Then, we have characterised S1BF 5-HT dynamics both in adult and developing mice. We expanded this work to study the effect of SERT, a major determinant of 5-HT developmental dynamics, in regulating early 5-HT fluctuations by using acute fluoxetine dosage and SERT-KO mice.

In chapter 3, we aim to characterise how genetic knockout of SERT affects emerging S1BF population dynamics, with a focus on its role in dictating excitatory-inhibitory cortical balance. For this we use longitudinal two-photon calcium imaging of SERT-KO mice from the first postnatal week to adulthood, in animals with interneuron subpopulations labelled with a red fluorophore.

In chapter 4, we aim to characterise the effects of postnatal exposure to fluoxetine in the emergence of S1BF cortical population dynamics, and defining cortical E-I balance, for which we employ the same longitudinal two-photon calcium imaging methodology in mice dosed orally with fluoxetine from P2 to P14.

In chapter 5, we aim to test the effect of 5-HT in adult S1BF cortical activity and its subsequent consequences for behaviour and learning. For this purpose, we use two-photon calcium imaging and localised S1BF optogenetics, in animals performing an air puff discrimination task with subsets of trials presenting misleading information. We expand this work to test the effects of 5-HT psychedelics in 5-HT dynamics, cortical activity and reversal learning.

In chapter 6, we aim to develop a biologically-grounded theoretical model to capture the different observations on cortical 5-HT obtained throughout this thesis. To this end, we employ gated deep neural networks with exact mathematical solutions and tasks comparable to our different datasets.

2 Monitoring cortical 5-HT dynamics throughout life

2.1 Introduction

How 5-HT fluctuates in the cortex of behaving mammals remains poorly understood. To date current studies are limited to high-pressure liquid chromatography combined with *in vivo* microdialysis (Collins et al., 2024; Lynne E. Rueter et al., 1997), which has limited temporal resolution, and electrophysiological studies of the DRN (Grossman et al., 2022; Paquelet et al., 2022; Ranade & Mainen, 2009), which provide an incomplete picture of 5-HT dynamics given the hodological diversity of the 5-HT system (Okaty et al., 2019) and confounding factors such as co-release of other neurotransmitters (e.g., GABA or Glu) (H. Li et al., 2024; Sengupta et al., 2017; H.-L. Wang et al., 2019). These studies suggest that the firing rate of 5-HT neurons correlates, among other things, with sleep-wake behavioural state (Kato et al., 2022), movement (Ranade & Mainen, 2009), reward (J. Y. Cohen et al., 2015; Ranade & Mainen, 2009), punishment (J. Y. Cohen et al., 2015), saliency (Paquelet et al., 2022), and uncertainty (Grossman et al., 2022). However, whether all these paradigms directly affect 5-HT release into adult cortical circuits remains untested.

The recent emergence of fluorescence 5-HT sensors like g5-HT1.0 and g5-HT3.0 - two recently developed GPCR-based 5-HT biosensors engineered from 5-HT_{2C} and 5-HT_{4} receptors respectively (Deng et al., 2024) - allows monitoring the dynamics of this neuromodulator *in vivo* with high temporal and spatial resolution (Deng et al., 2024; Kubitschke et al., 2022; Unger et al., 2020; Wan et al., 2021). However, the novelty of these sensors implies that they remain

untested in a number of settings, particularly *in vivo*. Current *in vivo* validations are limited to sleep-wake (Deng et al., 2024; Wan et al., 2021), movement (Kubitschke et al., 2022), MDMA-exposure (Wan et al., 2021) and epileptogenic activity (Deng et al., 2024), all of which trigger large changes in 5-HT dynamics. Thus, it is unclear whether these sensors will allow monitoring of 5-HT fluctuations in alive rodents during subtle changes in 5-HT supply. This gap highlights the need for studies validating these tools in a wide range of settings.

The dynamics of 5-HT in the developing cortex remain particularly elusive because of the experimental difficulty of performing DRN recordings in the developing brain. It is likely that 5-HT dynamics change across mammalian cortical development, given the transient developmental expression of genes involved in 5-HT dynamics and signalling, for example SERT and 5-HT_{1B} transient expression in thalamocortical projections to sensory cortices (Narboux-Nême et al., 2008; Verney et al., 2002). Given the clinical association between developmental disruption of 5-HT dynamics (e.g., embryonic SSRI exposure or SERT polymorphisms), and the emergence of neurodevelopmental disorders (Ames et al., 2021; Murphy & Lesch, 2008), understanding how 5-HT fluctuates in the developing brain is critical. SERT transient developmental expression in non-5-HT neurons is of particular interest given that it is the main target of SSRIs, the most commonly prescribed antidepressants (Luo et al., 2020). Two main hypotheses have been proposed for the role of this transient SERT expression: (1) that it buffers 5-HT from cortex in early development (Salichon et al., 2001) and (2) that it allows 5-HT release from non-5-HT-producing neurons (i.e., thalamus) (Lebrand et al., 1996). However, the difficulties of tracking 5-HT release with cellular resolution have hindered efforts of confirming either one of these hypotheses. The recent advent of surgical approaches to gain optical access to the developing brain (i.e., cranial windows in developing rodents) (Che & De Marco García, 2021), combined with fluorescence 5-HT biosensors (Deng et al., 2024; Kubitschke et al., 2022; Unger et al., 2020; Wan et al., 2021), has opened the door to monitor 5-HT dynamics in the early

postnatal cortex (from the end of 1st postnatal week) of awake head-fixed mice, allowing to answer these questions.

In this chapter, we have anatomically, pharmacologically and functionally validated the use of S1BF, and the fluorescence 5-HT sensor g5-HT3.0, to monitor 5-HT dynamics in awake head-fixed mice. Then, we have used these settings to characterise 5-HT dynamics in the S1BF of both adult and developing mice. Finally, we have tested the effects of pharmacologically (fluoxetine dosing) and genetically (SERT-KO) disrupting SERT on developmental cortical 5-HT fluctuations

2.2 Results

2.2.1 Anatomical validation of S1BF to study 5-HT cortical dynamics

We have anatomically validated S1BF as a model to explore 5-HT dynamics by confirming the presence of 5-HT axonal terminals in S1BF, while further exploring whether S1BF-projecting 5-HT neurons co-project to other cortical regions (Okaty et al., 2019). For this purpose, we have used multicolor retrograde tracing with cholera toxin subunit B (CTB) conjugated with diverse fluorophores (i.e., 488, and 647 nm) and dorsal raphe nuclei (DRN) immunohistochemistry with the 5-HT-neuron marker tryptophan hydroxylase 2 (tph2+) (**Figure 1a-c**). Namely, CTB647 was injected in S1BF (n=12 mice), while CTB488 was injected in a number of other cortical structures: prefrontal (PFC, n=4 mice), secondary somatosensory (S2, n=4 mice), endopiriform (EP, n=2 mice) and entorhinal cortex (EC, n=2 mice) (**Figure 1a,b & Supplementary figure 1**). Thus, the presence of CTB647+/tph2+ cells in DRN allowed us to establish the presence of

5-HTergic terminals in S1BF, while the presence of tph2+/CTB647+/CTB488+ allowed us to confirm the existence of 5-HT neurons co-projecting to another cortical region (e.g., S2 or PFC).

We observed consistent co-labelling with CTB647 of tph2+ (i.e., 5-HTergic) neurons distributed along the medio-lateral and dorso-ventral axis of DRN (**Figure 1d**), confirming the presence of 5-HT terminals in S1BF. Moreover, out of 95 S1BF-projecting 5-HT (CTB647+/Tph2+) cells labelled, only two showed co-projections to another area (i.e., CTB488+) and both were S2-projecting (**Figure 1e**). No PFC- and S1BF- co-projecting cells were found (**Figure 1f**). We cannot rule out the limited spread of CTB across these cortical areas (**Figure 1b & Supplementary figure 1**) providing an incomplete labelling of 5-HT subpopulations projecting to them. Nevertheless, these results suggest that 5-HT neurons in DRN have dedicated output streams to the somatosensory cortex, at least with respect to other major targets of the DRN (**Figure 1g**).

Altogether, while these results validate the use of S1BF as a model to study 5-HT dynamics they also highlight the possibility that these dynamics might differ in other cortical areas if diverse subpopulations of 5-HT neurons supply different cortical areas.

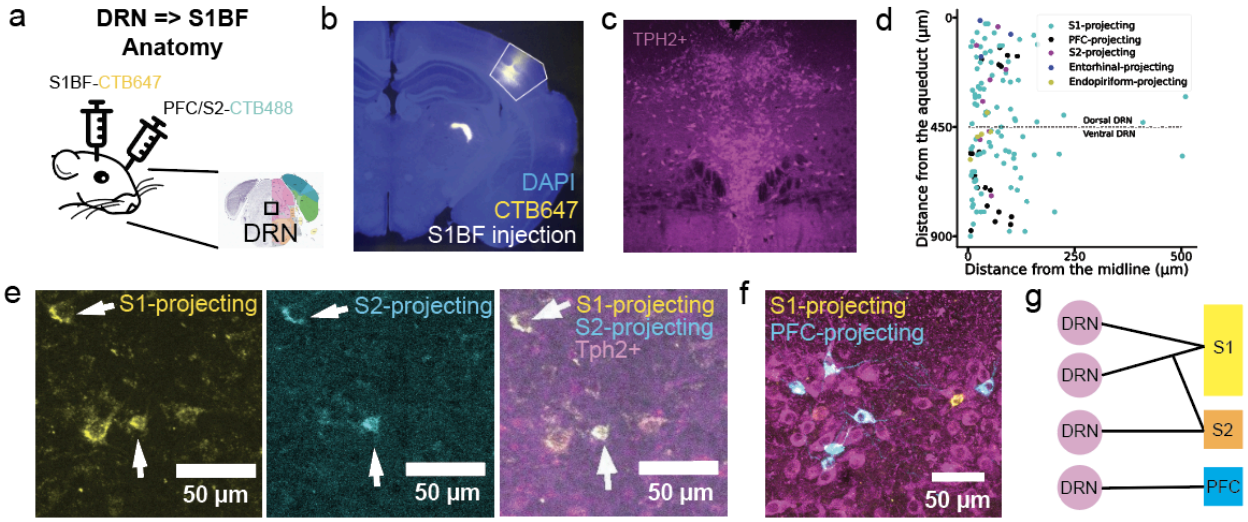

Figure 1. Anatomical characterization of S1BF-projecting 5-HT (tph2+) neurons with CTB retrograde tracing. a Diagram of dual colour retrograde tracing strategy with CTB647 intraparenchymal injection into S1BF (n = 12) and CTB488 in other cortical regions including S2 (n = 4), PFC (n = 4), EC (n = 2) and EP (n = 2). **b** Representative histological image acquired with an epifluorescence microscope showing S1BF injection site with CTB647 and VPM retrograde tracing which validates the tracing strategy (50µm slice). **c** 50µm DRN slice stained with the 5-HT marker tph2 using immunohistochemistry. Histological image acquired with a confocal microscope. **d** Dorso-ventral and medio-lateral positioning scatter plot of tph2+ retrogradely labelled cells coloured by projection target: S1 (n = 95 cells), PFC (n = 20 cells), S2 (n = 8 cells), EC (n = 3 cells) and EP (n = 5 cells). **e** Image of 2 only cells found to co-project to S1 (left) and S2 (middle), showing tracer co-localization (right). **f** Representative image showing distinct subpopulations projecting to either S1 or PFC. **g** Schematic representation of the hodological diversity of 5-HT neurons suggested by the retrograde tracing results. Sample sizes (number of animals): S1BF (n = 12), PFC (n = 4), S2 (n = 4), EC (n = 2) and EP (n = 2).

2.2.2 *In vivo* validation of 5-HT release in S1BF

While the above data suggested the presence of 5-HT terminals in S1BF (**Figure 1**), we decided to further validate the presence of 5-HT release in this cortical area. For this purpose, we used a small (n=3) subset of animals injected with the fluorescent green 5-HT sensor g5-HT1.0 - previous version of the g5-HT3.0 5-HT biosensor - in S1BF and intraperitoneal injection of 3,4-methylenedioxymethamphetamine (MDMA, 10 mg/kg of body weight). MDMA has been well established to induce increases in extracellular 5-HT in the central nervous system (Wan et al., 2021). We observed increases triggered by saline control injection that might be due to behavioural state changes triggered by the intraperitoneal injection (**Figure 2a,b)**. Nevertheless, intraperitoneal injection of MDMA led to longer-lasting g-5HT1.0 fluorescence increases in S1BF, indicating an increase in extracellular 5-HT (**Figure 2a,b**). This confirmed that S1BF not only has 5-HTergic terminals, but they also allow 5-HT release, thus supporting S1BF as a model to study 5-HT dynamics in cortex.

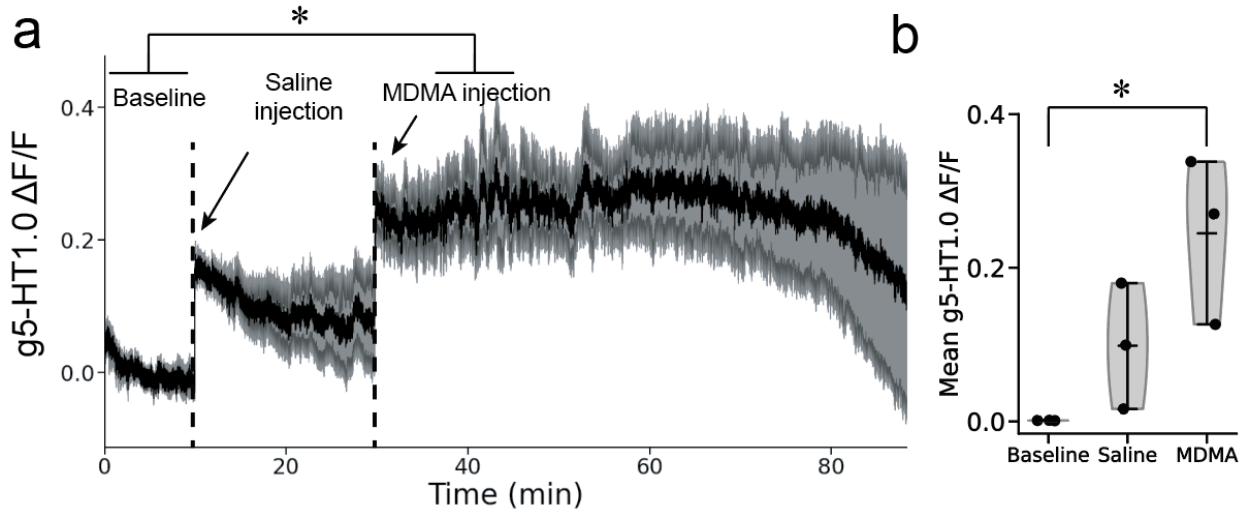

Figure 2. MDMA triggers increases in S1BF 5-HT. a Average *in vivo* g5-HT1.0 fluorescence of three WT animals during baseline (10 min), after intraperitoneal injection of saline (20 min) and after intraperitoneal injection of MDMA (10 mg/kg of body weight, 1h). ΔF/F g5-HT1.0 trace was calculated as the green sensor fluorescence signal at any time point subtracted and divided by the mean biosensor signal during the 10 min baseline. **b** Violin plot of average signal during 10 minute baseline or 20 minute after intraperitoneal injection of either saline control or MDMA. Sample size n = 3. One-way ANOVA p-value = 0.024. Posthoc Tukey test: baseline-saline p = 0.346; saline-MDMA p = 0.134 and baseline-MDMA p = 0.021.

2.2.3 Optimising *in vivo* 5-HT imaging in adult S1BF

While the use of the 5-HT sensors g5-HT1.0/3.0 has been validated to study *ex vivo* dynamics of 5-HT (Deng et al., 2024; Kubitschke et al., 2022; Unger et al., 2020; Wan et al., 2021), *in vivo* applications so far have been limited to contexts inducing large changes in 5-HT concentration (e.g., MDMA exposure, sleep-wake cycle and epilepsy) (Deng et al., 2024; Kubitschke et al., 2022; Unger et al., 2020; Wan et al., 2021). Therefore, these sensors remain untested in *in vivo* settings in which the changes in 5-HT concentrations might be smaller (e.g., sensation and complex behaviour). Here (Ocana-Santero et al., 2024), we address this gap in the field by using two-photon microscopy combined with g5-HT biosensors (Deng et al., 2024; Wan et al., 2021) to test the applicability of specific 5-HT biosensors *in vivo* within the context of a relatively simple but still unresolved question: are sensory responses in mammalian neocortex

accompanied by changes in 5-HT dynamics? The latter would be predicted since previous studies show changes in the firing of midbrain 5-HT neurons during the delivery of specific sensory stimuli (Ranade & Mainen, 2009)**.**

To test this hypothesis, we injected into the S1BF viral vectors genetically encoding g5-HT1.0 or g5-HT3.0 (**Figure 3a,b**). Mice were then imaged during periods of whisker stimulation using two-photon microscopy under awake, head-fixed conditions. Our experimental paradigm was well-suited to the study of possible contamination of the biosensor signal by intrinsic optical noise because whisker stimulation triggers strong neuronal activity accompanied by a robust intrinsic optical signal (Vasquez et al., 2023). As a control, other mice were injected with genetically encoded green fluorescent protein (GFP) which has no reported biosensor capability (**Figure 3c,d**).

2.2.3.1 Hemodynamic optical noise masks 5-HT signals in S1BF

We found that whisker stimulation triggered a pronounced, short-latency decrease followed by a delayed but marked increase in the fluorescence signal in g5-HT-expressing S1BF (**Figure 3b**). However, the dynamics of this fast decrease in fluorescence (1.1 ± 0.1 s poststimulus; n = 8 mice) were incompatible with the temporal resolution of the two 5-HT sensors tested (TauOFF g5-HT1.0 = 2.8 s (Wan et al., 2021); TauOFF g5-HT3.0 = 1.7 s (Deng et al., 2024)). Indeed, repeating the experiment in animals injected with GFP expressing viral vectors (**Figure 3c**) showed a similar decrease in fluorescence (peak decrease at 1.05 ± 0.2 s poststimulus, n = 3 mice) after whisker stimulation (**Figure 3d**), suggesting that the fast drop in fluorescence is not related to changes in 5-HT dynamics. Similar sensory responses have been observed in the primary visual cortex using widefield calcium imaging and have been associated with hemodynamic noise (Valley et al., 2020). Moreover, this finding aligns with prior literature

indicating that reduced light reflectance links to increased neuronal activity (L. B. Cohen et al., 1968; Grinvald et al., 1982; Hill & Keynes, 1949; Lipton, 1973; Salzberg et al., 1985; Tasaki et al., 1968).

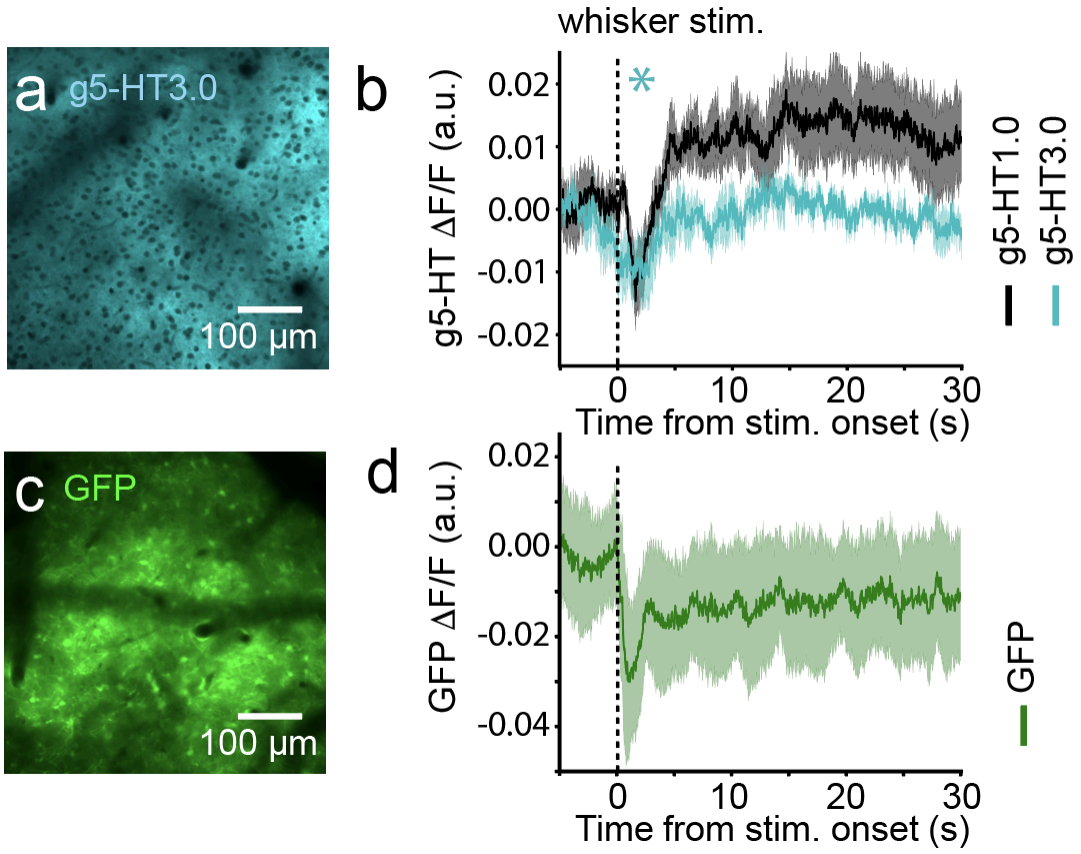

Figure 3. Effect of intrinsic optical signals on *in vivo* multiphoton imaging of 5-HT biosensor dynamics in the mouse S1BF. a,c Expression of (**a**) g5-HT3.0 and (**c**) GFP in S1BF delivered by intraparenchymal injection using a viral vector (AAV) under the human synapsin promoter. Images obtained using *in vivo* head-fixed two-photon imaging. **b,d** Peri-stimulus whole-field of view traces showing changes in (**b**) g5-HT1.0 (black trace, peak decrease at 1.2 ± 0.1 s poststimulus, n = 5) or g5-HT3.0 (cyan, peak decrease at 1.1 ± 0.4 s poststimulus, n = 3) and (**d**) GFP (green, peak decrease at 1.05 ± 0.2 s poststimulus, n = 3) in response to whisker stimulation (averaged across 10 stimulations); lines and shaded areas represent mean ± SEM values. ΔF/F traces were calculated as the green fluorescence at any time point subtracted and divided by the mean signal across the whole recording. Mean signal 5s pre-stim was then subtracted to normalize sensory responses. "n" indicates the number of mice in each group. * ($p < 0.05$): mean signal 1 s poststimulus is significantly decreased compared to 1 s prestimulus (Shapiro test, statistic = 0.99, p = 0.82; paired t test, statistic = 5.82, p = 0.02).

2.2.3.2 Spatial complexity of hemodynamic noise

To explore the spatial complexity of the source of intrinsic optical noise within the somatosensory cortex, we quantified changes in fluorescence at a higher spatial resolution (S1BF field of view divided into 256 subregions; **Figure 4a**). This revealed variability in g5-HT3.0 responses to whisker stimulation across the field of view, indicative of the local changes in signal. Thus, a combination of transient increases and decreases in signal, as well as no change, was observed (**Figure 4c**). There appeared to be no meaningful spatial distribution to these signals across the imaging field of view with increases and decreases in the signal often observed in adjacent subregions. Similar response variability was observed in control GFP-expressing mice, with subregions that present increasing, decreasing, or unaltered fluorescence signals upon whisker stimulation (**Figure 4b,d**). This suggests that changes in the intrinsic optical signal might underlie the changes in the g5-HT biosensor signal. Thus, artefactual changes in the 5-HT biosensor signal suspected on the basis of their fast signal dynamics were confirmed by the observation of similar changes in 5-HT biosensor and GFP signals at high spatial resolution, which highlights the complexity of this optical source of noise.

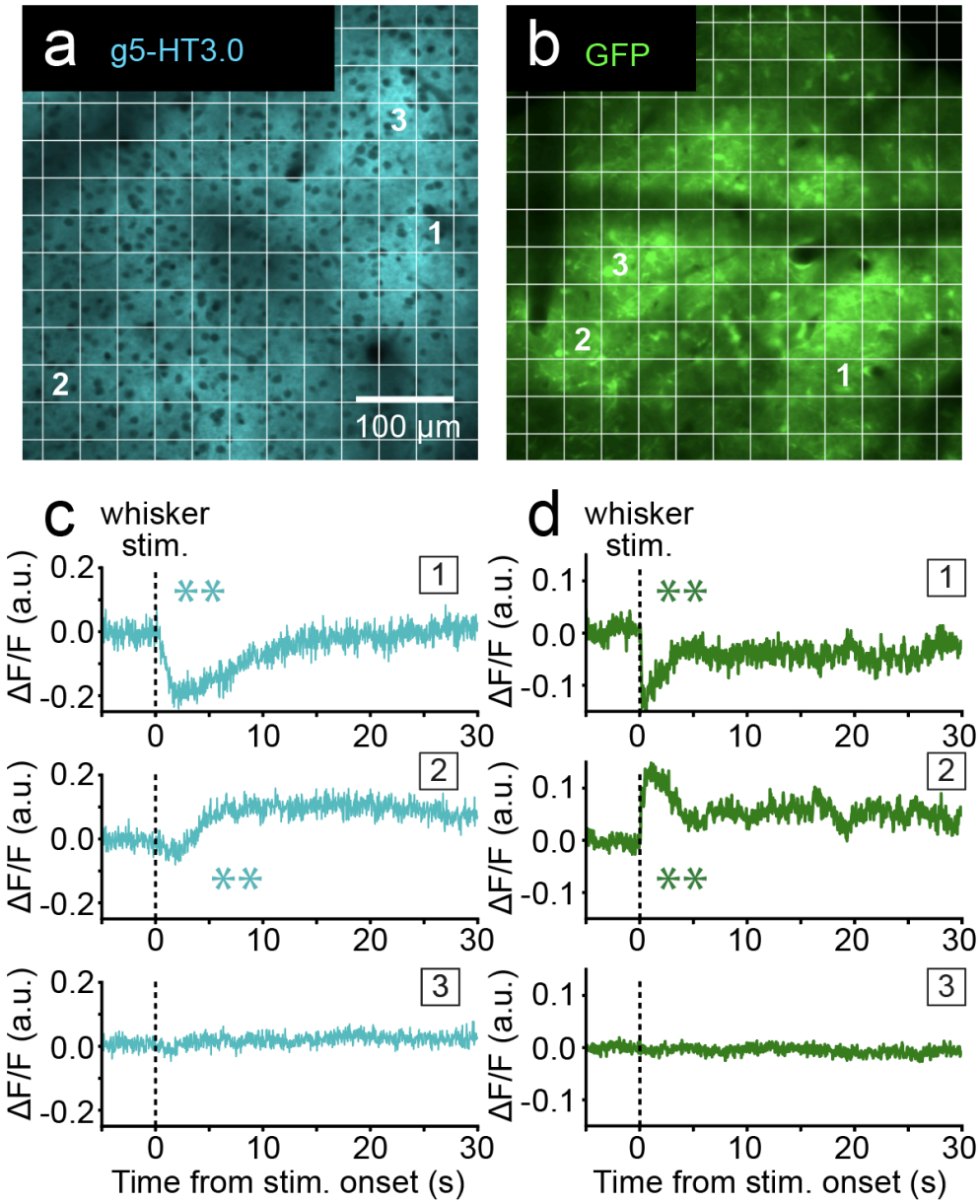

Figure 4. Whisker stimulus-evoked changes in intrinsic optical signals (GFP) and 5-HT biosensor signals show similar spatial variability. a g5-HT3.0 biosensor signal and **b** GFP fluorescence in field of view subregions of the S1BF, delivered by intraparenchymal injection of an AAV genetically encoding for either g5-HT1.0 (a) or GFP (b). Images obtained using *in vivo* head-fixed two-photon imaging. Acquisition of the data was performed simultaneously and region separation was conducted during analysis by subdividing the field of view in 256 square regions (with 32x32 pixels each). The mean fluorescence signal of each region was calculated. **c,d** Examples of peri-stimulus traces showing a diversity of whisker stimulus-evoked changes in (**c**) g5-HT3.0 or (**d**) GFP in different subregions of S1BF from a single animal in each group imaged simultaneously. The numbers (1–3) match the traces to the corresponding subregions of

the field of view. Same overall fields of view as shown in Figure 1. ΔF/F traces were calculated as the green fluorescence at any time point subtracted and divided by the mean signal across the whole recording. Mean signal 5s pre-stim was then subtracted to normalize sensory responses.**Paired t test, $p < 0.01$ (g5-HT3.0, subregion 1, $p = 0.002$; subregion 2, $p = 0.008$//GFP, subregion 1, $p = 6.20 \times 10–5$; subregion 2, $p = 0.0001$).

2.2.3.3 TdTomato provides a ratiometric control of hemodynamic noise revealing sensory-evoked 5-HT release in S1BF

To prevent the intrinsic optical signal obscuring changes in the 5-HT biosensor signal, we implemented a single-laser dual-fluorophore approach. Imaging of the 5-HT biosensor fluorophore simultaneously with a control fluorophore allowed subtraction of the intrinsic optical signal to reveal the 5-HT-specific signal. With a single laser the two fluorophores must have overlapping two-photon excitation spectra (**Figure 5a, top**) but distinguishable emission peaks that could be captured through separate recording channels (**Figure 5a, bottom**). Thus, we combined EGFP (the fluorescent protein of the 5-HT biosensor) and tdTomato, a red fluorophore that has previously been used to provide a readout of intrinsic optical signals (W.-T. Zhang et al., 2022) (**Figure 5a**). To this end, we virally delivered g5-HT3.0 to the S1BF of transgenic mice expressing tdTomato in either vasointestinal peptide (VIP) or Nkx2-1 positive GABAergic interneurons, the latter accounting for approximately 10% of the neurons in the field of view (**Figure 5c,d**). Indeed, both transgenic mice lines allowed targeting of populations present within our field of view, partially overlapping with the expression of the GRAB biosensor (under the control of the pan-neuronal hsyn promoter) and with widespread neuropil labelling thanks to the dense innervation exerted by these interneurons, which makes them ideal transgenics for the targeting of our control fluorophore.

Since we were expecting to record relatively small changes in fluorescence (Deng et al., 2024) (**Figure 5b,b′**), we utilised a smaller field of view, which at equal frame rate increased the dwell time per micron of tissue, thus increasing the signal-to-noise ratio. The dual-colour recordings revealed a whisker-evoked drop in signal in the red fluorophore (**Figure 5b**) as previously observed with a GFP signal (**Figure 3g**), confirming its utility as a control. By calculating the ratio of the green to red signal, it was possible to correct for the putative hemodynamic response and reveal a whisker-evoked increase in g5-HT3.0 signal (**Figure 5c′,d′**). These results are consistent with a human PET study showing increases in occipital cortex 5-HT release upon the presentation of visual stimuli (Hansen et al., 2020) and suggest that 5-HT may be involved in sensory processing (Marquez & Chacron, 2020). We measured comparable 5-HT responses in both VIP and Nkx2-1 transgenic mice (**Figure 5c′,d′**), suggesting that both serve as an appropriate control.

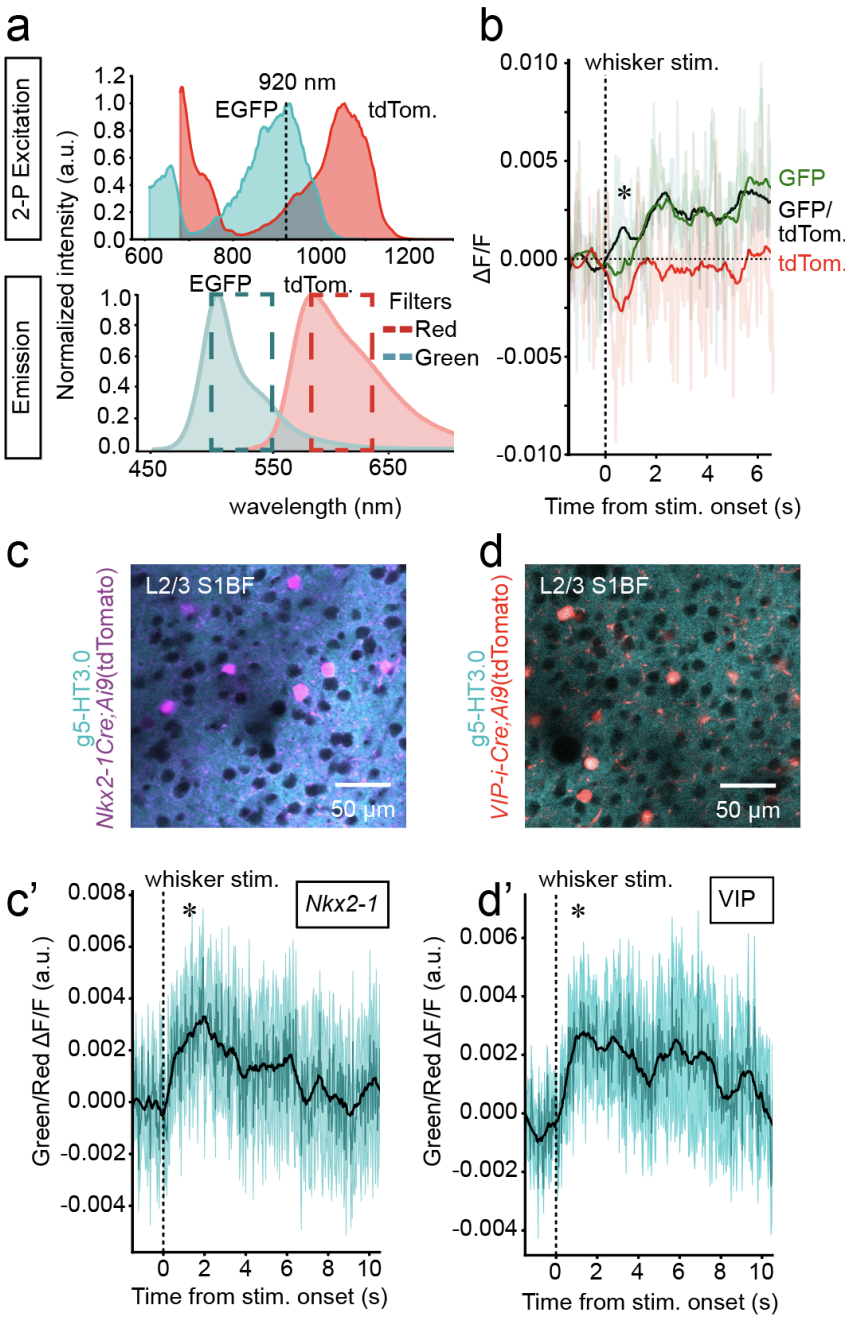

Figure 5. Evidence that dual-fluorophore imaging of g5-HT3.0 and a control red-fluorophore allows real-time hemodynamic correction when isosbestic correction is not possible. a Two-photon excitation (top) and emission (bottom) spectra of EGFP and tdTomato. A two-photon imaging wavelength of ~920 nm stimulates both fluorophores, while their emission peaks are sufficiently separate to allow recording via different channels (e.g., green and red) without major cross-contamination. The cyan and red dashed line boxes indicate the cutoff wavelengths for the green and red emission filters, respectively (green, 525 ± 25 nm; red, 595 ± 25 nm), which allow separation of EGFP and tdTomato signals in different recording

channels. Spectra plots made from data downloaded from the FPbase data set (Lambert, 2019). **b** Peri-stimulus traces showing a whisker stimulus-evoked drop in red tdTomato signal, a smaller drop in green g5-HT3.0 signal, and an increase in the ratiometrically corrected signal (black). * ($p < 0.05$): mean signal 1 s poststimulus is significantly increased compared to 1 s prestimulus for the black trace (Shapiro test, statistic = 0.91, p = 0.28; paired t test, statistic = 3.03, p = 0.01). Traces are the average response to 10 stimuli presentations recorded from a single representative animal. ΔF/F green and red traces were calculated as the green and red fluorescence, respectively, at any time point subtracted and divided by the mean signal across the whole recording. The black trace represents the ratio between the green and red fluorescence, subsequently normalized in the same ΔF/F manner. Mean signal 2s pre-stim was then subtracted to normalize sensory responses. Data obtained *in vivo* using two-photon head-fixed imaging of transgenic mice expressing tdTomato in either Nkx2-1 or VIP interneurons (Nkx2-1/VIP-Cre x Ai9) that were injected with an AAV vector genetically encoding the fluorescence sensor g5-HT3.0. **c** Field of view with g5-HT3.0 and tdTomato in Nkx2-1 positive neurons (top) and (**c′**) peri-stimulus traces (bottom, n = 4). **d** Field of view with g5-HT3.0 and VIP positive neurons (top) and (**d′**) peri-stimulus traces (bottom, n = 3). Peri-stimulus traces are the average of 10 stimulus presentations for four Nkx2-1+ and three VIP+ animals ΔF/F is the ratio between the green and red fluorescence signal an any time point, subtracted and divided by the mean ratio across the whole recording. Mean signal 2s pre-stim was then subtracted to normalize sensory responses. Shaded area represents the standard error of the mean, and the black trace represents the Savitzky–Golay filtered signal. “n” indicates the number of mice in each group. * ($p < 0.05$): mean signal 1 s poststimulus is significantly increased compared to 1 s prestimulus (Nkx2-1, Shapiro test, statistic = 0.96, p = 0.80; paired t test, statistic = 3.23, p = 0.048//VIP, Shapiro test, statistic = 0.85, p = 0.24; paired t test, statistic = 4.64, p = 0.043).

In conclusion, we recorded an increase in 5-HT biosensor dynamics in mouse somatosensory cortex in response to whisker stimulation using an approach that allows segregation of 5-HT signalling dynamics from confounding intrinsic optical signals. This was achieved using expression of a control fluorophore (tdTomato) in a subset of cortical neurons, which allows us to account for this source of noise across the field of view. These results validate the use of fluorescent biosensors to measure 5-HT dynamics *in vivo* with multiphoton imaging, when using appropriate controls. Moreover, this validation opens the door to studying 5-HT dynamics with unprecedented spatial resolution, at both the population and cellular level.

2.2.4 5-HT dynamics in the adult cortex during complex behaviour

Once the use of this sensor was validated in *in vivo* settings, we then monitored more complex 5-HT dynamics in the adult S1BF cortex (**Figure 6a**) guided by previous studies performing electrophysiological recordings of 5-HT neurons directly in the DRN (J. Y. Cohen et al., 2015; Grossman et al., 2022; Paquelet et al., 2022; Ranade & Mainen, 2009). For example, a recent study suggested that 5-HT neurons fire preferentially upon salient stimuli (Paquelet et al., 2022). To test whether more salient stimuli triggered bigger increases in 5-HT release, we used air puff whisker-deflection, in which stimulus saliency can be quantitatively controlled by varying the pressure of the air puff. We observed a linear increase in the area under the curve (AUC) of the fluorescence g5-HT3.0 response with increasing air puff pressure (**Figure 6b-c**).

5-HT neurons have also been shown to increase their firing rate upon reward (J. Y. Cohen et al., 2015). To test whether reward also led to release of 5-HT in S1BF, we monitored g5-HT3.0 in S1BF of water deprived animals in the initial phases of learning an association between an air puff (10psi) and a reward (water). Indeed, we observed a longer lasting increase in 5-HT when the stimulus was paired to reward (**Figure 6d**) indicating a reward-response of 5-HT release in S1BF.

Finally, previous studies have reported that 5-HT neurons in the DRN increase their firing rate upon novel and unexpected events (Grossman et al., 2022; Tapper & Molas, 2020). To test whether novelty triggered 5-HT release in S1BF, we compare reward responses to the first 5 versus the last 5 rewarded trials. We observed bigger responses to the first 5 trials, suggesting an encoding of novelty (**Figure 6e**). Thus, in line with previous electrophysiological studies of 5-HT neurons in the raphe nuclei, we confirmed that S1BF 5-HT dynamics reflect sensation, saliency, reward and novelty.

This is of particular interest in light of studies showing VIP interneuron responses to reward (Szadai et al., 2022), novelty (Tamboli et al., 2024) and behavioural state (Fu et al., 2014), suggesting that 5-HT release might mediate these responses. These cortical interneurons are characterised by their expression of the ionotropic depolarizing receptor 5-HT_{3A}R (S. Lee et al., 2010), their depolarization by 5-HT (Férézou et al., 2002), their localization in upper layers (Prönneke et al., 2015), and their role in mediating top-down modulation of activity in sensory cortices (Bastos et al., 2023; Fu et al., 2014; S. Lee et al., 2013). Thus, leveraging the spatial resolution of two-photon imaging, we further characterised the variability of 5-HT responses in S1BF upon a salient (100 PSI) air puff, by subdividing our field of view in 256 regions, in transgenic animals with tdTomato in VIP interneurons (**Figure 6f**). We observed a high degree of variability, with regions increasing, decreasing or not changing 5-HT release upon stimulus onset (**Figure 6f**). When we assessed the release in areas with VIP interneurons, we observed particularly high increases in 5-HT release into these interneurons (**Figure 6g**). These results suggest that the 5-HT system can perform 5-HT spatially localised release as a function of the postsynaptic targets with cellular resolution. Moreover, in light of the well-established role of these interneurons in mediating top-down regulation of cortical circuits (Bastos et al., 2023; Fu et al., 2014; S. Lee et al., 2013), these results suggest that 5-HT might potentiate top-down signalling.

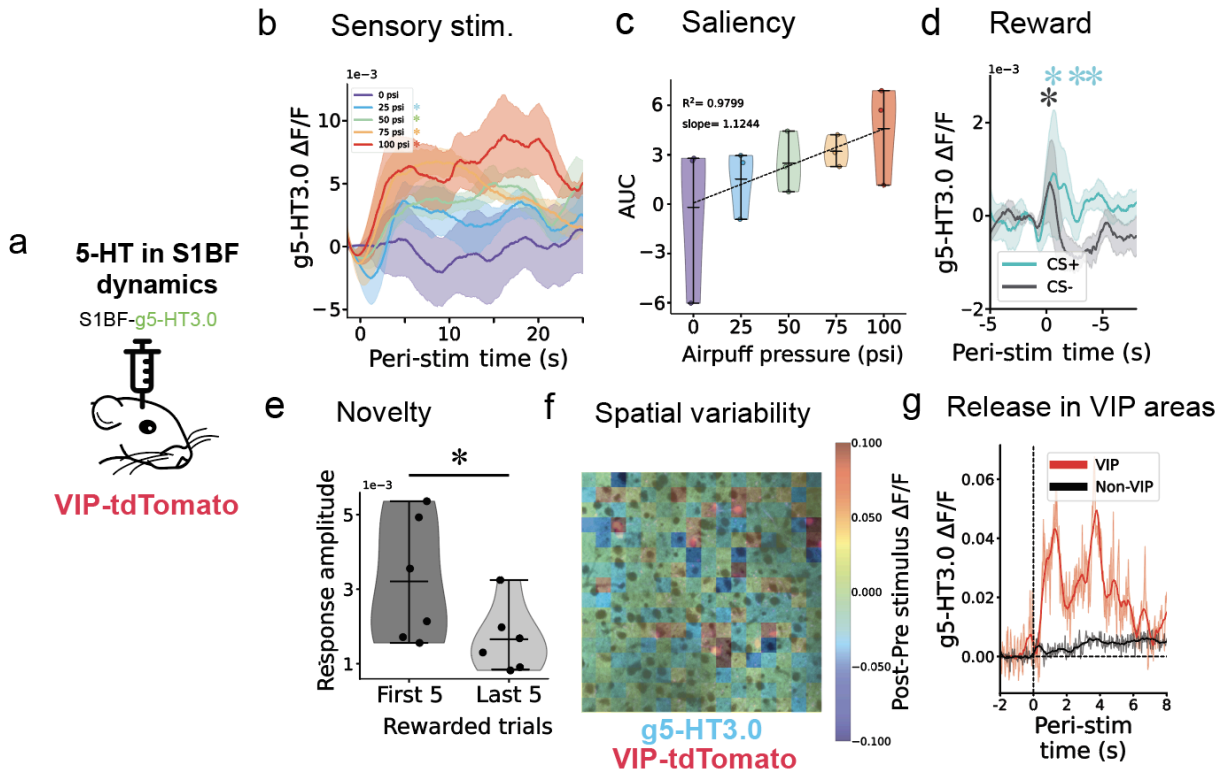

Figure 6. 5-HT dynamics in the adult cortex during salient sensation, reward and novelty. **a** Diagram of experimental settings, illustrating S1BF delivery of the sensor g5-HT3.0 to monitor 5-HT dynamics in adult mice (>8 weeks old) using in vivo head-fixed awake two-photon imaging. The sensor was delivered by intraparenchymal injection of an AAV vector genetically encoding the fluorescence sensor. Transgenic animals expressing tdTomato in VIP interneurons were used (VIP-Cre x Ai9). **b** Peri-stimulus average trace across 5 repeats of air puff whisker-deflection with varying pressure (0, 25, 50, 75 and 100 PSI) (n = 3). All stimuli, except for 0 PSI, showed increased g5-HT3.0 signal post- versus pre-stimulus (paired t-test $p < 0.05$). **c** Area under the curve of the 20s post-stimulus g-5HT3.0 trace for each air puff pressure, illustrating linear scaling of 5-HT response to air puff pressure as a proxy of stimulus saliency (n = 3) ($R2 = 0.9799$, slope = 1.1244). **d** Peri-stimulus trace in air puff stimulation (10 PSI) paired (CS+) or not (CS-) to water delivery in water-deprived mice learning an association to the stimulus, while mice licked in response to both stimuli (signal post- vs pre-stim paired t-test *p<0.05 for 1s in CS- and 3s in CS+, n = 6). **e** g-5HT3.0 fluctuations in response to reward-paired stimulus (air puff, 10 PSI) during the first/last 5 trials in mice learning a Pavlovian association between stimulus and reward, showing bigger release upon the former (paired t-test $p = 0.0254$, n = 6). **f** 256 regions grid heat-map of post-pre air puff onset (100 PSI) mean g5-HT3.0 signal average across 10 repeats in a single representative animal, overlaid on top of field of view with cyan g5-HT3.0 and red tdTomato VIP interneurons. **g** Mean peri-stimulus onset trace of VIP+ or VIP- regions in response to an air puff (100 PSI). For all panels ΔF/F is the ratio between the green and red fluorescence signal at any time point, subtracted and divided by the mean ratio across the whole recording. Mean signal 2s pre-stim was then subtracted to normalize sensory responses.

2.2.5 5-HT dynamics in the developing cortex

Given the validity of g.5-HT3.0 to monitor *in vivo* 5-HT dynamics in the adult S1BF and the developmental role of 5-HT (Daly et al., 2019), we proceeded to study how these dynamics differ in early development. We injected the fluorescence 5-HT sensor g5-HT3.0 into S1BF of neonatal mice to monitor 5-HT signalling dynamics both during the early period of transient thalamic SERT expression (Th-SERT; up to P10 (X. Chen et al., 2016; Narboux-Nême et al., 2008)) and subsequent adult pattern of raphe afferent-restricted SERT expression (adult-SERT) (**Figure 7a and Supplementary figure 2a,b**). During the Th-SERT period, multi-whisker deflection or presentation of a sound did not elicit a detectable 5-HT response while an aversive stimulus, an air puff directed to the face (J. Y. Cohen et al., 2015), resulted in a time-locked increase in 5-HT signal (**Figure 7b**). In the immediate time period of adult-like SERT expression (adult SERT; P11 to P13), 5-HT responses were observed to all stimuli albeit still larger following the aversive air puff (**Figure 7c**), a pattern that continued through juvenile life (**Supplementary figure 2c**).

Then, we studied the spatial variability of responses in both developmental periods (Th-SERT and Adult-SERT). For this, we subdivided our field of view in 256 regions, in transgenic animals with tdTomato in VIP interneurons. Analysis at the cellular level revealed a change in the spatial distribution of 5-HT signalling to the aversive air puff from a global response during the Th-SERT (**Figure 7d**) to more localised signalling in adult SERT (**Figure 7e**), a pattern consistent with developmental changes in 5-HT innervation of S1BF over this time (i.e., 5-HT axonal pruning in S1BF) (Maddaloni et al., 2017). It was evident that larger responses were present in regions with VIP interneurons (**Figure 7e**), indicative of targeted release of 5-HT at this later age, in line with our adult recordings (**Figure 6f-g**).

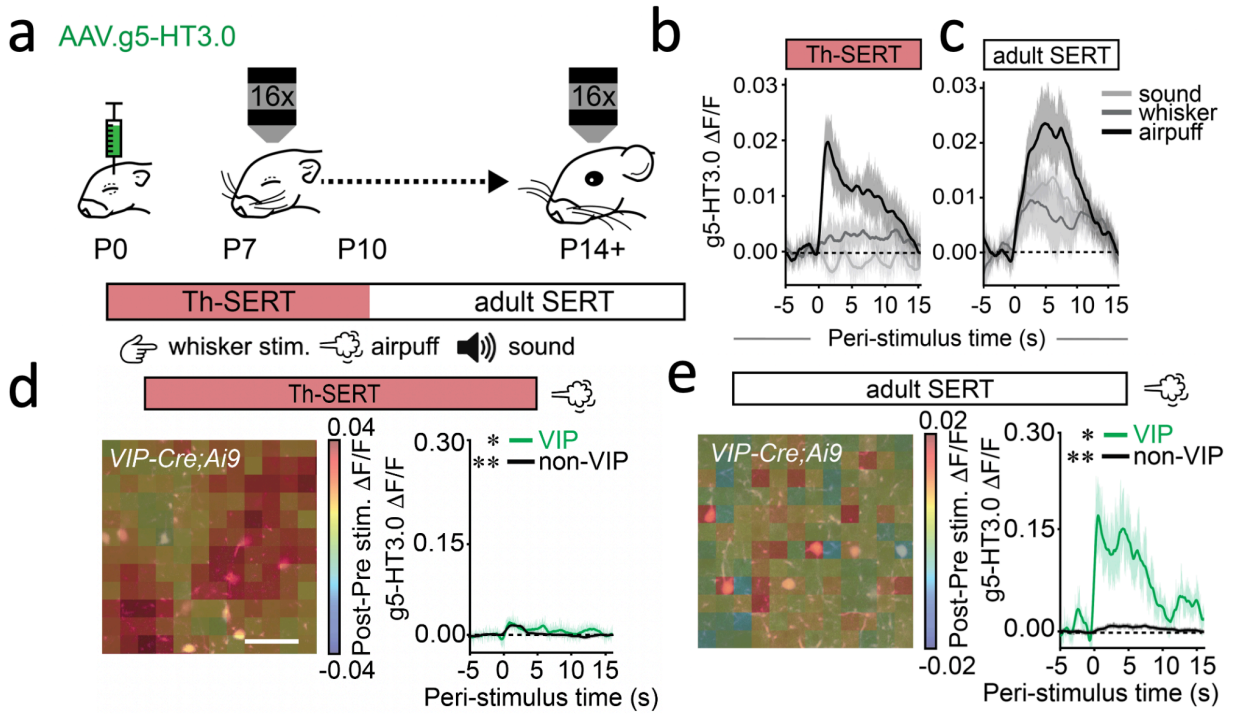

Figure 7. Postnatal 5-HT signalling fluctuates with adverse experience, but not sensory stimuli in early development. a VIP-tdTomato transgenic neonatal mice received an intraparenchymal injection of an AAV vector genetically encoding for the 5-HT sensor g5-HT3.0 in S1BF. Mice were then implanted with a cranial window at P6 and then imaged from P7 onwards, using two-photon awake head-fixed imaging, while recording their behaviour and performing auditory, whisker and air puff (80 PSI) stimulation. **b,c** 5-HT sensor g5-HT3.0 dynamics in response to air puff (**b,** 80 PSI, p = 0.031 **c,** p = 0.003), whisker (**b,** p = 0.189 **c,** p = 0.046) or auditory (**b,** p = 0.976 **c,** p = 0.010) stimulation show that only air puff triggers increases in signal at P7-P10 (**b**), while all stimuli trigger increases at P11-13 (**c**). **d,e, (left)** Average heatmaps from a single animal of g5-HT3.0 difference in signal after 10 air puff presentations compared to baseline, across 256 subregions overlaid on top of the field of view expressing tdTomato in Vip+ interneurons at P7-10 (**d**) or P11-13 (**e**). **d,e, (right)** Average response in subregions surrounding (**d,** p = 0.007 **e,** p = 0.043) or not (**d,** p < 0.001 **e,** p < 0.001) VIP+ interneurons at P7-10 (**d**) and P11-13 (**e**) all areas show increases on average. For all panels ΔF/F is the ratio between the green and red fluorescence signal at any time point, subtracted and divided by the mean ratio across the whole recording. Mean signal 2s pre-stim was then subtracted to normalize sensory responses.

2.2.6 SERT developmental regulation of 5-HT dynamics

Guided by previous studies (Salichon et al., 2001), we hypothesised that SERT transient overexpression (**Supplementary figure 2b**) in thalamocortical projections could be buffering 5-HT in the developing (<P10) cortex, thus being responsible for the lack of detectable 5-HT release in S1BF upon sensory stimulation. Therefore, we speculated that SERT disruption would lead to early detectable increases in 5-HT upon non-aversive sensory stimulation. To test this hypothesis, we first examined multi-whisker stimulation in SERT-KO mice. We observed an increased g5-HT3.0 signal in both heterozygous (SERT-Het) and knockout (SERT-KO) pups (**Figure 8a**).

To examine if this could be replicated with postnatal manipulation of SERT function, we dosed pups orally with the SSRI fluoxetine (10 mg/kg of body weight), or the vehicle sucrose, prior to imaging during the Th-SERT period (P7-10). Under these conditions, multi-whisker stimulation now resulted in a prolonged increase in 5-HT signal versus sucrose control (**Figure 8b**). Similarly, the aversive stimulus also triggered a longer-lasting response (**Figure 8c**) but no change was seen in response to auditory stimulus during this time window (**Figure 8d**). These results support the hypothesis that SERT actively clamps 5-HT release evoked by non-aversive modality-specific stimuli in postnatal S1BF. The lack of early auditory responses is likely explained by the delayed maturation of the auditory system (Martini et al., 2021), given that detectable responses were observed during the adult SERT period (**Figure 7c and Supplementary figure 2c**).

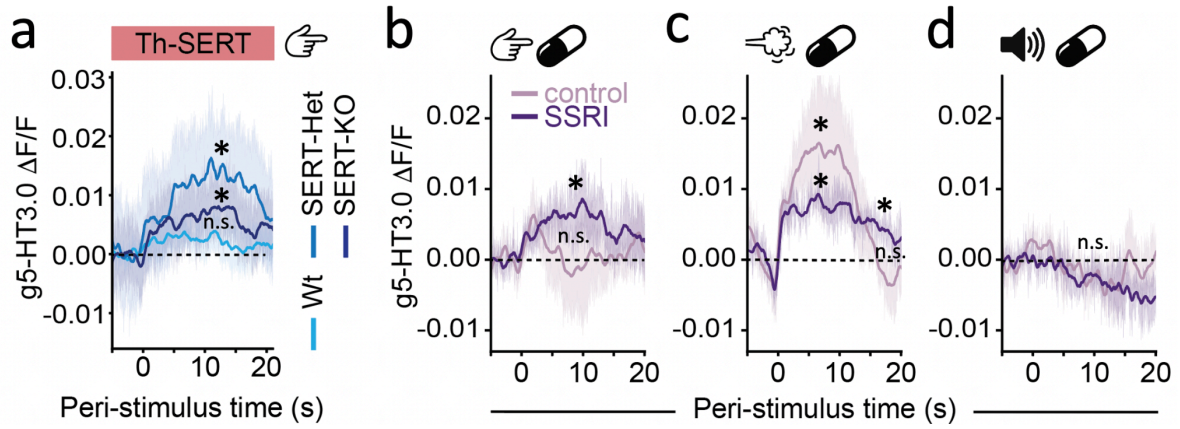

Figure 8. Transient SERT expression clamps 5-HT responses in early cortical development. Developmental two-photon head-fixed imaging of VIP-tdtomato transgenic mice injected neontally with an AAV vector genetically encoding g5-HT3.0 that were either SERT-WT/Het/KO or sucrose/fluoxetine-treated. **a** Peri-stimulus triggered average g5-HT3.0 signal in response to 10 whisker stimulations in WT ($p > 0.05$), SERT-Het ($p < 0.05$ for 14s post-stimulus) and SERT-KO mice ($p < 0.05$ for 15s post-stimulus). **b,c,d** Peri-stimulus triggered average g5-HT3.0 signal of sucrose- and SSRI-treated pups in response to 10 whisker (**b,** control: $p < 0.05$ for 1s; SSRI: $p < 0.05$ for 3s)**,** air puff (**c,** 80 PSI, control: $p < 0.05$ for 4s; SSRI: $p < 0.05$ for 20s) or auditory (**d,** not significant for both control and SSRI) stimuli.For all panels ΔF/F is the ratio between the green and red fluorescence signal at any time point, subtracted and divided by the mean ratio across the whole recording. Mean signal 5s pre-stim was then subtracted to normalize sensory responses.

2.2.7 5-HT developmental oscillations with behavioural state

Previous studies in adult rodents suggest that the firing rate of 5-HT neurons in the DRN oscillates during the sleep-wake cycle, with firing rates being maximal during wakefulness, decreasing during NREM and dropping during REM sleep (Kato et al., 2022). Recent work in adult mice has confirmed that extracellular 5-HT dynamics follow the same pattern (i.e., maximal during wakefulness and minimal during REM sleep) (Deng et al., 2024; Wan et al., 2021). Developing mammals present fast bouts of sleep-wake cycles in which REM sleep is a predominant behavioural state (Blumberg et al., 2022). Thus, we tested whether 5-HT oscillates with the sleep wake cycle early in development (P7-P10) in a similar manner to adults.

Based on previous work relating forelimb movement to particular sleep-wake states (Gómez et al., 2021), sleep was manually scored as a function of movement during infrared recordings (**Figure 9a, Supplementary figure 2d**): continuous movement, immobility and twitching were defined as wakefulness, quiet sleep (QS, developmental equivalent to adult NREM sleep) and active sleep (AS, developmental equivalent to adult REM sleep) respectively. Consistently with the adult literature (Deng et al., 2024; Kato et al., 2022; Wan et al., 2021), we observed the highest 5-HT levels during wakefulness (**Figure 9a-b**). No significant differences were observed in the 5-HT responses to whisker stimulation during different sleep states, albeit a trend to higher increases in quiet sleep stimulation suggested they might be awakening the pup (**Supplementary figure 2d-f**).

Finally, we tested whether these oscillations were also present in SSRI-treated mice and observed higher g5-HT3.0 signal in fluoxetine-treated mice during active sleep, (**Figure 9b left**). This suggests that SERT is important for the integrity of 5-HT fluctuations during the fast bouts of sleep-wake cycles that mice experience at this age. We also report a reduction in active sleep upon SSRI-treatment (**Figure 9b right**), consistent with a previous study showing that low 5-HT is necessary for active sleep (Kato et al., 2022), which suggests that SSRIs also disrupt sleep architecture. Taken together, these data identify tight state-dependent 5-HT neuromodulation in the postnatal mouse cortex.

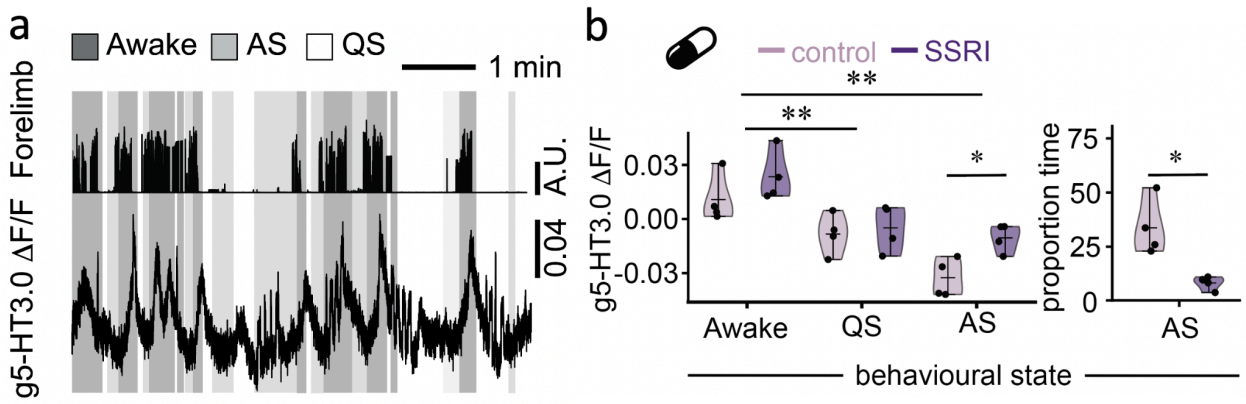

Figure 9. Behavioural state-dependent 5-HT oscillations. Developmental two-photon head-fixed imaging of VIP-tdtomato transgenic mice injected neontally with an AAV vector genetically encoding g5-HT3.0 that were either sucrose or fluoxetine-treated. **a** 5 minute representative time-locked trace of left forelimb movement and g5-HT3.0 S1BF signal during wakefulness (awake, dark grey), active sleep (AS, light grey) and quiet sleep (QS, white) from a single animal showing sleep-wake oscillations in signal. **b (left)** Mean g5-HT3.0 signal during wakefulness, quiet sleep and active sleep of animals treated with control sucrose or SSRIs (Shapiro-Wilk $p = 0.067$, Two-way ANOVA: sleep state $p < 0.001$, treatment condition $p = 0.017$, interaction state-treatment $p = 0.315$). ΔF/F is the ratio between the green and red fluorescence signal at any time point, subtracted and divided by the mean ratio across the whole recording. Sleep scoring was performed manually as a function of animal movement (i.e., continuous movement was defined as wakefulness, twitching as active sleep and immobility as quiet sleep). **b (right)** Proportion of time spent in active sleep for control and SSRI-treated mice (Shapiro-Wilk $p = 0.900$, t-test $p = 0.015$).

2.3 Conclusions

In this chapter, we have validated the use of S1BF as a model to study cortical 5-HT dynamics by reporting tph2+ cells in the DRN that project to S1BF, and by confirming 5-HT increases upon MDMA administration (**Figure 1,2**). We have also shown the potential of g5-HT3.0 to monitor 5-HT dynamics in sensory cortices of behaving mice throughout life, when the correct optical controls are in place (**Figure 3-5**). Namely, we propose the use of co-expressing fluorophores without biosensor capabilities, to use as a real-time ratiometric control for sources of optical noise. We particularly identify tdTomato as a fluorophore with an overlapping excitation spectrum with g5-HT3.0, allowing co-stimulation with the same laser, but separable emission

spectra which allows to monitor its dynamics in a different wavelength with low signal bleed-through (Ocana-Santero et al., 2024).

We report adult cortical 5-HT release during sensation (**Figure 5,6**) that scales with stimulus saliency, reward and novelty (**Figure 6**). Moreover, we report that beyond widespread 5-HT responses in S1BF, we also see cellular postsynaptic targeting, with 5-HT release being particularly high in cortical areas with VIP interneurons. This is of particular interest given that these interneurons express the excitatory ionotropic receptor 5-HT_{3A}R and are depolarized by 5-HT (Férézou et al., 2002). Therefore suggesting that the responses of VIP interneurons to reward (Szadai et al., 2022), novelty (Tamboli et al., 2024) and behavioural state (Piet et al., 2024) could be directly mediated by 5-HT signalling.

Then, we have shown that in early postnatal development (<P10), transient expression of SERT clamps these responses to sensory stimuli, but not aversive sensation or sleep-wake fluctuations (**Figure 7-9**). Genetic or pharmacological disruption of SERT can lead to early 5-HT increases in response to sensory stimuli (**Figure 8**). These results support the hypothesis that the role of the transient developmental expression of SERT is to buffer 5-HT from cortex in early ages (Salichon et al., 2001). However, given the retrograde transport of 5-HT to thalamic nuclei (Lebrand et al., 1996), with our results we cannot rule out the possibility that 5-HT is also being released by these non-5-HT-producing thalamic cells in other areas of the brain.

With intact SERT, sleep-wake oscillations were still observable (**Figure 7**), in a similar manner to the ones reported in the adult brain with the same g5-HT3.0 sensor, i.e., maximum signal during wakefulness, decrease in NREM sleep, and minimum signal during REM sleep (Deng et al., 2024; Wan et al., 2021). SSRI exposure also disrupted sleep-wake architecture by reducing REM-sleep, suggesting a causal role of 5-HT in shaping sleep-wake. This is consistent with a previous study in adult mice, showing that optogenetic activation of 5-HT neurons in the DRN during REM sleep induces wakefulness (Kato et al., 2022). REM-sleep disruption upon SSRI administration has also been observed in adult humans (Wilson & Argyropoulos, 2005). Given the crucial role of sleep in neurodevelopment (Blumberg et al., 2022), the observed sleep disturbances in SSRI postnatally-treated mice might be a contributing factor to their adult symptomatology (Cunha et al., 2021; Rebello et al., 2014).

Altogether, in this chapter we have characterised 5-HT dynamics in S1BF in the developing as well as the adult cortex, and identified SERT as a key regulator of 5-HT dynamics in the early postnatal neocortex.

3. Cortical population activity in SERT-KO mice

3.1 Introduction

SERT is thought to play a critical role in neurodevelopment, as evidenced by the large clinical literature associating polymorphisms in SERT with neurodevelopmental disorders (Brown et al., 2013; H.-J. Lee et al., 2005; Murphy & Lesch, 2008; Nicolini, 2010). The most studied polymorphism is a 44-base pair insertion/deletion in the gene promoter leading to a short and long allele (Lesch et al., 1996; Ramamoorthy et al., 1993). The short allele leads to reduced SERT transcription (Heinz et al., 2000; van Dyck et al., 2004) and has been associated with an increased risk for depression (Anguelova et al., 2003; Brown et al., 2013; Delli Colli et al., 2022; Ramamoorthy et al., 1993), eating disorders (Calati et al., 2011), PTSD (H.-J. Lee et al., 2005) and alcohol dependence (Feinn et al., 2005), while the long allele has been associated with increased risk of OCD (Nicolini, 2010; Tibrewal et al., 2010). These associations have also been suggested to interact with stressful events (Caspi et al., 2003; Chorbov et al., 2007; Delli Colli et al., 2022; Kendler et al., 2005; Murphy & Lesch, 2008). However, some studies have failed to replicate some of these findings (Border et al., 2019; Culverhouse et al., 2018). There is also a poor mechanistic understanding of how SERT polymorphisms could lead to these clinical associations.

Preclinical studies in rodents have tried to shed light on this mechanism using genetic models with either knockout (KO) (Kalueff et al., 2010) or overexpression (OE) of SERT (McHugh et al., 2015), the former being particularly well characterised. Behaviourally, adult SERT-KO rodents show anxiety-like behaviour (Tanaka et al., 2018), depression-related behaviours (Shoji et al.,

2023), altered nociception (Vogel et al., 2003), social deficits (Golebiowska et al., 2019; Kalueff et al., 2010), sleep disturbances (Wisor et al., 2003) and learning alterations (C. C.-G. Guo et al., 2021; Lima et al., 2019). This model has also been associated with neurodevelopmental alterations such as disruption in thalamocortical sensory map formation (Salichon et al., 2001), reduction in 5-HT neurons in the DRN (Lira et al., 2003), altered pyramidal neuron migration (Riccio et al., 2011), reduced feed-forward inhibition (Miceli et al., 2017), disrupted SST interneuron survival, as well as dendritogenesis (De Gregorio et al., 2020), and perturbed VIP interneuron migration (Frazer et al., 2015).

Of particular relevance to this thesis are studies characterising how 5-HT, and SERT transient expression in thalamocortical projections E15-P10, shape the development of cortical sensory circuits (Teissier et al., 2017). Sensory inputs, through glutamatergic transmission, play a key role in instructing barrel formation (Erzurumlu & Gaspar, 2012). In early development, 5-HT signalling modulates this process through presynaptic 5-HT_{1B} receptors, transiently expressed in thalamic neurons (Bennett-Clarke et al., 1993). Deleting the 5-HT_{1B}R gene rescues the lack of whisker barrels observed in the S1BF of monoamine oxidase A-KO and SERT-KO mice (Salichon et al., 2001). These results suggest that 5-HT inhibits excitatory thalamocortical synapses in the developing cortex, and SERT plays a key role in modulating this 5-HT signalling.

Despite this large literature characterising SERT-KO rodents, we have identified a major gap: understanding the effect of SERT disruption in emerging cortical population dynamics and the subsequent effect on adult sensory cortical encoding. This is of particular interest in light of our results showing that SERT regulates 5-HT dynamics in the early postnatal cortex, and that SERT-KO can lead to early increases in cortical 5-HT upon sensation (chapter 2). These observations were performed during a critical period for the activity-dependent maturation of

cortical microcircuitry (Teissier et al., 2017; Wong et al., 2018, 2022), during which previous studies suggest that 5-HT could be inhibiting thalamocortical projections (Bennett-Clarke et al., 1993; Salichon et al., 2001). Thus, we speculated that this increase in 5-HT triggered by SERT-KO would disrupt sensory-driven cortical activity in early development, subsequently impacting the activity-dependent maturation of cortical circuits. To test hypothesis, we used longitudinal two-photon calcium imaging of S1BF in SERT-KO mice with interneuron subpopulations (VIP and Nkx2-1) labelled with the red fluorophore tdTomato. This allowed us to characterise how SERT-KO shapes the emerging excitatory and inhibitory cortical dynamics.

3.2 Results

3.2.1 SERT-KO cortical dynamics manifest early cortical hypoactivity

To understand the impact of genetically disrupting SERT function on developing cortical activity, we performed *in vivo* two-photon imaging of GCaMP6s in S1BF through postnatal development in pups generated by breeding SERT-Het parents (**Figure 10a**). During the early postnatal time period, cortical activity is characterised by the presence of high- (H-) and low- (L-) synchronicity calcium events (**Figure 10a-c**) (Leighton et al., 2021; Siegel et al., 2012). L-events recruit between 20 to 80% of cells within the field of view, while H-events recruit more than 80% cells (general introduction, section 1.2.1). Analysis of these events in SERT-KO mice revealed a decrease in the amplitude (**Figure 10e**) and duration (**Figure 10f**), but an increased occurrence (**Figure 10d**) of H-events compared to wild-type (WT) mice, while L-events were unaltered (**Figure 10h-j**). The disruption of H-events led to a decorrelation of baseline cortical activity across distance in SERT-KO mice (**Figure 10g**). The net effect of these alterations was cortical hypoactivity, as evidenced by a left shift of the cumulative probability of ΔF/F values in both

SERT-Het and SERT-KO mice (**Figure 10k**), that indicates lower overall values of ΔF/F across the recording.

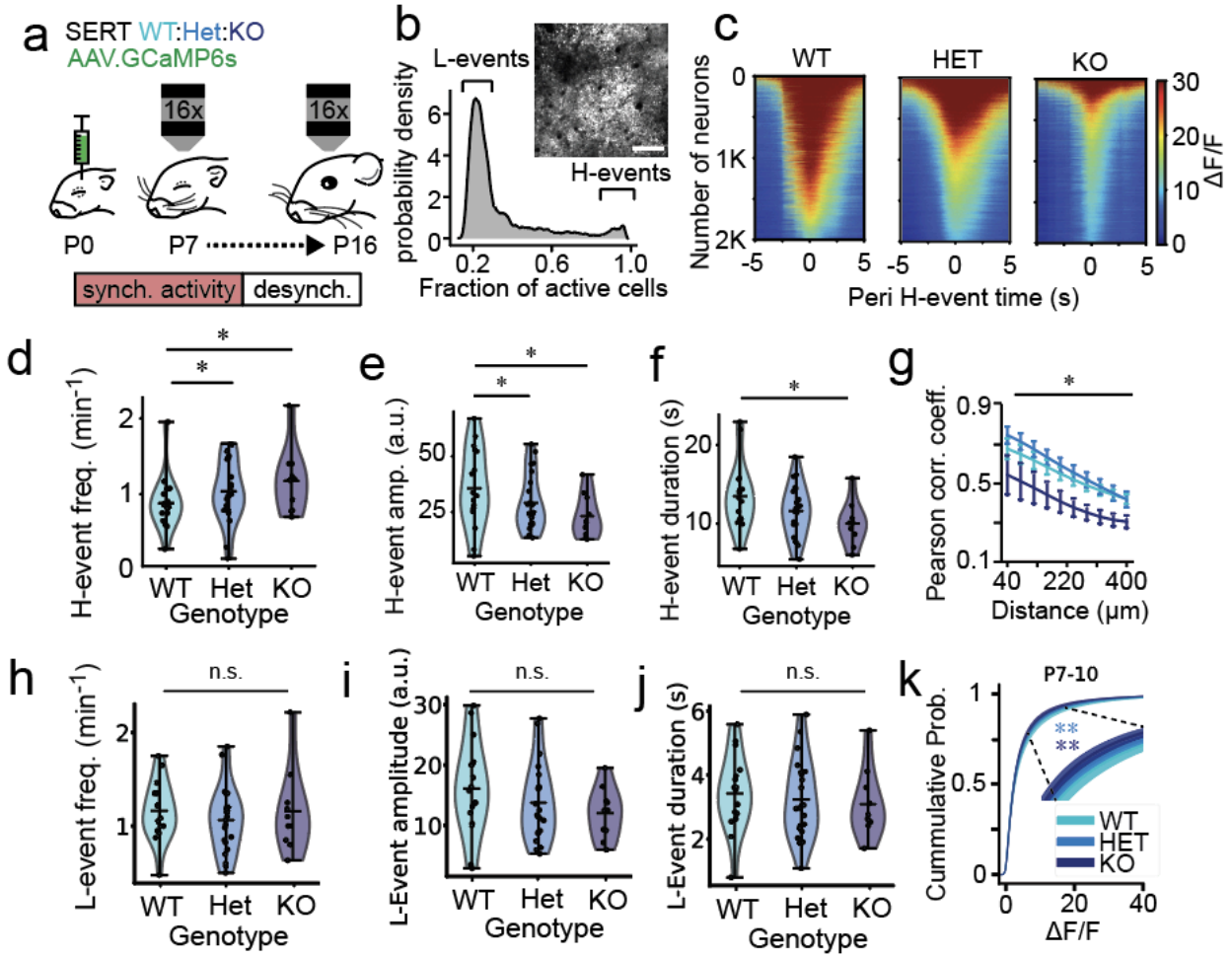

Figure 10. SERT-KO exhibits H, but not L, -event disruption with subsequent cortical hypoactivity. a SERT-WT/Het/KO neonates received an intraparenchymal injection of an AAV vector genetically encoding the fluorescence calcium indicator GCaMP6s in S1BF, they underwent the implantation of a cranial window, plus a head-fixing plate, at P6 and they were imaged P7-16 using two-photon head-fixed awake imaging. **b** Representative histogram of cell co-activation from a single WT animal at P8 showing the previously reported existence of low (L-) and high (H-) synchronicity calcium events, with a field of view of an H-event, showing the characteristic neuronal recruitment of more than 80% of cells. Image made from an average of 120 frames (scale bar = 100 μm). **c** Representative peri (+/- 5s) H-event GCCaMP6s signal heatmaps of 2000 cells in recordings from a single WT, SERT-Het and SERT-KO P8 mouse. Heat map constructed from averaging the signal across all H-events detected on each mouse during a 20 min recording. **d** Mean H-event frequency in SERT-WT/Het/KO mice at P7-10.

(ANOVA genotype p = 0.001. Pairwise comparisons: WT-Het p = 0.018; WT-KO p = 0.007; Het-KO p = 0.642). **e** Mean GCaMP6s signal amplitude of cells during H-events in SERT-WT/Het/KO mice at P7-10 (ANOVA genotype p = 0.003. Pairwise comparisons: WT-Het p = 0.033; WT-KO p = 0.011; Het-KO p = 0.604). **f** Average H-event duration in SERT-WT/Het/KO mice at P7-10 (ANOVA genotype p = 0.007. Pairwise comparisons: WT-Het p = 0.054; WT-KO p = 0.011; Het-KO p = 0.515). **g** Pairwise cell correlations across distance in SERT-WT/Het/KO mice at P8 ($p < 0.001$). **h** Mean L-event frequency in SERT-WT/Het/KO mice at P7-10. (ANOVA genotype p = 0.074). **i** Mean GCaMP6s signal amplitude of cells during L-events in SERT-WT/Het/KO mice at P7-10 (ANOVA genotype p = 0.062). **j** Average L-event duration in SERT-WT/Het/KO mice at P7-10 (ANOVA genotype p = 0.563). **k** P7-10 (b, Kolmogorov–Smirnov test: WT-HET p = 0.0002; WT-KO p = 0.0007). Sample sizes are 19 (WT), 23 (Het) and 10 (KO). ΔF/F is the green fluorescence signal at any time point, subtracted and divided by the mean signal across a 20 minute baseline.

3.2.2 H-events occur predominantly during wakefulness

The above results suggest a particular susceptibility of H-events, as opposed to L-events, to SERT disruption. Visual inspection during the recordings suggested that H-events take place predominantly during periods in which pups were moving (**Figure 11a**), suggesting that strong self-generated whisker deflection could be a major driver of H-events. This would be consistent with previous publications suggesting that movement is a major driver of developmental early neuronal activity (Dard et al., 2022). These movements take place during wakefulness, the behavioural state with the highest DRN firing rate (Kato et al., 2022), leading to the highest levels of 5-HT both in the adult (Deng et al., 2024; Kato et al., 2022; Wan et al., 2021) and the developing (**Figure 9**) brain. Thus, given the developmental expression of 5-HT_{1B} receptor in thalamocortical axons, activity taking place during wakefulness might be particularly impacted in SERT-KO mice, due to the higher release of 5-HT, while events taking place in REM sleep might be less impacted.

In young pups (<P14) whiskers are small and protracted which makes their tracking from an infrared recording difficult. We therefore tested this hypothesis in the right forelimb primary somatosensory cortex (S1FL) while tracking left forelimb movement (**Figure 11b**). Indeed we observed a higher correlation of forelimb movement with S1FL activity than with S1BF activity (**Figure 11c-e**). Visual inspection of time-locked forelimb and S1FL calcium dynamics suggests that H-events take place predominantly during continuous movement (i.e., wakefulness), while L-events were distributed between periods of continuous movement and sharp twitches (i.e., active sleep) (**Figure 11d**). Sleep-wake classification from forelimb tracking with deeplabcut (Nath et al., 2019) confirmed that H-events occurred predominantly during wakefulness (**Figure 11f**). Therefore suggesting that H-events might be particularly susceptible to SERT-KO due to the heightened levels of 5-HT release in the awake developing cortex (**Figure 9**) and the inhibitory effect of 5-HT in bottom-up sensory activity (Bennett-Clarke et al., 1993; Laurent et al., 2002; Leslie et al., 1992; Salichon et al., 2001).

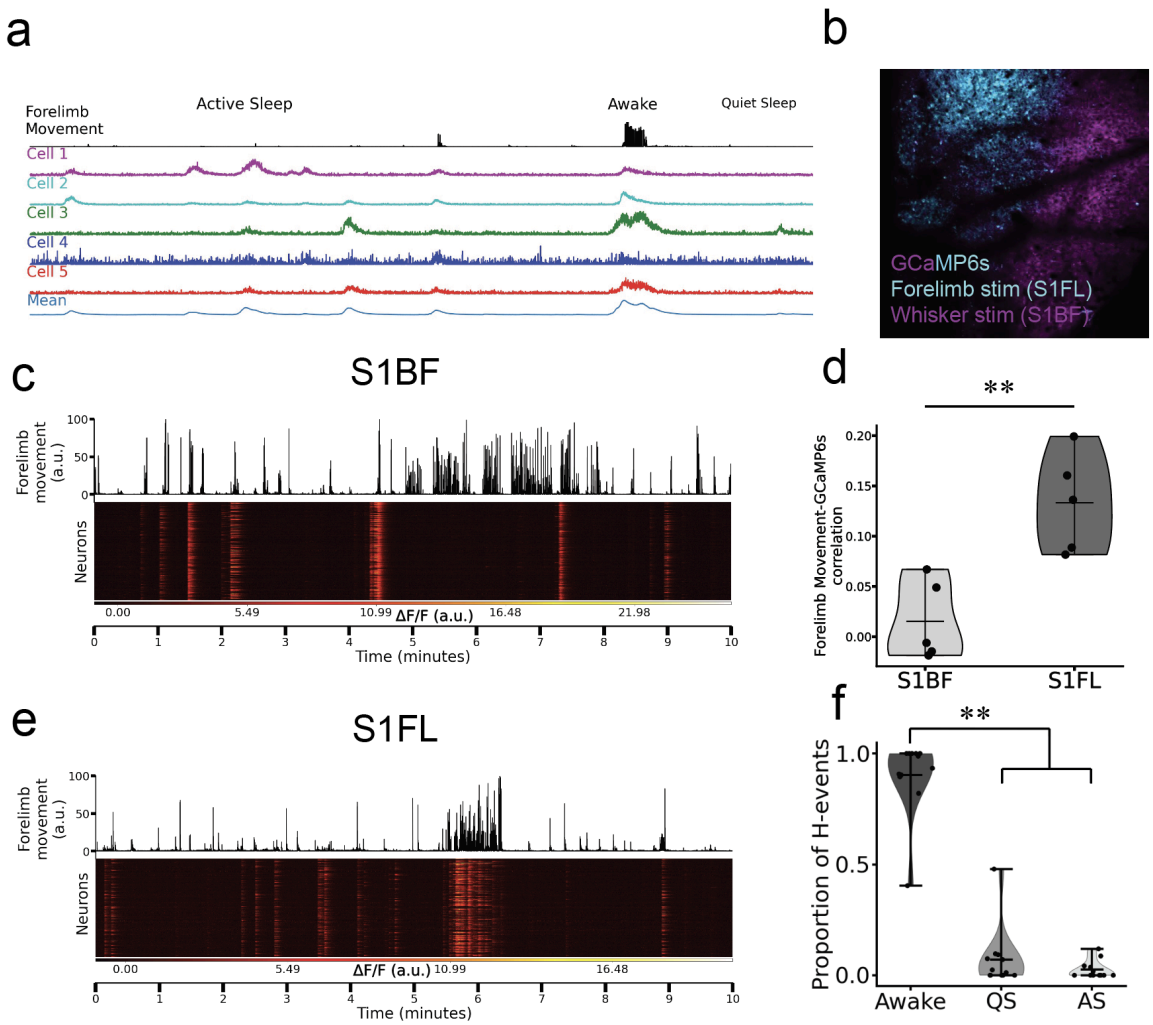

Figure 11. H-events are predominantly driven by self-generated movement during wakefulness. WT neonates received an intraparenchymal injection of an AAV vector genetically encoding the fluorescence calcium indicator GCaMP6s in S1BF or S1FL, they underwent the implantation of a cranial window, plus a head-fixing plate, at P6 and they were imaged P7-10 using two-photon head-fixed awake imaging. **a** Example of time-locked S1BF ΔF/F calcium traces from 5 cortical cells, and the average of all cells, with left forelimb movement trace for 3.5 min during postnatal day 8. **b** Field of view within a P8 mouse somatosensory cortex (L2/3) showing responsive cells to forelimb (cyan) and whisker (magenta) somatosensory stimulation with the calcium indicator GCaMP6s. Image generated by averaging stimulus-responses across 10 repeats of each modality in a single animal. **c** Representative traces from a single P8 mouse of forelimb movement time-locked to calcium heatmap of cell activity during a 10 minute baseline in S1BF. **d** Pearson correlation coefficient between S1BF/S1FL activity and forelimb movement during a 20 min recording. (paired t-test, ** $p < 0.01$, $n = 5$ mice imaged in both S1BF and S1FL) in P8 mice. **e** Representative traces from a single P8 mouse of forelimb movement time-locked to calcium heatmap of cell activity during a 10 minute baseline in S1FL. **f** Violin plot of proportion of H-events during wakefulness, quiet sleep (QS) or active sleep (AS).

(Kruskal-Wallis test p < 0.001, post hoc Dunn test: awake-QS p < 0.001, awake-AS p < 0.001, AS-QS p = 0.553, n = 11 mice). S1FL: forelimb primary somatosensory cortex. ΔF/F is the green fluorescence signal at any time point, subtracted and divided by the mean signal across a 20 minute baseline.

3.2.3 SERT-KO transitions into cortical hyper-excitability

At P11 cortical activity desynchronises (Dard et al., 2022; Golshani et al., 2009), concurrent with the disappearance of the transient SERT expression (De Gregorio et al., 2020; Narboux-Nême et al., 2008), through the rise of GABAergic inhibition (Mòdol et al., 2024), that leads to the disappearance of H- and L-events. We speculated that the early hypoactivity in SERT-KO mice could be disrupting S1BF maturation and leading to altered cortical dynamics after cortical decorrelation. Thus, we characterised S1BF cortical activity in SERT-KO mice after cortical decorrelation (P11) with two-photon calcium imaging of S1BF in head-fixed mice during whisker deflection. During this period, we observed an increase in the amplitude of cortical responses to whisker stimuli in SERT-KO mice (**Figure 12a-b**) that is accentuated in response to a more salient sensory stimuli, a high-pressure air puff (**Figure 12c**). Thus at P11 cortical dynamics paradoxically transition from hypo- to hyperactivity, as illustrated by the right-shift of the cumulative probability distribution of GCaMP6s ΔF/F values (**Figure 12d**), in mutant SERT-KO animals compared to WT control littermates.

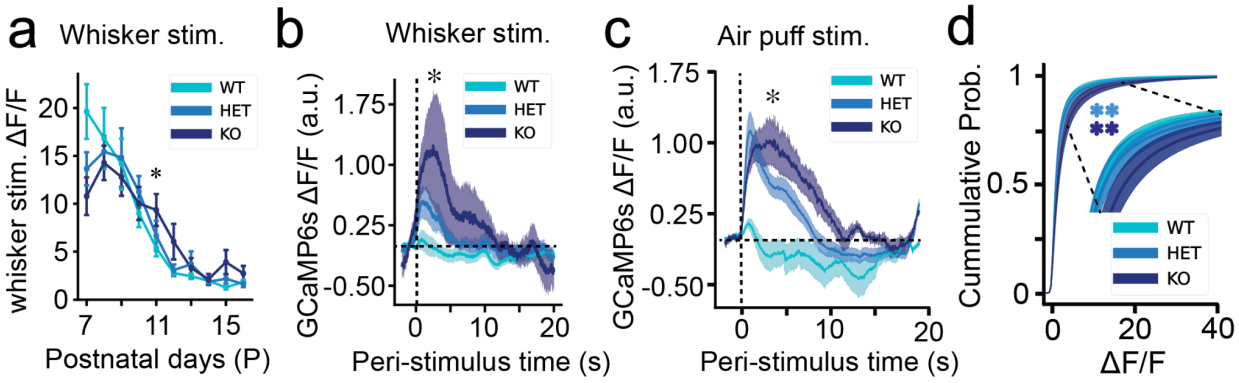

Figure 12. SERT-KO transitions into cortical hyper-excitability and hyper-responsiveness. SERT-WT/Het/KO neonates received an intraparenchymal injection of an AAV vector genetically encoding the fluorescence calcium indicator GCaMP6s in S1BF, they underwent the implantation of a cranial window, plus a head-fixing plate, at P6 and they were imaged P7-16 using two-photon head-fixed awake imaging. **a** Mean whisker-response amplitude across development in SERT-KO mice showing increases after decorrelation at P11 (ANOVA genotype $p = 0.006$, pairwise WT-Het: $p = 0.900$, WT-KO: $p = 0.038$, Het-KO: $p = 0.0579$). **b** Stimulus-triggered average GCaMP6s signal across all cells and mice showing increased whisker-response amplitude at P11-13 (ANOVA $p = 0.040$, pairwise WT-HET $p = 0.246$, WT-KO $p = 0.010$). **c** Stimulus-triggered average GCaMP6s signal across all cells and mice in response to a 80 PSI air puff at P11-13 (ANOVA $p = 0.047$, pairwise WT-HET $p = 0.198$, WT-KO $p = 0.038$). **d** Cumulative probability of ΔF/F 20 minute baseline values of all SERT-WT/Het/KO at P11-13 (Kolmogorov–Smirnov test: WT-HET $p < 0.001$; WT-KO $p < 0.001$). Sample sizes are 19 (WT), 23 (Het) and 10 (KO) mice. ΔF/F is the green fluorescence signal at any time point, subtracted and divided by the mean signal across a 20 minute baseline. Mean signal 2s pre-stim was then subtracted to normalize sensory responses.

3.2.4 SERT-KO interneuron neurophysiology

SERT-KO S1BF switched from hypo- to hyper-activity with respect to WT animals, at P11. Thus, this transition occurs during the onset of inhibition that decorrelates cortical activity (Mòdol et al., 2024). This process requires the emergence of PV inhibition, but its timing is orchestrated by SST interneurons (Mòdol et al., 2024) (introduction, section 1.2.2). The early SERT-KO hypoactivity was observed during a key period for the activity dependent maturation of MGE inhibition (Wong et al., 2018). This is also the period in which CGE interneurons decorrelate (Che et al., 2018), and in fact the survival (Wong et al., 2022) and migration (Frazer et al., 2015; Murthy et al., 2014) of these neurons depends on 5-HT signalling. Thus, a likely cause of this hypo- to hyperactivity switch in SERT-KO mice is the dysregulation of interneuron development. We hypothesised that increased 5-HT would promote activity in 5-HT_{3A}R-expressing interneurons including those defined by expression of VIP, whereas other interneurons originating from the Nkx2-1-expressing MGE would be down-regulated due to the overall hypoactive cortex (**Figure 13a**).

To test this, we generated pups in which either VIP or Nkx2-1 interneurons were labelled with tdTomato on the SERT-KO background (**Figure 13b**). *In vivo* imaging revealed that VIP interneurons exhibit higher amplitude calcium transients during H-events (**Figure 13c**), and enhanced whisker responses (**Figure 13d**) in SERT-KO mice compared to WT littermate controls. In contrast, we observed decreased H-event (**Figure 13e**) and predominantly reduced whisker sensory-evoked (**Figure 13f**) responses in Nkx2-1 interneurons in SERT-Het animals. No SERT-KO animals born on the *Nkx2-1Cre* background survived beyond P11 precluding *in vivo* analysis. We speculated that the overexpression of tdTomato in Nkx2-1 neurons, potentially already impaired in SERT-KO mice, could be increasing cell death of these neurons and leading to premature death of the pups by epilepsy at the onset of inhibition (P10), however we did not confirm this hypothesis experimentally. Altogether we observed that the transition from hypo-to-hyper function (**Figure 10,12**) coincides with alterations in interneuron neurophysiology, namely VIP hyperfunction in SERT-KO and Nkx2-1 early hypoactivity in SERT-Het.

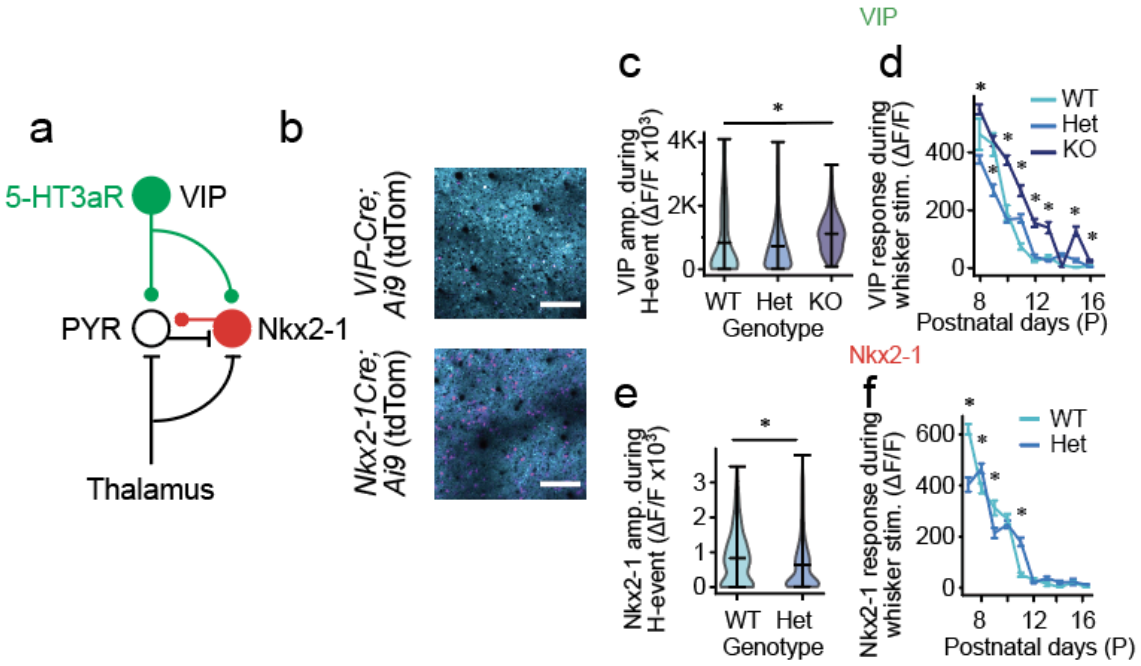

Figure 13. SERT-KO hypo-to-hyper activity presents concomitant alterations in VIP/Nkx2-1 interneuron neurophysiology. SERT-WT/Het/KO VIP- or Nkx2-1-tdTomato transgenic neonatal mice received an intraparenchymal injection of an AAV vector genetically encoding the fluorescence calcium indicator GCaMP6s in S1BF, they underwent the implantation of a cranial window, plus a head-fixing plate, at P6 and they were imaged P7-16 using two-photon head-fixed awake imaging. **a** Circuit diagram illustrating that Nkx2-1 provides bottom-up feed-forward inhibition, while VIP interneurons cause both direct inhibition of pyramidal neurons, as well as disinhibition of these neurons by inhibiting Nkx2-1 interneurons. **b** Representative fields of view of murine S1BF cortex expressing GCaMP6s under the hSyn promoter and tdTomato in VIP (**top**) or Nkx2-1 (**bottom**) interneurons. **c** Violin plot of average amplitude of VIP interneurons during H-events in SERT-WT/Het/KO mice at P7-10 (Kruskal–Wallis $p < 0.001$, pairwise WT-HET: $p = 0.087$, WT-KO: $P = 0.001$, HET-KO: $p = 0.001$). **d** Whisker response amplitudes of VIP+ interneurons in SERT-WT/Het/KO mice from P8 to P16 (* $p < 0.05$). **e** Violin plot of average amplitude of Nkx2-1+ interneurons during H-events in SERT-WT/Het mice at P7-10 ($p < 0.001$). **f** Whisker response amplitudes of Nkx2-1 interneurons in SERT-WT/Het mice from P7 to P16 (* $p < 0.05$). (**c-d**) Sample sizes for the VIP dataset are: 201 cells from 4 animals (WT), 1361 cells from 9 animals (Het) and 546 cells from 5 animals (KO). (**e-f**) Sample sizes for the Nkx2-1 dataset are: 555 cells from 6 animals (WT) and 1020 cells from 8 animals (Het)**.** ΔF/F is the green fluorescence signal at any time point, subtracted and divided by the mean signal across a 20 minute baseline. Mean signal 2s pre-stim was then subtracted to normalize sensory responses. Nkx2-1/VIP interneurons were identified by their expression of tdTomato using a 20s two-photon imaging recording with a 765nm excitation wavelength and a red filter. Amplitude is defined as the maximum fluorescence signal during H-events or 10s post-stimulus onset in the case of whisker responses.

3.2.5 SERT-KO cortical population dynamics

To explore how the above alterations in cortical activity change information encoding, we explored the effect in cortical population dynamics. For this, we used two commonly employed measurements in both rodent and human systems neuroscience studies: representational similarity analysis (RSA) (Kriegeskorte et al., 2008) and entropy (Keshmiri, 2020).

Firstly, we performed RSA using correlation distance as a measure of representational dissimilarity. Namely, we used RSA to identify how constant the representation of the same sensory stimuli is in the S1BF of SERT-KO mice compared to littermate WT animals. We observed a decrease in the representational dissimilarity of identical air puff stimulations in SERT-KO mice compared to WT (**Figure 14a-b**). This result is of particular interest in light of a recent theoretical study suggesting that representational variability plays a role in learning generalisation (Shang et al., 2021) and the fact that SERT-KO rats have alterations in learning generalisation (C. C.-G. Guo et al., 2021). Thereby suggesting that reduced representational dissimilarity could be a potential neurophysiological correlate of this learning dysfunction. From a mechanistic perspective, a deficit in inhibition could be underlying this increase in representational dissimilarity, on the basis of a study suggesting that inhibition plays a key role in representational variability (Haroush & Marom, 2019).

Secondly, we used our calcium recordings to compute the population entropy of SERT-KO, HET and WT controls. This quantity from the field of information theory, provides a readout of the information encoded by a system. It is a particularly interesting metric in systems neuroscience, as alterations in brain entropy have been reported in a wide range of neuropsychiatric conditions (e.g., schizophrenia or ADHD) (Ji et al., 2022). We speculated that the observed alteration in the cortical activity of SERT-KO mice would have an impact on cortical population

entropy. However, we did not observe any alterations in entropy of SERT-KO, compared to WT, mice (**Figure 14c**).

Altogether, these results highlight the complex effects that neuromodulatory perturbations can have in the encoding of information throughout cortical development, and that will likely manifest in an intricate manner at a behavioural level.

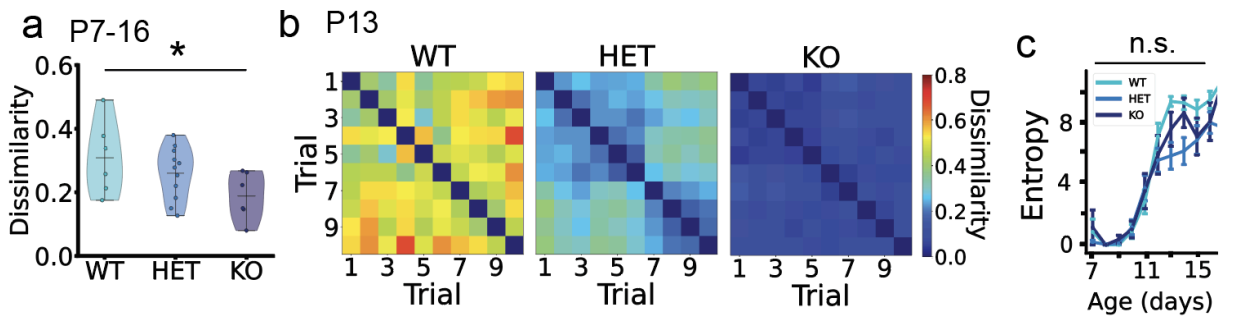

Figure 14. SERT-KO mice present decreased representational dissimilarity of air puff repeats throughout postnatal development. SERT-WT/Het/KO neonates received an intraparenchymal injection of an AAV vector genetically encoding the fluorescence calcium indicator GCaMP6s in S1BF, they underwent the implantation of a cranial window, plus a head-fixing plate, at P6 and they were imaged P7-16 using two-photon head-fixed awake imaging. **a** P7-16 average correlation distance, as a measure of representational dissimilarity, of air puff stimulation responses in S1BF of WT, SERT-Het and SERT-KO mice. Data is average since the same trend was observed throughout the recordings. (One-way ANOVA $p = 0.017$, Tukey's test multiple comparison: $p = 0.3422$ for WT-HET and $p = 0.0135$ for WT-KO). **b** Representative example of representational similarity matrices heatmaps at P13 for WT, SERT-Het and SERT-KO mice. **c** Population entropy in S1BF cortex across second week postnatal development in WT, SERT-Het and SERT-KO mice (genotype Kruskal-Wallis test $p = 0.872$).

3.2.6 SERT-KO lack of adult neurophysiological S1BF phenotype

Our findings point to a complex effect of SERT-KO in S1BF activity throughout development. In light of the complex adult behavioural phenotype of SERT-KO mice (introduction), we speculated that cortical dynamics might remain altered in the adult cortex. Thus, we explored

the impact of these developmental alterations in adult cortical sensory encoding. For this, we monitored cortical calcium dynamics in the S1BF cortex of adult (8-12 weeks old) head-fixed SERT-KO mice exposed to an array of different types of sensory stimulation: single-whisker deflection, multi-whisker deflection, rough vibrating surface, smooth vibrating surface, air puff and sound (**Supplementary figure 4a,b**).

We observed no differences in the sensory response to any of the stimuli in SERT-KO mice compared to littermate WT controls (**Figure 15a-d**, single-whisker and air puff stimulation). To confirm the lack of differences in sensory encoding, we perform logistic regression analysis. We aimed to study whether animal genotypes could be classified purely from the patterns of cortical activity, which would have confirmed an alteration in cortical activity. Thus, we trained classifiers to distinguish the genotype of the animal (SERT- WT, Het or KO) from the average response of 500 randomly sub-sampled cells. We trained a different classifier for each trial type, and we performed inter-individual cross-validation to ensure that individual overfitting was not a confounding factor (Saeb et al., 2017). To establish the statistical significance of the classification we run bootstrapping analysis by training logistic regression models with randomly permuted traces (**Supplementary figure 4f**). None of the classifiers showed significant accuracy (**Figure 15e-f**), further confirming the lack of cortical activity differences in the SERT-KO, versus WT, mice. Given the differences in developmental cortical activity and the life-long nature of the genetic alteration, these results suggest a compensatory mechanism in the adult cortex.

Notably, in WT animals, we were able to classify the genotype of the animal's dam as a function of baseline and sound recordings, but not from somatosensory stimulation trials (**Figure 15e-f**). These results indicate that baseline, but not stimulation trials, present different patterns of cortical activity in WT mice from SERT-Het dams, compared to WT mice from WT dams. This

suggests an alteration in baseline, or resting state, dynamics that is compensated during stimulation trials. These results align with an alteration observed in the offspring of SERT-Het dams that lack transient inhibitory circuits from L5b to L4 in early postnatal development (**Supplementary figure 3k-p**). Moreover, they are consistent with clinical literature suggesting pathological associations between maternal SERT polymorphisms and offspring neurodevelopmental disorders (Ames et al., 2021; Beversdorf et al., 2021; Côté et al., 2007; Hecht et al., 2016; Jones et al., 2010; Montgomery et al., 2018; Sjaarda et al., 2017). Of note, in the offspring of SERT-Het dams compared to the offspring of WT dams we did not observe any detectable neurophysiological alteration in calcium dynamics during postnatal development (**Supplementary figure 3q-t**).

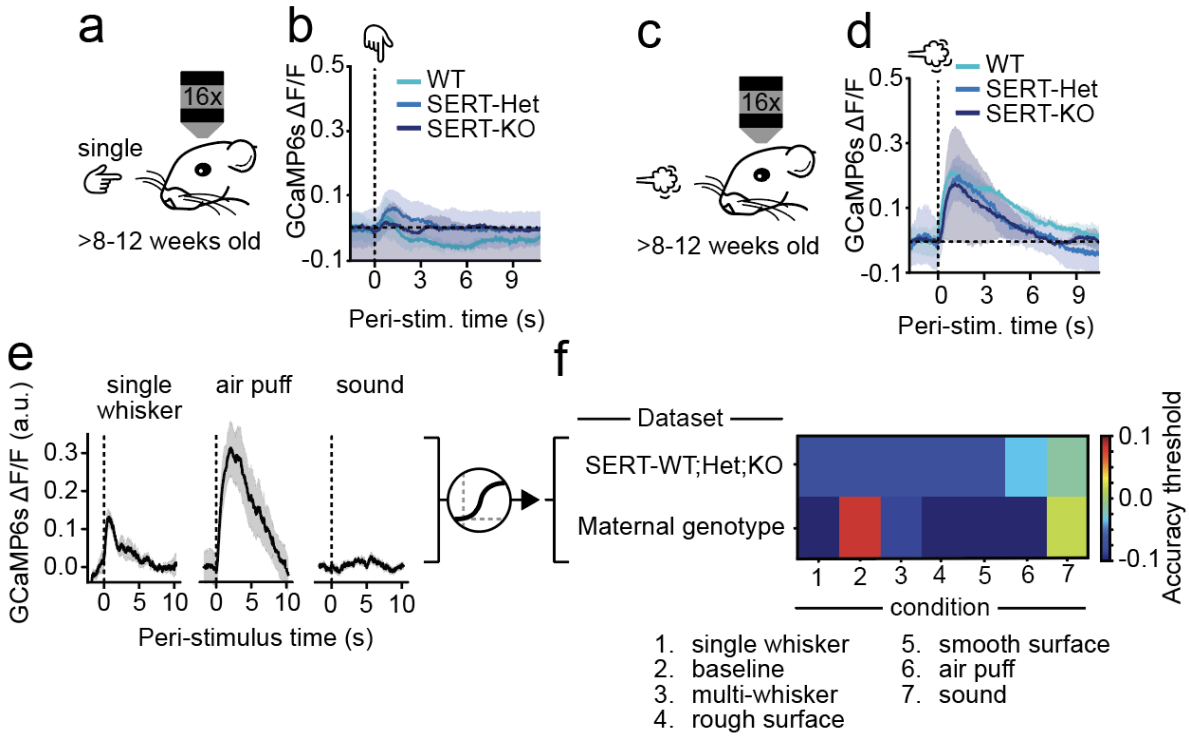

Figure 15. SERT-KO S1BF adult cortical activity is indistinguishable from WT mice. SERT-WT/Het/KO mice received an intraparenchymal injection of an AAV vector genetically encoding the fluorescence calcium indicator GCaMP6s in S1BF and they underwent the implantation of a cranial window, plus a head-fixing plate to perform two-photon head-fixed awake recordings. **a** Schematic illustrating that adult mice (8-12 weeks) were exposed to single whisker deflection. **b** GCaMP6s single-whisker stimulus triggered average response to 10

stimuli in SERT-WT/Het/KO mice. **c** Diagram illustrating that adult mice (8-12 weeks) were exposed to air puff stimulation (80 psi). **d** GCaMP6s air puff triggered average response to 10 stimuli in SERT-WT/Het/KO mice. **e** Diagram illustrating that post-stimulus calcium responses to the different stimuli were used for logistic regression analysis. **f** Heat map with the decoding accuracy of the different logistic regression classifiers trained to discriminate across genotypes from the post-stimulus responses of the different types of stimuli. The colour indicates accuracy minus threshold for significance of the classification as defined by bootstrapping. Thus, positive values indicate significant classification accuracy. Sample sizes are 10 (WT), 8 (HET) and 5 (KO). ΔF/F is the green fluorescence signal at any time point, subtracted and divided by the mean signal across the whole recording. Mean signal 2s pre-stim was then subtracted to normalize sensory responses.Response amplitude is defined as the maximum fluorescence signal 10s post-stimulus onset. Cell responsiveness was addressed by comparing the mean signal pre- and post-stimulus onset across the 10 repeats (paired t-test or Wilcoxon signed-rank test after addressing normality with Shapiro-Wilk test)..

3.2.7 SERT-KO mice exhibit histological alterations in adult interneuron subpopulations

Despite the lack of an adult phenotype, we wanted to confirm that the early cortical hypoactivity of SERT-KO, that was taking place during a critical period for activity-dependent interneuron survival (Wong et al., 2018, 2022), was not altering interneuron numbers in the adult S1BF. Thus, we quantified interneuron numbers in S1BF using histology for VIP(tdTomato) and PV alongside automated DAPI cell detection (**Figure 16a; Supplementary figure 5**). Due to the failure of Nkx2-1(tdTomato) SERT-KO animals to survive to adulthood, we were reliant on PV immunohistochemistry (**Figure 16a-b**). This revealed a decrease in PV expression across the depth of cortex, while the distribution and number of VIP interneurons remained unchanged (**Figure 16a-b**) in contrast to previous reports (Frazer et al., 2015). Given that the developmental hypoactivity observed in SERT-KO mice (**Figure 10**) takes place during a critical period for MGE-interneuron survival (Wong et al., 2018), these results suggest that the early impairment of H-events could be increasing PV cell death. This reduction in PV interneurons is likely underlying the cortical hyperactivity observed in the third week of postnatal development (**Figure 11**). The lack of a phenotype in the neuronal activity of adult SERT-KO mice compared to control WT littermates, further suggests a compensatory mechanism to this inhibitory deficit.

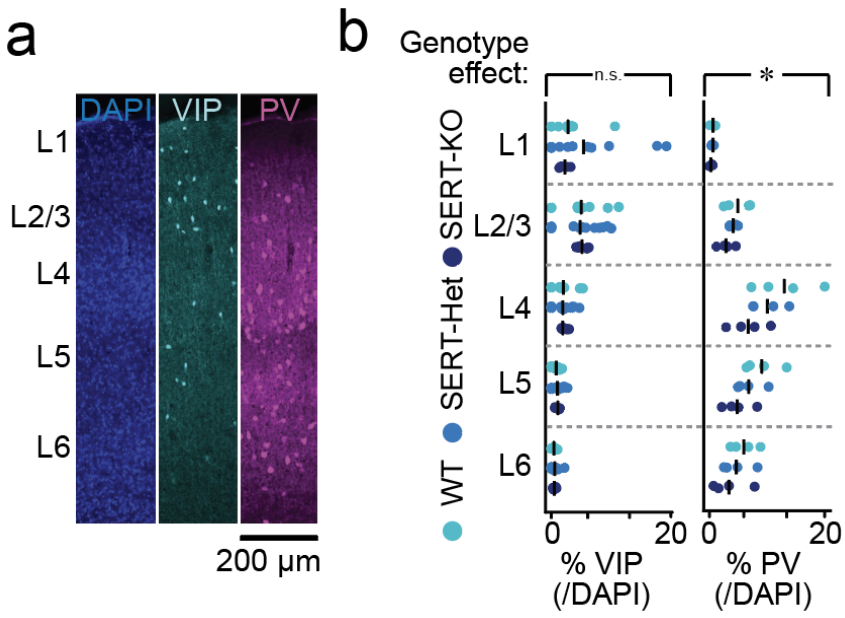

Figure 16 SERT-KO mice have a decrease in PV-expressing cells. a Confocal histological image of a S1BF cortical column (200 µm wide) on an adult WT cortex, illustrating DAPI (blue, left), VIP (cyan, centre) and PV (magenta, right) layer distribution. VIP was labelled by using transgenic VIP-CrexAi9 mice while PV was labelled by immunohistochemistry. **b** Biodistribution of VIP (Two-way ANOVA: genotype $p = 0.766$, layer $p < 0.001$, genotype-layer interaction = 0.946) and PV (Two-way ANOVA: genotype $p = 0.004$, layer $p < 0.001$, genotype-layer interaction = 0.625) interneurons across layers for SERT-WT/Het/KO mice. VIP Sample size: 5 WT, 8 SERT-Het and 5 SERT-KO. PV sample size: 4 WT, 4 SERT-Het and 4 SERT-KO.

3.3 Conclusions

In this chapter we report early postnatal (P7-10) cortical hypoactivity in the S1BF of SERT-KO mice during the period of transient SERT expression (**Figure 10**). This hypoactivity is likely driven by two mechanisms. Firstly, the transient expression of 5-HT_{1B}R in thalamocortical terminals during this period (Bennett-Clarke et al., 1993). Previous studies have speculated that 5-HT inhibits sensory-driven thalamocortical glutamate release through this transient expression of 5-HT_{1B} (Salichon et al., 2001; Teissier et al., 2017), and therefore the activation of these receptors could be driving the observed hypoactivity. Secondly, the activation of 5-HT_{3A}R interneurons. We report that VIP interneurons, that express 5-HT_{3A}R, showed increased activity in the developing cortex (P7-16) of SERT-KO mice (**Figure 13**). These interneurons located in

upper layers have been reported to restrict pyramidal cell activation in early development (Che et al., 2018), and therefore their activation could also be driving this hypoactivity. Thus, we speculate that SERT-KO increases extracellular 5-HT (**Figure 8**) which in turn leads to both excessive inhibition of thalamocortical release and higher activation of 5-HT_{3A}R interneurons, thereby driving the observed early hypoactivity.

We report this hypoactivity during a critical period for the activity-dependent survival of interneurons, in which we also observed that SERT-Het mice have hypoactive Nkx2-1 interneurons (**Figure 13**). Consistently we observed a reduction in PV immunohistochemistry in SERT-KO animals (**Figure 16**), that suggested increased cell death of these interneurons. Although, we cannot rule out the possibility that this is driven by a decrease in PV expression. We could not confirm a reduction in MGE cells due to the premature death of SERT-KO Nkx2-1-tdTomato animals. However, these results point towards a deficit in MGE inhibition, consistent with the previously reported reduction in feed-forward inhibition in juvenile SERT-KO rats (Miceli et al., 2017). VIP interneurons showed increased activity throughout development (**Figure 13**). Surprisingly, we did not observe any changes in VIP interneuron survival nor their cortical layering (**Figure 16**). These results contrast with previous histological studies in SERT-KO mice suggesting a disruption of their migration leading to decreasing VIP counts in upper layers and an increase in deeper layers (Frazer et al., 2015).

This early hypoactivity is underlied by a reduction in the amplitude and duration of H-events, albeit an increase in their frequency, while L-events remain unaltered (**Figure 10**). The increase in H-event frequency can be explained from literature suggesting that these early events are partly terminated by synaptic short-term depression (Kirmse & Zhang, 2022). The shorter H-events observed in SERT-KO mice could increase the frequency in which the cortex is in a state of excitability that allows an H-event to take place. Regarding H-event, versus L-event,

susceptibility we have identified two potential explanations. Firstly, H-events might be susceptible given that they take place in S1BF predominantly during wakefulness (**Figure 11**), the behavioural state with highest 5-HT release (**Figure 9**) (Deng et al., 2024; Wan et al., 2021). While events taking place during REM sleep, in which 5-HT release is reduced, might be spared. Secondly, H and L events might be regulated by different inhibitory circuits, as SST interneurons have been shown to restrict the spread of L, but not H, calcium events in the visual cortex (Leighton et al., 2021). In this case, H-events could be regulated by 5-HT_{3A}R interneurons, and over-restricted by the observed increased activation of these interneurons during H-events (**Figure 13**). While our results show H-events taking place during wakefulness, we do not provide causal evidence to disambiguate among these hypotheses, and future studies should explore the mechanism behind this susceptibility of H-events in SERT-KO mice.

While we observed cortical hyperexcitability in SERT-KO mice (**Figure 12**), studying adult cortical dynamics revealed normal sensory responses (**Figure 15**), despite a reduction in the number of cortical PV-expressing interneurons (**Figure 16**). These results suggest a compensatory mechanism in the adult cortex of SERT-KO mice. This compensation could be taking place in two ways. Firstly, 5-HT release might adjust to the levels of SERT in the adult cortex. This is consistent with a reduction in the number of 5-HT neurons in the DRN of SERT-KO mice (Lira et al., 2003), although some studies have reported alterations in 5-HT dynamics in these mice during adulthood (Jennings et al., 2010). Secondly, if 5-HT plays a similar inhibitory role in the adult cortex, the putative reduction in PV that we observe might compensate for the increased inhibitory tone provided by higher levels of 5-HT. This would suggest that the levels of cortical inhibition develop to match the levels of 5-HT neuromodulation.

Finally, we observed an alteration of adult cortical baseline activity in animals originating from SERT-Het dams (**Figure 15**). This alteration was correlated with an alteration of transient translaminar GABAergic circuits in development (**Supplementary figure 3**). These observations are consistent with previous clinical associations between maternal SERT genotype and neurodevelopmental disorders in the offspring (Beversdorf et al., 2021; Hecht et al., 2016; Jones et al., 2010; Sjaarda et al., 2017), however it is challenging to interpret how this alteration in baseline activity would subsequently shape behaviour and to understand why sensory-evoked activity is not altered in the offspring of maternal SERT-Het mice.

Altogether, we unveil a developmental alteration in the cortical dynamics of SERT-KO mice with concomitant alterations in the GABAergic system.

4. Cortical population activity in SSRI postnatally-treated mice

4.1 Introduction

SERT-KO mice present a developmental transition from early cortical hypoactivity to hyperactivity, that is accompanied by alterations in VIP and Nkx2-1 interneuron neurophysiology, as well as a decrease in PV survival. This is particularly relevant, given the association between SERT polymorphisms and the emergence of neuropsychiatric conditions (Brown et al., 2013; Hesse et al., 2011; Murphy & Lesch, 2008; Veenstra-VanderWeele et al., 2012) (e.g., ASD) that present interneuron alterations (Contractor et al., 2021). However, SERT-KO mice present two major limitations as a model: firstly, the life-long nature of this alteration makes it hard to delineate the precise critical period responsible for their phenotype; secondly, in humans, clinical associations with neurodevelopmental disorders have been made upon polymorphisms in its promoter, but not a complete knockout of the gene, which limits the translational potential of this model. Thus, we decided to expand this work, by characterising a more temporally acute and translationally-relevant model (Ames et al., 2021; Koc et al., 2023; Morales et al., 2018; Suarez et al., 2022): developmental exposure to SSRIs, the most commonly prescribed antidepressants.

Our first aim with this model was to delineate the critical period of this mechanism, that we speculated to be postnatal. For this, we used a previously described model of SSRI postnatal treatment in mice: dosing orally with fluoxetine from P2-P14. This treatment has been shown to trigger alterations in prefrontal cortex connectivity (Soiza-Reilly et al., 2019). Moreover, treatment during this window of development avoids the previously described critical period for

5-HT-sensitive thalamocortical plasticity (up to P2) (Sinclair-Wilson et al., 2023; Toda et al., 2013) and allows an overlap of the treatment with our longitudinal imaging protocol (>P6). This treatment period also captured the developmental window of interneuron activity-dependent cell death that we speculated was altered in SERT-KO mice based on the observed reduction in PV interneurons.

Our second aim was to characterise the effects of disrupting 5-HT dynamics developmentally in a more translationally relevant context. SSRIs cross the placenta and *in utero* exposure to SSRIs has been linked to acute 5-HT-mediated adverse effects in newborns (Halvorsen et al., 2019; Stein et al., 2014). Moreover, large scale meta-analyses frequently report that *in utero* exposure to SSRIs is associated with increased risk of neurodevelopmental disorders such as ADHD and ASD in offspring (Morales et al., 2018). This association does not necessarily reflect a causal relationship with maternal psychiatric diagnosis being one residual confound, and indeed there is some conflicting literature (Ames et al., 2021). Nevertheless, a recent study accounting for maternal diagnosis has reported alterations in white matter microstructure in the developing offspring (Koc et al., 2023). In light of SSRIs being the most commonly prescribed antidepressants (Luo et al., 2020), a complete understanding of their effect in cortical mammalian development is critical.

Thus, we set out to characterise the effects of postnatal SSRIs (P2-14) in cortical population dynamics, with an identical methodology to chapter 3, i.e., longitudinal two-photon imaging of calcium dynamics in S1BF from P7 to P16, and subsequently in the adult cortex, while monitoring interneuron subpopulations.

4.2 Results

4.2.1 Postnatal exposure to fluoxetine reproduces SERT-KO early cortical hypoactivity

Our results point to a critical role for perinatal 5-HT in the formation of cortical interneuron microcircuitry. To explore the exclusively postnatal effects, we next switched to dosing of WT mice with the SSRI fluoxetine (10 mg/kg of body weight) from P2 to P14 (**Figure 17A**); a window previously identified as SSRI-sensitive for cortical development (Rebello et al., 2014; Soiza-Reilly et al., 2019). Two-photon developmental calcium imaging revealed that SSRI-treated mice exhibited altered H-events (**Figure 17b,c**): a reduction in amplitude (**Figure 17b,c**), an increase in frequency (**Figure 17d**), but no change in event duration (**Figure 17e**) in SSRI-dosed pups compared to vehicle control (sucrose)-treated littermates. No differences were found in L-events **(Figure 17f-h).** We also observed a decreased correlation across distance (**Figure 17i**) and a reduction in the amplitude of whisker-stimulus evoked responses during the initial imaging window (≤P10) (**Figure 17j,k**). The net effect of these alterations was early cortical hypoactivity as highlighted by the left-shift of the cumulative probability distribution of ΔF/F values in SSRI-treated mice (**Figure 17l**). The sum of these observations indicates that both genetic (**Figure 10**) and pharmacological (**Figure 17**) disruption of SERT cause cortical hypoactivity during the Th-SERT period, by particularly impacting H-events. In line with the results of the previous chapter (**Figure 11**), we speculate that the susceptibility of H-events is due to the fact that these events are driven by large whisker deflections triggered by self-generated movements taking place during wakefulness, the behavioural state with the highest DRN firing (Kato et al., 2022) and extracellular 5-HT levels (Deng et al., 2024; Wan et al., 2021).

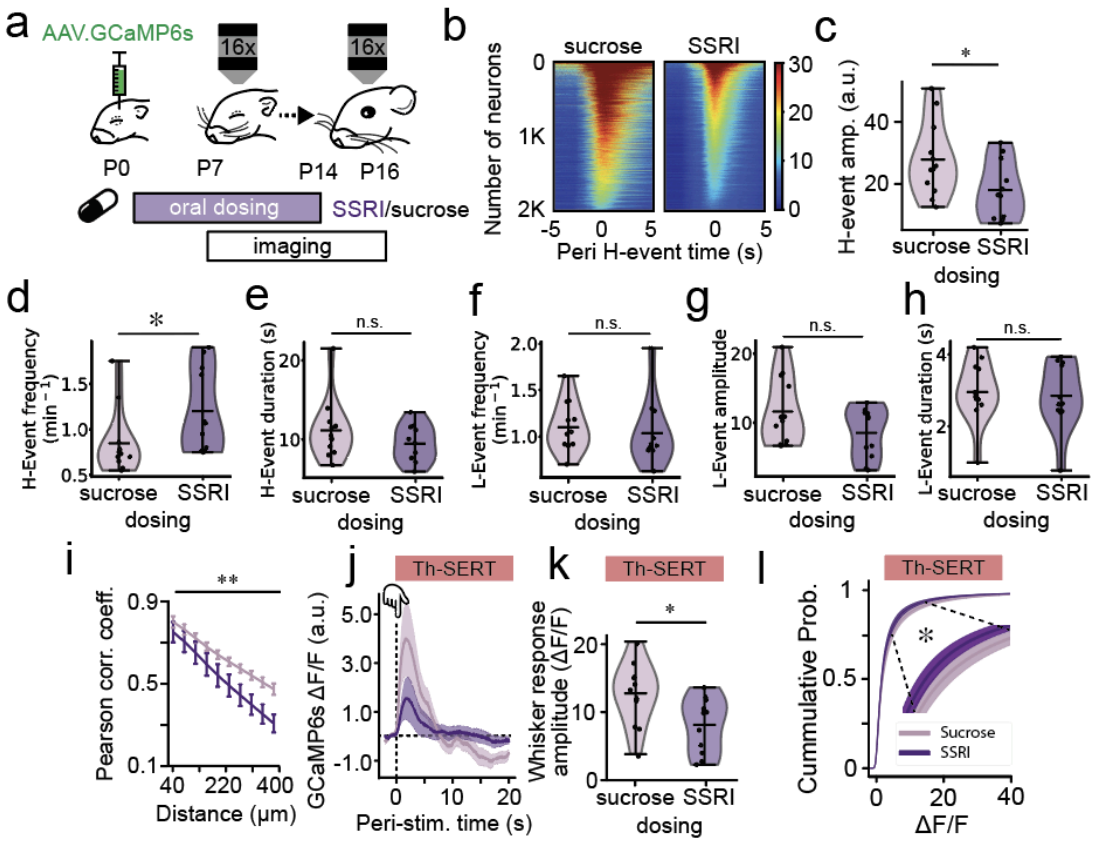

Figure 17. Postnatal exposure to SSRI induces early cortical hypoactivity by reducing H-event amplitude. a Animals were dosed orally with either 10% sucrose (control vehicle) or 10 mg/kg of fluoxetine in 10% sucrose (SSRI) daily from P2 to P14, injected neonatally with GCaMP6s, implanted with a cranial window and head-fixing plate at P6 and imaged from P7 to P16 using two-photon head-fixed awake recordings. **b** Representative peri (+/- 5s) H-event GCaMP6s signal heatmaps of 2000 cells in recordings from a single sucrose- (left) and SSRI-treated (right) P8 mouse. Heat map constructed from averaging the signal across all H-events detected on each mouse during a 20 min baseline recording. **c** Violin plot of mean amplitude of GCaMP6s across all cells during H-events in SSRI- versus sucrose-treated P7-10 mice (t-test p = 0.040). **d** Mean H-event frequency (Mann–Whitney U: p = 0.016) and **e** duration (Mann–Whitney U: p = 0.310) in sucrose- or SSRI-treated mice at P7-10. **f,g,h** Mean L-event frequency (Mann–Whitney U: p = 0.160), amplitude (t-test: p = 0.098) and duration (t-test: p = 0.774) in sucrose- or SSRI-treated mice at P7-10. **i** Baseline pairwise cell correlations across distance in SSRI-treated mice compared to sucrose-treated littermate controls at P9 (Two-way ANOVA, treatment p < 0.001). **j,k** Stimulus-triggered average GCaMP6s signal across all cells and mice at P7-10 in SSRI- or sucrose- treated mice (response amplitude (**k**) t-test p = 0.018). **l** Cumulative probability of ΔF/F 20-minute baseline values of all sucrose/SSRI treated animals at P7-10 (a, Kolmogorov–Smirnov test: p = 0.022). Sample sizes are 12 (Control) and 12 (SSRI). ΔF/F is the green fluorescence signal at any time point, subtracted and divided by the mean signal across a 20 minute baseline. Mean signal 2s pre-stim was then subtracted to normalize sensory responses.

Following desynchrony (~P11), whisker-evoked responses of SSRI postnatally-treated mice had an increased mean calcium signal (**Figure 18a**) but no changes in response amplitude (**Figure 18b**) compared to sucrose-treated mice. Moreover the cumulative probability of ΔF/F values during a 20-minute baseline, was unaltered in SSRI treated mice (**Figure 18c**). These results illustrate that the prominent cortical hyperexcitability in SERT-KO mice during the immediate Adult-SERT period is not directly replicated by postnatal SSRI-dosage.

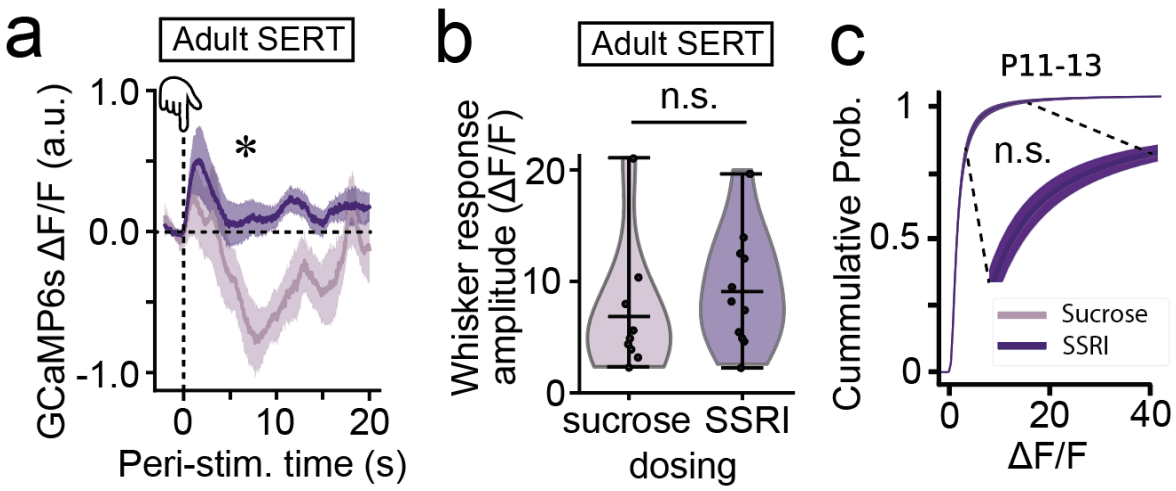

Figure 18. Lack of early hyperactivity at the time of cortical desynchronization in SSRI postnatally treated mice. Animals were dosed orally with either 10% sucrose (control vehicle) or 10 mg/kg of fluoxetine in 10% sucrose (SSRI) daily from P2 to P14, injected neonatally with GCaMP6s, implanted with a cranial window and head-fixing plate at P6 and imaged from P7 to P16 using two-photon head-fixed awake recordings. **a**,**b** Whisker stimulus-triggered average GCaMP6s signal across all cells and mice at P11-13 (**a**,mean signal post-stimulus: t-test p = 0.006) and the corresponding response amplitude (**b,** Mann–Whitney U p = 0.254). **c** Cumulative probability of ΔF/F values during a 20 min baseline of all sucrose/SSRI treated animals at P7-10 (Kolmogorov–Smirnov test: p = 0.253). Sample sizes are 12 (Control) and 12 (SSRI). ΔF/F is the green fluorescence signal at any time point, subtracted and divided by the mean signal across a 20 minute baseline. Mean signal 2s pre-stim was then subtracted to normalize sensory responses. Response amplitude is defined as the maximum fluorescence signal 10s post-stimulus onset.

4.2.2 SSRI postnatally-treated mice interneuron neurophysiology

SERT-KO mice presented hyperactive VIP interneurons throughout development, and SERT-Het showed hypoactive Nkx2-1 interneurons mice during Th-SERT period (chapter 3). The window of SSRI postnatal treatment (P2-14) overlapped with a critical period for the integration of both Nkx2-1 and VIP interneurons in S1BF (Wong et al., 2018, 2022). We speculated that similar alterations would be observable in this pharmacological model, and thereby we performed the analogous experiment in these mice. Analysis of interneuron recruitment in SSRI-treated animals (**Figure 19a**) revealed that VIP interneurons have no changes in H-event amplitude (**Figure 19b**), and an early (<P10) decrease in response amplitude to whisker deflection that switches to an increased response from P13 (**Figure 19c**). Nkx2-1 interneurons showed an increased recruitment during the Th-SERT period (**Figure 19d,e**) followed by hyporesponsiveness during early Adult-SERT (**Figure 19e**). Previous studies suggest that Nkx2-1 developmental overactivation can restrict early cortical activity and accentuate the programmed cell death taking place during this period (Duan et al., 2020; Leighton et al., 2021). Thus, this Nkx2-1 overactivation could be contributing to the early hypoactivity observed. Altogether, while we also observed alterations in Vip/Nkx2-1 interneuron neurophysiology, these were markedly different to the ones observed in SERT-KO mice (**Figure 13**), highlighting the differences between this postnatal pharmacological disruption and the life-long genetic alteration of SERT-KO mice.

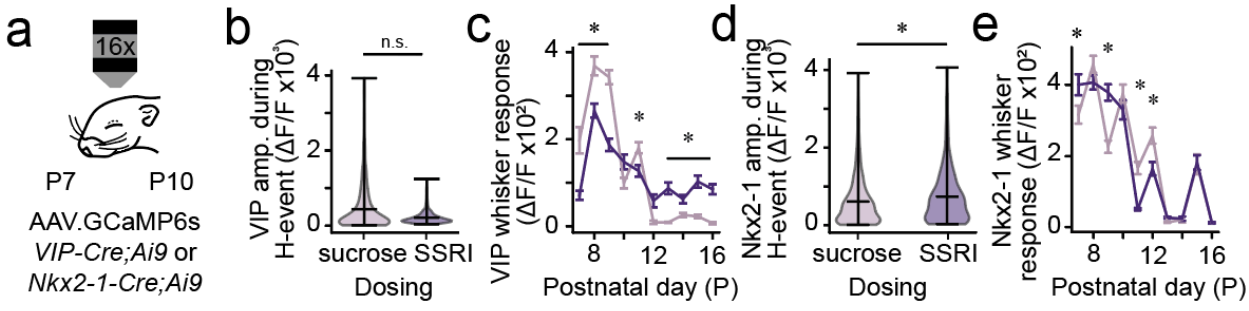

Figure 19. SSRI postnatally-treated mice presents alterations in VIP/Nkx2-1 interneuron neurophysiology a Diagram of experimental settings illustrating the use of transgenic animals with tdTomato in either Vip+ or Nkx2-1+ interneurons to identify GCaMP6s traces from these interneuron subpopulations. These animals were dosed orally with either 10% sucrose (control vehicle) or 10 mg/kg of fluoxetine in 10% sucrose (SSRI) daily from P2 to P14, injected neonatally with GCaMP6s, implanted with a cranial window and head-fixing plate at P6 and imaged from P7 to P16 using two-photon head-fixed awake recordings. **b** H-event VIP+ interneuron GCaMP6s mean amplitude in sucrose- or SSRI-treated pups P7-10 (Mann–Whitney U $p = 0.401$). **c** VIP+ interneuron whisker response GCaMP6s amplitude in SSRI- and sucrose-treated mice across development (*$p<0.05$). **d** H-event Nkx2-1+ interneuron GCaMP6s mean amplitude in sucrose- or SSRI-treated pups P7-10 (Mann–Whitney U $p < 0.001$). **e** Nkx2-1+ interneuron whisker response GCaMP6s amplitude in SSRI- and sucrose-treated mice across development (*$p<0.05$). VIP sample sizes are 870 cells from 5 animals (Control) and 576 cells from 6 animals (SSRI) (b-c), while Nkx2-1 are 1291 cells from 5 animals (Control) and 775 cells from 4 animals (SSRI) (d-e). Amplitude is defined as the maximum fluorescence signal during H-events or 10s post-stimulus onset in the case of whisker responses. Nkx2-1/VIP interneurons were identified by their expression of tdTomato using a 20s two-photon imaging recording with a 765nm excitation wavelength and a red filter.

4.2.3 SSRI postnatally-treated mice cortical population dynamics

Next, we decided to explore how these changes in cortical activity alter information encoding, for which we analysed cortical population dynamics using the same two metrics as in the previous chapter: representational similarity analysis (RSA) and entropy (chapter 3).

First, we used RSA (Kriegeskorte et al., 2008) to estimate how stable the representation of the same stimuli was, as a function of the treatment. In contrast to the results observed in SERT-KO mice, RSA did not reveal any changes in SSRI vs Sucrose treated mice (**Figure 20a-b**). Then, we explored the change in cortical population entropy. This measure from information theory, is used as an estimation of the information encoded by a system. In SSRI postnatally-treated mice we observed a transient increase in entropy at the onset of cortical desynchronization (P11, **Figure 20c-d**). This is of particular interest in light of clinical studies that have previously reported transient developmental increases in the entropy of the parietal cortex in ASD

individuals (Maximo et al., 2021), a condition in which SSRI developmental exposure has been suggested to be a risk factor (Koc et al., 2023; Morales et al., 2018). This increase in entropy could be mechanistically explained by a deficit in inhibition increasing the state space of the circuit (i.e., the number of firing rate combinations in which the neurons integrating the circuit can be). These results differ from our observations in SERT-KO mice (**Figure 13**) suggesting that life-long genetic SERT-KO and transient postnatal pharmacological SERT blockage with SSRIs lead to different perturbations in cortical population dynamics.

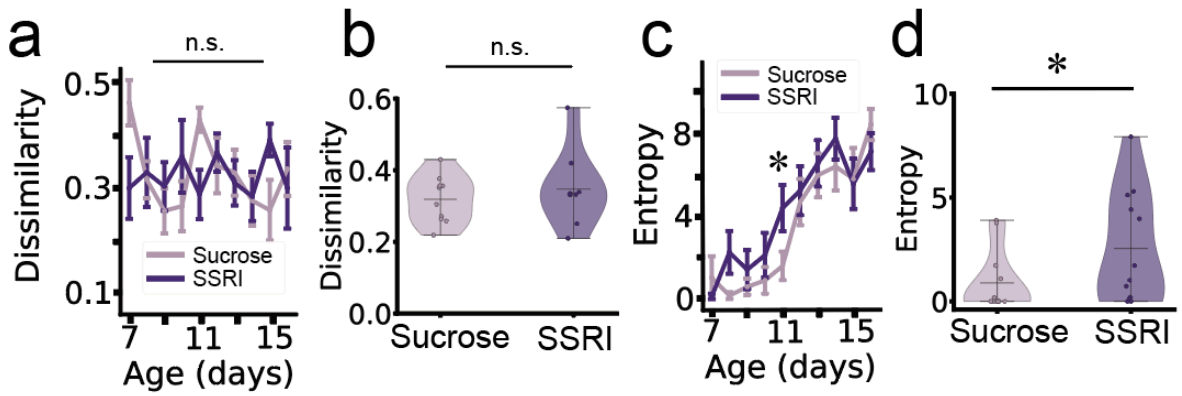

Figure 20. Transient increase in cortical entropy of SSRI postnatally-treated mice. a,b Neonates were dosed orally with either 10% sucrose (control vehicle) or 10 mg/kg of fluoxetine in 10% sucrose (SSRI) daily from P2 to P14, injected neonatally with GCaMP6s, implanted with a cranial window and head-fixing plate at P6 and imaged from P7 to P16 using two-photon head-fixed awake recordings. Representational dissimilarity (i.e., correlation distance) of air puff responses in S1BF across postnatal development (**a,** P7-16) or averaged (**b**) in sucrose- vs SSRI postnatally-treated mice (treatment condition t-test p = 0.691). **c, d** Population entropy across development (**c,** P7-15) and averaged (**d**) in sucrose- vs SSRI postnatally-treated mice (treatment condition Mann-Whitney U test p = 0.041). Entropy is defined as the number of states in which the recorded neurons are found across the whole recording (see methods for more detailed description).

4.2.4 Disruption of glutamatergic co-transmission is not the main driver of early cortical hypoactivity

A previous study demonstrated that perinatal exposure to SSRIs disrupts glutamatergic co-transmission from 5-HT neurons to the VTA, with consequences for motor coordination (Cunha et al., 2021). Thus, we hypothesised that a similar disruption of glutamatergic co-transmission into cortical circuits could be the driver of the early hypoactivity observed in our postnatally SSRI-treated mice. To address this question, we imaged cortical activity through development in animals knocked-out for VGlut3 in SERT+ neurons, a validated model of disrupted glutamatergic co-transmission from 5-HT neurons (Gullino et al., 2024). Thus, we tested whether a disruption of glutamatergic co-transmission could trigger a similar early hypoactivity. During the period of transient SERT expression, knocking out VGlut3 in 5-HT neurons did not alter H- (**Figure 21a-c**) nor L-event (**Figure 21d-f**) features. We also did not observe any differences in whisker stimulus triggered responses (**Figure 21g**) nor in the overall cumulative probability distribution of ΔF/F values over a 20-minute baseline recording (**Figure 21h**). The fact that disruption of glutamatergic co-transmission does not trigger early hypoactivity suggests that this is likely not the driver of the early cortical hypoactivity observed in SSRI postnatally treated mice (**Figure 17**).

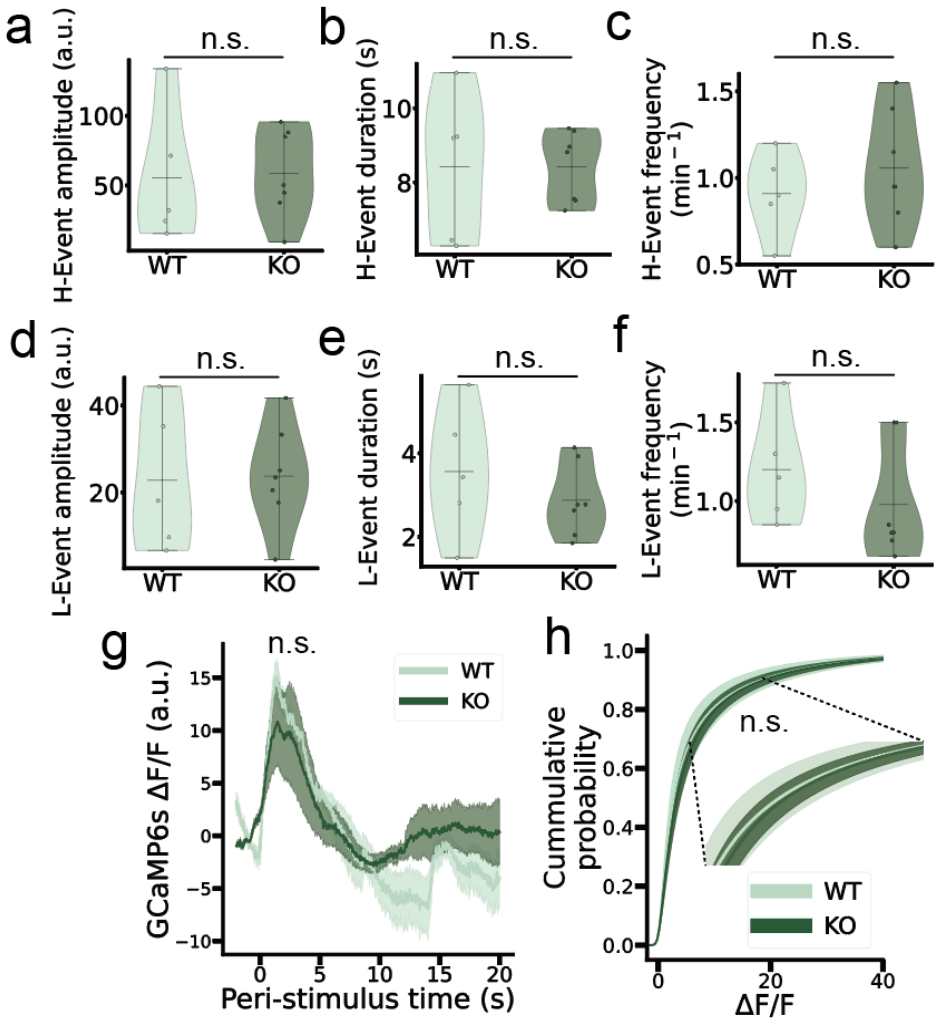

Figure 21. Glutamatergic co-transmission disruption from 5-HT neurons with SERT-Cre-flx-VGlut3 conditional KO does not cause early cortical hypoactivity. Neonates that were VGlut3-KO in SERT-Cre neurons received an intraparenchymal injection of an AAV vector genetically encoding the fluorescence calcium indicator GCaMP6s in S1BF. Then they underwent the implantation of a cranial window, plus a head-fixing plate, at P6 and they were imaged P7-10 using two-photon head-fixed awake imaging. **a**,**b,c** Amplitude (t-test p = 0.878), duration (t-test p = 0.495) and frequency (t-test p = 0.746) of H-events in WT and VGlut3 conditional KO in SERT+ neurons. **d,e,f** Amplitude (t-test p = 0.931), duration (t-test p = 0.344) and frequency (t-test p = 0.934) of L-events in WT and VGlut3 conditional KO in SERT+ neurons. **g** Average calcium trace in response to 10 whisker-deflection stimuli across all cells in the field of view, in WT and VGlut3 conditional KO in SERT+ neurons (Mann-Whitney U test p = 0.533). **h** Cumulative probability of ΔF/F values during a 20-minute baseline of all WT/VGlut3 conditional KO treated animals at P7-10. Sample sizes are 5 (Control) and 7 (VGlut3 conditional KO in SERT+ neurons). ΔF/F is the green fluorescence signal at any time point, subtracted and divided by the mean signal across a 20 minute baseline. Mean signal 2s pre-stim was then subtracted to normalize sensory responses.

4.2.5 Postnatal SSRI exposure causes adult cortical hyperexcitability

Altered 5-HT signalling during development has been linked to life-long deficits in sensory processing (Kepser & Homberg, 2015; Murphy & Lesch, 2008). To explore if this is the case in our transient development SSRI-exposure model, we studied the effects in adult sensory encoding as we had done with SERT-KO mice (**Figure 15**). In brief, we first mapped single barrels using online stimulus-triggered averaging (**Supplementary figure 4a**) and probed adult somatosensory cortical encoding within that field of view by presenting an array of different stimuli: single-whisker, multi-whisker, air puff, sound as well as smooth and rough vibrating surfaces, all of which triggered an average sensory response in cortex, except for sound (**Supplementary figure 4b**). Single-whisker stimulation revealed increases in cortical response amplitude and neuronal recruitment in SSRI-treated mice (**Figure 22a-d**). We observed a similar, but more pronounced, hyperresponsivity upon the presentation of an air puff (**Figure 22e-h**) consistent with a prolonged deficit in inhibitory control of information transfer.

Then, we performed logistic regression analysis (**Figure 22i**), as previously done in SERT-KO mice (chapter 3), to confirm an alteration in cortical dynamics during somatosensory stimulation. Indeed, we observed that postnatal (P2-14) treatment conditions (sucrose vs SSRI) could be classified purely from the cortical responses to somatosensory stimuli (**Figure 22j**), but not baseline nor sound trials. Thus, highlighting a difference in cortical sensory encoding of mice treated with SSRIs postnatally. We conclude that SSRI postnatally-treated mice exhibit S1BF neuronal hyperresponsivity upon somatosensory stimuli, altering sensory encoding.

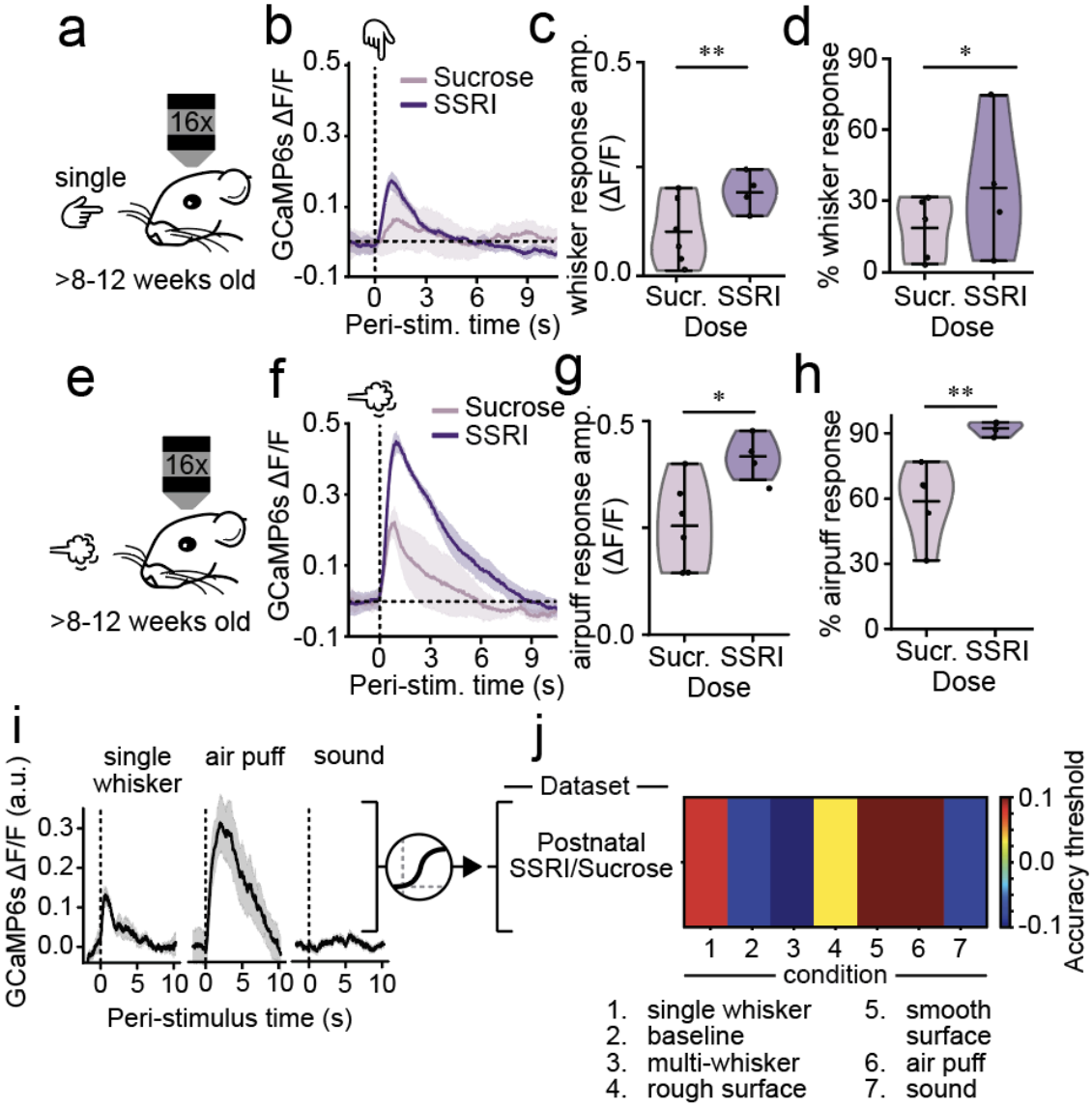

Figure 22. Long lasting cortical hyperexcitability in adult mice postnatally-treated with SSRIs. Mice that had been postnatally (P2-14) treated with either sucrose or fluoxetine, received an intraparenchymal injection of an AAV vector genetically encoding the fluorescence calcium indicator GCaMP6s in S1BF and they underwent the implantation of a cranial window, plus a head-fixing plate to perform two-photon head-fixed awake recordings. **a** Adult mice (8-12 weeks) were exposed to single whisker deflection. **b** GCaMP6s single-whisker stimulus triggered average response to 10 stimuli in sucrose-/SSRI- postnatally treated mice. **c,d** Violin plots of single-whisker stimulus response amplitude (**c,** Mann–Whitney U p = 0.004) and cell recruitment (**d,** t-test p = 0.032) in sucrose- or SSRI- postnatally treated mice. **e** Adult mice (8-12 weeks) were exposed to air puff stimulation**. f,** GCaMP6s air puff stimulus triggered average response to 10 stimuli in sucrose-/SSRI- postnatally treated mice. **g,h,** Violin plots of air puff stimulus response amplitude (**g,** t-test p = 0.046) and cell recruitment (**h,** t-test p = 0.007) in sucrose- or SSRI- postnatally treated mice. **i** Diagram illustrating that post-stimulus calcium

responses to the different stimuli were used for logistic regression analysis. **j** Heat map with the decoding accuracy of the different logistic regression classifiers trained to discriminate across postnatal treatment conditions from the post-stimulus responses of the different types of stimuli. The colour indicates accuracy minus threshold for significance of the classification as defined by bootstrapping. Thus, positive values indicate significant classification accuracy. Sample sizes are 6 (Control) and 4 (SSRI). ΔF/F is the green fluorescence signal at any time point, subtracted and divided by the mean signal across the whole recording. Mean signal 2s pre-stim was then subtracted to normalize sensory responses.Response amplitude is defined as the maximum fluorescence signal 10s post-stimulus onset. Cell responsiveness was addressed by comparing the mean signal pre- and post-stimulus onset across the 10 repeats (paired t-test or Wilcoxon signed-rank test after addressing normality with Shapiro-Wilk test).

4.2.6 SSRI postnatally-treated mice exhibit adult histological alterations in interneuron subpopulations

Given that SSRI-treated mice, similarly to SERT-KO, showed developmental cortical hypoactivity during a critical period for activity-dependent programmed interneuron cell death (Wong et al., 2018, 2022), we hypothesised that the adult cortex of these mice would also have a reduction in MGE-derived interneurons. Moreover, a recent study suggested that postnatal SSRI exposure during an overlapping window of time (P7-10) increases the survival of bipolar 5-HT_{3A}R-expressing interneurons (VIP-expressing) (Wong et al., 2022). To test the effect of our treatment settings (P2-14) in MGE and CGE interneuron survival, we quantified interneuron numbers in S1BF using histology for VIP(tdTomato) and Nkx2-1(tdTomato) alongside automated DAPI cell detection (**Figure 23a; Supplementary figure 5**). We identified a decrease in Nkx2-1 interneuron survival across the depth of cortex in SSRI postnatally-treated mice, particularly significant at L2/3 (**Figure 23b**). We also reproduced the previously observed increased VIP interneuron survival (**Figure 23b**) in SSRI postnatally-treated mice. These results further support that early 5-HT increases and impaired H-events lead to increased MGE-derived interneuron apoptosis. Thus, the increase in disinhibitory neurons (VIP interneurons (Kullander & Topolnik, 2021)) concomitant with a decrease in the major subpopulation of cortical inhibitory

neurons (Nkx2-1 interneurons) are likely the drivers of the adult hyperexcitability observed (**Figure 22**).

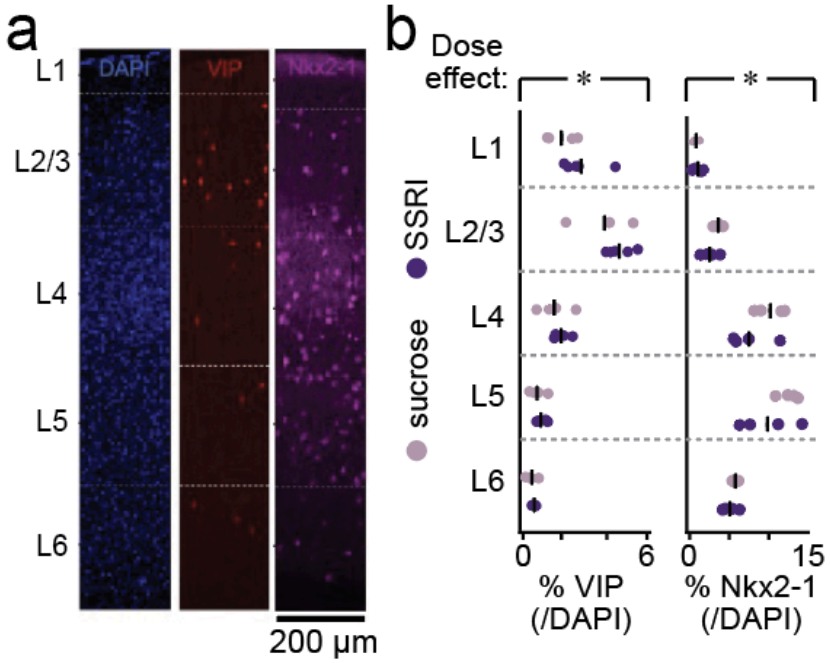

Figure 23. SSRI postnatal treatment leads to increased VIP and decreased Nkx2-1 interneuron survival in S1BF. a Confocal histological image of a S1BF cortical column (200 µm wide) on an adult (>8 weeks old) WT cortex, illustrating DAPI (blue, left), VIP (cyan, centre) and Nkx2-1 (magenta, right) layer distribution. VIP and Nkx2-1 were labelled by using transgenic VIP- or Nkx2-1-Cre mice crossed with Ai9 (flx-tdTomato) mice. **b** Biodistribution of VIP (Two-way ANOVA: treatment $p = 0.032$, layer $p < 0.001$, treatment-layer interaction = 0.691) and Nkx2-1 (Two-way ANOVA: treatment $p = 0.032$, layer $p < 0.001$, treatment-layer interaction = 0.789) interneurons across layers for sucrose- or SSRI- postnatally treated mice. Sample sizes: 5 sucrose and 4 SSRI mice.

4.3 Conclusions

Our findings reveal that postnatal SSRI exposure leads to early cortical hypoactivity, marked by a reduction in the amplitude and an increase in the frequency of H-events in the developing cortex (<P10) (**Figure 17**). This period of hypoactivity aligns with a critical developmental window for the integration of Nkx2-1 and VIP interneurons into S1BF (Wong et al., 2018, 2022). Analysis of these interneuron populations showed that SSRI-treated mice exhibited an increased recruitment of Nkx2-1 interneurons early on (**Figure 19**), which based on previous

studies could be contributing to the observed hypoactivity by restricting cortical activity (Leighton et al., 2021) and subsequently promoting programmed cell death (Duan et al., 2020). While alterations in VIP and Nkx2-1 interneuron activity were observed, these changes differed from our previous findings in SERT-KO mice, indicating distinct effects of SSRI 5-HT disruption during postnatal development.

The analysis of cortical population dynamics revealed no significant changes in representational similarity but identified a transient increase in entropy at the onset of cortical desynchronization (**Figure 20**), a pattern that has been noted in certain neurodevelopmental disorders such as ASD (Maximo et al., 2021). Alterations in brain entropy are also observed in OCD (Jiang et al., 2021), ADHD (Sato et al., 2013) and MDD (X. Liu et al., 2020) patients, all of which are also associated with developmental 5-HT alterations (Beversdorf et al., 2021; Brown et al., 2013; Hesse et al., 2011; Morales et al., 2018, 2018; Nicolini, 2010). This suggests that early alterations in 5-HT levels can affect the stability and diversity of cortical activity patterns, possibly leading to long-term changes in brain function.

Our results also demonstrate that the early cortical hypoactivity observed in SSRI-treated mice is not due to disrupted glutamatergic co-transmission from 5-HT neurons (**Figure 21**), as previously observed in VTA upon perinatal SSRI exposure (Cunha et al., 2021). This suggests that other mechanisms, likely through direct 5-HT signalling, are at play. It has been reported that SERT developmental disruption inhibits S1BF thalamocortical activity through 5-HT_{1B} receptors (Cases et al., 1996; Laurent et al., 2002; Salichon et al., 2001), suggesting that 5-HT direct inhibition of thalamocortical projections might be a major driver of this early cortical hypoactivity. This is supported by the transient overexpression of 5-HT_{1B} receptors in thalamocortical projections to S1BF (Laurent et al., 2002). In adulthood, SSRI postnatally-treated mice exhibit persistent cortical hyperexcitability and altered sensory

processing (**Figure 22**), with increased survival of VIP interneurons and decreased survival of Nkx2-1 interneurons (**Figure 23**). This shift in interneuron balance likely contributes to the long-lasting changes in cortical excitability and sensory encoding observed.

The fact that transient SSRIs, but not life-long SERT-KO, cause adult hyperexcitability suggest that a reversible alteration of 5-HT dynamics is more detrimental. One possible explanation is that the establishment of excitation-inhibition balance taking place during this critical period depends on 5-HT dynamics too, such that once 5-HT dynamics revert to baseline, the inhibition levels established are insufficient in SSRI postnatally-treated animals. Another explanation is that the increase in VIP+ interneurons observed in SSRI postnatally-treated, but not SERT-KO, mice is the major driver of the hyperactivity, given their disinhibitory role (Kullander & Topolnik, 2021). Altogether, we report similarities between the effects of SSRI postnatal-treatment and SERT-KO (i.e., early cortical hypoactivity), but with idiosyncrasies, such as the long-lasting neurophysiological effects of the former. These differences likely stem from the temporal difference of these SERT disruptions (postnatal versus life-long) and the nature of the disruption (genetic versus pharmacological).

Finally, these findings have important clinical implications. Given that SSRIs are widely prescribed (Luo et al., 2020), including during pregnancy and postpartum, understanding their impact on early brain development is crucial. The results suggest that transient exposure to SSRIs during critical developmental periods can lead to significant and lasting changes in cortical circuitry, adding pre-clinical evidence to the previously suggested association between embryonic exposure to SSRIs and neurodevelopmental disorders (Ames et al., 2021; Koc et al., 2023; Morales et al., 2018; Suarez et al., 2022).

5. The role of 5-HT in adult cortical dynamics and learning

5.1 Introduction

In previous chapters, we have identified a prominent role of cortical 5-HT fluctuations in early S1BF activity and subsequently its development (chapter 2-4). Next, we explored the role of 5-HT dynamics in the adult S1BF cortex, and its subsequent shaping of behaviour.

Previous studies in rodents have characterised the neurophysiology and behaviour of adult animal models with life-long genetic alterations in 5-HT dynamics (i.e., SERT-KO, TPH2-KO), and identified disruptions in sensory responses (W. Pan et al., 2021), sleep-wake (Wisor et al., 2003), learning (C. C.-G. Guo et al., 2021; Lima et al., 2019), anxiety (Aboagye et al., 2018; Johnson et al., 2019) and aggression (Meng et al., 2022; Mosienko et al., 2012). However, these results are likely confounded by the developmental alterations of these models (introduction, chapter 3 & 4). With the advent of optogenetic approaches a number of acute studies have characterised the role of 5-HT manipulation in adult neuronal activity (Azimi et al., 2020; Puig & Gener, 2015; Seillier et al., 2017), behaviour (Dugué et al., 2014; K. W. Miyazaki et al., 2014) and learning (Grossman et al., 2022; Iigaya et al., 2018; Michely et al., 2022). Studies in rodents and non-human primates suggest that 5-HT has a predominantly inhibitory effect on spontaneous activity of adult cortices, and exerts gain-control of sensory-evoked activity (Azimi et al., 2020; Lottem et al., 2016; Puig & Gener, 2015; Seillier et al., 2017; Tian et al., 2017), with a minority of studies reporting excitatory effects (Hamada et al., 2022; Puig & Gener, 2015). 5-HT manipulations yield a complex mixture of effects in behaviour and learning, including changes in aggression (Audero et al., 2013), social interaction (Zou et al., 2020) or

patience (K. W. Miyazaki et al., 2014), as well as increases and decreases in learning (Grossman et al., 2022; Iigaya et al., 2018; Michely et al., 2022). A major confounding factor of the majority of these studies is that they perform bulk optogenetic activation of the dorsal raphe nucleus. Thus, the complexity of the results can be understood in light of the great heterogeneity of the mammalian 5-HT system, particularly in terms of postsynaptic targets (Okaty et al., 2019). For example, the fact that the VTA is excited by DRN-projections (H.-L. Wang et al., 2019) implies that bulk DRN optogenetic activation will concomitantly trigger dopamine increases. Moreover, a majority of these studies have employed activity monitoring techniques that also lack cellular resolution such as 1-photon calcium imaging (Azimi et al., 2020) or fMRI (Hamada et al., 2022). More precise manipulation of 5-HT circuits and recording in particular projection targets is required to understand the role of 5-HT in cortical circuits. For this purpose, we used optogenetic stimulation of 5-HT terminals in S1BF to study the neurophysiological and behavioural effects of 5-HT in the somatosensory cortex.

Understanding the effects of 5-HT within cortical circuits is crucial to make sense of the involvement of this monoamine in translationally relevant contexts. For example, how SSRIs influence 5-HT dynamics, and its involvement in the therapeutic effect of these drugs, has been extensively characterised (Blier & de Montigny, 1994; Celada et al., 2004; Celada & Artigas, 1993; Collins et al., 2024; Fritze et al., 2017). Less well known is the effect of psychedelics in 5-HT dynamics and its involvement in their use to treat depression and addiction (Korkmaz et al., 2024). A number of studies from 50 years ago, described that 5-HT psychedelics such as LSD and psilocin decrease the tonic firing of 5-HT neurons (Foote et al., 1969; Rogawski & Aghajanian, 1979; Trulson & Jacobs, 1979). But how this affects cortical 5-HT dynamics and whether it is involved in the therapeutic role of psychedelics remains unexplored. Thus, we extend our optogenetic study of the effects of cortical 5-HT in adult neurophysiology and

behaviour, to a pharmacological translationally-relevant model: acute exposure to 5-HT psychedelics.

5.2 Results

5.2.1 5-HT effects in adult S1BF cortical activity

To circumvent the lack of spatial resolution in previous studies, we have used two-photon imaging of a red calcium indicator (jRCaMP1a) (Dana et al., 2016) in S1BF with simultaneous holographic two-photon stimulation of 5-HT axonal projections to S1BF (**Figure 24a**). For this, we have used SERT-Cre animals injected with jRCaMP1a and g5-HT3.0 in S1BF, as well as the opsin flex-Chrimson in the DRN. This ensures high spatial resolution in both the recording and the stimulation. While we cannot rule out the possibility of a certain degree of antidromic activation leading to 5-HT increases in other areas, we maximise the likelihood of locally-constrained release of 5-HT in S1BF, by only activating terminals within our field of view (**Figure 24a**). Then, we confirmed the local release of 5-HT with the green 5-HT fluorescence indicator g5-HT3.0 (**Appendix 6**). As a control, we used WT littermate mice that underwent the same surgical and imaging procedures, but that did not express the opsin due to the lack of cre recombinase.

Given the complexity of the 5-HT receptome across the cortical column (e.g., 5-HT_{3A}R-expressing interneurons primarily populate upper layers (Prönneke et al., 2015) while 5-HT_{2A}R is preferentially found in L5 pyramidal neurons (Andrade & Weber, 2010)), we performed recordings with local optogenetic stimulation of 5-HT axons at two cortical depths: 150 µm (L2/3) and 350 µm (L4) from the surface of the brain. Recordings in L2/3 showed a mixed response of excitation and inhibition with an average flat response (**Figure 24b,d**) while recordings in L4 showed a strong suppression of calcium signal (**Figure 24c-d**). The canonical

model of sensory processing in cortex identifies L4 as the primary thalamo-recipient layer, while L2/3 integrates feed-forward excitation from L4 with cortico-cortical inputs (Miller, 2016). Thus, our imaging is consistent with 5-HT having a suppressive effect in the thalamo-recipient layer of cortex, down-scaling bottom-up activity. These results align with previous studies suggesting that 5-HT leads to gain-control of cortical sensory responses (Azimi et al., 2020; Lottem et al., 2016; Seillier et al., 2017). In light of the previously described excitation of VIP interneurons (involved in top-down control (Bastos et al., 2023; Schuman et al., 2021; S. Zhang et al., 2014)) by 5-HT (Férézou et al., 2002), an interpretation of these results is that 5-HT promotes top-down over thalamo-cortical (bottom-up) information transfer (**Figure 24e**).

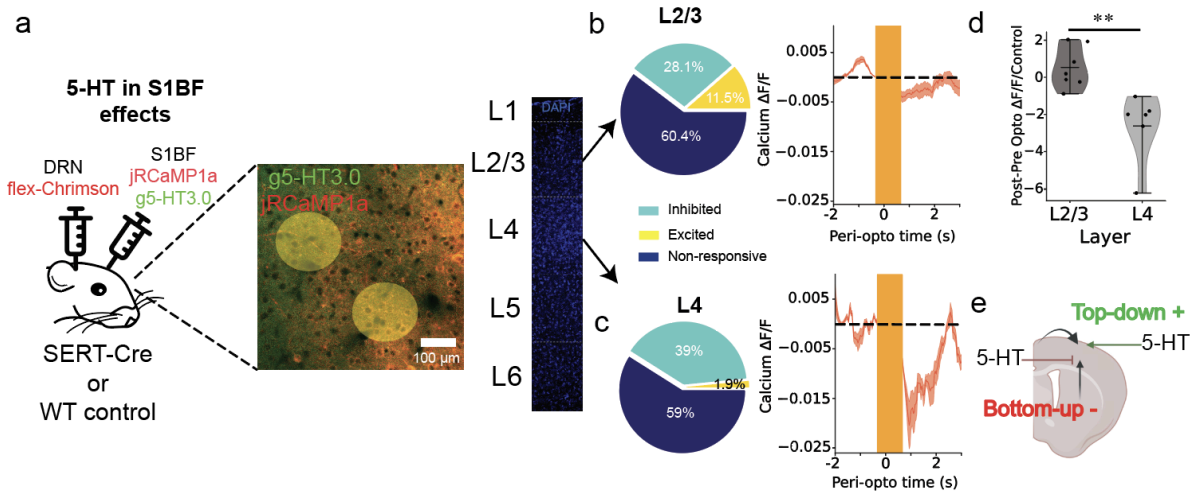

Figure 24. 5-HT inhibits S1BF L4 spontaneous activity. a (left) Diagram illustrating surgical approach for all-optical experiments: DRN intraparenchymal injection of an AAV vector genetically encoding the floxed opsin flex-Chrimson into S1BF and S1BF intraparenchymal injection of an AAV vector encoding the red calcium sensor jRCaMP1a and another AAV vector encoding the green 5-HT sensor g5-HT3.0 in SERT-Cre animals. These animals also received a cranial window and head-fixing plate implantation. Then, two-photon imaging of S1BF in awake head-fixed animals was used to record calcium and 5-HT dynamics, while two-photon holographic stimulation was used to activate 5-HT terminals that innervated S1BF. g5-HT3.0 injection was used to confirm 5-HT release (Appendix 6). Control animals were WT mice that underwent the same surgical and imaging procedure but did not express Chrimson due to the lack of cre recombinase. (right) Representative field of view, with holographically stimulated area with a 1040 nm laser, to release 5-HT within our field of view. **b** (left) Pie chart illustrating excited (11.5%), inhibited (28.1%) and non-responsive (60.4%) cells within the whole field of view of all animals (n = 7 mice, cells =121) and (right) the average response in L2/3. **c** (left) Pie chart

illustrating excited (1.9%), inhibited (39%) and non-responsive (59%) cells within the whole field of view of all animals (n = 7 mice, cells = 105) and (right) the average response in L4. **d** Average response in L2/3 and L4, normalised by changes in control animals (SERT-Cre negative littermates) (Mann-Whitney U statistic=42.0, p=0.0012, n = 7 opsin-expressing animals and n = 4 non-opsin expressing control animals). ΔF/F is the green fluorescence signal at any time point, subtracted and divided by the mean signal across the whole recording. Mean signal 2s pre-stim was then subtracted to normalize sensory responses. Response amplitude is defined as the maximum fluorescence signal 10s post-stimulus onset.

5.2.2 An air puff discrimination task to study S1BF 5-HT

To study how these effects of 5-HT balancing of bottom-up versus top-down integration in S1BF cortex translated to behaviour and learning, we developed a behavioural paradigm that captured several elements of 5-HT dynamics: sensation (Ranade & Mainen, 2009), stimulus saliency (Paquelet et al., 2022) and uncertainty (Grossman et al., 2022). We used a Pavlovian air puff discrimination task that has been shown to trigger neuroplastic changes in S1BF, in which water-deprived mice learn to associate one of two, orthogonally oriented, air puffs with water-delivery (**Figure 25a**) (Benezra et al., 2024). To study the effects of uncertain information, during this 10 day learning paradigm, we introduced two days (5 and 7) in which the opposite rule provided misleading trials with a prevalence of 25% (**Figure 25b,c**). To study the effect of stimulus saliency, the first misleading day (i.e., day 5) air puff pressure was kept the same as in previous days (10 PSI), while in the second misleading day (i.e., day 7) air puff pressure was 5 times higher (50 PSI) (**Figure 25c**). Based on our previously observed 5-HT dynamics (chapter 2) and its inhibitory effects in L4 (**Figure 24**), we hypothesised that while misleading trials would disrupt learning as a function of their saliency (i.e., stimulus pressure), 5-HT dynamics would track these learning perturbations and mitigate their effect on learning.

As previously reported (Benezra et al., 2024), we were able to train animals in this task within 10 days, during which animals first licked in response to both air puffs, and then progressively

started to lick only to the rewarded stimulus (CS+) (**Figure 25d and Supplementary figure 7**), which correlated with changes in cortical calcium dynamics (**Supplementary figure 8a-i**). When stimulus saliency was kept constant, we observed that 25% of misleading trials had no effect on next day performance (**Figure 25e**), suggesting that mice could account for this degree of reward uncertainty in this task environment. In contrast, at high stimulus saliency, 25% misleading trials significantly decreased next day performance (**Figure 25f**). This suggests that the higher stimulus saliency, triggered an increase in learning rate, making the animal overfit to misleading trials.

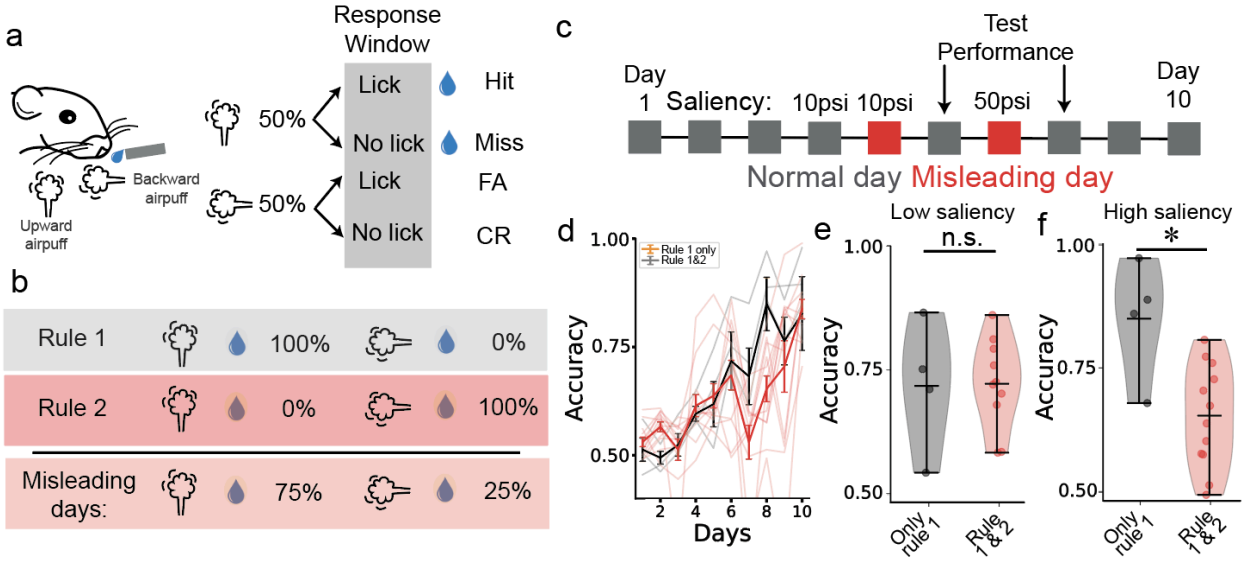

Figure 25. An air puff discrimination task with misleading information a. Diagram of mice performing a head-fixed pavlovian air puff discrimination task in which only one of two orthogonal directions is associated with reward, with equal trial probability. **b.** Reward probability for each air puff based on each rule, and the combination of both in misleading days, with a 25% prevalence of rule 2. **c.** Diagram of behavioural paradigm indicating the misleading days, 5 and 7, and their corresponding stimulus pressure (i.e., salience), which is 10 and 50 PSI respectively. **d.** Task accuracy (i.e., % of hits and correct rejections) across learning days for animals with (red) and without (black) misleading days (Rule 1 only n = 4 mice, rule 1 & 2 n = 11 mice). **e.** Accuracy on day 6, i.e., the day after low saliency misleading trials (Mann-Whitney U test p-value = 0.605). **f.** Accuracy on day 8, i.e, the day after high saliency misleading trials. (Mann-Whitney U test p-value =0.033). Accuracy was defined as the sum of hit and correct rejection (CR) trials, divided by total number of trials. A hit trial was considered if the animal licked after CS+ stim onset, but before reward delivery (0.5s after).

5.2.3 S1BF 5-HT tracks behaviourally-relevant environment statistics

Next, we used the 5-HT sensor g5-HT3.0 to track the evolution of 5-HT release into the same cells of L2/3 S1BF across 3 learning stages of this task (naive, learning and expert) (**Figure 26a,b**). We observed an increase in 5-HT release paired with reward during CS+ (compared to CS-) in naive animals, that then decreased across learning (**Figure 26c,d**). Introduction of low saliency misleading trials that did not disrupt learning (**Figure 25e)** did not alter the lack of 5-HT release upon reward at this learning stage to neither expected (rule 1) nor unexpected (rule 2) trials (**Figure 26e**). However, high stimulus saliency misleading trials that disrupt learning (**Figure 25f**) led to high 5-HT release, which was longer lasting during unexpected (rule 2) rewards (**Figure 26f**). These results show that 5-HT release in S1BF tracks the regularity of different behaviourally-relevant stimulus statistics, such as its magnitude or its association to reward, across learning, with higher release during salient uncertain settings.

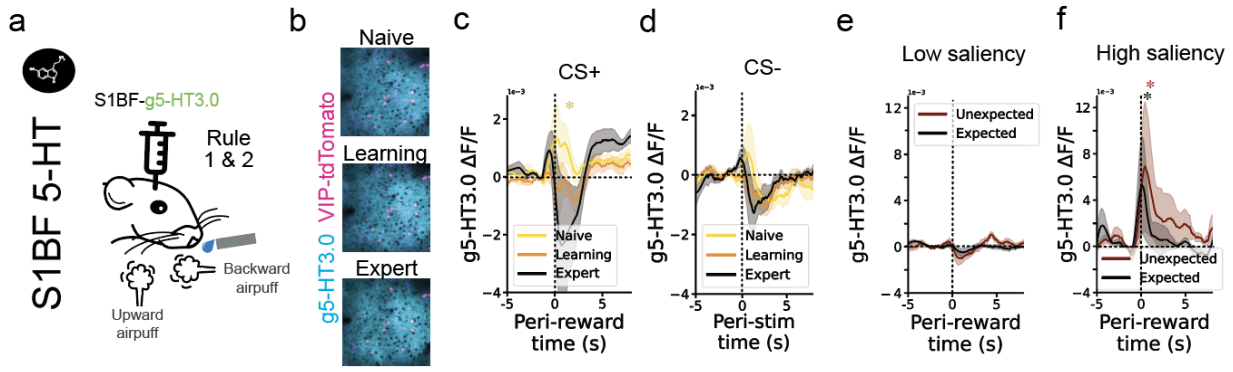

Figure 26. Cortical 5-HT tracks behaviourally-relevant environment statistics. Adult mice performed a head-fixed pavlovian air puff discrimination task in which only one of two orthogonal directions is associated with reward, with equal trial probability, and misleading trials in which this rule was inverted. **a.** Diagram of g5-HT3.0 5-HT fluorescence sensor injection in S1BF to monitor 5-HT dynamics in awake head-fixed animals performing the air puff discrimination task. **b** Exact same field of view in a representative animal expressing g5-HT3.0 under the hSyn promoter and tdTomato in VIP interneurons, across three learning stages (day 3 naive, day 6 learning and day 10 expert). **c** g5-HT3.0 peri-reward signal for naive, learning and expert animals, showing only significant increases to reward during naive state (post- vs pre- mean signal, paired t-test : naive p = 0.004, learning p = 0.07 and expert p = 0.255). **d** g5-HT3.0 peri-stimulus onset signal for naive, learning and expert animals, during CS- trials. **e.** g5-HT3.0

peri-reward signal during day 5 (i.e., low saliency misleading day), for expected (rule 1) and unexpected (rule 2) rewards. **f.** g5-HT3.0 peri-reward signal during day 7 (i.e., high saliency misleading day), for expected (rule 1) and unexpected (rule 2) rewards. N = 6 mice. For all panels ΔF/F is the ratio between the green and red fluorescence signal at any time point, subtracted and divided by the mean ratio across the whole recording. Mean signal 5s pre-stim was then subtracted to normalize stimulus-locked responses.

5.2.4 Cortical 5-HT decreases learning from misleading information

Given 5-HT downregulation of bottom-up activity (**Figure 24)**, and the fact that 5-HT dynamics track the uncertainty and saliency of the disruptive misleading trials (**Figure 26**), we speculated that 5-HT could be gating sensory input from uncertain information that can disrupt learning trajectories, thus downregulating the learning from these trials. To test this hypothesis we used SERT-Cre mice injected with the opsin flex-Chrimson (**Figure 27a**) in the DRN, allowing to optogenetically stimulate 5-HT neurons. We used one-photon optogenetics with light shed directly into S1BF, to maximise the release over this area. Thus, misleading trials were paired with the presentation of an orange (595 nm) light on top of S1BF (through a cranial window) to induce 5-HT release (**Supplementary figure 8j-l**). Firstly, we characterised the effect of this optogenetic 5-HT release on S1BF cortical calcium dynamics. We observed that the proportion of excited and inhibited neurons was unchanged for CS+ (**Figure 27b**), while a higher inhibition and reduced excitation was observed in CS- (**Figure 27c**). This result illustrates that the effect of 5-HT release depends on other variables (e.g., reward). Given the role of VIP interneurons, that are excited by 5-HT (Férézou et al., 2002), in the cortical signalling of reward (Szadai et al., 2022) and in top-down modulation (Bastos et al., 2023; Fu et al., 2014; S. Lee et al., 2013), this effect only in CS- could be underlied by a mixture of bottom-up and top-down sources of activity in L2/3 during CS+, with 5-HT gating the former and potentiating the latter.

Secondly, we studied the effects of 5-HT release during misleading trials in performance. Behavioural analysis revealed that 5-HT optogenetic release during low saliency misleading trials did not change next day performance in the task (**Figure 27d**), consistent with the fact that these misleading trials were not altering the behaviour. These results suggest that the mice were able to ignore them. Moreover, 5-HT optogenetic release during high-saliency misleading trials rescued the learning disruption generated by these trials (**Figure 27e**), providing causal evidence of the role of cortical 5-HT in decreasing internal model update from potentially-disruptive misleading predictive errors. Notably, the effects were limited to learning and not trial performance (i.e., within trial probability of lick, **Supplementary figure 9**), which can be understood in the light of a larger literature proposing that the cortex plays a key role in learning actions but not performing them (Kawai et al., 2015; Ostlund & Balleine, 2005). Altogether these results provide causal evidence of 5-HT modulation of bottom-up and top-down activity to control cortical learning rate from sensory experience.

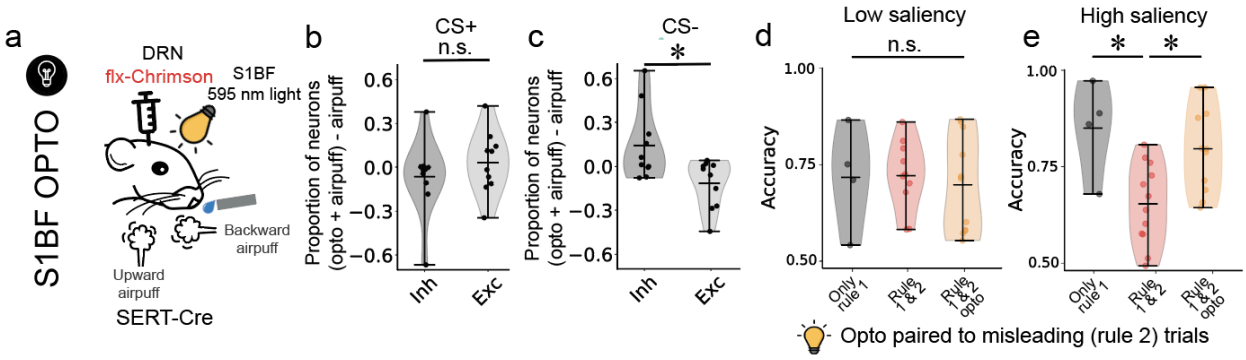

Figure 27. S1BF 5-HT decreases learning from misleading information a Diagram of optogenetic experimental settings, illustrating the intraparenchymal injection of a viral vector genetically encoding flex-Chrimson into the DRN of SERT-Cre mice and the application of 595 nm light (20 Hz pulses) directly in S1BF through a cranial window. These mice performed a head-fixed pavlovian air puff discrimination task in which only one of two orthogonal directions is associated with reward, with equal trial probability, and misleading trials in which this rule was inverted. Light was delivered paired to misleading trials. **b,c** Violin plot showing the change in cells inhibited and excited upon pairing the air puff with optogenetic stimulation, compared to just the air puff for (**b**) CS+ (Wilcoxon signed-rank test p = 0.922, n = 11 mice) and (**c**) CS- (Wilcoxon signed-rank test p = 0.048, n = 11 mice). Cell responsiveness was addressed by comparing the mean signal pre- and post- optogenetic light onset across all repeats (paired

t-test or Wilcoxon signed-rank test after addressing normality with Shapiro-Wilk test). (**d**) Accuracy on day 6, i.e., the day after low saliency misleading trials (One-way ANOVA p = 0.862). (**e**) Accuracy on day 8, i.e, the day after high saliency misleading trials. (One-way ANOVA p=0.021, post hoc: rule 1&2 vs rule 1&2 with optogenetics p = 0.021; rule 1 vs rule 1&2 with optogenetics p = 0.486). Rule 1&2 animals were SERT-Cre negative, thus not expressing the opsin, but were presented with the optogenetic light too as a control. Control data from panels d,e is the same as the data in panels e,f of figure 25. Rule 1 only n = 4 mice, rule 1 & 2 n = 11 mice, rule 1 & 2 opto n = 11 mice). Accuracy was defined as the sum of hit and correct rejection (CR) trials, divided by total number of trials. A hit trial was considered if the animal licked after CS+ stim onset, but before reward delivery (0.5s after).

5.2.5 Psychedelics decrease cortical 5-HT and increase learning

Then, we went onto studying whether a similar gating mechanism could account for the effects of altering cortical 5-HT dynamics beyond physiological learning. Of particular interest are 5-HT psychedelics, i.e., 5-HT agonists, with therapeutic potential for the treatment of depression and addiction (Korkmaz et al., 2024). A number of studies have described that 5-HT psychedelics decrease the tonic firing rate of 5-HT neurons in the dorsal raphe nuclei (Foote et al., 1969; Trulson et al., 1981; Trulson & Jacobs, 1979), which is likely due to the strong inhibitory feedback of the 5-HT system. Thus, we sought to confirm that this decrease in 5-HT firing, reduced S1BF 5-HT release. Indeed, intraperitoneal injection of the psychedelics LSD and psilocin, as well as the non-hallucinogenic analogue lisuride all caused a significant reduction in extracellular S1BF 5-HT, compared to vehicle injection (**Figure 28a,b**), as measured by the fluorescence 5-HT sensor g5-HT3.0.

In line with our model, we speculated that this decrease in 5-HT would lead to more dominant bottom-up versus top-down activity and increase the learning rate at which the internal model of the animal is updated from sensory experience. To test this, we trained animals that were experts in the previous air puff discrimination task in the reversal rule (i.e., reward associated with previous CS- and *vice versa*) 1h after injection of psilocin or vehicle control (**Figure 28c**).

We observed a recovery of increased 5-HT release in response to reward during CS+ (**Supplementary figure 10**) as observed in the previous task in naive animals (**Figure 25**).

Next, we looked at the effects of psilocin on cortical calcium dynamics. We observed a reduction in CS+ rewarded responses (**Figure 28d,e**) but not CS- sensory responses (**Figure 28f,g**) in psilocin- versus vehicle-injected animals. These results can be explained if the effects of reward in S1BF activity are mediated by 5-HT signalling of VIP interneurons (Szadai et al., 2022), while CS- responses are predominantly sensory bottom-up information. The reduction in S1BF 5-HT upon psychedelic administration would reduce VIP reward responses justifying the reduction in the overall calcium S1BF signal. Representational similarity analysis also revealed an increased representational dissimilarity in the cortical encoding of CS+ and CS- stimuli in psilocin-treated mice (**Figure 28h,i**). These results suggest that psilocin-treated mice have cortical representations of these two air puffs that are more distinct from each other, which is consistent with an increased differentiation of these stimuli and potentially beneficial for the performance of a discrimination task.

Then, we looked at the effects of psilocin on behaviour, i.e., task performance. Reversal of task contingencies led to animals reverting to their initial strategy of licking to both CS- and CS+ (**Figure 28j,k**). We observed that psilocin-treated mice have increased next-day accuracy in the reversal task (**Figure 28l,m**), driven by an increased licking in response to CS+ trials (**Figure 28n,o**). These results are consistent with previous studies illustrating the neuroplastic role of psychedelics (de Vos et al., 2021; Woodburn et al., 2024). The fact that the non-hallucinogenic analogue lisuride presents 5-HT decreases suggests that this 5-HT reduction is likely not a driver of the hallucinogenic effect of psychedelics. However, lisuride also has antidepressant effects (Qu et al., 2023), suggesting that 5-HT reduction in cortex could be a contributing

element to the neuroplasticity induced by these drugs. Thus, these results provide correlative evidence in favour of decreases in cortical 5-HT leading to increases in learning rate.

Altogether, the effect of psychedelics on 5-HT dynamics, cortical activity and reversal learning, are consistent with the suggested role of 5-HT in balancing bottom-up and top-down activity to regulate the learning rate of internal model update. However, the multifactorial effects of these drugs (de Vos et al., 2021) requires more spatially localised reductions in cortical 5-HT (e.g., inhibitory opsins (Mahn et al., 2021)) to causally link the decrease in 5-HT with the observed effects in cortical activity and learning.

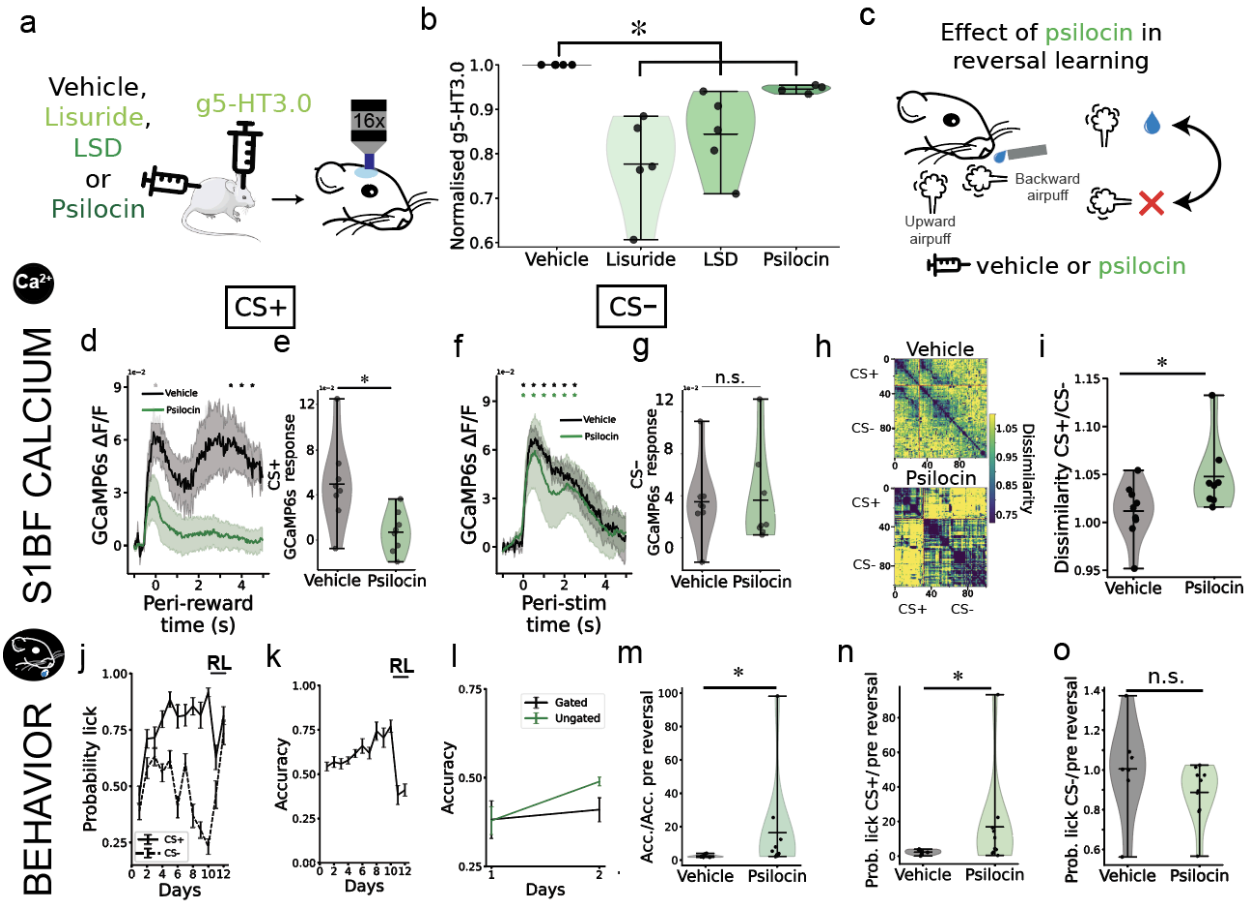

Figure 28. Psychedelics decrease cortical 5-HT while increasing representational dissimilarity and reversal learning. Adult mice received intraparenchymal injection of an AAV vector genetically encoding the 5-HT sensor g5-HT3.0 or the calcium indicator GCaMP6s into S1BF, followed by the implantation of a head-fixing plate and a cranial window. Two-photon head-fixed awake imaging was used to monitor calcium and 5-HT dynamics. g5-HT3.0 was injected in transgenic animals expressing tdTomato in VIP interneurons (VIP-Cre x Ai9) to account for intrinsic optical noise. **a** Diagram of experimental timeline: mice were injected intraperitoneally with the drug vehicle (control), then g5-HT3.0 signal in L2/3 was recorded for 20 minutes. After 5-10 minutes, mice were injected intraperitoneally with a psychedelic (psilocin or LSD), or the non-hallucinogenic analogue lisuride, and g5-HT3.0 was imaged again for 20 minutes. **b** Vehicle-normalised g5-HT3.0 signal across a 5 minute baseline recording post-injection of either vehicle, lisuride (n = 5), LSD (n = 5) or psilocin (n = 4) (Kruskal Wallis test p = 0.036, paired t-test against vehicle: lisuride p = 0.010; LSD p = 0.018; psilocin p = 0.001). g5-HT3.0 is the raw green fluorescence normalized by the mean value after vehicle injection. **c** Experimental set-up: mice were trained two consecutive days in the reversal task of the previously described air puff discrimination task once they reached expertise in the original task (accuracy over 75%). During the first day of reversal learning animals were injected with either vehicle (n = 8) or psilocin (n = 8) 1h before training. **d** Mean calcium trace during CS+ trials in S1BF L2/3 after treatment with vehicle or psilocin. **e** Violin plot illustrating a change in mean (0 to 5s after reward onset in CS+trials) GCaMP6s signal (t-test, p = 0.012) in vehicle- versus psilocin-treated mice. **f** Mean calcium trace during CS- trials in S1BF L2/3 after treatment with vehicle or psilocin. **g** Violin plot illustrating the lack of a change in mean (0 to 5s after CS- stimulus onset) GCaMP6s signal (t-test, p = 0.164) in vehicle- versus psilocin-treated mice. **h** Heat map of representative representational dissimilarity matrices to CS+ and CS- in a vehicle (top) and psilocin (bottom) treated mice. **i** Average representational dissimilarity of CS+ and CS- L2/3 S1BF representations for vehicle and psilocin treated mice (Mann-Whitney U test, p = 0.027). **j** Animal lick probability to CS+ and CS- across a 10 days learning paradigm, followed by a two days of reversal learning. **k** Evolution of accuracy across both learning and reversal learning paradigms. **l** First and second day mice average accuracy after treatment with psilocin (green) or control vehicle (black). **m** Second day accuracy (day 12) in the reversal task of mice treated with vehicle or psilocin, normalised by accuracy in previous task pre-reversal (day 10) (Mann-Whitney U test, p = 0.013). **n,o** Second reversal day (i.e., day 12) probability of licking, normalised by probability pre-reversal (day 10), to CS+ **(n)** (Mann-Whitney U test, p = 0.043) or CS- **(o)** (t-test, p = 0.215) in vehicle or psilocin injected mice. GCaMP6s ΔF/F is the green fluorescence signal at any time point, subtracted and divided by the mean signal across the whole recording. Mean signal 2s pre-stim was then subtracted to normalize sensory responses. Response is defined as the mean fluorescence signal 6s post-stimulus onset.

5.3 Conclusions

In this chapter, we obtained evidence that cortical 5-HT modulates learning by balancing bottom-up and top-down information processing. The use of two-photon imaging and holographic optogenetic stimulation allowed us to achieve high spatial resolution (Packer et al., 2015) in recording cortical activity while activating 5-HT axonal projections, demonstrating that 5-HT release within S1BF has a suppressive effect in the thalamic-input layer (L4) (**Figure 24**), which suggests a down-scaling of bottom-up sensory input. This aligns with previous studies indicating that 5-HT serves as a gain control mechanism for cortical sensory responses (Azimi et al., 2020; Lottem et al., 2016; Seillier et al., 2017). The mixed inhibition-excitation observed in L2/3 (**Figure 24**), where top-down and bottom-up activity integrate, suggests that 5-HT could be promoting top-down pathways. Particularly, in light of the cortical VIP interneuron excitation by 5-HT (Férézou et al., 2002), a circuit involved in top-down modulation by several previous studies (Bastos et al., 2023; Kullander & Topolnik, 2021; Schuman et al., 2021; S. Zhang et al., 2014).

We also showed that cortical 5-HT tracks the uncertainty and saliency of stimuli during the learning of an air puff discrimination task (**Figure 26**), mitigating the disruptive effects of misleading trials by reducing the learning rate during exposure to unreliable information (**Figure 27**). These results are consistent with previous studies in mice characterising how DRN neurons increase their firing rate in response to salient stimuli (Paquelet et al., 2022) and to unexpected outcomes (i.e., unexpected uncertainty) during the learning of a task (Grossman et al., 2022). Our findings demonstrate that increasing S1BF 5-HT release during misleading trials using an optogenetic strategy can rescue learning performance. Previous studies have reported a mixture of increases and decreases in learning upon 5-HT manipulation (Colwell et al., 2024; Grossman et al., 2022; Kanen et al., 2021; Michely et al., 2022), and even that the effects of 5-HT depend on interval duration (Iigaya et al., 2018), type of learning (e.g., associative vs

reversal learning) (Kanen et al., 2021), trial outcome (i.e., reward versus punishment) (Michely et al., 2022), and reward probability (K. Miyazaki et al., 2018). In contrast to these studies, our optogenetic manipulations were directly targeted to terminals of DRN axons in S1BF, allowing us to discern the effects of 5-HT release in a very precise circuit (DRN-S1BF). However, it is unclear whether changing the task contingencies will affect the effects of S1BF 5-HT in learning. Future studies should address the effects of similar localised S1BF 5-HT release during learning in different task settings.

We also observed that psychedelic administration decreases 5-HT (**Figure 28**), which is consistent with previous electrophysiological studies showing that 5-HT psychedelics silence DRN neurons (Rogawski & Aghajanian, 1979; Trulson et al., 1981; Trulson & Jacobs, 1979). Psychedelic administration also reduced CS+, but not CS-, cortical calcium responses. A potential explanation is that the previously reported signalling of reward by VIP interneurons (Szadai et al., 2022), is reduced due to the psychedelic-induced 5-HT decrease in S1BF. Previous studies have suggested that this reward signalling is a form of top-down modulation of sensory representations (Wilmes & Clopath, 2019), in which case these results can be interpreted as a reduction in top-down activity. This would be in line with previous observations in human studies reporting that psychedelics promote bottom-up versus top-down signalling (Alonso et al., 2015; Aqil & Roseman, 2023). The observed decrease in 5-HT correlates with an increase in learning rates during reversal learning of the previous air puff discrimination task (**Figure 28**). These results are in line with previous literature suggesting that 5-HT psychedelics (e.g., psilocin) facilitate reversal learning (Woodburn et al., 2024). This increase in learning rate concomitant with 5-HT decreases provides correlative evidence of a bidirectional modulation of learning rates on a translationally-relevant context. Moreover, this is of particular interest given the antidepressant and anti-addiction effect of these drugs (Korkmaz et al., 2024).

Altogether, these results suggest a role for 5-HT in balancing bottom-up and top-down sources activity in S1BF, in a way capable of adjusting the learning rate from sensory experience. In parallel, our findings provide a framework to better understand the potential mechanism underpinning the neuroplastic effect of psychedelics.

6. Modelling the role of cortical 5-HT throughout mammalian life with gated deep neural networks

6.1 Introduction

Throughout this thesis we have characterised 5-HT dynamics in the developing and adult cortex. We have also explored the effects of optical, genetic and pharmacological manipulations of 5-HT fluctuations in cortical population activity. As a final chapter, we aim to reconcile these results in a single theoretical model that can account for how 5-HT dynamics relate to its consequences in the mammalian cortex, subsequently shaping animal behaviour.

For this, we exploited the recent advent of neuroAI that opens the door to understand neuronal processes by modelling them with biologically-plausible architectures, allowing an analytical understanding of their second order effects (Garcia et al., 2023; Kanwisher et al., 2023). Moreover, by finding exact mathematical solutions, from the field of statistical physics, we can find an analytical description of the dynamics of these models throughout learning, an emergent approach known as analytical connectionism (Mannelli et al., 2024).

To model monoaminergic neuromodulation in a biologically-plausible manner, we propose the use of gated deep neural networks, in which the action of the neuromodulator is modelled as a multiplicative gating mechanism, re-scaling the output of the neuron. Then, we study the consequences on learning as second order effects emerging from the change in neuronal

activation. This approach is biologically-plausible as we know that neuromodulators (e.g., 5-HT) alter cortical activity (Azimi et al., 2020; Lottem et al., 2016; Seillier et al., 2017), and that there is activity-dependent neuroplasticity taking place in cortex (Y. Pan & Monje, 2020). However, we cannot rule out the existence of other mechanisms altering learning directly through 5-HT signalling pathways (Sahu et al., 2018).

Thus, in this chapter we used deep gated neural networks with exact solutions to model the effects of 5-HT in cortex, observed in the diverse experimental results obtained throughout this thesis. Thereby, we provide one possible framework for the comprehensive interpretation of these results.

6.2 Results

6.2.1 A gated deep neural network model to formalise the role of 5-HT

Our results suggest that bottom-up (sensory-driven) S1BF activity is inhibited by 5-HT. Moreover, we observed that 5-HT dynamics track uncertainty and scale with stimulus saliency and reward, playing a major role in learning from noisy environments (chapter 5). To understand the impact that these dynamics and effects of cortical 5-HT would have in shaping behaviour, we used our previous results to design a biologically-grounded model using non-linear deep gated neural networks with exact solutions. We developed a theoretical model using a two-layer neural network trained in the teacher-student framework (Engel & Van den Broeck, 2001) in a discrimination task using Gaussian-distributed data. Based on the observed gating of bottom-up inputs by 5-HT (**Figure 24**), we modelled 5-HT as a gate in the first set of weights multiplicatively scaling down the inputs. Since we observed a proportional increase of 5-HT with input saliency, the value of the gating in the model scaled with the input variance (used as a proxy of saliency for mathematical simplicity) (**Figure 29a**). Given that the scaling of learning

with neuronal activation is evident in Hebbian learning, we decided to use a more complex learning rule (i.e., online stochastic gradient descent) with the intention that our results would extrapolate to other learning rules.

The task of the model was designed to incorporate components of 5-HT dynamics: sensation, uncertainty and saliency. During training, the student network approximates a N-to-one dimensional mapping from a primary teacher (rule 1), despite interference from a secondary teacher (rule 2) with an opposing rule and variable input variance (**Figure 29a**). In the high-dimensional regime we obtained analytical solutions that can be efficiently evaluated free of the intrinsic variability present in simulations (**Figure 29b-d, Supplementary figure 11**). Thus, our results only depend on the initialization of the teacher and student networks (**Figure 29d**) — done at random — which furthers the biological analogy given the elevated inter-individual variability in the animal realm.

Our analysis shows that learning is disrupted by introducing a few trials (5%) in which the opposite rule (or label) is provided, which is reflected both in the loss (**Figure 29b and Supplementary figure 11a**) and in the accuracy (**Figure 29c,d**). This disruption increases with the variance of the input in misleading trials, as evidenced by an increase in the final loss (**Supplementary figure 11b**) and a decrease in the final accuracy (**Figure 29e**). Implementing a 5-HT-like gating of the input in the first set of weights, that scales with input variance, can mitigate the effects of this learning disruption (**Figure 29b-d**). These theoretical results confirm that salient misleading information can disrupt learning and showcase the benefit of having a 5-HT-like gating function.

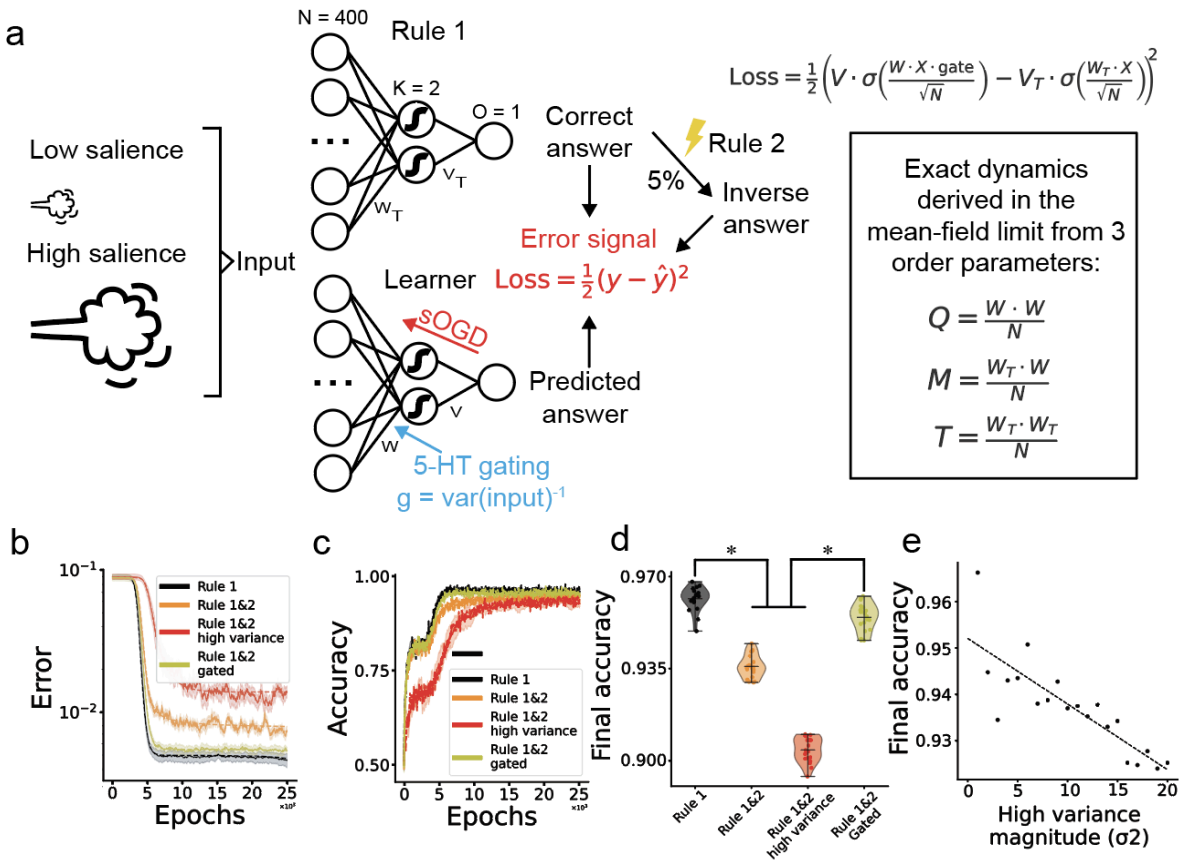

Figure 29.A biologically-grounded gated deep neural network model of cortical 5-HT Gated deep neural network model incorporating experimental 5-HT dynamics and effects was constructed to simulate 5-HT cortical modulation. **a** Diagram describing the model with a teacher-student setup, in which both the teacher and student are 2 layer neural networks with 400 inputs, 1 hidden layer with two nodes that have error function non-linear activation, and a single output node. The student needs to learn, through stochastic online gradient descent, the randomly initialised teacher mapping of 400 gaussian inputs to 1 output, despite interference from a second teacher with opposite label, that provides 5% of the trials, during which inputs have higher variance. 5-HT is implemented as a gate in the first set of weights that inversely scales with the input variance. Q, M and T are the order parameters that describe the dynamics of the system, respectively: the student weight correlations, the teacher-student weight correlations and the teacher weight correlations (a constant). **b** Analytical mean square error loss of student neural network across 25,000 epochs with rule 1 only (black trace), same variance rule 1&2 (orange trace), rule 1 & and high variance rule 2 (red trace) or a gated student with rule 1 & high variance rule 2 (yellow). Continuous traces are the average simulation (n = 10), while the discontinuous line represents the analytical evolution of the loss. **c** Evolution of accuracy across 25,000 epochs, for the same 4 conditions. **d** Violin plot with analytical mean final accuracy upon different initializations for rule 1, rule 1&2 (low/high variance) or gated rule 1 & 2/ (n = 20 initializations, Kruskall-wallis test $p < 0.001$, Dunn post hoc test rule 1-rule 1&2 $p < 0.001$; rule 1-rule 1&2 high variance $p < 0.001$; rule 1- rule 1&2 gated $p = 0.268$; rule 1&2 high

variance - rule 1&2 gated p < 0.001; rule 1&2- rule 1&2 gated p = 0.012). **e** Scaling of final accuracy with the value of the input variance of rule 2-labelled trials (linear fit, R^2 = 0.688, slope = -0.001 and p <0.001). sOGD = stochastic online gradient descent. Analytical accuracy was calculated by Monte Carlo integration.

6.2.2 Modelling cortical 5-HT in adult sensory discrimination

Fitting our model to the settings of the behavioural air puff discrimination paradigm (i.e., sequential low and high saliency misleading trials in a subset of training days) (**Figure 25-28**), accounted for the behavioural results (**Figure 30a**). Namely, we observed no effect of the low saliency misleading trials, nor of the gating, in the performance (**Figure 30b**), while high saliency misleading trials disrupted learning and 5-HT-like gating mitigated this effect (**Figure 30c**). These results illustrate that this 5-HT implementation can account for the effects of 5-HT in cortical circuits during adult learning.

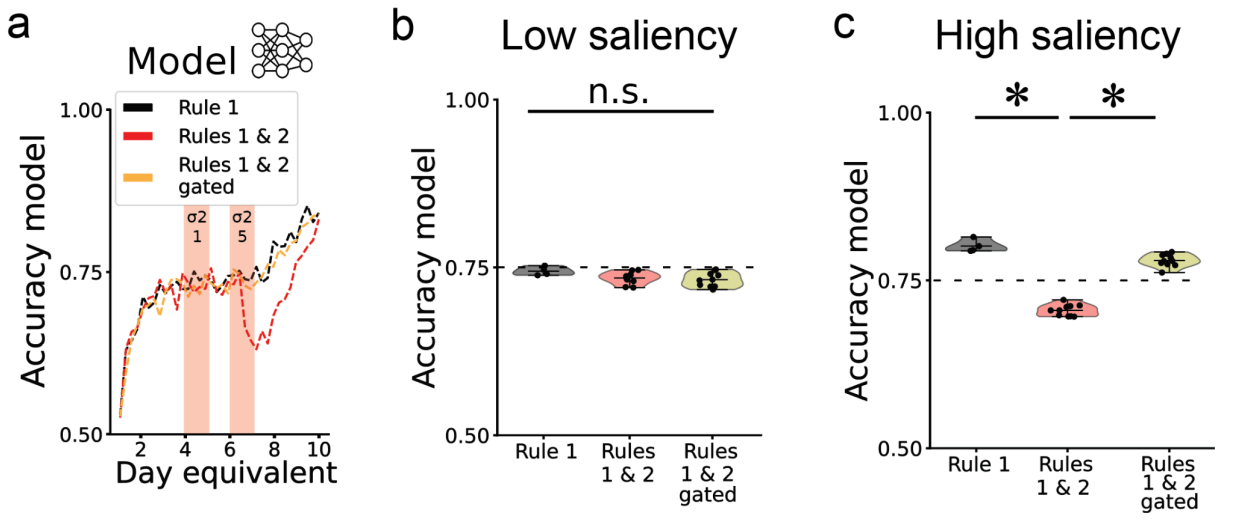

Figure 30. A gated deep neural network model accounts for the effects of misleading salient trials and paired 5-HT release in learning. Model settings (e.g., number of epochs, proportion and location of misleading trials…) were adjusted to the behavioural task to make more precise predictions. **a** Evolution of accuracy across 1800 epochs (1 day equivalent = 180 epochs), for neural networks trained without (yellow, single teacher) or with perturbation (black, dual teacher), as well as with 5-HT like gating (green, gated dual teacher). Model parameters fitted to the task settings, see methods for detailed description. **b** Average accuracy across 180 epochs (900-1080 epochs) after the low saliency perturbation epoch range (one-way ANOVA p = 0.890, N = 10 different initializations). **c** Average accuracy across 180 epochs (1260-1440

epochs) after the high saliency perturbation epoch range (one-way ANOVA p = $3.42e^{-12}$, Tukey post hoc test: rule 1 vs rule 1&2 p < 0.001; rule 1&2 vs gated rule 1&2 p < 0.001; N = 10 different initializations).

6.2.3 Modelling cortical 5-HT role in the effect of psychedelics on reversal learning

We next sought to capture the behavioural effect of psychedelics in reversal learning with this same model. We modelled the decrease of 5-HT triggered by psychedelics by removing the 5-HT-like gate implemented. For this, we trained deep neural networks to expertise (i.e., accuracy > 0.9) on the primary task (**Figure 31a**), and then re-trained them in the reversal rule, with or without gating (**Figure 31b**). We observed that removal of the gate during reversal learning can improve performance in the task by implicitly increasing the learning rate (**Figure 31c,d**), as we observed in mice (**Figure 31**). Thus, our model accounts for the behavioural effects of psychedelics in reversal learning, as a function of the observed 5-HT dynamics.

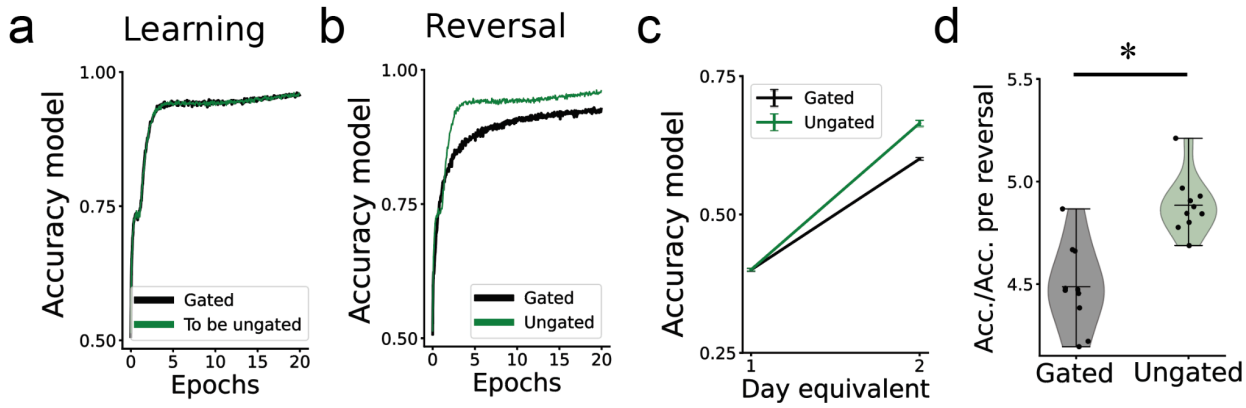

Figure 31. A gated deep neural network model accounts for the effects of psychedelics in reversal learning. The effect of psychedelics was mimicked by removing the gating mechanism during reversal learning trials. **a** Dynamics of accuracy for two gated neural networks trained with a single teacher (rule 1 only), to identical accuracy across 25,000 epochs. **b** Dynamics of accuracy for the previous two neural networks trained in reversal task (rule 2 all trials) with (black) or without (green) the gate, for 25,000 epochs. **c,d** Final accuracy for the two neural networks with parameters fitting mice task settings (see methods), showing an increased accuracy, normalised by pre-reversal accuracy, on day 2 (n = 10 initializations, t-test p < 0.001).

6.2.4 Modelling the role of cortical 5-HT in the developing cortex

Finally, we tested whether this model could account for the observed effects of 5-HT in cortical development, by using our previously described results in SERT genetic (SERT-KO, chapter 3) and pharmacological (postnatal SSRI, chapter 4) developmental disruption. Firstly, we showed that gate removal in early epochs can accelerate learning (**Figure 32a)**. This is consistent with the heightened neuroplasticity in early development (Blumberg et al., 2022), and a potential lack of top-down modulation prior to the onset of active sensation (i.e., eye opening and active whisking at postnatal day 14). This result suggests that the role of the transient SERT expression in thalamocortical axons could be to buffer 5-HT as a mechanism to increase neuroplasticity in early cortical development (E15-P10). Secondly, we showed that early 5-HT-like gating can explain the early hypoactivity observed upon SERT disruption (**Figure 32b**). Thirdly, we demonstrated that if we implement activity-dependent pruning, we can recreate the early cell death observed (**Figure 32c**) by implementing 5-HT-like gating. Altogether this gating implementation of 5-HT can account for observations on the effects of 5-HT in the developing cortex.

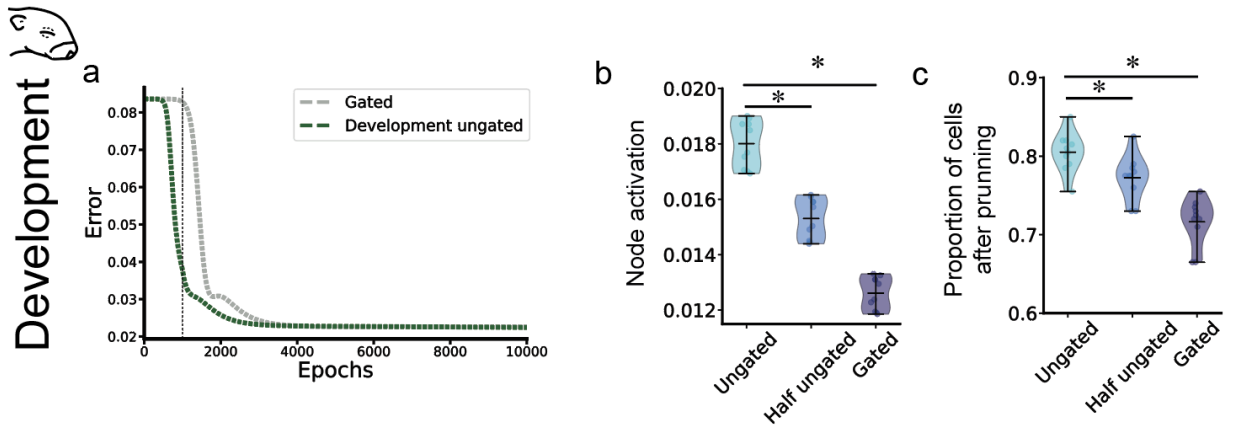

Figure 32. A gated deep neural network model accounts for the effects of SERT transient overexpression in early postnatal development. The effect that transient SERT overexpression in development has on cortical 5-HT activity was modelled using a gated deep neural network model. **a** Evolution of the loss across 10,000 epochs in a gated deep neural

network, or a neural network that is ungated during the first 1000 epochs, showing faster convergence to the asymptote. **b** Average node activation in these first 1000 epochs with ungated, half-gated or fully gated settings (n = 10 initializations, one-way ANOVA $p<0.001$, Tukey post hoc ungated-half ungated $p < 0.001$ and half ungated-gated $p < 0.001$). **c** Average number of cells pruned as a function of the degree of gating (n = 10 initializations, one-way ANOVA $p < 0.001$, ungated-half ungated Tukey post hoc $p = 0.014$, half ungated-gate $p < 0.001$).

6.3 Conclusions

This chapter presents a unified model of cortical 5-HT function based on input gating, which accounts for its diverse roles in adult associative learning, the effects of psychedelics on reversal learning, and its involvement in cortical development. By implementing 5-HT as a multiplicative gating mechanism that scales down inputs according to their uncertainty and saliency, the model successfully replicates the inhibition of misleading sensory information, thereby enhancing learning accuracy in noisy environments (**Figure 29**). In adult learning tasks, the model demonstrates how 5-HT mitigates the disruptive impact of high-saliency misleading stimuli by reducing their influence in internal model updates (**Figure 30**), aligning with observed behavioural effects in chapter 5. For reversal learning, simulating the removal of this gating mechanism — analogous to the decreased extracellular 5-HT in S1BF following psychedelic administration — predicts an increased learning rate (**Figure 31**), accurately capturing the improved performance observed in chapter 5. Additionally, the model provides a potential explanation to the overexpression of SERT as a way of increasing cortical neuroplasticity in early mammalian development. Moreover, the model accounts for how early 5-HT increases, triggered by SERT genetic or pharmacological disruption, can decrease node activation and increase cell death during a period of activity-dependent pruning (**Figure 32**), as we observed in chapters 2-4.

This input-gating deep neural network framework offers a mechanistic account that integrates multiple roles of 5-HT, suggesting its broader applicability to other areas of 5-HT research. Our model is amenable to increasing its complexity to capture other phenomena through changes in task settings, architecture and other hyperparameters. Moreover, the ability of the model to replicate diverse experimental results indicates that input gating might be a general principle underlying the function of 5-HT in cortical microcircuits. Further application of this model may provide new insights into the complex and multifaceted functions of 5-HT in both health and pathology.

7. General Discussion

7.1 Summary of main findings

This thesis investigates the role of cortical 5-HT in shaping cortical population dynamics, and its subsequent effects in cortical neurodevelopment and adult behaviour using head-fixed two-photon imaging combined with genetic, pharmacological and optogenetic manipulations of cortical 5-HT.

In chapter 2, we used a novel 5-HT biosensor to identify the release of 5-HT in S1BF in response to sensory stimulation (i.e., whisker deflection) that scaled with stimulus saliency, novelty, and presence of reward, as well as during developmental sleep-wake 5-HT fluctuations. We also observed evidence that 5-HT release is buffered in early development (until P10) through the transient overexpression of SERT in thalamocortical projections, leading to a lack of detectable increases in 5-HT release upon sensory stimulation. However, sleep-wake 5-HT fluctuations and 5-HT increases in response to salient stimuli were still detectable at this stage in early life. In this chapter, we also observed localised release of 5-HT in S1BF L2/3, particularly in regions rich in VIP interneurons, proving the potential for targeted synaptic release of 5-HT release, beyond volumetric transmission.

In chapter 3, we used *in vivo* two-photon calcium imaging in S1BF to characterise how life-long genetic knockout of the developmental 5-HT buffering system SERT leads to an impairment of H-events, resulting in early cortical hypoactivity. At the age of cortical decorrelation (P11), the cortical activity of SERT-KO mice transitioned into hyperresponsivity to sensory stimulation which was still observable by P16. This hyperactivity was concomitant with evidence of an overactivation of VIP interneurons in the SERT-KO mice, together with underactivation of

Nkx2-1 interneurons. In adult SERT-KO animals (>8 weeks), there was a reduction in the number of PV-expressing interneurons in S1BF. Notably, in the adult cortex of these animals, we did not observe any alterations in sensory encoding as revealed by calcium imaging during exposure to diverse somatosensory stimuli, thus suggesting a compensatory mechanism.

In chapter 4, using *in vivo* two-photon calcium imaging, we expanded this work by studying the effects of postnatal exposure (P2-14) to the SSRI fluoxetine, a model of transient pharmacological SERT disruption. In S1BF of SSRI postnatally-treated mice, we observed an impairment of H-events and early hypoactivity, with a transition into hyperactivity that was still observable in the adult cortex. We also observed a decrease in the number of Nkx2-1 interneurons and an increase in VIP interneurons in SSRI postnatally-treated mice, evidencing that early SERT disruption interferes with the survival of diverse interneuron subpopulations. This finding also highlighted a long-lasting cortical hyperactivity phenotype in response to this transient developmental alteration in 5-HT.

In chapter 5, we used all-optical two-photon calcium imaging and two-photon optogenetics of 5-HT terminals in S1BF to study the effects of local 5-HT release in cortical activity. We observed that optogenetically-evoked 5-HT release inhibited calcium signals in S1BF L4, the canonical thalamo-recipient layer of cortex, while producing a mixture of inhibition and excitation in L2/3. Then, we studied the effects of S1BF 5-HT on learning. For this, we trained water-restricted SERT-Cre animals, with an opsin in DRN, in an air puff discrimination paradigm in which misleading information was presented. Optogenetically-evoked 5-HT release in S1BF during misleading trials reduced the learning disruption evoked by these trials. Thereby, we identified a role for S1BF 5-HT in gating unreliable streams of bottom-up information. Moreover, we found that systemic administration of the psychedelic drug psilocin reduced S1BF 5-HT and

increased the learning rate during a reversal learning air puff discrimination task. This provided correlative evidence of decreases in S1BF 5-HT increasing learning rate.

In chapter 6, we used theoretical neuroscience approaches to design a deep gated neural network model with exact analytical solutions that captured how 5-HT dynamics and its effects in cortex can lead to the shaping of learning dynamics in adult and developing mice. Thus, we provide a theoretical framework for the interpretation of the experimental findings obtained in this thesis.

7.2 Discussion of main findings

7.2.1 Role of 5-HT in cortical development

Our results suggest that 5-HT signalling in the early postnatal cerebral cortex is tightly regulated to ensure appropriate instruction of bottom-up sensory circuits. We found that 5-HT fluctuated with behavioural state in the early postnatal cortex, as previously reported in adults (Deng et al., 2024; Kato et al., 2022). We also observed that aversive stimulation triggered detectable 5-HT increases in S1BF as previously reported in adult electrophysiological recordings of the DRN (J. Y. Cohen et al., 2015). However, early transient SERT expression ensured a lack of detectable 5-HT increases in S1BF upon non-aversive sensation. These results support previous speculation that the role of transient SERT expression in thalamocortical axons to sensory cortices is buffering extracellular 5-HT in early ages (E15-P10) (Salichon et al., 2001; Teissier et al., 2017). Disruption of this early buffering by either genetic SERT-KO or exposure to the SSRI fluoxetine resulted in early decreased cortical activity (<P10), likely due to the overactivation of 5-HT_{1B} receptors in thalamocortical projections (Bennett-Clarke et al., 1993; Salichon et al., 2001) and 5-HT_{3A} receptors in interneurons located in upper layers (Che et al., 2018). These

results are also consistent with findings from previous electrophysiological and imaging studies of a predominantly inhibitory effect of 5-HT in adult sensory cortices (Azimi et al., 2020; Lottem et al., 2016; Seillier et al., 2017). Further, in light of 5-HT sleep-wake fluctuations, this early 5-HT neuromodulation of cortical activity can provide a state-dependent mechanism for the previously reported regulation of developmental cortical activity (Blumberg et al., 2022).

Subsequently we observed altered development of interneuron subtypes involved in bottom-up, feedforward inhibition (Nkx2-1) (Marques-Smith et al., 2016) and top-down inhibitory control (VIP) (S. Zhang et al., 2014). Namely, in SERT-KO mice we observed VIP hyperactivity and Nkx2-1 early hypoactivity with subsequent reduced PV expressing interneurons in the adult cortex. In SSRI postnatally-treated mice, we observed an early hyper-recruitment of Nkx2-1 interneurons, as well as an increase in VIP and a decrease Nkx2-1 survival in the adult cortex. As such, these findings support the idea that 5-HT is a critical modulator of activity within cortical microcircuits in a manner consistent with the reported role of 5-HT in interneuron development (De Gregorio et al., 2020; Frazer et al., 2015; Murthy et al., 2014; Wong et al., 2022).

Disrupted early regulation (i.e, SERT-KO and postnatal-SSRIs) resulted in a developmentally hyperexcitable S1BF that persisted into adulthood in the case of mice postnatally-treated with a SSRI. These results provide a neurophysiological account that builds on reported alterations of sensory map formation in sensory cortices of SERT-KO rodents (Cases et al., 1996; De Gregorio et al., 2020, 2020; Salichon et al., 2001). We further observed an effect arising from maternal phenotype (Jones et al., 2010; Sjaarda et al., 2017), namely that wildtype mice generated by breeding SERT-het dams exhibited a distinct and subtle change to early supragranular GABAergic innervation (**Supplementary figure 3**) (Marques-Smith et al., 2016), one that leads to life-long changes in baseline dynamics.

While the cortical hyperexcitability of SSRI postnatally-treated mice remained present in the adult cortex, this effect was not present in adult SERT-KO mice, despite reduced PV interneuron numbers, suggesting the involvement of a compensatory mechanism. This result suggests that a transient alteration of 5-HT dynamics during a critical period (P2-14 SSRI exposure) might be more disruptive than life-long changes in 5-HT (SERT-KO). There are three potential explanations for the different effects of short term pharmacological inhibition of SERT and long term genetic knockout. The first is that since the levels of cortical inhibition mature to match levels of pyramidal excitation (Wong et al., 2018), increased 5-HT during this period of interneuron plasticity leads to an irreversible imbalance in cortical excitation and inhibition. This hypothesis is particularly interesting in light of our adult results reporting that 5-HT leads to bottom-up thalamic input gating. Thus, with a higher input gating, less inhibition might be required, and the levels of gating could influence the levels of inhibition defined in this critical period. Then, given that the increased bottom-up gating is life-long in SERT-KO mice but not in the developmental SSRI exposure, it would justify why only the latter presents adult hyper-excitability.

The second explanation is that the observed increase in survival of VIP interneurons in SSRI-treated mice is responsible for the long-lasting hyperexcitability, given the previously reported disinhibitory motif of these interneurons in cortical microcircuits (Kullander & Topolnik, 2021; S. Lee et al., 2013). Notably, the lack of alterations in VIP interneuron numbers of SERT-KO mice across S1BF layers is in contradiction with a previous study reporting migration deficits leading to increases in VIP interneurons in deep layers and a reduction in upper layers (Frazer et al., 2015).

The third explanation for the observed differences between SSRI-treated and SERT-KO mice lies in the off-target effects of SSRIs beyond SERT inhibition. SSRIs are known to interact with

other molecular targets, including various 5-HT receptor subtypes, norepinephrine transporters, (Owens et al., 1997) and the Trkβ receptor (Casarotto et al., 2021). These off-target interactions could influence neuronal development and circuit formation in ways distinct from the effects of elevated extracellular 5-HT due to SERT disruption. For example, SSRI binding to Trkβ receptors could alter intracellular signalling pathways and calcium dynamics, potentially contributing to the observed phenotypes in SSRI-treated mice. Additionally, modulation of norepinephrine reuptake may further amplify neuromodulatory imbalances during critical developmental windows. These off-target effects might explain why transient SSRI exposure produces a phenotype distinct from the lifelong genetic absence of SERT. To disentangle the contribution of off-target effects, future studies should investigate the effects of SSRI treatment in SERT-KO mice as a control. Such experiments would allow to isolate the impact of SSRI-induced SERT-independent mechanisms on cortical development and activity, providing a more in-depth understanding of SSRI pharmacology in the developing brain.

The current findings that altered 5-HT signalling in early life alters cortical excitability connects with evidence that both genetic variation in *SERT* (H.-J. Lee et al., 2005; Murphy & Lesch, 2008; Nicolini, 2010; Pezawas et al., 2005; Veenstra-VanderWeele et al., 2012) and developmental exposure to SSRIs (Koc et al., 2023; Morales et al., 2018) are risk factors for psychiatric neurodevelopmental disorders. Notably, the majority of these disorders (e.g., ASD) have also been associated with alterations in the integration of bottom-up and top-down pathways (LeDuke et al., 2023; Ursino et al., 2022) as well as excitation-inhibition balance (Contractor et al., 2021; Fogaça & Duman, 2019; Girgenti et al., 2021), two phenotypes observed in our models of early-life disruption of 5-HT dynamics. Further, our observations of hyperexcitability in adult S1BF of SSRI postnatally-treated mice are in accord with the pathophysiology of sensory hypersensitivity, present in neurodevelopmental disorders such as ASD (Marco et al., 2011), and associated with altered GABAergic signalling (Green et al., 2015; Sapey-Triomphe et al.,

2019) (Kourdougli et al., 2023). Finally the observed 5-HT responses to aversive stimuli even with intact SERT, might provide a neurophysiological basis for the previously suggested interaction of SERT disruptions and early exposure to trauma in neurodevelopmental disorders (Brown et al., 2013; Delli Colli et al., 2022; Murphy & Lesch, 2008), in that both SERT disruption and aversive experience trigger early cortical 5-HT increases.

In summary, our results suggest that pharmacological and genetic disruptions of perinatal 5-HT dynamics can alter cortical patterns of activity, thereby perturbing interneuron integration and function with consequences for cortical information transfer and sensory encoding in later life.

7.2.2 Role of 5-HT in the adult cortex

Our results with the 5-HT biosensor g5-HT3.0 demonstrate that cortical 5-HT tracks task-relevant sensory information from the environment including uncertainty, saliency and reward, in line with previous electrophysiological recordings of 5-HT neurons in the DRN (Feng et al., 2024; Grossman et al., 2022; Y. Li et al., 2016; Z. Liu et al., 2014; Ocana-Santero et al., 2024; Paquelet et al., 2022; Ranade & Mainen, 2009). Our all-optical experiments showed that optogenetically-evoked 5-HT release in S1BF suppresses calcium signals in the thalamo-recipient layer of S1BF (L4), suggesting inhibition of bottom-up inputs, while producing a mixture of excitation and inhibition in L2/3. 5-HT release in L2/3 was particularly high in VIP interneurons that are well-established to be involved in top-down regulation (Bastos et al., 2023; Piet et al., 2024; Schuman et al., 2021; Wilmes & Clopath, 2019; S. Zhang et al., 2014) and are excited by 5-HT (Férézou et al., 2002). These results suggest that 5-HT is a critical regulator of bottom-up versus top-down sources of activity. We also reported that optogenetically-increasing 5-HT downregulates learning from misleading information in an air puff discrimination task. Under the light of these results, 5-HT scaling with saliency and reward might reflect a need to

scale the suppression of misleading information by any factor that increases learning (i.e., reward or saliency), as we report that particularly salient misleading information can represent a major overfitting risk. This role of 5-HT in modulating bottom-up and top-down sources of activity, can be understood from the light of predictive coding as promoting predictions over sensation. Moreover, these results align with previous speculation in the field of predictive coding suggesting that neuromodulatory gating can balance bottom-up and top-down activity to adjust the rate of update of internal representations (Keller & Mrsic-Flogel, 2018; Yu & Dayan, 2005). However, whether the role of cortex really is predictive coding is still a matter of debate (Furutachi et al., 2024).

Interestingly, we did not observe differences in licking behaviour (i.e., trial performance) during the optogenetic 5-HT stimulation, as other studies performing bulk optogenetic activation of 5-HT neurons in the DRN, through the implantation of an optic fibre, have reported (Dugué et al., 2014; Fonseca et al., 2015; K. W. Miyazaki et al., 2014). Namely, these studies have reported an increased mechanosensory threshold for perception and promotion of waiting for future rewards. However, our optogenetically-evoked 5-HT release was performed by shedding light directly on top of S1BF through a cranial window, thus inducing more localised 5-HT release. Our results can be understood from previous studies suggesting that the cortex is crucial for the learning of behaviours but not their performance (Kawai et al., 2015; Ostlund & Balleine, 2005). Thus, we hypothesise that cortical 5-HT gating of bottom-up inputs in sensory cortices might be playing a predominant role in regulating the learning rate of internal model update, rather than affecting ongoing behaviour.

In summary, we have identified a key role of cortical 5-HT in dictating the balance of bottom-up and top-down activity, with second order effects in learning.

7.2.3 5-HT psychedelics drug action in cortex

In our 5-HT biosensor experiments we found that systemic administration of the psychedelics psilocin or LSD, as well as the non-hallucinogenic analogue lisuride, all decreased cortical 5-HT release. Moreover, we observed that psilocin injection also triggered increases in reversal learning. Since we have previously reported that 5-HT increases in S1BF decrease bottom-up inputs and learning rate, we speculate that the decrease in 5-HT triggered by psilocin injection could be causally linked to the increase in reversal learning. In agreement with this hypothesis, fMRI human studies have shown an overactivation of bottom-up, and depression of top-down, pathways upon psychedelic drug exposure (Alonso et al., 2015; Aqil & Roseman, 2023). We speculate that this increased bottom-up information transfer may upregulate learning rate and partly account for the neuroplastic effect of psychedelics (de Vos et al., 2021).

In support of this role of cortical 5-HT in downregulating learning rate, a study in rodents showed that pharmacologically elevating 5-HT decreases the transition from cocaine consumption to compulsion through 5-HT_{1B} receptor activation in orbitofrontal cortex projections to striatum. Reciprocally, reducing this signalling through a knockout of 5-HT_{1B} in this pathway increases the transition to compulsion (Y. Li et al., 2021). This decrease of the transition to compulsion by 5-HT can be interpreted as a decrease in learning rate, reducing overfitting to a particular source of reward. Another study in agreement has shown that increasing synaptic 5-HT release in humans, using a selective 5-HT releasing agent, decreases learning in aversive contexts (Colwell et al., 2024). However, while we argue towards a role of 5-HT decreases in upregulating learning, it is not the only mechanism having this effect of psychedelics, since these drugs induce neuroplasticity — subsequently impacting learning — through several pathways. This is illustrated by the fact that psychedelics can induce neuritogenesis and spinogenesis in cell culture, without changes in 5-HT supply (Ly et al., 2018). In fact, psychedelics also trigger directly signalling pathways involved in neuroplasticity such as

intracellular 5-HT_{2A}R (Vargas et al., 2023) and direct binding to TRk (Moliner et al., 2023) receptors.

The fact that the non-hallucinogenic analogue lisuride also triggers a strong 5-HT decrease, suggests that this mechanism does not underlie hallucinogenic experience. In fact this argument has been previously used to rule out the 5-HT theory of the hallucinogenic effect of psychedelics (Rogawski & Aghajanian, 1979; Trulson et al., 1981) . However, lisuride has also been ascribed anti-depressants effects (Qu et al., 2023), supporting the possibility that 5-HT decreases, through increasing learning rate, contribute to the neuroplastic effect of these drugs.

In summary, we provide correlative evidence that 5-HT cortical decreases triggered by acute psychedelics lead to an increase in learning rate and, subsequently, contribute to the neuroplastic effect of these drugs. While the correlative nature of these results makes this theory highly speculative, we believe its translational relevance as a potential non-hallucinogenic neuroplasticity-inducer mechanism grants further research.

7.2.4 5-HT modelling to support a theory of 5-HT action in the CNS

We have developed a deep gated neural network theoretical model of 5-HT to account for our experimental results. In our model the consequences of changes in cortical 5-HT on learning are second order effects of input gating that impact the activation of the neurons. While this is biologically plausible, we cannot rule out the possibility that changes in learning rates are mediated by signalling pathways beyond activity-dependent mechanisms. Nevertheless, our model successfully captures how the dynamics and effects of 5-HT in learning, psychedelic drug action and cortical neurodevelopment, relate to their shaping of learning dynamics as measured in our behavioural task.

Beyond the phenomena that we have modelled, this model could be conceptually expanded to address other roles of 5-HT. For example, a major change in 5-HT dynamics is observed during

sleep-wake (Deng et al., 2024; Kato et al., 2022), with 5-HT release dropping during REM sleep, consistent with the heightened neuroplasticity observed in cortex during this sleep stage (Aime et al., 2022). 5-HT dynamics have also been found to change with movement (Kubitschke et al., 2022), which is interesting since a gating mechanism of bottom-up sensory information self-generated by movement has been suggested as critical for the cortical predictive coding framework (Keller & Mrsic-Flogel, 2018) and could thus be implemented by 5-HT. From this model, a potential relationship of 5-HT with neuropsychiatric conditions such as MDD or PTSD (Pourhamzeh et al., 2022) can be made through the lens of changes in learning rate making the brain susceptible to overfitting to traumatic experiences, well-known triggers of these conditions (S.-K. Wang et al., 2023).

Our model of cortical 5-HT aligns with previous theories of the role of 5-HT in the CNS. The opponency theory proposes that 5-HT plays antagonic effects to other neuromodulators such as dopamine and noradrenaline to balance behaviour and decision-making (Boureau & Dayan, 2011). In line with this theory, our results and model situate 5-HT as a downregulator of cortical plasticity, exerting antagonic effects to other monoamines such as dopamine and noradrenaline that might increase learning rate. The cognitive flux theory suggests that 5-HT tone sets different cognitive modes as a function of how demanding tasks are (Shine et al., 2022). Our study suggests that 5-HT promotes top-down information and reduces learning rate, both of which would be beneficial in cognitively demanding tasks in which associations are not evident. Finally, the recent suggestion that 5-HT dynamics encode state value, suggests that the firing rate of 5-HT neurons can be accounted for by a model encoding predicted value of actions (Harkin et al., 2023). From our model, this could be understood from this cortical role as an scaling of the gating by the expected value, to avoid overfitting to unreliable experiences despite their high predicted value.

In summary, we have developed a theoretical framework that accounts for our experimental results, and that could potentially be expanded to capture further results in the field of 5-HT research.

7.3 Limitations and future directions

7.3.1 Beyond early postnatal development

Our developmental study of the effects of SERT disruption is limited to measurements during postnatal development. We identify P2-14 as a critical period for the 5-HT neuromodulatory control of excitatory-inhibitory balance in S1BF. However, the 5-HT innervation of cortex predates this critical period, and maternal supply of 5-HT also takes place early in embryonic development (Bonnin & Levitt, 2011). Indeed, alterations in maternal 5-HT supply in rodent models (e.g., maternal KO of the 5-HT producing enzyme tryptophan hydroxylase 1 (tph1)) result in changes to embryonic morphogenesis (Côté et al., 2007), and maternal SERT polymorphisms are also associated with neurodevelopmental disorders (Beversdorf et al., 2021; Jones et al., 2010; Sjaarda et al., 2017). Neonatal alterations in 5-HT (P0-P2) can also disrupt thalamocortical map formation (Sinclair-Wilson et al., 2023; Toda et al., 2013). Moreover, cortical interneurons still undergo developmental processes during adolescence (Caballero et al., 2014; Larsen & Luna, 2018), and disruption in 5-HT_{1A} receptors during adolescence in a rodent model can trigger a depression-like phenotype (Garcia-Garcia et al., 2017). Altogether, these studies highlight that 5-HT plays a plurality of roles in cortical development, all of which have the potential to impact the emergence of cortical population dynamics. Future studies should characterise the effects of disrupting SERT, or 5-HT dynamics, in different developmental windows while employing similar longitudinal imaging approaches, in order to fully elucidate the complex roles of 5-HT in cortical development.

7.3.2 Beyond voltage-dependent mechanisms

Our findings are limited in their ability to disentangle the metabotropic effects of 5-HT GPCRs on calcium signalling from direct voltage-dependent mechanisms. The calcium signals recorded using the GCaMP6s sensor may include components driven by receptor-mediated calcium release from intracellular stores, beyond changes in membrane potential. For instance, activation of 5-HT2A receptors via Gq-mediated pathways could enhance intracellular calcium through phospholipase C activity, potentially confounding interpretations of synaptic activity derived from calcium sensor readouts. This highlights the need for electrophysiological recordings to provide a more comprehensive understanding of the voltage-dependent mechanisms underlying 5-HT effects (Akhmetshina et al., 2016).

Moreover, the distinct phenotypes observed in SERT-KO and SSRI postnatally-treated mice may reflect broader second messenger dysregulation beyond the immediate voltage-dependent effects of 5-HT. Alterations in 5-HT availability could influence downstream pathways, such as cAMP or IP3/DAG cascades, resulting in long-term effects on gene expression and neurodevelopment. These findings suggest that some of the observed behavioral and cellular changes might stem from altered second messenger signalling rather than solely activity-dependent mechanisms.

To address these limitations, future work should leverage emerging tools that allow cell-type-specific and receptor-specific activation or inhibition, such as optogenetically-activated GCPRs (e.g., (Barzan et al., 2024) use optogenetically-activated 5-HT_{2A}R). These approaches enable precise manipulation of GPCR pathways in distinct neuronal populations and provide valuable insights into the network-level consequences of receptor-specific 5-HT signalling. Combining such advanced techniques with electrophysiological recording strategies will help

disambiguate the contributions of specific receptors and their downstream signalling pathways in shaping neural circuit function.

7.3.3 Beyond S1BF

Our study is limited to the characterization of 5-HT dynamics in S1BF. The neurodevelopmental consequences of SERT disruption, and subsequent 5-HT increases, are potentially similar in other sensory cortices, given the widespread transient overexpression of SERT in thalamocortical projections (Narboux-Nême et al., 2008; W. Pan et al., 2021). However, the developmental timelines and processes involved in the cortical development of different sensory cortices such as S1 and V1 are markedly different (Ghezzi et al., 2023), therefore challenging the assumption that an identical 5-HT developmental mechanism will be taking place. Association cortices also present transient SERT overexpression, which could suggest a similar buffering role. However, this expression is confined to deep layer pyramidal neurons (Narboux-Nême et al., 2008; Rebello et al., 2014) instead of thalamocortical projections to L4. Previous work has identified this transient SERT expression in association cortices as a critical regulator of PFC-to-DRN synaptic connectivity, and whose disruption leads to anxiety/depressive-like symptoms (Soiza-Reilly et al., 2019). Future studies using longitudinal imaging approaches should address whether altered 5-HT signalling has similar effects on emerging cortical population dynamics in this cortical region as observed here in S1BF.

Regarding our findings in the S1BF of adult mice, It is possible that the proposed 5-HT control of bottom-up input gating occurs in other sensory cortices. This is especially so given that gain-evoked effects of 5-HT are reported on sensory-driven activity in V1 (Azimi et al., 2020; Seillier et al., 2017) and olfactory cortex (Lottem et al., 2016). The promotion of top-down activity by 5-HT is also likely common in other cortical circuits, given the widespread distribution

of 5-HT_{3A}R-expressing VIP interneurons across cortex (Szadai et al., 2022). Moreover, some neurophysiological studies have also suggested a role of 5-HT in gating inputs into association cortices (Kjaerby et al., 2016), thalamus (Reggiani et al., 2023) or amygdala (J.-D. Guo et al., 2017), suggesting that this mechanism could be implemented across diverse 5-HT targets. Nevertheless, the widespread distribution and functional diversity of the 5-HT system (Okaty et al., 2019) indicates that it likely plays a plethora of roles in other regions. This is well exemplified by a study characterising the functional diversity of the 5-HT system in which they describe the involvement of DRN-to-frontal cortex projections in active coping and the role of DRN-to-amygdala projections in anxiety-like behaviours (Ren et al., 2018).

Thus, future studies should use similar approaches to characterise the dynamics and effects of 5-HT in other cortical and subcortical circuits across mammalian life, to clarify whether a common gating mechanism, as well as developmental effect, is observed in other regions, and elucidate other roles of 5-HT sub-circuitry.

7.3.4 Beyond associative learning

Our study of the effects of 5-HT in learning is limited to the application of optogenetically-released 5-HT during misleading trials on an associative Pavlovian learning task and psilocin-induced changes in 5-HT function during reversal learning. Previous studies have found a high variability in the effects of bulk activation of 5-HT neurons in the DRN during learning as a function of inter-stimulus interval duration (Iigaya et al., 2018), type of learning (e.g., associative vs reversal learning) (Kanen et al., 2021), trial outcome (i.e., reward vs punishment) (Michely et al., 2022), reward probability and timing uncertainty (K. Miyazaki et al., 2018). All these studies highlight the complexity of the effects of 5-HT in different tasks. Thus, future studies could optogenetically-evoke a local release of 5-HT during different types of learning paradigms, to fully clarify the effects of cortical 5-HT on learning dynamics.

7.3.5 Beyond 5-HT

This thesis is devoted to the exploration of the functions of cortical 5-HT. However, cortical circuits are influenced by a mix of neuromodulators, including dopamine, noradrenaline, acetylcholine, histamine and oxytocin (Galvin & Disney, 2023). All of these neuromodulators present complex dynamics and effects (Galvin & Disney, 2023). Moreover, these neuromodulatory systems interact with each other (Avery & Krichmar, 2017). For example 5-HT DRN neurons excite VTA dopaminergic neurons (H.-L. Wang et al., 2019) and noradrenergic neurons in the locus coeruleus excite DRN 5-HT neurons (Pudovkina et al., 2002). This complex arrangement of neuromodulators likely shapes cortical population dynamics throughout mammalian life, thus effects extend beyond that of a single neuromodulator. Future studies could explore how other neuromodulators shape cortical dynamics and subsequently behaviour using similar approaches to the ones applied in this thesis.

7.3.6 Beyond a gated deep neural network model

In this project, we account for the effects of 5-HT in adult learning, psychedelic neuroplasticity and cortical neurodevelopment, using a gated deep neural network model. However, our model comes with several limitations. Firstly, we do not perform comparisons of our model with other alternative theoretical models (e.g., theory of state value (Harkin et al., 2023)). Secondly, our model is focused on the role of 5-HT in gatting bottom-up cortical inputs and did not implement 5-HT promotion of top-down circuits. Thirdly, our model of the effects of 5-HT in learning enforces the observed 5-HT dynamics in cortex as known values of the gate, and as such it does not provide a model of how 5-HT dynamics evolve across learning (see reference (Harkin et al., 2023) for a model accounting for 5-HT dynamics). Fourthly, while deep neural networks

represent a plausible model of the cortical architecture, they do not fully recreate the biological complexity of cortical circuits in terms of neuronal subpopulations, connectivity and learning rules. Thus, future studies could aim to build onto this mechanistic implementation of 5-HT, by increasing its architectural complexity and by applying biological constraints (e.g., top-down modulation, inhibitory/disinhibitory nodes, recurrent connections…), to provide a more precise theoretical depiction of the function of cortical 5-HT.

7.4 Conclusions

Throughout this thesis, we have characterised the dynamics and effects of cortical 5-HT using S1BF as a canonical model of cortical circuitry and sensory processing. This work highlights the likely role of 5-HT in modulating bottom-up and top-down activity, in order to adjust the learning rate of internal model update throughout mammalian life. This role of 5-HT appears particularly critical in early postnatal development as it influences the establishment of excitatory-inhibitory circuits through distinct effects on interneuron subpopulations. We have characterised this role of 5-HT using translationally-pertinent contexts relevant to neuropsychiatric treatment (psychedelics) and pathology (postnatal SSRIs and SERT polymorphisms). Finally, we have created a mechanistic theoretical model to account for our results, that is amenable to model future findings, with the aim of achieving a comprehensive theory of 5-HT in the CNS.

8. Materials and Methods

8.1 Animals

Experiments were approved by the local ethical review committee at the University of Oxford and performed in accordance with UK Home Office project licences P861F9BB7, PE5B24716 and PP8136190 under the UK Animals (Scientific Procedures) 1986 Act. The following mouse lines were used *SERT-* mutant (Slc6a4(tm1Kpl/J)), *Nkx2-1-Cre* (Tg(Nkx2-1-cre)2Sand/J), *VIP-Cre (Viptm1(cre)Zjh/J)*, *Ai9* (Cg-Gt(ROSA)26Sortm9(CAG-tdTomato)Hze/J), SERT-Cre (B6.129(Cg)-Slc6a4tm1(cre)Xz/J) *VGLUT3* conditional KO ($VGLUT3^{LoxP/LoxP}$) and wild type C57BL/6J mice. Mice of either sex were generated via targeted breeding and housed in a temperature-controlled room under a 12 h light/12 h dark cycle with free access to food and water *ad libitum*. Number of animals (i.e., experimental sample sizes) are specified at each figure caption.

8.2 Surgery

8.2.1 Neonatal injections

Intracranial injections were performed at postnatal day 0-1 as in previous work (Hoerder-Suabedissen et al., 2022). Mice were anaesthetized with 3.5% isoflurane (1 L/min) in an induction chamber, and were then kept under anaesthesia using a custom designed nose cone (Ho et al., 2020). With a Nanoject III injector (Drummond) and a motorised stereotaxic arm (MCI), animals were injected in S1BF (AP 1.4 ML 1.5 from lambda) penetrating through the skull (right hemisphere). Pups were injected with 300 nL of either AAV9.hSyn-g5-HT3.0 (WZBiosciences, titre ≥ 1x10^13 v.g./mL), and AAV1.hSyn.GCaMP6s.WPRE.SV40 (Addgene,

titre > 1x10^13 v.g./mL). Injections of 100 nL were performed at a rate of 23 nL/sec at 3 different depths from skull surface: 600, 450 and 300 µm. After ~20 sec the capillary needle was extracted and the pups were placed on a Thermacage (Datesand technologies) for recovery. In order to remove surgical odours, pups were rubbed in nesting material before being returned to their dam.

8.2.2 Adult intracerebral injections

Mice were anaesthetised with isoflurane, head-fixed in a stereotaxic frame (Stoelting) and a 1 cm incision was performed on the scalp prior to craniotomy. A <0.5 mm craniotomy was drilled at the injection coordinates. Then the viral vector or CTB solutions were loaded into a glass micropipette (Drummond) and injected over 3 min. After a further 3 min waiting period, the micropipette was withdrawn, and the wound was closed with absorbable surgical stitches (Vicryl). Mice were then placed on a heating pad until recovery.

Viral vectors, and CTB, volumes as well as concentrations for adult injections were as follow:

Reagent	Titre/Concentration	Volume	Injection site coordinates (mm)
AAV9.hsyn.g5HT1.0 (Addgene)	≥1×10¹³ vg/mL	100 nL (x3 injections)	S1BF (AP = -1.9, ML = 3.0 and DV = 0.3)
AAV9.hsyn.g5HT3.0 (WZBiosciences)	≥1×10¹³ vg/mL	100 nL (x3 injections)	S1BF (AP = -1.9, ML = 3.0 and DV = 0.3)
AAV-Syn-FLEX-rc[ChrimsonR-tdTomato] (Addgene)	1×10¹³ vg/mL	30 nL (x3 injections)	DRN (AP = -4.75, ML = 0.1 and DV = 2.6)
AAV1Syn.GCaMP6s.WPRE.SV40 (Addgene)	1×10¹³ vg/mL	100 nL (x3 injections)	S1BF (AP = -1.9, ML = 3.0 and DV = 0.3)
AAV.1Syn.NES.jRCaMP1a.WPRE.SV40 (addgene)	1.9×10¹³ vg/mL	100 nL (x3 injections)	S1BF (AP = -1.9, ML = 3.0 and DV = 0.3)

Cholera Toxin Subunit B (Recombinant), Alexa Fluor™ 647 Conjugate (Invitrogen)	1.0 mg/mL	180 nL (x1 injections)	S1BF (AP = -1.9, ML = 3.0 and DV = 0.3)
Cholera Toxin Subunit B (Recombinant), Alexa Fluor™ 488 Conjugate (Invitrogen)	1.0 mg/mL	180 nL (x1 injections)	S2 (AP = -1.4, ML = 4.3 and DV = 0.75) PFC (AP = 1.8, ML = 0.3 and DV = 1.8)

Table 1. Injection reagents with concentration, volume and coordinates. AP: Antero-Posterior (from bregma), ML: Medio-Lateral (from the closest point of the midline) and DV: Dorso-Ventral (from the brain surface).

8.2.3 Developmental cranial windows

P6-7 mice were kept on a heating pad to avoid hypothermia and anaesthetized with 4% Isoflurane (1 L/min) in an induction chamber. Then, mice were placed in a face mask delivering isoflurane, the concentration was constantly adjusted to keep the mice in a safe anaesthetic depth (1-4%), and fixed with earbars in a stereotaxic frame. Following incision and partial removal of the scalp, 0.5% lidocaine was applied at the wounded area and a blue lamp with a GFP filter mounted on a miner helmet (BLS) were used to identify the region of GCaMP expression. g5-HT3.0 was generally not detectable through the skull and coordinates AP = 2.4, ML = 2.8 were used. Then, a manually thinned head-fixing plate (<0.3 g) was cemented (Super-bond, Dental Prestige) over the region of interest and, once dry, the animal was head-fixed and a 3 mm craniotomy was performed over the injected area (~S1BF) using an insulin syringe (BD). Once hemostasis was achieved, two coverslips (3mm and 4mm) (Warner instruments) glued together with optical adhesive (Norland) were placed over the craniotomy. Then, the craniotomy was sealed with Vetbond (3M) and fixed with dental cement (Super-bond, Dental Prestige). Animals were allowed to recover for at least 30 min on a heat-pad before being returned to their homecage. No signs of abnormal skull or brain development were

observed in these animals (**Supplementary figure 12**). Moreover, their developmental timeline (e.g., eye opening) was similar to animals that did not undergo the procedure (**Supplementary figure 12**). Good cranial window visibility was maintained throughout development (**Supplementary figure12**).

8.2.4 Adult cranial windows

Mice were anaesthetised with isoflurane and subcutaneously injected with Metacamp (Boehringer Ingelheim) and Vetergesic (Ceva). Then mice were head-fixed in a stereotaxic frame (Stoelting) and the scalp was removed to allow placement of a head-fixing plate (0.6-0.8g) which was fixed to the skull using dental cement (Superbond, Sun Medical). A craniotomy (3 mm diameter) was performed over the right hemisphere S1BF (centre of the window AP = −1.9, ML = 3.0) using a surgical drill (Volvere Surgical Drill i7 NSK Monobloc) and two coverslips (3 and 4 mm diameter) (Warner Instruments) attached to each other with optical glue (Norland) were placed over the craniotomy, sealed with vetbond (3M), and immobilised with dental cement. Mice were then placed on a heating pad until recovery (15-30 min).

8.3 Drug delivery

8.3.1 Postnatal SSRIs

Pups were gently scruffed and 10% sucrose or fluoxetine (10 mg/kg of body weight, Supelco) diluted in 10% sucrose were delivered with a P10 micropipette delicately introduced on the tip of the mouth. The dam was kept in a different cage during pup-treatment and the procedure was kept under 15 minutes, to avoid excessive maternal separations. Animals were dosed using a fresh drug dilution of 0.1 mg/ml, daily from P2 to P14, both included, maintaining a regular time of the day for dosage within the same litter. On surgery days, pups were dosed prior to surgery. During imaging days, each animal was dosed 5 minutes before the start of its first recording to keep time from dosing homogeneous across animals.

8.3.2 Other drugs

While postnatal SSRI dosage was performed orally, 5-HT psychedelics and MDMA were delivered intraperitoneally in adult mice, the following reagents, solution vehicles and concentrations were used:

Drug	Supplier	Concentration	Vehicle
Psilocin	Cayman Chemical	2 mg/kg	Tartaric acid + NaOH (to bring pH to 5-7) and diluted in saline + glucosaline
Lisuride	Biotechne Tocris	2 mg/kg	Saline
LSD	Sigma-Aldrich	0.2 mg/kg	Saline
MDMA	Sigma-Aldrich	10 mg/kg	Saline

Table 2. Psychedelics used with respective supplier, concentration and vehicle. All concentrations and vehicles were chosen based on previous published studies (de la Fuente Revenga et al., 2022; González-Maeso et al., 2003).

8.4 Two-photon imaging

8.4.1 Microscope and settings

Recordings were performed on a resonant galvo scanning 2-photon microscope (Bruker) with a Chameleon Ultra II laser (Coherent) and 50 mW of power on sample (except for L4 jRCaMP1a recordings, in which 80 mW were used). A 16x/0.8-NA water immersion objective lens (Nikon) was used. g5-HT3.0, and GCaMP6s were imaged using a 920 nm beam, tdTomato was imaged at 765 nm, and jRCaMP1a at 980 nm. Imaging was performed at a frame rate of 30 Hz in a square field of view (643x643 µm for GCaMP6s and 287x287 µm for g5-HT3.0). All recordings were obtained at ~150 µm from the brain surface (cortical L2/3), except for L4 recordings in chapter 5 (**Figure 24**) in which recordings were made at 350 µm from the brain surface.

8.4.2 Developmental recordings

Animals were imaged daily during a 20 minute baseline session and a 12 minute whisker stimuli delivery session from P7 to P16 for developmental imaging. The first day of recordings, the field of view was chosen based on whisker-stimulation responsiveness. Then, the same field of view was found by matching the sparse patterns of interneurons at the start of the first recording every day (**Supplementary figure 13c**), ensuring the same region was recorded. Pups were surrounded by padding material to minimise heat-loss and homecage nesting material was added to this padding to reduce stress by adding homecage odours.

8.4.3 Adult recordings

The first day of recordings, the field of view was chosen based on whisker-stimulation responsiveness. For developmental windows, imaging in adults was performed in mice 8 weeks or older, only when the window maintained good visibility and excessively bright cells (potentially calcium-filled) were not present, or very sparsely so (<1% of total cells), in the field of view. For air puff discrimination behaviour (**Figure 26**), imaging was performed on days 0, 3, 5, 7 and 10, while for the reversal learning paradigm (**Figure 28**) imaging was performed both days. Then, for longitudinal experiments, the same field of view was found by matching either blood vessel distribution or the sparse patterns of interneurons at the start of the recording every day, ensuring the same region was recorded. For g5-HT3.0 recordings, the centre of the image was recorded (i.e., AP = -1.9, ML = 3.0).

8.5 Optogenetics

8.5.1 One-photon optogenetics

An optic fibre (Thorlabs) was placed directly on top of the S1BF cranial window. 595 nm light pulses at 20 Hz and 1.5 mW of power on sample during 1.1s total stimulation duration were used to induce 5-HT release. 5-HT release was confirmed with the g5-HT3.0 sensor (**Supplementary figure 8j-l**). When paired to an air puff, the optogenetic stimulation started 1s before the air puff and ended simultaneously. Black electrical tape was attached around the fibre and objective to avoid the light being perceived by the mice. To prevent damage to the photomultiplier tubes, the imaging shutter was closed 0.1 s before light onset, and reopened 0.1 s after light offset, using a custom-made arduino-based circuit. This limited the temporal resolution of the analysis of the direct one-photon optogenetic effects on cortical activity.

8.5.2 Two-photon optogenetics

Two-photon optogenetics: a 1040 nm laser (Monaco, Coherent) and a spatial light modulator (BNS, incorporated into the Bruker microscope) were used. Axonal 5-HT stimulation was performed by creating two masks with 60 targets each with 6 mW of power per target in areas where tdTomato axons were observed (**Figure 24**). The stimulation settings consisted of 10 trials of spiral stimulations at 20 Hz lasting 1 second. Optogenetic settings and phase masks for target stimulation were generated with custom made code (Naparm) (Russell, 2019/2024).

8.6 Behavioural paradigms

8.6.1 Sensory stimulation

Sensory stimuli were generated pseudo-randomly using custom python code. Whisker stimulation was delivered with a piezoelectric actuator (Physik Instrumente) connected to a custom-designed (3D printed) whisker stimulator with modules for single-whisker (glass capillary), multi whisker (brush), air puff (picospritzer III at 80 psi), smooth surface (velcro), or rough surface (sand paper). All whisker stimuli were delivered oscillating at 20 Hz within the mouse left whiskers, with a duration of 40ms. For adult passive sensation (chapter 3 and 4) stimuli were presented 10 times with inter-stimulus intervals between 20 to 30s. The auditory stimulus was an amplitude and frequency modulated complex tone with a 5 kHz carrier frequency delivered with a speaker (Dell). All traces were time-locked using PackIO (Watson et al., 2016).

8.6.2 Air puff discrimination

For “rule 1 only” animals were exposed to the same behavioural paradigm previously described (Benezra et al., 2024). In brief, adult water-deprived mice (85-90% of their original weight) were trained over 10 days in the discrimination of two orthogonally oriented air puffs, with only one associated with reward. Association was measured through licking response, using a custom-made lickometer. Both air puffs were kept constant at a pressure of 10 PSI across the 10 days, with a duration of 100 ms. Air puff stimulation was delivered with a Picospritzer III (Parker) plus a custom made (3D printed) holder. The task was Pavlovian, in that the reward was delivered independently of the mouse’s behaviour. 10 µL rewards were delivered 0.5 s after the onset of the conditions stimulus (CS+). Out of the two directions, the choice of air puff

rewarded was randomised for each animal on day 1, and kept constant thereafter. Rewards were delivered through a gravity system gated by a solenoid surrounded by noise-absorbing material. White noise was played throughout the task to ensure the mice did not hear the solenoid reward delivery. This was confirmed by observing a lack of licking in response to 0 PSI control air puffs where a reward was delivered (**Supplementary figure 7d**). Mice performed 180 trials every day (~90 CS+/90 CS-), in randomised order, for a maximum water delivery of 0.9 mL over 30 min. The intertrial interval was a randomised gap of 8-12 s. Mice were head-fixed and exposed to non-rewarded air puffs two-days before the start of the training; no other task shaping was performed. For animals exposed to “rule 1 & 2”, as well as “rule 1 & 2 opto”, this paradigm was modified during day 5 and 7 by introducing 25% of trials in which the unrewarded air puff was paired to reward delivery and *vice versa*. The air puff pressure for day 5 and 7 was respectively 10 and 50 PSI. All rule 2 trials were paired with 595 nm light delivery on top of S1BF (hidden from the animal view with black electrical tape). “rule 1 & 2” (opsin-negative controls) and “rule 1 & 2 opto” (opsin-expressing experimental animals) underwent the exact same protocol (including opsin injection), but they were SERT-cre (-) and SERT-cre (+) littermates (generated from a SERT-cre Het x WT crossing) respectively. Experiments were performed blind to animal genotype, although Chrimson-tdTomato expression was observable in S1BF in 5-HT axons (**Supplementary figure 7a**), limiting our ability to fully blind the experimenter. All learning paradigms were programmed and delivered using custom-made Python code and PackIO (Watson et al., 2016).

8.6.3 Reversal learning

Animals were trained to expert-level in the previous air puff discrimination task, defined as >= 70% accuracy, during the 10 day described paradigm. Then, animals were trained in the reversal of the task by pairing reward delivery only with the old unconditioned stimulus, during a two day paradigm. The first day of reversal, animals were injected intraperitoneally with either vehicle or psilocin (2 mg/kg of body weight) 1h before training. Animals were trained for 180 trials, i.e., 30 min, each day.

8.7 Theoretical model

8.7.1 Gated deep neural network model

We developed a two-layer gated deep neural network model in the teacher-student framework. Both teacher and student had 400 inputs, a single layer with two nodes that had the error function as a non-linear activation function, and a single output node. The mean squared error was used as the loss function. For simulations, accuracy was calculated averaging the number of trials in which the student output sign (+ or -) matched the output sign of the teacher. For the analytical solution, accuracy was estimated from monte carlo sampling (from 1000 samples). Teacher neural networks were initialised at random from a Gaussian distribution of mean 0 and variance 1. Student neural networks were initialised at random from a Gaussian distribution of mean 0 and variance 0.001. The student network had to learn the N-to-1 dimensional mapping of the teacher network through online stochastic gradient descent. Parameters were optimised for each model comparison. For the general testing of the effect of saliency and misleading trials (**Figure 29**), second rule trials (5% of the trials) had Gaussian inputs drawn from N(0,5), while first rule trials (95% of the trials) were drawn from N(0,1). Misleading trials were randomly

presented across the whole learning paradigm. The value of the 5-HT-like gate was the inverted of the variance. Learning rate was 2.5, and the total number of epochs used for training was 25,000. For comparison to the behavioural air puff discrimination paradigm (**Figure 30**). In order to account for the behavioural air puff discrimination results, the model settings were adjusted. Namely, misleading trials were only presented between epochs 720-900 (low variance, all inputs ~ N(0,1)) and 1080-1260 (high variance, all inputs ~ N(0,5)), the learning rate was 7.5, the prevalence of misleading rule 2 trials was 25% and the total number of training epochs was 1800 (180 epochs per day-equivalent during 10 day-equivalents of training). The 5-HT-like gating was computed as:

$$gate = \frac{1}{\sigma^2(input)*5}$$

Where $\sigma^2(input)$ is the variance of the input for that trial and is only in place during that epoch range.

In the case of the reversal learning modelling (**Figure 31**), gated deep neural networks with the same architecture were trained in rule 1 for 1800 epochs at a learning rate of 7.5 and using the gating implementation described above. From epoch 1801, networks were trained in rule 2 for another 1800 trials after removal or not of the gating mechanism. Finally, to model the role of 5-HT in development (**Figure 32**), the same neural networks were trained in rule 1 with a learning rate of 12.5 during 1800 epochs, of which the first 1000 were (or not) gated with the implementation described above. Activation magnitude as a function of the gating was also calculated from this same model. Pruning was implemented using a similar model simulated with pytorch, in which the hidden layer had 200 nodes, and training lasted only 100 epochs, that were ungated, gated as above, or gated by half the value. Pruning was calculated using the 20th percentile of activation of neurons in the ungated model as a threshold for neuron (i.e., node) survival.

8.7.2 Sketch of the derivation of the ODE description

Here we provide additional details on the derivation of the ODE system underlying the analytical solution of our model, i.e., online learning in the teacher-student setup for a 2-layer network in the high-dimensional limit, d → ∞, with K neurons and i.i.d. Gaussian inputs. Thus, to recover the low-dimensional deterministic description we are going to consider the asymptotic limit where the input size d → ∞. Note that the full derivation was first derived (Biehl & Schwarze, 1995; Saad & Solla, 1995), and then rigorously proven in (Goldt et al., 2019). The network is trained using one-pass stochastic gradient descent on MSE loss.

$$MSE\ (y, \hat{y})\ = \frac{1}{2}\ (\hat{y}\ -\ y)^2$$

Given an input-output pair (X, y), we define the receptive field of any student (i) and teacher ($\boldsymbol{\alpha}$) hidden layer neuron as:

$$\lambda i\ = \frac{Wi \cdot X}{\sqrt{N}} \quad \lambda\boldsymbol{\alpha}\ = \frac{W\boldsymbol{\alpha} \cdot X}{\sqrt{N}}$$

and the error as:

$$Loss\ = \frac{1}{2}\ (Vi \cdot \sigma(\lambda i)\ \ -\ \ V\boldsymbol{\alpha} \cdot \sigma(\lambda\boldsymbol{\alpha}))^2$$

Where σ() is the activation function (i.e., the error function in our case), V is the second set of weights and N is the number of inputs.

The discrete time oSGD updates:

$$\Delta W = W(t+1)i - W(t)i = -\eta \cdot \frac{dLoss}{dW}$$

$$\Delta W = W(t)i - \eta \cdot (Vi \cdot \sigma(\lambda i) - V\boldsymbol{\alpha} \cdot \sigma(\lambda \boldsymbol{\alpha})) \cdot Vi \cdot \sigma'(\lambda i) \cdot \frac{X}{\sqrt{N}}$$

$$\Delta V = V(t+1)i - W(t)i = -\frac{\eta}{N} \cdot \frac{dLoss}{dV}$$

$$\Delta V = W(t)i - \frac{\eta}{N} \cdot (Vi \cdot \sigma(\lambda i) - V\boldsymbol{\alpha} \cdot \sigma(\lambda \boldsymbol{\alpha})) \cdot \sigma(\lambda i)$$

where η represents the learning rate. We then describe the evolution of the model across learning as a function of three order parameters:

$$Q = \frac{W \cdot W}{N} \quad M = \frac{W_T \cdot W}{N} \quad T = \frac{W_T \cdot W_T}{N}$$

where Q is the student hidden layer weight correlation, M the teacher-student hidden layer weight correlations and T the teacher hidden layer weight correlations. Since only the student parameters are updated across learning, T is a constant. Using the SGD update equations for the first layer weights we can described the evolution of M and Q as:

$$\Delta M = M_{t+1} - M = \frac{(W_i + \Delta W_i) \cdot W_\alpha - W_i \cdot W_\alpha}{N} = \frac{\Delta W_i \cdot W_\alpha}{N}$$

$$= \frac{\eta}{N} \cdot (Vi \cdot \sigma(\lambda i) - V\boldsymbol{\alpha} \cdot \sigma(\lambda \boldsymbol{\alpha})) \cdot Vi \cdot \sigma'(\lambda i) \cdot \lambda \boldsymbol{\alpha}$$

$$\Delta Q = Q_{t+1} - Q = \frac{W_i \cdot W_j + W_i \cdot \Delta W_j + W_j \cdot \Delta W_i + \Delta W_i \cdot \Delta W_j - Q}{N}$$

$$= \frac{1}{N} \cdot (W_i \cdot \eta \cdot (V_j \cdot \sigma(\lambda_j) - V_{\alpha j} \cdot \sigma(\lambda_{\alpha j})) \cdot V_j \cdot \sigma'(\lambda_j) \cdot \frac{X}{\sqrt{N}} +$$

$$W_j \cdot \eta \cdot (V_i \cdot \sigma(\lambda_i) - V_{\alpha i} \cdot \sigma(\lambda_{\alpha i})) \cdot V_i \cdot \sigma'(\lambda_i) \cdot \frac{X}{\sqrt{N}} +$$

$$\frac{\eta^2}{N} \cdot V_i \cdot V_j \cdot \sigma'(\lambda_i) \cdot \sigma'(\lambda_j) \cdot \frac{X^2}{N} \cdot (\Sigma V_{i/j} \cdot \sigma(\lambda_{i/j}) - \Sigma V_{\alpha(i/j)} \cdot \sigma(\lambda_{\alpha(i/j)}))^2)$$

$$= \frac{\eta}{N} \cdot [(\Sigma V_j \cdot \sigma(\lambda_j) - \Sigma V_{\alpha j} \cdot \sigma(\lambda_{\alpha j})) \cdot V_j \cdot \sigma'(\lambda_j) \cdot \lambda_i + (\Sigma V_i \cdot \sigma(\lambda_i) - \Sigma V_{\alpha i} \cdot \sigma(\lambda_{\alpha i})) \cdot V_i \cdot \sigma'(\lambda_i) \cdot \lambda_j +$$

$$\frac{\eta \cdot X^2}{N^2 \sqrt{N}} \cdot V_i \cdot V_j \cdot \sigma'(\lambda_i) \cdot \sigma'(\lambda_j) \cdot (\Sigma V_i \cdot V_j \cdot \sigma(\lambda_i) \cdot \sigma(\lambda_j) - 2 \cdot \Sigma V_i \cdot V_\alpha \cdot \sigma(\lambda_i) \cdot \sigma(\lambda_\alpha) + \Sigma V_\alpha \cdot V_\beta \cdot \sigma(\lambda_\alpha) \cdot \sigma(\lambda_\beta))]$$

where i,j, are any student hidden layer nodes; α, β are any teacher hidden nodes and X are i.i.d gaussian inputs. Then the generalisation error is calculated:

$$\epsilon_g = \frac{1}{2} \cdot (\hat{y} - y)^2 = \frac{1}{2} \cdot (\Sigma V_i \cdot \sigma(\lambda_i) - \Sigma V_\alpha \cdot \sigma(\lambda_\alpha))^2$$

$$= \frac{1}{2} \cdot (\Sigma V_i \cdot V_j \cdot \sigma(\lambda_i) \cdot \sigma(\lambda_j) - 2 \cdot \Sigma V_i \cdot V_\alpha \cdot \sigma(\lambda_i) \cdot \sigma(\lambda_\alpha) + \Sigma V_\alpha \cdot V_\beta \cdot \sigma(\lambda_\alpha) \cdot \sigma(\lambda_\beta))$$

From these equations, in $d \to \infty$, we can obtain the expectation of the update of each parameter as a function of three types of integrals.

$$I_2 = E_{Z1,Z2}[\sigma(Z_1) \cdot \sigma(Z_2)]$$

$$I_3 = E_{Z1,Z2,Z3}[Z_1 \cdot \sigma(Z_2) \cdot \sigma'(Z_3)]$$

$$I_4 = E_{Z1,Z2,Z3,Z4}[\sigma(Z_1) \cdot \sigma(Z_2) \cdot \sigma'(Z_3) \cdot \sigma'(Z_4)]$$

8.8 Histology

8.8.1 Perfusion and slicing

Mice were anaesthetized in an induction chamber with isoflurane (5%, 1 L/min) and then injected intraperitoneally with a non-recovery dose of pentobarbital (Pentoject, Animalcare Ltd) (adjusted by mouse weight). The mice received intracardiac perfusion with 0.01 M PBS followed by 4% PFA (Sigma-Aldrich 37% Formaldehyde stock) for tissue fixation. The brain was dissected and left in 4% PFA for 24 h at 4 °C. Brains were placed in 0.01M PBS, embedded in agarose 5%, and sliced using a vibrating microtome (Leica VT1000S). Coronal sections of 50 µm were made. Brain slices were conserved in 0.01 M PBS with 0.05% sodium azide, at 4 °C.

8.8.2 Immunohistochemistry

Three brain sections from each animal were placed for 2 h in 2% goat or donkey serum in PBS-T (0.2% Triton in PBS) at room temperature. The tissue was incubated at 4 °C overnight with a primary antibody (rabbit anti-PV, AB2631173, goat anti-Tph2, 1:250, ab121013 Abcam) in blocking solution. Sections were washed with 0.01 M PBS 3 times and incubated for 2 h with the goat anti-Rabbit-Alexa647 (AB_2535813) or donkey anti-goat IgG;Alexa Fluor-405 (1:250 ab175664 Abcam) at room temperature. Tissue was washed with PBS and incubated with 1 mL of DAPI (1:1000) for 30 min. Finally, samples were washed with PBS again and mounted onto superfrost slides (ThermoScientific) with 0.01M PBS. A cover slide (VWR) was placed on top of the slide and sealed with nail polish (Superstay 7 days Maybelline).

8.8.3 Histological imaging

All imaging was performed blind to the sample genotype/treatment. Histological imaging was conducted with an epifluorescence microscope (Zeiss) for injection site confirmation and a confocal microscope (Olympus Fluoview FV1000) for interneuron imaging. Imaging settings were kept constant within the experimental batch (SERT-KO: WT, HET, KO and SSRI: Fluoxetine and sucrose). In both cases, z-stacks of the whole slice depth were obtained (~11 images per slice). 3 brain slices from each animal across both hemispheres were imaged.

8.9 Analysis

8.9.1 Behavioural analysis

Probability of lick was calculated as the proportion of trials in which the animal licked at least once after the onset of the air puff in a window of 0.5s (i.e., before the onset of reward for CS+). Accuracy was estimated as the proportion of true positives (or hit trials) and true negatives (or correct rejections) out of the total number of trials. For reversal learning, accuracy on the new task was normalised against the last recorded accuracy on the previous task (day 10), to account for the variability in expertise (70-100%).

For behavioural-state tracking analysis, time-locked recordings at ~30 frames/second of the mice while performing two-photon imaging were obtained with a camera (point grey CM3-U3-13Y3M-CS) and an infrared light (BW 48 LED). Movies were then used to train a ResNet-50 artificial neural network with 200 manually-labelled frames from 20 recordings, extracted with K-means clustering, to track 3 markers (nose, left and right forelimbs) using DeepLabCut (Nath et al., 2019). Successful tracking was achieved after 500 000 epochs and pose estimation was performed for all recordings. Movement was calculated as the euclidean distance between the two dimensional coordinates of consecutive frames for each marker.

Sleep state was estimated from the left forelimb (i.e., the marker with best visibility) movement with the following criteria: continuous movement was considered wakefulness, lack of movement quiet sleep and sharp twitches active sleep.

8.9.2 5-HT sensor analysis

All images were pre-processed by registration with Turboreg (Thevenaz et al., 1998) against a mean-intensity average of 200 frames in Fiji (Schindelin et al., 2012). All fluorescent (F) traces are presented as ΔF/F:

$$\Delta F/F \ = \frac{(F - Fmean)}{Fmean}$$

where Fmean is the mean fluorescence of the recording session. For stimulus responses in animals P14 or older, when a hemodynamic response was observable, tdTomato fluorescence was used as a ratiometric control, as in our previous work (Ocana-Santero et al., 2024). Signal filtering was performed using the Savitzky–Golay filter with a third order polynomial on windows of 31 frames (~1s). For subregion analysis, custom-designed code in Fiji was used to quantify mean fluorescence in a 256 subregion grid.

8.9.3 Calcium sensor analysis

Suite2p (Pachitariu et al., 2017) was used to perform registration, cell detection and fluorescent trace extraction of all calcium recordings. Given the difficulty of finding the right correction factor under conditions of high cell density (**Supplementary figure 13b**) and very high cell-neuropil correlation (**Supplementary figure 13a**) (Dipoppa et al., 2018), neuropil subtraction was not performed. Regarding signal normalisation, due to the change in calcium neurophysiology

across development, and the importance of the baselining strategy to compare measurements from different animals, we chose to normalise against the first percentile, as this showed the highest stability across development (**Supplementary figure 13e**). Thus calcium developmental recordings are presented as ΔF/F:

$$\Delta F/F \ = \frac{F - F(1st\ percentile)}{F(1st\ percentile)}$$

Where F(1st percentile) is the first percentile of the raw fluorescence values of each cell across the whole recording. Adult recordings were normalised against the mean as in our previous work (Rowland et al., 2023).

High (H-) and low (L-) synchronicity developmental calcium events were detected with a custom made algorithm optimised in control animals until good detection was achieved (**Supplementary figure 13d**), yielding similar event frequency to previous studies (Siegel et al., 2012). Given the duration of events is ~2-20 seconds (**Figure 10f,j**), detection was performed in six second time bins from the 20 minute baseline recording session. First, if the mean fluorescence across all cells was ever greater than the mean ΔF/F, the maximum was selected as the event peak. Next, adjacent bins were searched to determine if any maximum reached in those bins exceeded the selected event peak in the current bin, implying that the event stretched across more than one time bin. The event peak was therefore defined as the maximal peak across the bin and adjacent bins. Event duration was defined as the period around the event peak where the mean ΔF/F of all cells was greater than the mean. Single cells were considered to participate in an event when their mean fluorescence within the event period was greater than the mean fluorescence of the individual cell. H-events were defined as events with more than 80% of cells participating, and L-events as 20-80% of cells being recruited, based on previous studies (Leighton et al., 2021; Siegel et al., 2012).

Automatic interneuron detection based on tdTomato expression was optimised to minimise false positives, allowing identification of a subset of interneurons within the field of view. Cells were identified as interneurons when their mean fluorescence during a 20-second 765nm-laser recording was equal or higher than the 97th percentile.

Correlations were calculated between all cell pairs using Pearson's correlation coefficient. For correlations across distance, suite2p ROIs coordinates were used to calculate the euclidean distance between cells and the average cell-to-cell correlation was obtained on bins of ~40 μm distance. Whisker response amplitude was defined as the maximum ΔF/F value on a 20s post-stimulus window of time (i.e., within the interstimulus interval). Cell-neuropil correlations were calculated with Pearson's correlation coefficient between the entire trace from the 20 min baseline session of the suite2p-extracted ROI and its surrounding neuropil region.

Neuronal recruitment upon sensory stimuli was determined by calculating the proportion of responsive neurons. Responsiveness was defined as statistically significant differences between the 1s mean pre- versus post- stimulus onset with paired t-test or Wilcoxon signed-rank test after addressing normality with Shapiro-Wilk test and correcting for multiple comparisons with Benjamini/Hochberg method.

Genotype logistic regression classifiers used a logistic regression model with an L2 penalty term to the weights with a regularisation strength of 0.001 (after parameter optimization). The Scikit-learn implementation of logistic regression was used (Pedregosa et al., 2011) on average fluorescence of 500 ms time bins for 500 randomly selected cells, on a 20s post-stimulus window of time, creating 500-elements feature vectors. A classifier was trained for each stimulus type and time bin. A 60/40 random train/test split was performed across individual animals to ensure subject-wise cross-validation (Saeb et al., 2017). Test decoding accuracy was calculated for each time bin and the maximum decoding accuracy was selected (**Figure 15,22**). The accuracy of 7000 classifiers trained in permuted data were used to define significance

thresholds (**Supplementary figure 4f**) for each classifier. Logistic regression classifiers for stimulus type (**Supplementary figure 4d**) were implemented without time bins or averaging, but by using a 20 second post-stimulus window (600 frames) of 500 randomly selected cells to create a 300,000 feature vector. A single classifier was generated for each animal, and cross-validation was performed recording-wise.

Representational similarity analysis was performed with the Scipy (Virtanen et al., 2020) implementation of correlation distance (1 - Pearson's correlation coefficient), as a measure of representational dissimilarity. Correlation distance was calculated across every trial, using the mean 15 frames (0.5 seconds) post-stimulus onset (i.e., before reward onset). For mean dissimilarity the average of the relevant section of the representational dissimilarity matrix was used.

8.9.4 Histological analysis

For injection site confirmation, GCaMP6s fluorescence was visually confirmed in S1BF. For interneuron quantification, all imaging was performed blind to the sample genotype/treatment. Z-stacks were collapsed into z-projections using the max (SERT-KOs) or the mean (Fluoxetine/sucrose) with Fiji (ImageJ). Using QuPath (Bankhead et al., 2017), annotations were drawn over several 200 μm wide cortical columns (~5 per image). Sub-annotations were manually drawn in the columns for each layer, based on DAPI cytoarchitecture (**Supplementary figure 7**). Automatic cell detection was done with the DAPI channel in Qupath by optimising signal intensity, nuclei expected size, and cytoplasmic expansion thresholds. Interneuron classification was performed in QuPath (Bankhead et al., 2017) by training random trees classifiers in a subset of images until human-like classification performance was achieved. A classifier was trained on each marker (VIP, Nkx2-1 and PV). Automatic classification was run throughout annotations and images with custom-made workflow scripts. Counts for each layer

were averaged across columns, hemispheres, and slices for each animal, such that all plotting and statistics were done using animals as independent data points.

8.10 Statistics

Statistical analyses were conducted using python 3.9 and all were two-sided tests unless otherwise indicated. Normality was assessed by the Shapiro–Wilk test. Two-group comparisons were performed with t-test/paired t-test and Mann–Whitney U test/ Wilcoxon signed-rank test for parametric and non-parametric tests of measurements in the same/different mice respectively. Multigroup testing across a single variable was performed with either one-way ANOVA or Kruskal–Wallis test for parametric and non-parametric testing respectively. Multigroup testing across two variables (e.g., across genotype and age) were performed by two-way ANOVA for normally distributed data, and two-way permANOVA, i.e., with permutation testing, for non-normally distributed data. Pairwise comparisons were performed with Fisher's Least Significant Difference (LSD) for three groups, Tukey's HSD test for more than three groups when the data was parametric and Dunn's test for non-parametric data. Multiple comparison correction was performed with Bonferroni-Holm correction unless otherwise indicated. Kolmogorov–Smirnov test was used to compare distributions. Bootstrapping was used to test the significance of logistic regression classifiers. All statistical analysis was performed using single animals as independent points, except when population analysis was performed (interneuron analysis), in which case cells were used as independent points, but similar trends were confirmed when averaging by animals. The precise statistical test is described in the figure legends. Statistical significance was considered for *$p<0.05$ and **$p<0.01$.

8.11 Software

Microscopy images were processed with Fiji (Schindelin et al., 2012) (processing package based on ImageJ). Automatic cell detection and classification were performed with Qupath (Bankhead et al., 2017). Turboreg (Thevenaz et al., 1998) was used for g5-HT3.0 image registration and Suite2p for GCaMP6s recording registration, cell detection and signal extraction (Pachitariu et al., 2017). DeepLabCut was used for behavioural tracking (Nath et al., 2019). Figures were created from panels using Adobe Illustrator. Images for diagrams were obtained from SERVIER medical arts kits (https://smart.servier.com/). All *in vivo and in vitro* analysis, statistics and plotting were performed in python 3.9.

9. Supplementary figures

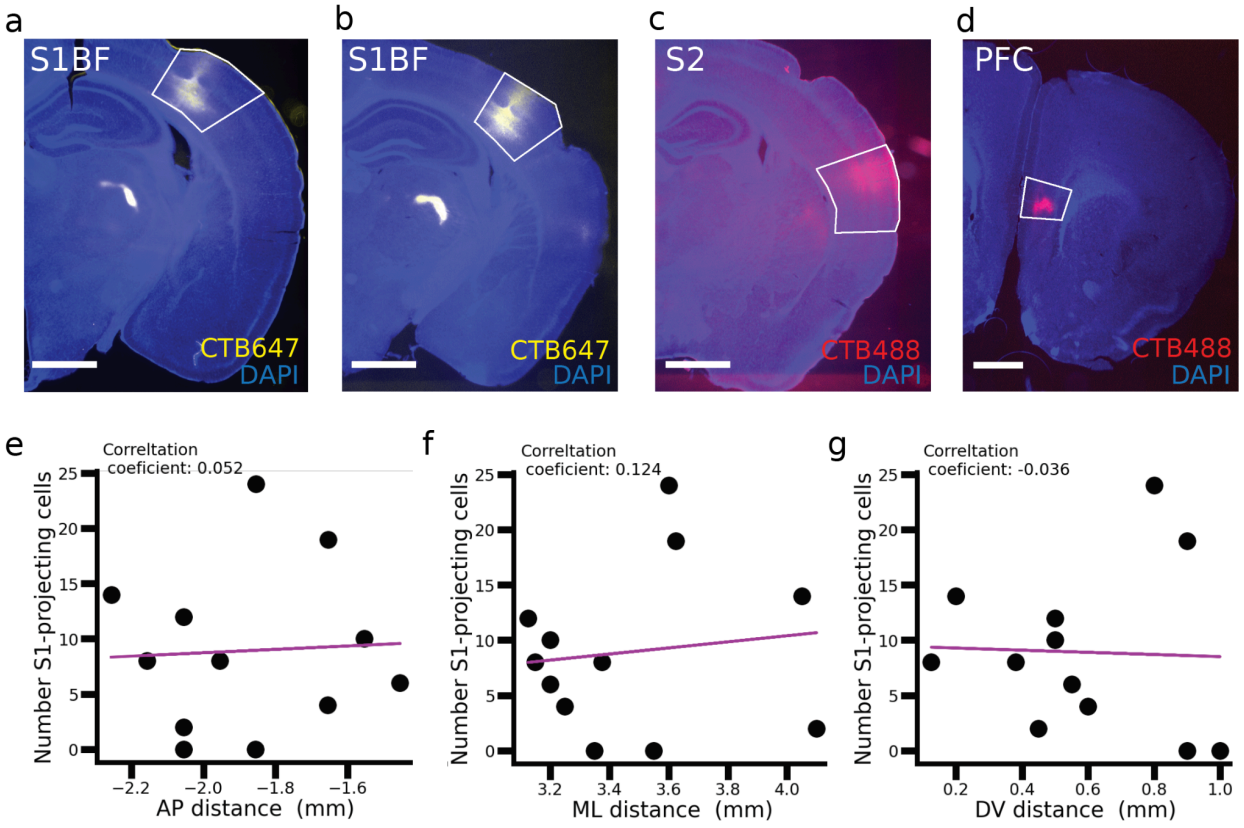

Supplementary figure 1. CTB retrograde tracing representative injection sites and S1BF injection variability. (A-D) Epifluorescence microscope images showing representative injection sites for CTB647 or CTB488 in S1BF (**A,B**), S2 (**C**), and PFC (**D**), using DAPI-stained slices. (scale bar = 1mm). **(E-F)** Scatter plot of S1BF-retrogradely labelled tph2+ cell number and injection site coordinates in the antero-posterior (**E**), medio-lateral (**F**) and dorso-ventral (**G**) axes, suggesting comparable amount of 5-HT projections across different S1BF locations.

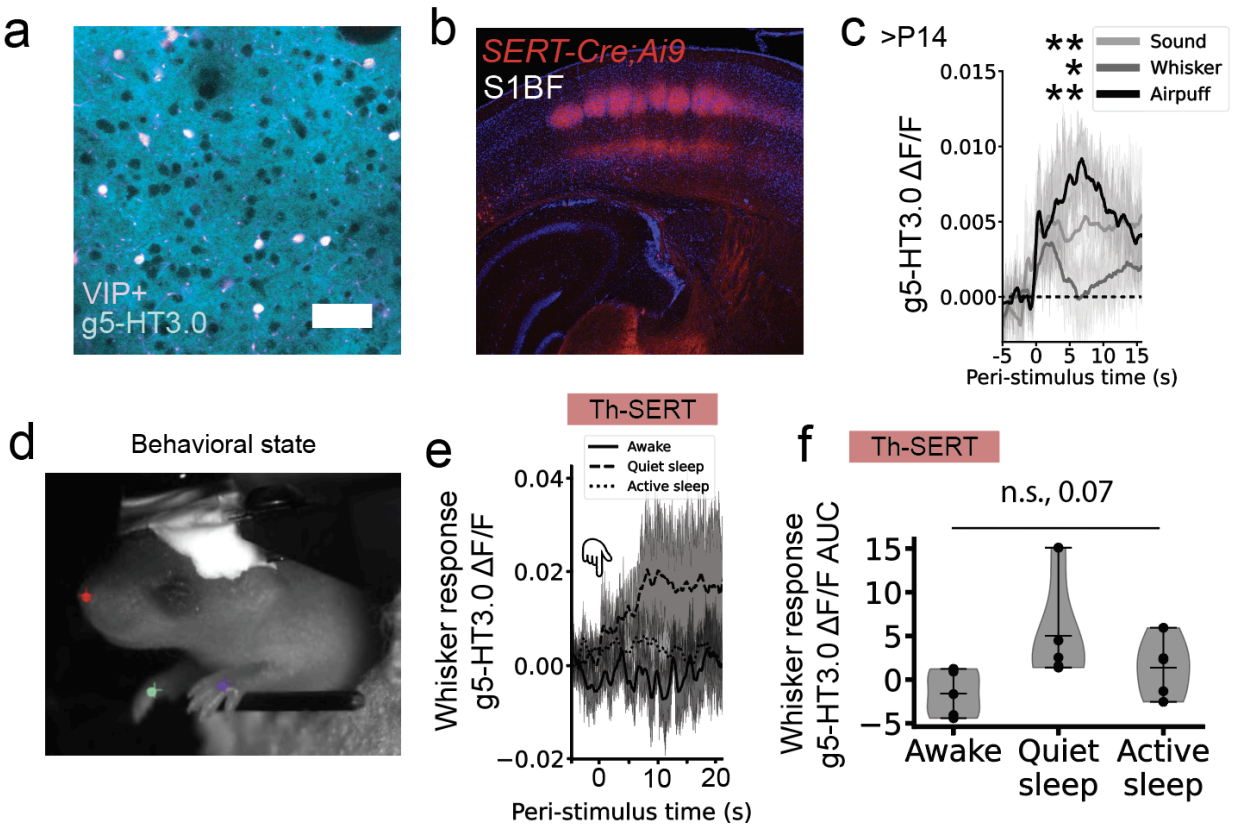

Supplementary figure 2. Developmental 5-HT dynamics. a, S1BF L2/3 field of view in a P21 mouse expressing the genetically encoded fluorescent 5-HT sensor g5-HT3.0 and tdTomato in VIP+ interneurons. **b,** Confocal image of S1BF from a transgenic SERT-Cre;Ai9 animal expressing tdTomato in SERT+ neurons, shows strong thalamo-cortical labelling that delineates the barrels, illustrating the previously reported SERT transient developmental expression. **c,** Average g5-HT3.0 signal in S1BF upon the presentation of 10 whisker (paired t-test p = 0.019), air puff (paired t-test p = 0.006) or sound (paired t-test p = 0.009) stimuli in WT animals older than P14 (n=6). **d** Frame from an infrared camera while 2-photon imaging was performed in a P8 pup. Manually labelled (circle) and deeplabcut predicted (cross) markers overlap, showing tracking of nose (red), green (right forelimb) and purple (left forelimb), the latter used for behavioural state scoring. **e** Average peri-stimulus g5-HT3.0 trace in response to whisker stimulation in P7-10 WT animals, as a function of behavioural state (i.e., awake, quiet sleep or active sleep) and the corresponding areas under the curve (**f,** ANOVA sleep-state p = 0.07, n = 4).

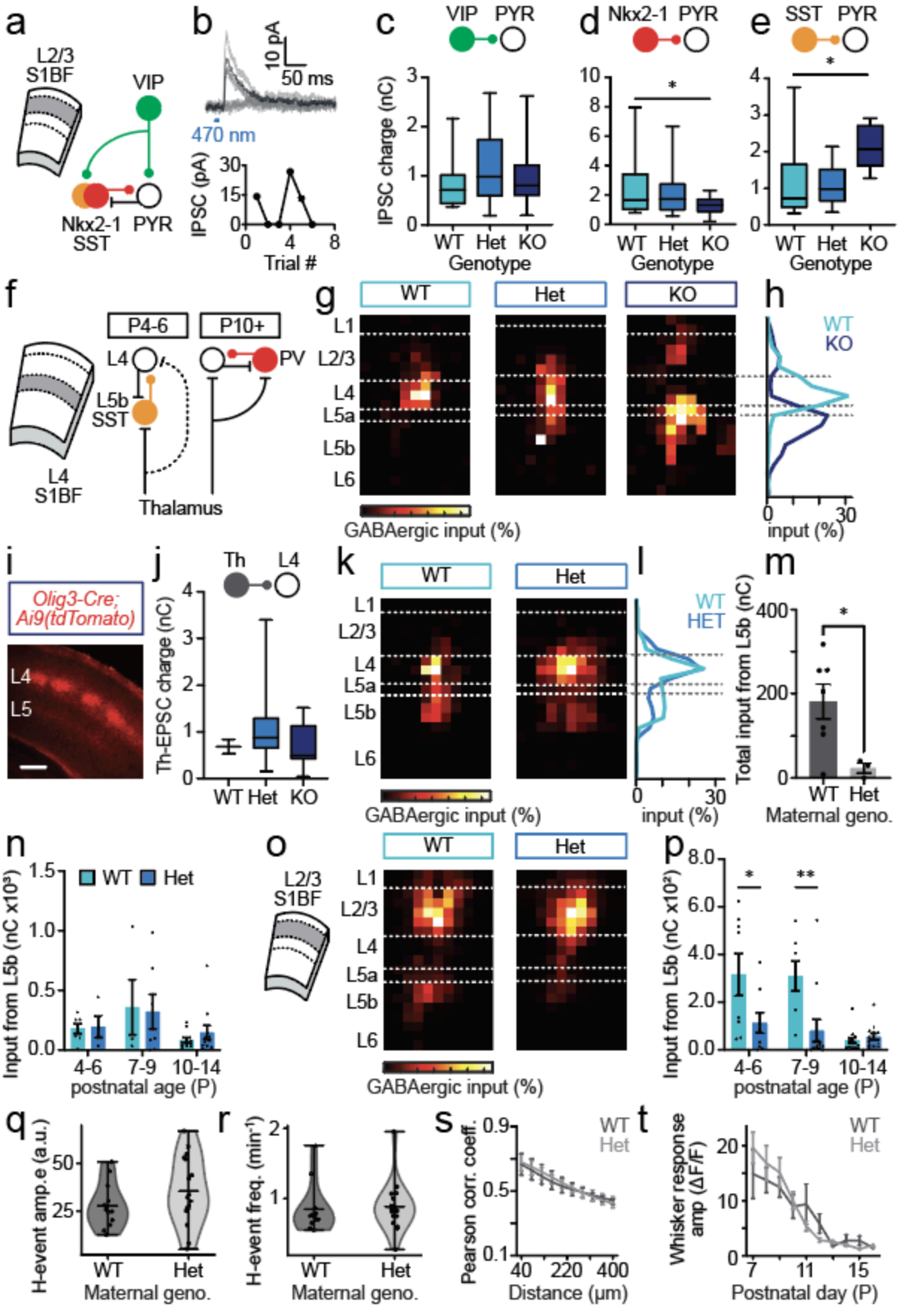
a
L2/3
S1BF
VIP
Nkx2-1
SST
PYR
b
10 pA
50 ms
470 nm
IPSC (pA)
Trial #
c
VIP PYR
IPSC charge (nC)
WT Het KO
Genotype
d
Nkx2-1 PYR
e
SST PYR
f
P4-6
P10+
L4
L5b
SST
PV
L4
S1BF
Thalamus
g
WT
Het
KO
L1
L2/3
L4
L5a
L5b
L6
GABAergic input (%)
h
WT
KO
input (%)
i
Olig3-Cre;
Ai9(tdTomato)
L4
L5
j
Th L4
Th-EPSC charge (nC)
WT Het KO
k
WT
Het
GABAergic input (%)
l
WT
HET
input (%)
m
Total input from L5b (nC)
WT Het
Maternal geno.
n
WT Het
Input from L5b (nC x10³)
4-6 7-9 10-14
postnatal age (P)
o
L2/3
S1BF
WT
Het
GABAergic input (%)
p
Input from L5b (nC x10²)
4-6 7-9 10-14
postnatal age (P)
q
H-event amp.e (a.u.)
WT Het
Maternal geno.
r
H-event freq. (min⁻¹)
WT Het
Maternal geno.
s
WT
Het
Pearson corr. coeff.
Distance (µm)
t
WT
Het
Whisker response amp (ΔF/F)
Postnatal day (P)

Supplementary figure 3. Perinatal 5-HT regulates the development of local GABAergic circuits. a, schematic showing the relationship between interneuron subtypes and pyramidal cells (PYR) in L2/3 of S1BF. **b,** representative superimposed traces and plot of repeat ChR2-mediated stimulation of Nkx2-1 interneuron synaptic input onto a L2/3 pyramidal cell demonstrating minimal stimulation protocol (~50% failure rate). Average minimal interneuron input recorded across the 3 genotypes generated by the SERT-Het x SERT-Het breeding paradigm for VIP (**c**), Nkx2-1 (**d**) and SST (**e**) interneuron subtypes; * a significant difference was observed in Nkx2-1 (**d**)(one-way ANOVA, genotype p = 0.07, Pairwise comparisons: WT-Het p = 0.666; WT-KO p = 0.047) and SST (**e**)((one-way ANOVA, genotype p = 0.0191, Pairwise comparisons: WT-Het p = 0.973; WT-KO p = 0.0187) synaptic input between SERT-WT and SERT-KO L2/3 pyramidal cells. **f**, schematic of the transient L5b SST input onto L4 spiny stellate neurons (SSNs) present in S1BF prior to P10, after which PV interneurons provide feed-forward inhibition. **g**, average LSPS maps of total GABAergic input onto L4 SSNs across the 3 SERT genotypes recorded during the P4-6 time window. Dashed white lines, average layer boundaries to the nearest 50 µm pixel. **h**, average profile of GABAergic input across the depth of the cortical column recording in SERT-WT and SERT-KO L4 SSNs. **i**, representative image showing conditional *Olig3-Cre*-dependent tdTomato expression in thalamic afferent fibres innervating S1BF in a SERT-KO P7 pup. **j**, minimum thalamic afferent input recorded in L4 SSNs across all 3 SERT genotypes. **k**, average LSPS maps for total GABAergic input onto L4 SSNs recorded in pups generated from breeding SERT-Het male and WT female mice during the P4-6 time window. **l**, profile of GABAergic input across the depth of cortex from the data shown in (**k**). **m**, reduction in total L5b GABAergic input onto L4 SSNs observed in WT pups born from either WT or SERT-Het (Het) females; (t-test p = 0.0414). **n**, total L5b GABAergic input onto L4 SSNs recorded in animals bred from SERT-Het male and WT female pairs across postnatal development. Corresponding data from the same WT female breeding paradigm is shown in panels (**o**) GABAergic input maps for L2/3 PYRs during the P7-9 time window and (**p**) timeline of L5b GABAergic innervation of L2/3; (t-test: P4-6 p = 0.0478, P7-9 p = 0.009, P10-14 p = 0.344) **q,** Mean H-event frequency in WT mice from SERT-WT/Het dams at P7-10. (Mann–Whitney U p = 0.277). **r,** Mean GCaMP6s signal amplitude of cells during H-events in WT mice from SERT-WT/Het dams at P7-10 (t-test p = 0.916). **s,** Pairwise cell correlations across distance in WT mice from SERT-WT/Het dams at P8 (two-way ANOVA, genotype p = 0.790). **t** Mean GCaMP6s whisker response amplitude across development (two-way ANOVA, genotype p = 0.746).

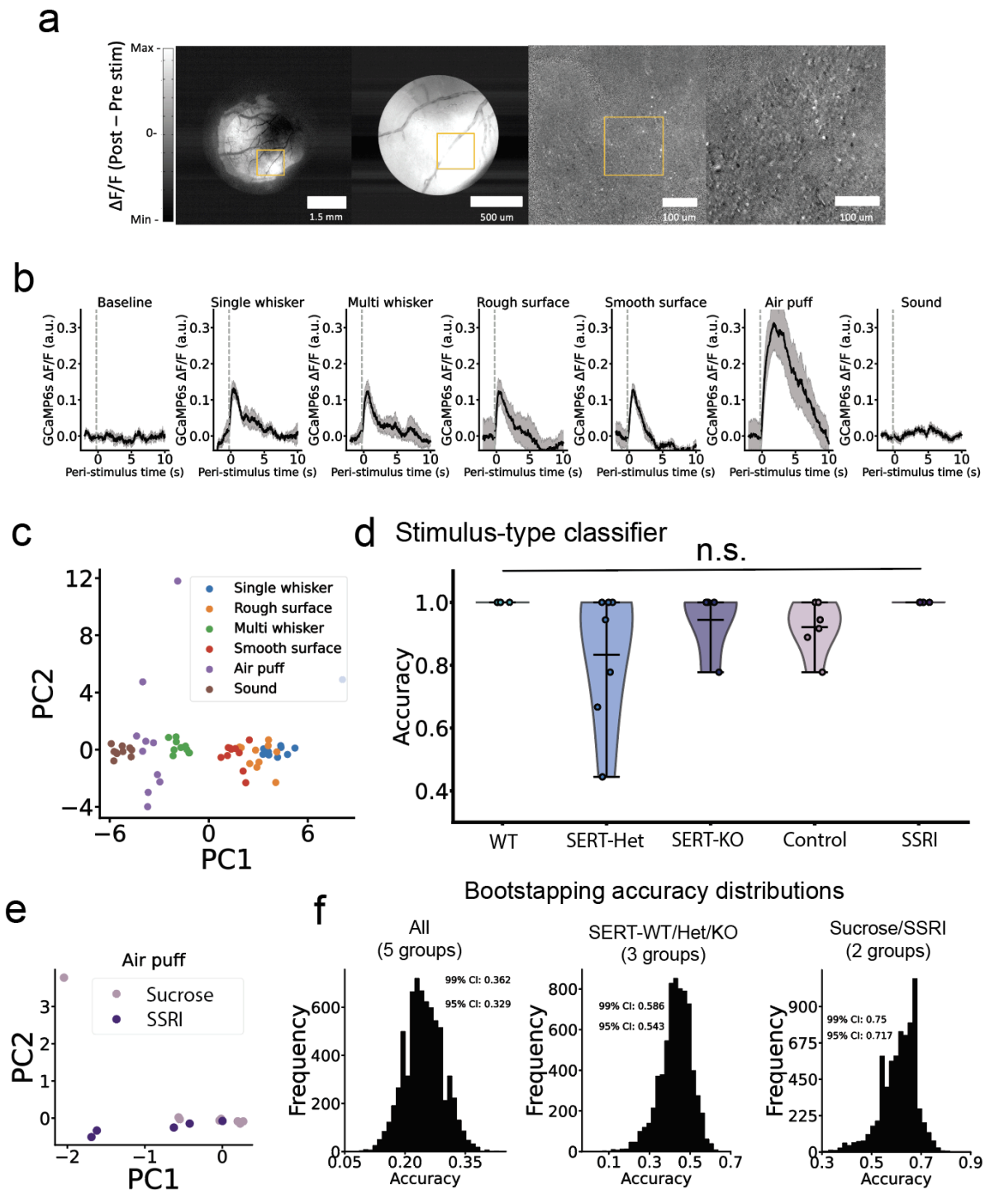
a
ΔF/F (Post – Pre stim)
Max
0
Min
1.5 mm
500 um
100 um
100 um
b
Baseline
Single whisker
Multi whisker
Rough surface
Smooth surface
Air puff
Sound
GCaMP6s ΔF/F (a.u.)
Peri-stimulus time (s)
c
Single whisker
Rough surface
Multi whisker
Smooth surface
Air puff
Sound
PC1
PC2
d
Stimulus-type classifier
n.s.
Accuracy
WT
SERT-Het
SERT-KO
Control
SSRI
e
Air puff
Sucrose
SSRI
PC1
PC2
f
Bootstapping accuracy distributions
All
(5 groups)
99% CI: 0.362
95% CI: 0.329
SERT-WT/Het/KO
(3 groups)
99% CI: 0.586
95% CI: 0.543
Sucrose/SSRI
(2 groups)
99% CI: 0.75
95% CI: 0.717
Frequency
Accuracy

Supplementary figure 4. Sensory encoding in adult somatosensory cortex of mice with developmental disruptions of SERT. a, Example of the online analysis used to map single barrels: Stimulus-triggered average fluorescence post- minus pre- single whisker stimulation in 1-photon (left) or 2-photon (right) microscopy. Images are the average of 10 stimuli. **b,** Stimulus-triggered average calcium trace of 10 repeats of each stimulus type for a representative WT animal, from left to right: baseline, single-whisker, multi-whisker, rough surface, smooth surface, air puff and sound. **c,** Principal component analysis showing the spread of neuronal responses to the repeats of the different stimuli (colour-coded) along the two first components. Data from a single representative WT mouse. **d,** Testing classification accuracy of logistic regression classifiers for the decoding of the different types of stimulation from the neuronal responses for WT, SERT-Het, SERT-KO, Sucrose-treated or SSRI-treated animals. A different classifier was trained for each animal. **e,** Principal component analysis showing the spread of neuronal responses to air puff stimulation along the two first components, for sucrose- and SSRI-treated animals. Each dot is a different animal. **f**, Null accuracy distributions generated by bootstrapping, i.e., training genotype/treatment classifiers on datasets with permuted labels. Sample sizes are 10 (WT), 8 (HET), 5 (KO), 6 (Control) and 5 (SSRI).

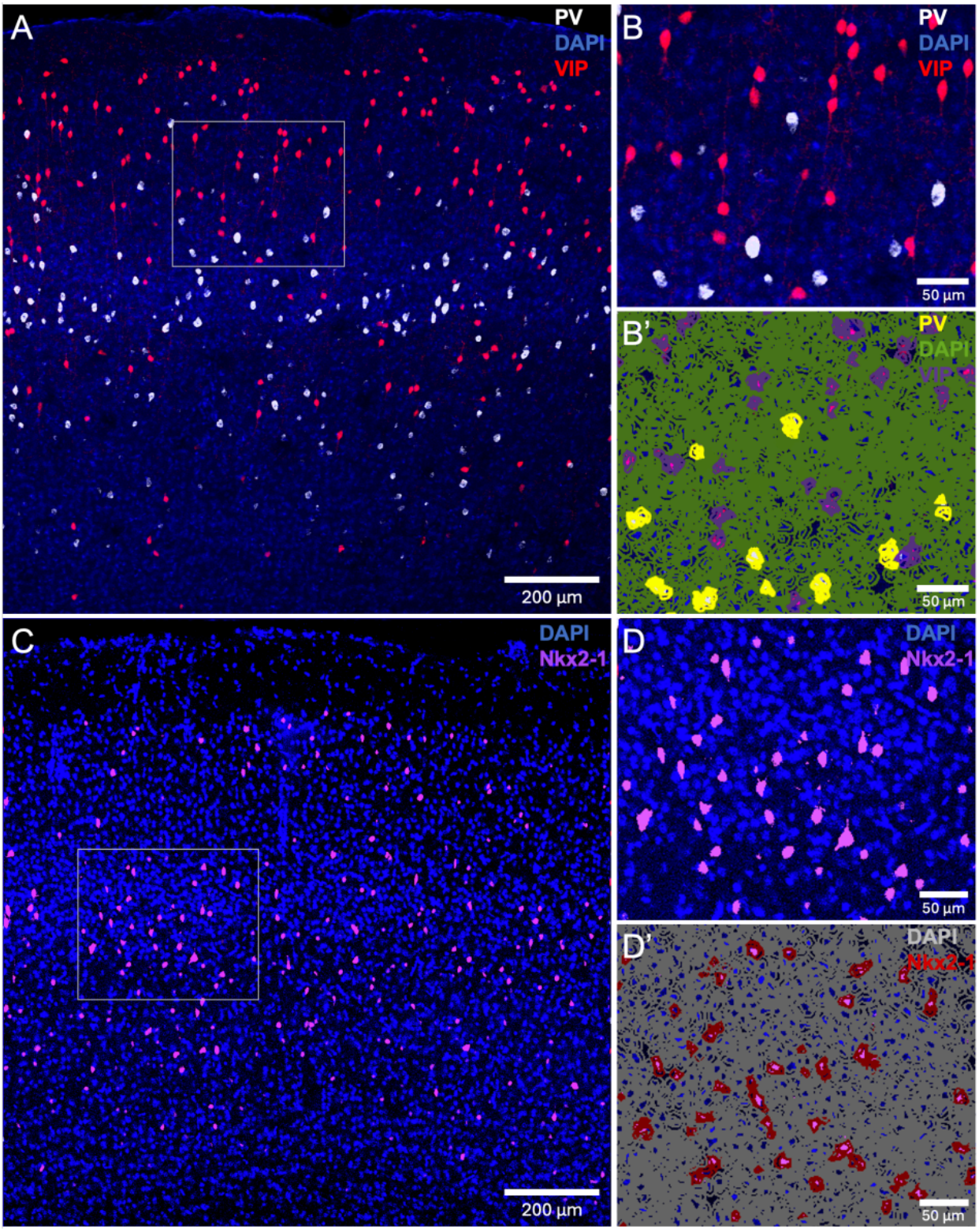
A
PV
DAPI
VIP
200 µm
B
PV
DAPI
VIP
50 µm
B'
PV
DAPI
VIP
50 µm
C
DAPI
Nkx2-1
200 µm
D
DAPI
Nkx2-1
50 µm
D'
DAPI
Nkx2-1
50 µm

Supplementary figure 5. Validation of automated interneuron classifiers. a, Confocal image of S1BF on an adult VIP-tdTomato. **b,** Same confocal image magnified ~2x, with comparisons to automated PV and VIP classifier detections, demonstrating consistent overlap (**b'**). **c,** Confocal image of S1BF on an adult Nkx2-1-tdTomato. **d,** Same confocal image magnified ~2x, with comparisons to automated Nkx2-1 classifier detections, demonstrating consistent overlap (**d'**).

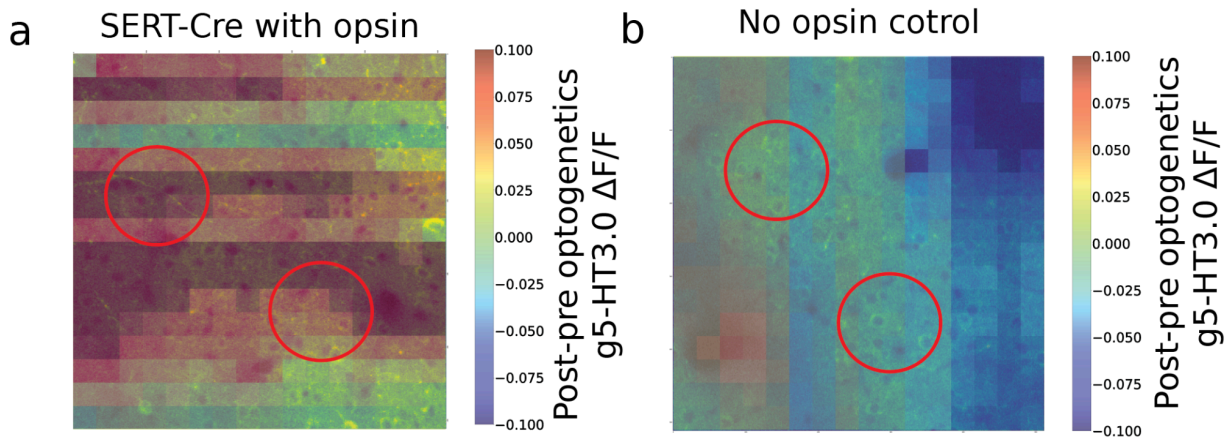

Supplementary figure 6. All-optical stimulation of DRN-SERT+ axons in S1BF triggers 5-HT increases. a,b Heat-map of g5-HT3.0 fluorescence signal post minus pre holographic localised optogenetic stimulation in animals expressing Chrimson in SERT+ DRN neurons (**A**) or control littermates (**b**), overlaid on top of the field of view for representative animals, illustrating localised 5-HT release in opsin-expressing animals. Red circles delineate area of two-photon optogenetic stimulation.

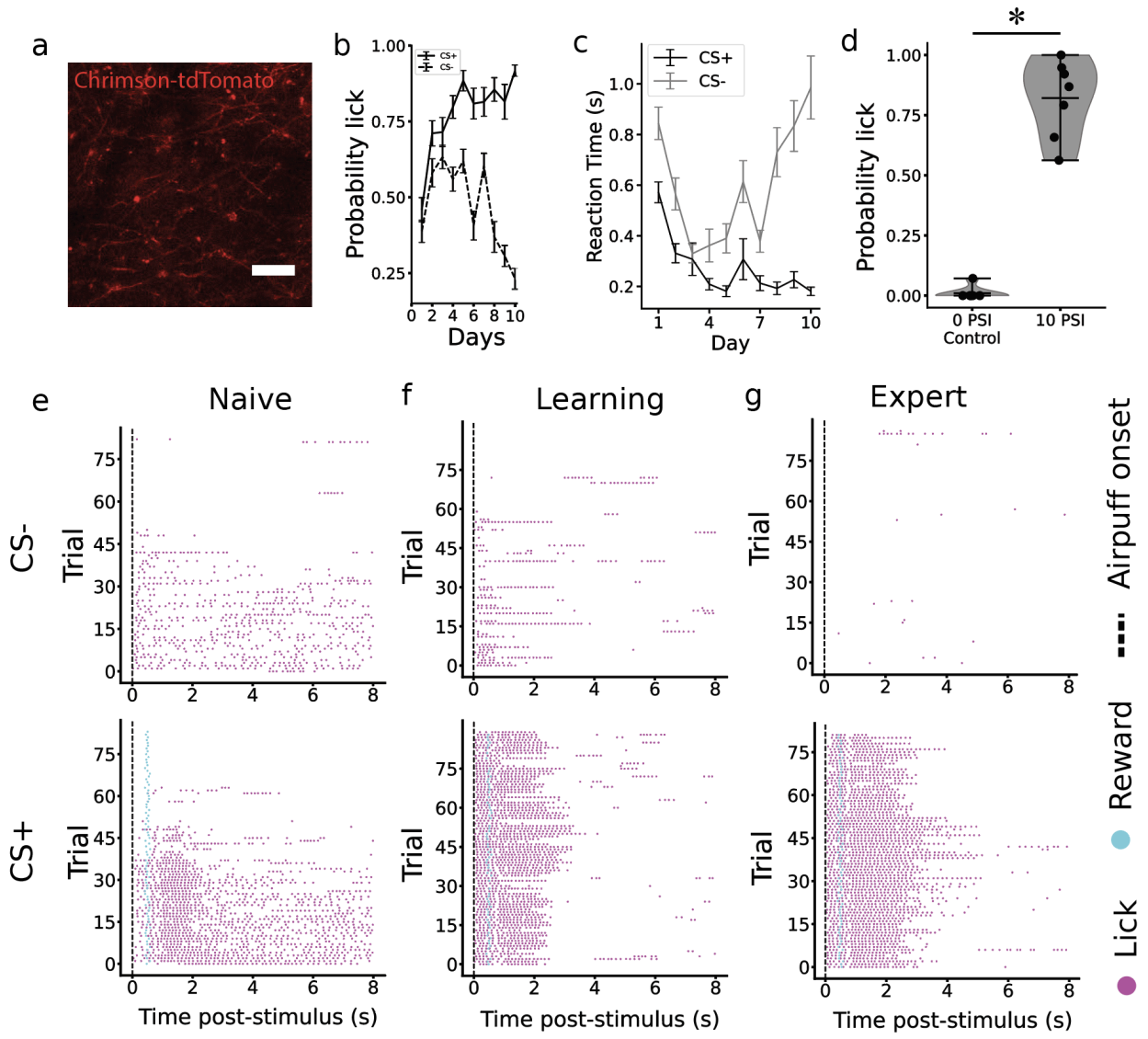

Supplementary figure 7. Learning of an air puff discrimination task. a Two-photon microscopy image showing Chrimson tdTomato-positive axons in S1BF from SERT+ DRN neurons *in vivo*. **b** Probability of licking to the conditioned (CS+, continuous line) or the unconditioned (CS-, discontinuous line) stimulus across a 10 day learning paradigm of the air puff discrimination task, before the onset of reward (0.5s after air puff onset) (n = 27 mice). **c** Evolution of mice reaction time to air puff presentation for both the conditioned (black) and unconditioned (grey) stimuli (n = 27 mice). **d** Probability of licking to a conditioned air puff paired to reward, at 0 (control) or 10 (normal) PSI stimulus pressure in expert (day 11) mice. This control illustrates that mice associate the reward to air puff, and not other correlating cues such as the solenoid noise (n = 7, Wilcoxon signed-rank test p = 0.016). **e-g** Raster plots of licking in response to unconditioned (top) or conditioned (bottom) air puff presentations in naive (**e**), learning (**f**) and expert (**g**) stages for a representative mouse.

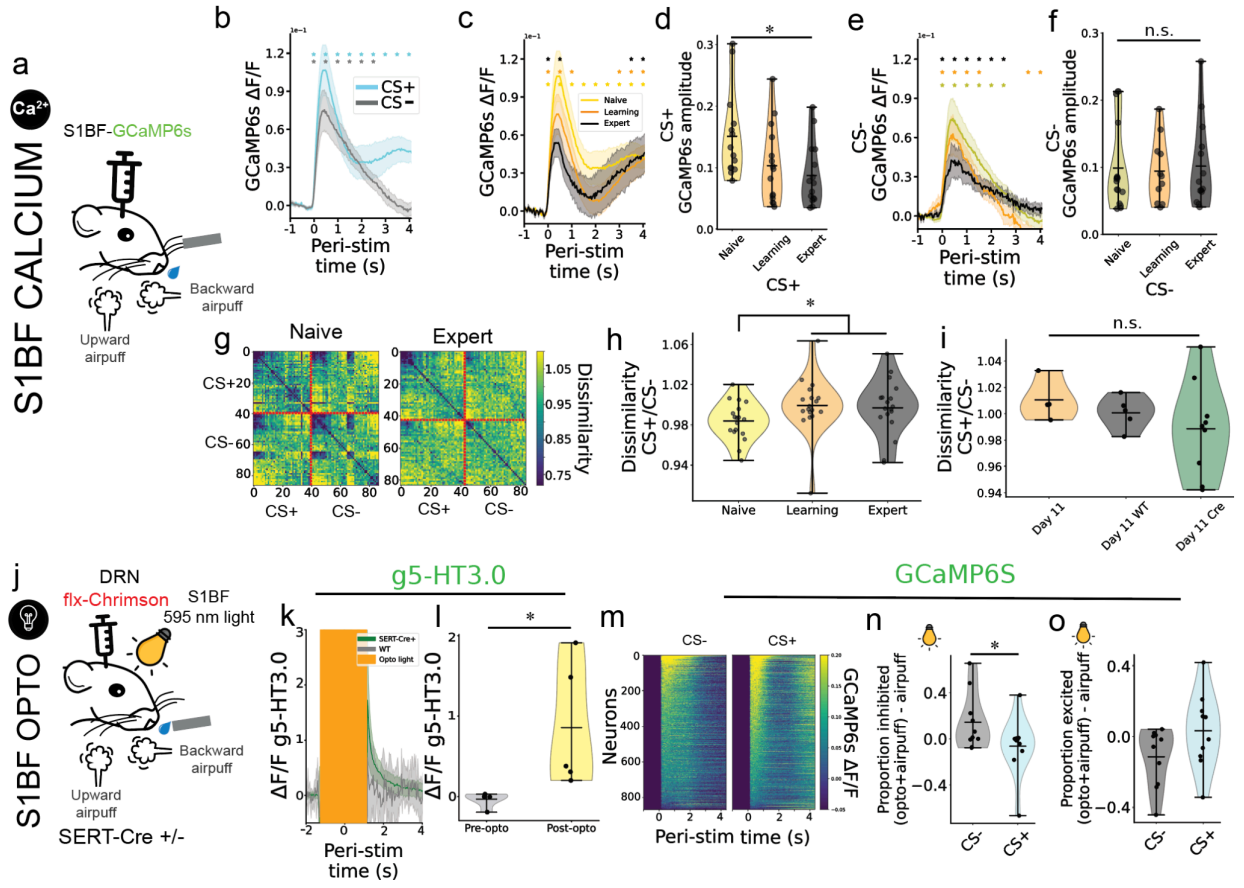

Supplementary figure 8. Neurophysiological correlates of the air puff discrimination task. **a** Diagram illustrating that animals injected with the green fluorescence calcium indicator GCaMP6s where trained in the air puff discrimination task. **b** Mean GCaMP6s peri-stimulus trace, in response to the conditioned and unconditioned air puff in naive (day 3) animals (n = 13, *p<0.05 paired t-test of post versus pre-stimulus signal in bins of 0.5s). **c,e** Mean GCaMP6s peri-stimulus trace, in response to the conditioned (**c**) and unconditioned (**e**) air puff in naive, learning or expert animals and (**d,f**) the respective violin plot of the maximum signal amplitude (n = 13, *p<0.05 paired t-test of post versus pre-stimulus signal in bins of 0.5s for traces **c** and **e**; one-way ANOVA for **d** p = 0.022, Tukey post hoc test naive-learning p = 0.104, naive-expert p = 0.021; one-way ANOVA for **f** p = 0.952). **g** Representative representational dissimilarity matrices for one naive and expert example mouse, calculated with correlation distance from calcium responses within 0.5s of stimulus onset during condition and unconditioned air puffs. **h** Mean calcium dissimilarity between the representation of condition and unconditioned air puffs in naive, learning and expert mice (n = 17, one-way ANOVA p = 0.028, Tukey post hoc test naive-learning p = 0.014, learning-expert p = 0.031). Mean calcium dissimilarity between the representation of condition and unconditioned air puffs in Rule 1 only (n = 4), rule 1&2 (n = 5) and rule 1&2 with optogenetics (n = 9) mice (Kruskal-Wallis test p = 0.223). **j** Diagram illustrating mice performing the air puff discrimination behaviour with misleading trials being paired to optogenetic activation of 5-HT neurons. (**k,l**) 5-HT green fluorescence sensor (g5-HT3.0) signal upon optogenetic stimulation in control (WT) or SERT-Cre animals showing 5-HT release in

S1BF (n = 5 mice, t-test p = 0.0361). **m** Perit-stimulus heat map of calcium responses (GCaMP6s) in a representative animal to the conditioned and unconditioned air puff during optogenetic stimulation. **n,o** Proportion of neurons inhibited (**n**) or excited (**o)** during optogenetic stimulation paired to an unconditioned (grey) or conditioned (blue) air puff, normalised by subtraction with just the same air puff stimulation (n = 9, Wilcoxon signed-rank test p = 0.019 (**n**) and paired t-test p = 0.211 (**o**)).

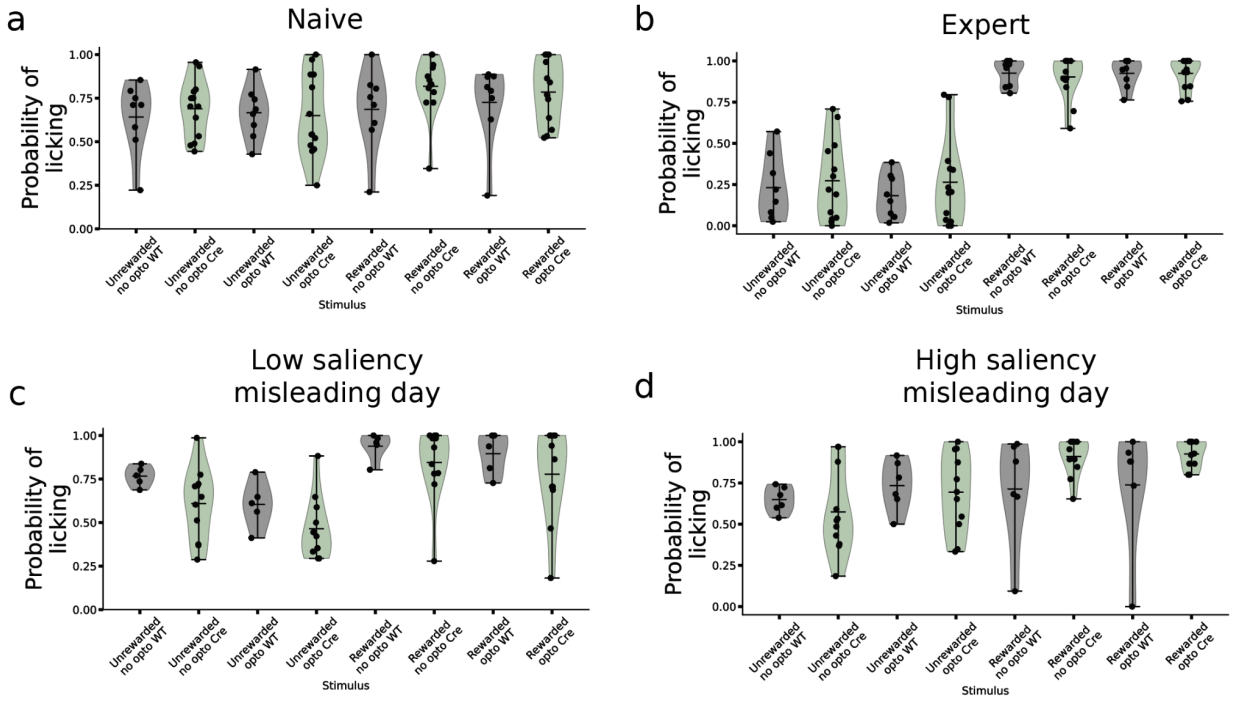

Supplementary figure 9. 5-HT optogenetics do not change the within-trial probability of licking. a-d Probability of licking during trials rewarded or unrewarded, paired or not with optogenetic stimulation, in WT and SERT-Cre animals, the latter expressing an opsin in SERT-Cre neurons of the DRN. Effects tested in naive (**a**) and expert (**b**) mice, as well as in learning animals during the low salience (**c**) and high saliency (**d**) misleading days. All conditions showed no significant effects of opsin expression during opto-trials on licking probability. Two-way ANOVA genotype p-values: p = 0.302 (**a**, n = 8 WTs & 11 SERT-Cres**)**, p = 0.071 (**b**, n = 8 WTs & 12 SERT-Cres), p = 0.302 (**c**, n = 5 WTs & 9 SERT-Cres), and p = 0.533 (**d**, n = 6 WTs & 10 SERT-Cres); while the pairing of a stimulus with reward affected the probability of licking in all except naive animals, reward p-values: p = 0.139 (**a)**, p < 0.001 (**b**), p = 0.004 (**c**), and p < 0.001.

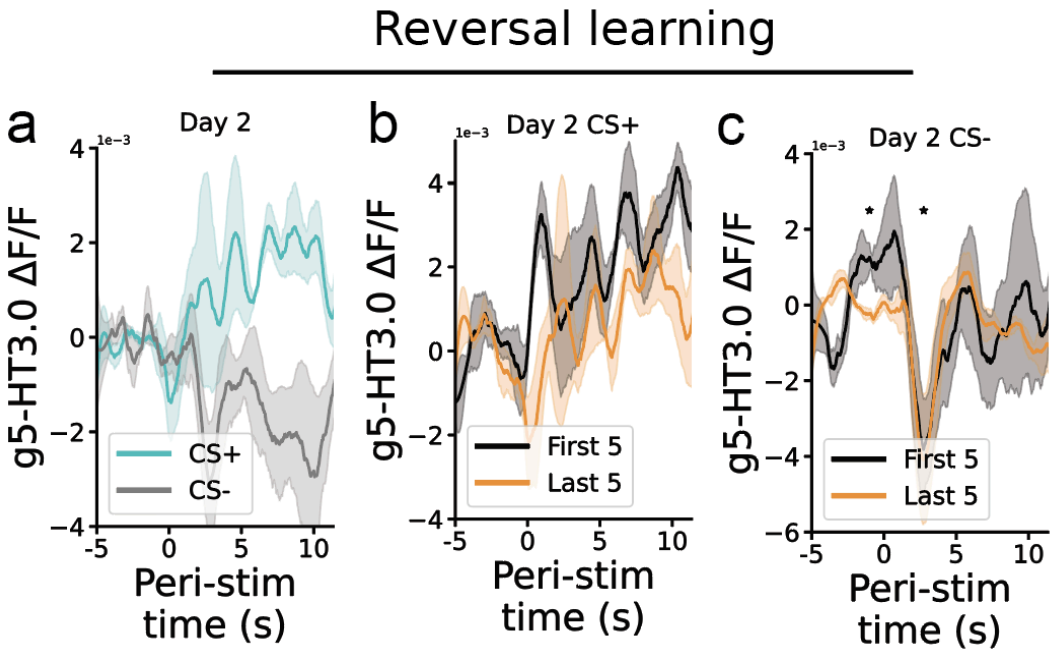

Supplementary figure 10. 5-HT dynamics during LSD-exposure and reversal learning. a,b g5-HT3.0 green fluorescence 5-HT biosensor signal in response to an air puff directed to the whiskers in animals previously injected with LSD or vehicle control (**b,** n = 5, t-test p = 0.784). (**c**) g5-HT3.0 dynamics in response to a 10 PSI air puff paired or not to reward delivery during the second day of reversal learning (n = 6 mice). (**d,e**) g5-HT3.0 peri-stimulus trace during the first five (black) or the last five (orange) presentations of conditioned (**d**) and unconditioned (**e**) air puffs (n = 6 mice).

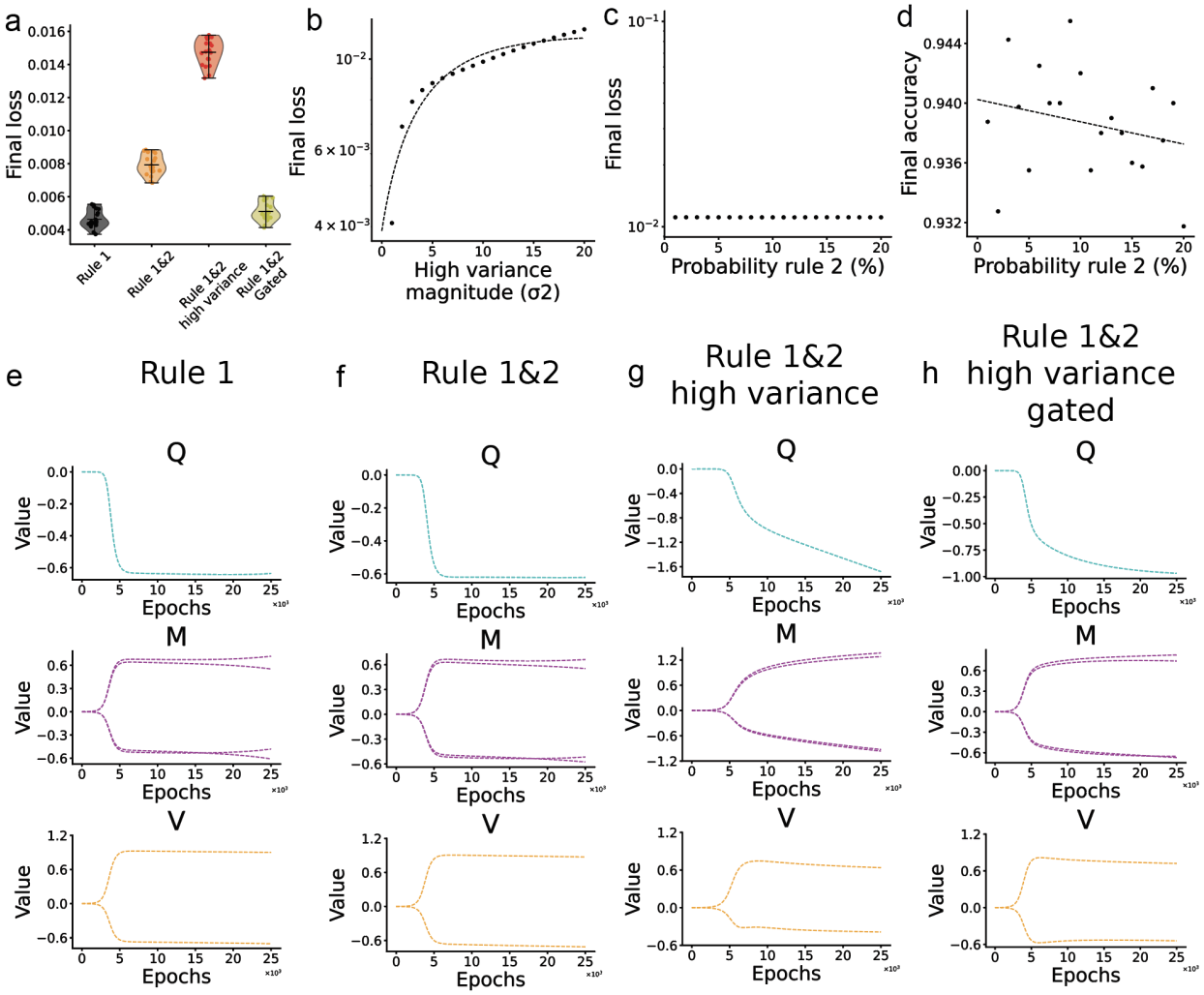

Supplementary figure 11. Loss and order parameters in a gated deep neural network model of cortical 5-HT learning in a noisy environment upon different task settings. (A) Analytical mean-squared error loss, at epoch 25,000, for a deep neural network trained on rule 1 only (black), on rule 1&2 trials with equal variance (orange) or on rule 1&2 trials with 10 times higher input variance in rule 2 trials without (red) or with (yellow) gating. **(B)** Exponential scaling of the loss with the increasing variance of the input during rule 2 trials. Scattered points are the loss, and the discontinuous line is the exponential fit (using “Scipy optimise”). (**C,D**) Scatter of final loss (**C**) or accuracy (**D**) against the probability of a rule 2 epoch at a fixed 5 times higher variance. Accuracy linear fit: R^2 = 0.063, p-value = 0.287 and slope = -0.0001. (**E-H**) Evolution of order parameters Q and M, as well as second layer weights V, across 25,000 epochs for each model settings.

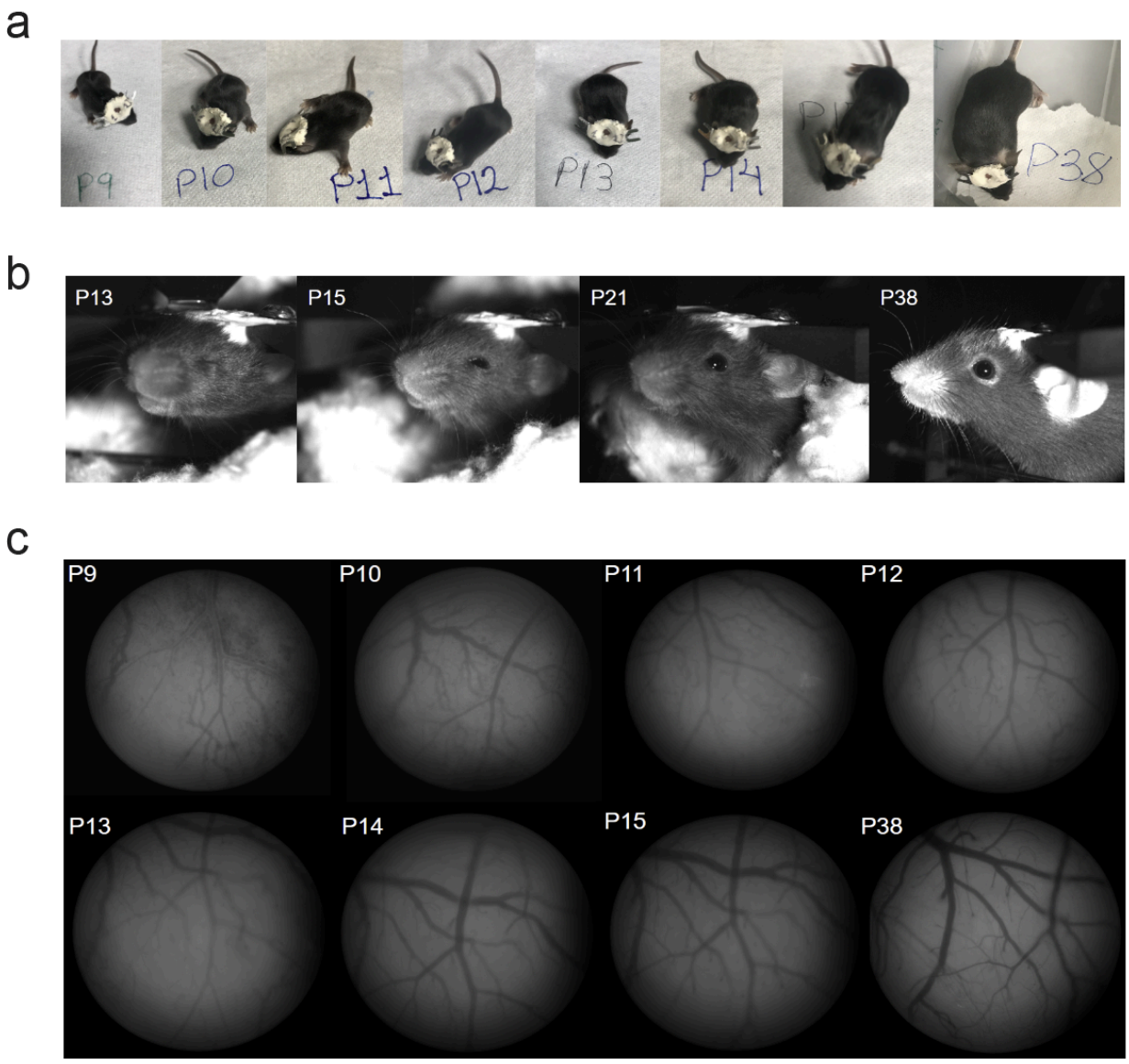

Supplementary figure 12. Physiological development of mice with developmental implantation of a cranial window and a head-fixing plate. a, Pictures of the same animal across development with the implants. **b,** Infrared pictures of the same animal head-fixed in different developmental stages, illustrating normal eye opening timeline. **c,** 1-photon low-magnification pictures of the craniotomy showing estable visibility without skull regrowth throughout development.

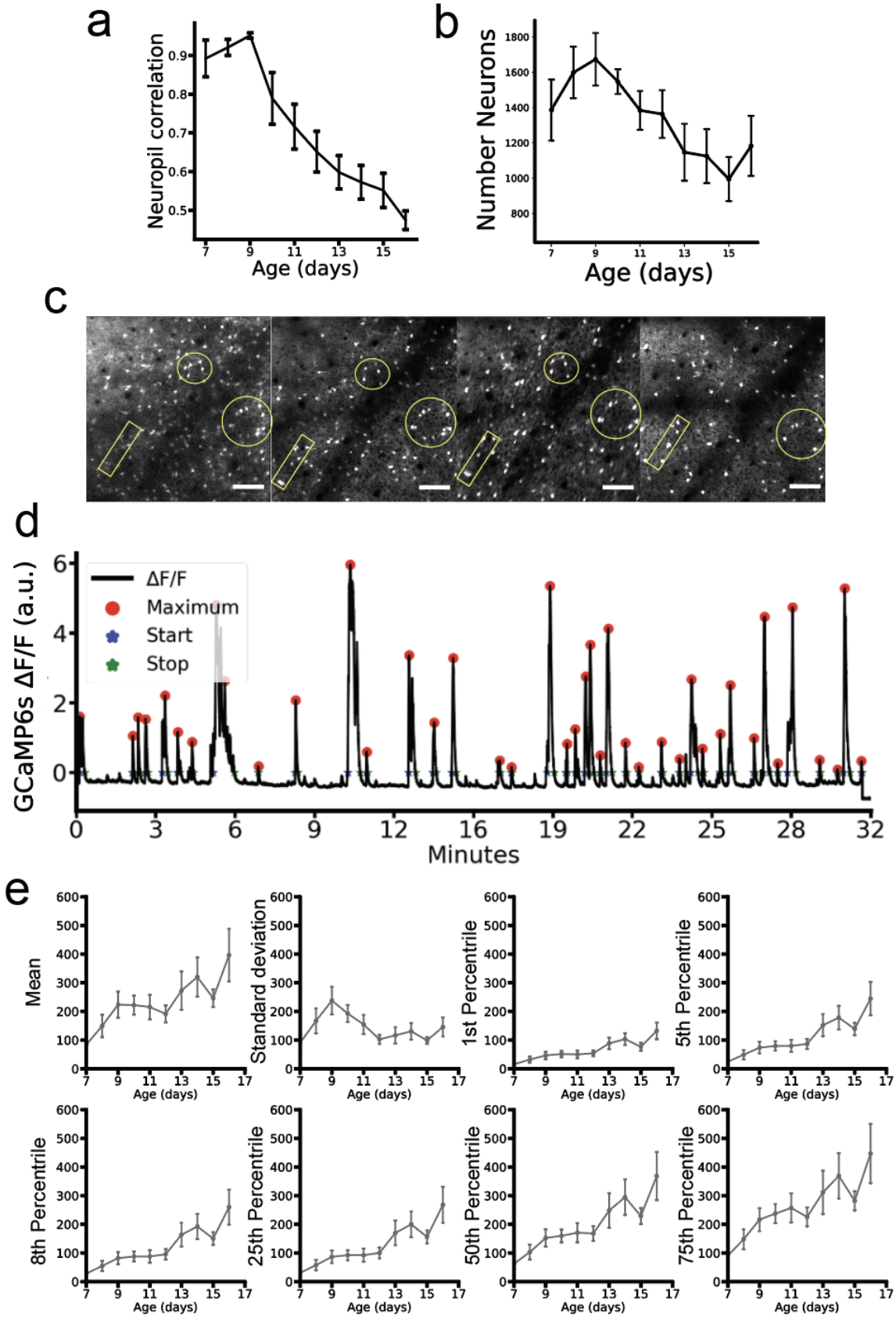
a
Neuropil correlation
0.9
0.8
0.7
0.6
0.5
7
9
11
13
15
Age (days)
b
Number Neurons
1800
1600
1400
1200
1000
800
7
9
11
13
15
Age (days)
c
d
GCaMP6s ΔF/F (a.u.)
ΔF/F
Maximum
Start
Stop
6
4
2
0
0
3
6
9
12
16
19
22
25
28
32
Minutes
e
Mean
Standard deviation
1st Percentrile
5th Percentrile
8th Percentrile
25th Percentrile
50th Percentrile
75th Percentrile
600
500
400
300
200
100
0
7
9
11
13
15
17
Age (days)

Supplementary figure 13. Developmental imaging of calcium traces from the same neurons throughout development. a, Average neuropil-neuron Pearson's correlation coefficient during 20 minute baseline through development (P7-16) for all animals imaged. **b,** Average number of neurons detected in the field of view through development (P7-16) for all animals imaged. **c,** Tracking of the same interneurons (VIP+) across development (from left to right: P8, P10, P12 and P14). Images are averages of 128 frames used to locate the same FOV every imaging day. **d,** Representative average calcium trace of all cells in the field of view from a single animal, with the result of the calcium event automatic detection algorithm showing the maximum, start and end of each event, demonstrating high-accuracy to identify H- and L-events. **e,** Errorbar plots of the change of different statistics (mean, standard deviation, 1st, 5th, 8th, 25th, 50th and 75th percentile) in calcium dynamics, across development, to select the right normalisation approach for developmental recordings. Traces are the average of all animals imaged.

10. Bibliography

Aboagye, B., Weber, T., Bartsch, D., Waider, J., & Klaus-Peter, L. (2018). P.2.027—Inducible tryptophan hydroxylase 2 knockout mice as model for anxiety and fear like behaviour. *European Neuropsychopharmacology*, *28*, S41–S42. https://doi.org/10.1016/j.euroneuro.2017.12.066

Aime, M., Calcini, N., Borsa, M., Campelo, T., Rusterholz, T., Sattin, A., Fellin, T., & Adamantidis, A. (2022). Paradoxical somatodendritic decoupling supports cortical plasticity during REM sleep. *Science*, *376*(6594), 724–730. https://doi.org/10.1126/science.abk2734

Ajibola, M. I., Wu, J.-W., Abdulmajeed, W. I., & Lien, C.-C. (2021). Hypothalamic Glutamate/GABA Cotransmission Modulates Hippocampal Circuits and Supports Long-Term Potentiation. *The Journal of Neuroscience: The Official Journal of the Society for Neuroscience*, *41*(39), 8181–8196. https://doi.org/10.1523/JNEUROSCI.0410-21.2021

Akhmetshina, D., Zakharov, A., Vinokurova, D., Nasretdinov, A., Valeeva, G., & Khazipov, R. (2016). The serotonin reuptake inhibitor citalopram suppresses activity in the neonatal rat barrel cortex in vivo. *Brain Research Bulletin*, *124*, 48–54. https://doi.org/10.1016/j.brainresbull.2016.03.011

Allers, K. A., & Sharp, T. (2003). Neurochemical and anatomical identification of fast- and slow-firing neurones in the rat dorsal raphe nucleus using juxtacellular labelling methods in vivo. *Neuroscience*, *122*(1), 193–204. https://doi.org/10.1016/s0306-4522(03)00518-9

Alonso, J. F., Romero, S., Mañanas, M. À., & Riba, J. (2015). Serotonergic psychedelics temporarily modify information transfer in humans. *The International Journal of Neuropsychopharmacology*, *18*(8), pyv039. https://doi.org/10.1093/ijnp/pyv039

Ames, J. L., Ladd-Acosta, C., Fallin, M. D., Qian, Y., Schieve, L. A., DiGuiseppi, C., Lee, L.-C., Kasten, E. P., Zhou, G., Pinto-Martin, J., Howerton, E., Eaton, C. L., & Croen, L. A. (2021). Maternal Psychiatric Conditions, Treatment with SSRIs, and Neurodevelopmental Disorders. *Biological Psychiatry*, *90*(4), 253–262. https://doi.org/10.1016/j.biopsych.2021.04.002

Anastasiades, P. G., Marques-Smith, A., Lyngholm, D., Lickiss, T., Raffiq, S., Kätzel, D., Miesenböck, G., & Butt, S. J. B. (2016). GABAergic interneurons form transient layer-specific circuits in early postnatal neocortex. *Nature Communications*, *7*(1), 10584. https://doi.org/10.1038/ncomms10584

Andrade, R., & Weber, E. (2010). Htr2a Gene and 5-HT2A Receptor Expression in the Cerebral Cortex Studied Using Genetically Modified Mice. *Frontiers in Neuroscience*, *4*. https://www.frontiersin.org/articles/10.3389/fnins.2010.00036

Anguelova, M., Benkelfat, C., & Turecki, G. (2003). A systematic review of association studies investigating genes coding for serotonin receptors and the serotonin transporter: II. Suicidal behavior. *Molecular Psychiatry*, *8*(7), 646–653. https://doi.org/10.1038/sj.mp.4001336

Aqil, M., & Roseman, L. (2023). More than meets the eye: The role of sensory dimensions in psychedelic brain dynamics, experience, and therapeutics. *Neuropharmacology*, *223*, 109300. https://doi.org/10.1016/j.neuropharm.2022.109300

Audero, E., Mlinar, B., Baccini, G., Skachokova, Z. K., Corradetti, R., & Gross, C. (2013). Suppression of Serotonin Neuron Firing Increases Aggression in Mice. *Journal of Neuroscience*, *33*(20), 8678–8688. https://doi.org/10.1523/JNEUROSCI.2067-12.2013

Avery, M. C., & Krichmar, J. L. (2017). Neuromodulatory Systems and Their Interactions: A Review of Models, Theories, and Experiments. *Frontiers in Neural Circuits*, *11*, 108. https://doi.org/10.3389/fncir.2017.00108

Azimi, Z., Barzan, R., Spoida, K., Surdin, T., Wollenweber, P., Mark, M. D., Herlitze, S., &

Jancke, D. (2020). Separable gain control of ongoing and evoked activity in the visual cortex by serotonergic input. *eLife*, *9*, e53552. https://doi.org/10.7554/eLife.53552

Azmitia, E. C., Gannon, P. J., Kheck, N. M., & Whitaker-Azmitia, P. M. (1996). Cellular localization of the 5-HT1A receptor in primate brain neurons and glial cells. *Neuropsychopharmacology: Official Publication of the American College of Neuropsychopharmacology*, *14*(1), 35–46. https://doi.org/10.1016/S0893-133X(96)80057-1

Babij, R., Ferrer, C., Donatelle, A., Wacks, S., Buch, A. M., Niemeyer, J. E., Ma, H., Duan, Z. R. S., Fetcho, R. N., Che, A., Otsuka, T., Schwartz, T. H., Huang, B. S., Liston, C., & García, N. V. D. M. (2023). Gabrb3 is required for the functional integration of pyramidal neuron subtypes in the somatosensory cortex. *Neuron*, *111*(2), 256-274.e10. https://doi.org/10.1016/j.neuron.2022.10.037

Bankhead, P., Loughrey, M. B., Fernández, J. A., Dombrowski, Y., McArt, D. G., Dunne, P. D., McQuaid, S., Gray, R. T., Murray, L. J., Coleman, H. G., James, J. A., Salto-Tellez, M., & Hamilton, P. W. (2017). QuPath: Open source software for digital pathology image analysis. *Scientific Reports*, *7*(1), Article 1. https://doi.org/10.1038/s41598-017-17204-5

Barnes, N. M., Ahern, G. P., Becamel, C., Bockaert, J., Camilleri, M., Chaumont-Dubel, S., Claeysen, S., Cunningham, K. A., Fone, K. C., Gershon, M., Di Giovanni, G., Goodfellow, N. M., Halberstadt, A. L., Hartley, R. M., Hassaine, G., Herrick-Davis, K., Hovius, R., Lacivita, E., Lambe, E. K., … Hoyer, D. (2021). International Union of Basic and Clinical Pharmacology. CX. Classification of Receptors for 5-hydroxytryptamine; Pharmacology and Function. *Pharmacological Reviews*, *73*(1), 310–520. https://doi.org/10.1124/pr.118.015552

Barzan, R., Bozkurt, B., Nejad, M. M., Süß, S. T., Surdin, T., Böke, H., Spoida, K., Azimi, Z., Grömmke, M., Eickelbeck, D., Mark, M. D., Rohr, L., Siveke, I., Cheng, S., Herlitze, S., & Jancke, D. (2024). Gain control of sensory input across polysynaptic circuitries in mouse

visual cortex by a single G protein-coupled receptor type (5-HT2A). *Nature Communications*, *15*(1), 8078. https://doi.org/10.1038/s41467-024-51861-1

Bastos, G., Holmes, J. T., Ross, J. M., Rader, A. M., Gallimore, C. G., Wargo, J. A., Peterka, D. S., & Hamm, J. P. (2023). Top-down input modulates visual context processing through an interneuron-specific circuit. *Cell Reports*, *42*(9), 113133. https://doi.org/10.1016/j.celrep.2023.113133

Benezra, S. E., Patel, K. B., Campos, C. P., Hillman, E. M. C., & Bruno, R. M. (2024). Learning enhances behaviorally relevant representations in apical dendrites. *eLife*, *13*. https://doi.org/10.7554/eLife.98349.1

Bennett-Clarke, C. A., Leslie, M. J., Chiaia, N. L., & Rhoades, R. W. (1993). Serotonin 1B receptors in the developing somatosensory and visual cortices are located on thalamocortical axons. *Proceedings of the National Academy of Sciences of the United States of America*, *90*(1), 153–157.

Benninger, R. K. P., & Piston, D. W. (2013). Two-Photon Excitation Microscopy for the Study of Living Cells and Tissues. *Current Protocols in Cell Biology / Editorial Board, Juan S. Bonifacino ... [et Al.]*, *0 4*, Unit-4.1124. https://doi.org/10.1002/0471143030.cb0411s59

Beversdorf, D. Q., Shah, A., Jhin, A., Noel-MacDonnell, J., Hecht, P., Ferguson, B. J., Bruce, D., Tilley, M., & Talebizadeh, Z. (2021). microRNAs and Gene–Environment Interactions in Autism: Effects of Prenatal Maternal Stress and the SERT Gene on Maternal microRNA Expression. *Frontiers in Psychiatry*, *12*. https://doi.org/10.3389/fpsyt.2021.668577

Biehl, M., & Schwarze, H. (1995). Learning by on-line gradient descent. *Journal of Physics A: Mathematical and General*, *28*(3), 643. https://doi.org/10.1088/0305-4470/28/3/018

Blier, P., & de Montigny, C. (1994). Current advances and trends in the treatment of depression. *Trends in Pharmacological Sciences*, *15*(7), 220–226. https://doi.org/10.1016/0165-6147(94)90315-8

Blumberg, M. S., Dooley, J. C., & Tiriac, A. (2022). Sleep, plasticity, and sensory

neurodevelopment. *Neuron*, *110*(20), 3230–3242. https://doi.org/10.1016/j.neuron.2022.08.005

Bocchio, M., McHugh, S. B., Bannerman, D. M., Sharp, T., & Capogna, M. (2016). Serotonin, Amygdala and Fear: Assembling the Puzzle. *Frontiers in Neural Circuits*, *10*. https://doi.org/10.3389/fncir.2016.00024

Bonnin, A., & Levitt, P. (2011). Fetal, Maternal and Placental Sources of Serotonin and New Implications for Developmental Programming of the Brain. *Neuroscience*, *197*, 1–7. https://doi.org/10.1016/j.neuroscience.2011.10.005

Border, R., Johnson, E. C., Evans, L. M., Smolen, A., Berley, N., Sullivan, P. F., & Keller, M. C. (2019). No Support for Historical Candidate Gene or Candidate Gene-by-Interaction Hypotheses for Major Depression Across Multiple Large Samples. *The American Journal of Psychiatry*, *176*(5), 376–387. https://doi.org/10.1176/appi.ajp.2018.18070881

Boureau, Y.-L., & Dayan, P. (2011). Opponency Revisited: Competition and Cooperation Between Dopamine and Serotonin. *Neuropsychopharmacology*, *36*(1), 74–97. https://doi.org/10.1038/npp.2010.151

Brown, G. W., Ban, M., Craig, T. K. J., Harris, T. O., Herbert, J., & Uher, R. (2013). Serotonin Transporter Length Polymorphism, Childhood Maltreatment, and Chronic Depression: A Specific Gene–Environment Interaction. *Depression and Anxiety*, *30*(1), 5–13. https://doi.org/10.1002/da.21982

Bystron, I., Blakemore, C., & Rakic, P. (2008). Development of the human cerebral cortex: Boulder Committee revisited. *Nature Reviews Neuroscience*, *9*(2), 110–122. https://doi.org/10.1038/nrn2252

Caballero, A., Flores-Barrera, E., Cass, D. K., & Tseng, K. Y. (2014). Differential regulation of parvalbumin and calretinin interneurons in the prefrontal cortex during adolescence. *Brain Structure & Function*, *219*(1), 10.1007/s00429-013-0508–8. https://doi.org/10.1007/s00429-013-0508-8

Calati, R., De Ronchi, D., Bellini, M., & Serretti, A. (2011). The 5-HTTLPR polymorphism and eating disorders: A meta-analysis. *The International Journal of Eating Disorders*, *44*(3), 191–199. https://doi.org/10.1002/eat.20811

Cameron, L. P., Benetatos, J., Lewis, V., Bonniwell, E. M., Jaster, A. M., Moliner, R., Castrén, E., McCorvy, J. D., Palner, M., & Aguilar-Valles, A. (2023). Beyond the 5-HT2A Receptor: Classic and Nonclassic Targets in Psychedelic Drug Action. *Journal of Neuroscience*, *43*(45), 7472–7482. https://doi.org/10.1523/JNEUROSCI.1384-23.2023

Cameron, L. P., Patel, S. D., Vargas, M. V., Barragan, E. V., Saeger, H. N., Warren, H. T., Chow, W. L., Gray, J. A., & Olson, D. E. (2023). 5-HT2ARs Mediate Therapeutic Behavioral Effects of Psychedelic Tryptamines. *ACS Chemical Neuroscience*, *14*(3), 351–358. https://doi.org/10.1021/acschemneuro.2c00718

Casarotto, P. C., Girych, M., Fred, S. M., Kovaleva, V., Moliner, R., Enkavi, G., Biojone, C., Cannarozzo, C., Sahu, M. P., Kaurinkoski, K., Brunello, C. A., Steinzeig, A., Winkel, F., Patil, S., Vestring, S., Serchov, T., Diniz, C. R. A. F., Laukkanen, L., Cardon, I., … Castrén, E. (2021). Antidepressant drugs act by directly binding to TRKB neurotrophin receptors. *Cell*, *184*(5), 1299-1313.e19. https://doi.org/10.1016/j.cell.2021.01.034

Cases, O., Vitalis, T., Seif, I., De Maeyer, E., Sotelo, C., & Gaspar, P. (1996). Lack of barrels in the somatosensory cortex of monoamine oxidase A-deficient mice: Role of a serotonin excess during the critical period. *Neuron*, *16*(2), 297–307. https://doi.org/10.1016/s0896-6273(00)80048-3

Caspi, A., Sugden, K., Moffitt, T. E., Taylor, A., Craig, I. W., Harrington, H., McClay, J., Mill, J., Martin, J., Braithwaite, A., & Poulton, R. (2003). Influence of life stress on depression: Moderation by a polymorphism in the 5-HTT gene. *Science (New York, N.Y.)*, *301*(5631), 386–389. https://doi.org/10.1126/science.1083968

Celada, P., & Artigas, F. (1993). Monoamine oxidase inhibitors increase preferentially extracellular 5-hydroxytryptamine in the midbrain raphe nuclei. A brain microdialysis

study in the awake rat. *Naunyn-Schmiedeberg's Archives of Pharmacology*, *347*(6), 583–590. https://doi.org/10.1007/BF00166940

Celada, P., Puig, M. V., Amargós-Bosch, M., Adell, A., & Artigas, F. (2004). The therapeutic role of 5-HT1A and 5-HT2A receptors in depression. *Journal of Psychiatry and Neuroscience*, *29*(4), 252–265.

Che, A., Babij, R., Iannone, A. F., Fetcho, R. N., Ferrer, M., Liston, C., Fishell, G., & De Marco García, N. V. (2018). Layer I Interneurons Sharpen Sensory Maps during Neonatal Development. *Neuron*, *99*(1), 98-116.e7. https://doi.org/10.1016/j.neuron.2018.06.002

Che, A., & De Marco García, N. V. (2021). An in vivo Calcium Imaging Approach for the Identification of Cell-Type Specific Patterns in the Developing Cortex. *Frontiers in Neural Circuits*, *15*. https://www.frontiersin.org/articles/10.3389/fncir.2021.747724

Chen, T.-W., Wardill, T. J., Sun, Y., Pulver, S. R., Renninger, S. L., Baohan, A., Schreiter, E. R., Kerr, R. A., Orger, M. B., Jayaraman, V., Looger, L. L., Svoboda, K., & Kim, D. S. (2013). Ultra-sensitive fluorescent proteins for imaging neuronal activity. *Nature*, *499*(7458), 295–300. https://doi.org/10.1038/nature12354

Chen, X., Petit, E. I., Dobrenis, K., & Sze, J. Y. (2016). Spatiotemporal SERT expression in cortical map development. *Neurochemistry International*, *98*, 129–137. https://doi.org/10.1016/j.neuint.2016.05.010

Chorbov, V. M., Lobos, E. A., Todorov, A. A., Heath, A. C., Botteron, K. N., & Todd, R. D. (2007). Relationship of 5-HTTLPR genotypes and depression risk in the presence of trauma in a female twin sample. *American Journal of Medical Genetics. Part B, Neuropsychiatric Genetics: The Official Publication of the International Society of Psychiatric Genetics*, *144B*(6), 830–833. https://doi.org/10.1002/ajmg.b.30534

Cipriani, A., Furukawa, T. A., Salanti, G., Chaimani, A., Atkinson, L. Z., Ogawa, Y., Leucht, S., Ruhe, H. G., Turner, E. H., Higgins, J. P. T., Egger, M., Takeshima, N., Hayasaka, Y., Imai, H., Shinohara, K., Tajika, A., Ioannidis, J. P. A., & Geddes, J. R. (2018).

Comparative efficacy and acceptability of 21 antidepressant drugs for the acute treatment of adults with major depressive disorder: A systematic review and network meta-analysis. *The Lancet*, *391*(10128), 1357–1366. https://doi.org/10.1016/S0140-6736(17)32802-7

Cohen, J. Y., Amoroso, M. W., & Uchida, N. (n.d.). Serotonergic neurons signal reward and punishment on multiple timescales. *eLife*, *4*, e06346. https://doi.org/10.7554/eLife.06346

Cohen, L. B., Keynes, R. D., & Hille, B. (1968). Light Scattering and Birefringence Changes during Nerve Activity. *Nature*, *218*(5140), Article 5140. https://doi.org/10.1038/218438a0

Collins, H. M., Gullino, L. S., Ozdemir, D., Lazarenco, C., Sudarikova, Y., Daly, E., Pilar Cuéllar, F., Pinacho, R., Bannerman, D. M., & Sharp, T. (2024). Rebound activation of 5-HT neurons following SSRI discontinuation. *Neuropsychopharmacology*, *49*(10), 1580–1589. https://doi.org/10.1038/s41386-024-01857-8

Colwell, M. J., Tagomori, H., Shang, F., Cheng, H. I., Wigg, C. E., Browning, M., Cowen, P. J., Murphy, S. E., & Harmer, C. J. (2024). Direct serotonin release in humans shapes aversive learning and inhibition. *Nature Communications*, *15*(1), 6617. https://doi.org/10.1038/s41467-024-50394-x

Contractor, A., Ethell, I. M., & Portera-Cailliau, C. (2021). Cortical interneurons in autism. *Nature Neuroscience*, *24*(12), Article 12. https://doi.org/10.1038/s41593-021-00967-6

Coppen, A. (1967). The biochemistry of affective disorders. *The British Journal of Psychiatry: The Journal of Mental Science*, *113*(504), 1237–1264. https://doi.org/10.1192/bjp.113.504.1237

Correia, A. S., & Vale, N. (2022). Tryptophan Metabolism in Depression: A Narrative Review with a Focus on Serotonin and Kynurenine Pathways. *International Journal of Molecular Sciences*, *23*(15), 8493. https://doi.org/10.3390/ijms23158493

Côté, F., Fligny, C., Bayard, E., Launay, J.-M., Gershon, M. D., Mallet, J., & Vodjdani, G. (2007). Maternal serotonin is crucial for murine embryonic development. *Proceedings of the*

National Academy of Sciences, *104*(1), 329–334. https://doi.org/10.1073/pnas.0606722104

Culverhouse, R. C., Saccone, N. L., Horton, A. C., Ma, Y., Anstey, K. J., Banaschewski, T., Burmeister, M., Cohen-Woods, S., Etain, B., Fisher, H. L., Goldman, N., Guillaume, S., Horwood, J., Juhasz, G., Lester, K. J., Mandelli, L., Middeldorp, C. M., Olié, E., Villafuerte, S., … Bierut, L. J. (2018). Collaborative meta-analysis finds no evidence of a strong interaction between stress and 5-HTTLPR genotype contributing to the development of depression. *Molecular Psychiatry*, *23*(1), 133–142. https://doi.org/10.1038/mp.2017.44

Cunha, C., Smiley, J. F., Chuhma, N., Shah, R., Bleiwas, C., Menezes, E. C., Seal, R. P., Edwards, R. H., Rayport, S., Ansorge, M. S., Castellanos, F. X., & Teixeira, C. M. (2021). Perinatal interference with the serotonergic system affects VTA function in the adult via glutamate co-transmission. *Molecular Psychiatry*, *26*(9), 4795–4812. https://doi.org/10.1038/s41380-020-0763-z

da Cunha-Bang, S., & Knudsen, G. M. (2021). The Modulatory Role of Serotonin on Human Impulsive Aggression. *Biological Psychiatry*, *90*(7), 447–457. https://doi.org/10.1016/j.biopsych.2021.05.016

Daly, E., D. Tricklebank, M., & Wichers, R. (2019). Chapter Two—Neurodevelopmental roles and the serotonin hypothesis of autism spectrum disorder. In M. D. Tricklebank & E. Daly (Eds.), *The Serotonin System* (pp. 23–44). Academic Press. https://doi.org/10.1016/B978-0-12-813323-1.00002-5

Dana, H., Mohar, B., Sun, Y., Narayan, S., Gordus, A., Hasseman, J. P., Tsegaye, G., Holt, G. T., Hu, A., Walpita, D., Patel, R., Macklin, J. J., Bargmann, C. I., Ahrens, M. B., Schreiter, E. R., Jayaraman, V., Looger, L. L., Svoboda, K., & Kim, D. S. (2016). Sensitive red protein calcium indicators for imaging neural activity. *eLife*, *5*, e12727. https://doi.org/10.7554/eLife.12727

Dard, R. F., Leprince, E., Denis, J., Rao Balappa, S., Suchkov, D., Boyce, R., Lopez, C., Giorgi-Kurz, M., Szwagier, T., Dumont, T., Rouault, H., Minlebaev, M., Baude, A., Cossart, R., & Picardo, M. A. (2022). The rapid developmental rise of somatic inhibition disengages hippocampal dynamics from self-motion. *eLife*, *11*, e78116. https://doi.org/10.7554/eLife.78116

Davis, L. L., Suris, A., Lambert, M. T., Heimberg, C., & Petty, F. (1997). Post-traumatic stress disorder and serotonin: New directions for research and treatment. *Journal of Psychiatry and Neuroscience*, *22*(5), 318–326.

De Gregorio, R., Chen, X., Petit, E. I., Dobrenis, K., & Sze, J. Y. (2020). Disruption of Transient SERT Expression in Thalamic Glutamatergic Neurons Alters Trajectory of Postnatal Interneuron Development in the Mouse Cortex. *Cerebral Cortex*, *30*(3), 1623–1636. https://doi.org/10.1093/cercor/bhz191

de la Fuente Revenga, M., Jaster, A. M., McGinn, J., Silva, G., Saha, S., & González-Maeso, J. (2022). Tolerance and Cross-Tolerance among Psychedelic and Nonpsychedelic 5-HT2A Receptor Agonists in Mice. *ACS Chemical Neuroscience*, *13*(16), 2436–2448. https://doi.org/10.1021/acschemneuro.2c00170

De Marco García, N. V., Priya, R., Tuncdemir, S. N., Fishell, G., & Karayannis, T. (2015). Sensory inputs control the integration of neurogliaform interneurons into cortical circuits. *Nature Neuroscience*, *18*(3), 393–401. https://doi.org/10.1038/nn.3946

de Vos, C. M. H., Mason, N. L., & Kuypers, K. P. C. (2021). Psychedelics and Neuroplasticity: A Systematic Review Unraveling the Biological Underpinnings of Psychedelics. *Frontiers in Psychiatry*, *12*. https://www.frontiersin.org/articles/10.3389/fpsyt.2021.724606

Delli Colli, C., Borgi, M., Poggini, S., Chiarotti, F., Cirulli, F., Penninx, B. W. J. H., Benedetti, F., Vai, B., & Branchi, I. (2022). Time moderates the interplay between 5-HTTLPR and stress on depression risk: Gene x environment interaction as a dynamic process. *Translational Psychiatry*, *12*(1), Article 1. https://doi.org/10.1038/s41398-022-02035-4

Deng, F., Wan, J., Li, G., Dong, H., Xia, X., Wang, Y., Li, X., Zhuang, C., Zheng, Y., Liu, L., Yan, Y., Feng, J., Zhao, Y., Xie, H., & Li, Y. (2024). Improved green and red GRAB sensors for monitoring spatiotemporal serotonin release in vivo. *Nature Methods*, *21*(4), 692–702. https://doi.org/10.1038/s41592-024-02188-8

Descarries, L., Alain, B., & Watkins, K. C. (1975). Serotonin nerve terminals in adult rat neocortex. *Brain Research*, *100*(3), 563–588. https://doi.org/10.1016/0006-8993(75)90158-4

Desrochers, S. S., Spring, M. G., & Nautiyal, K. M. (2022). A Role for Serotonin in Modulating Opposing Drive and Brake Circuits of Impulsivity. *Frontiers in Behavioral Neuroscience*, *16*, 791749. https://doi.org/10.3389/fnbeh.2022.791749

Dipoppa, M., Ranson, A., Krumin, M., Pachitariu, M., Carandini, M., & Harris, K. D. (2018). Vision and Locomotion Shape the Interactions between Neuron Types in Mouse Visual Cortex. *Neuron*, *98*(3), 602-615.e8. https://doi.org/10.1016/j.neuron.2018.03.037

Domínguez, S., Ma, L., Yu, H., Pouchelon, G., Mayer, C., Spyropoulos, G. D., Cea, C., Buzsáki, G., Fishell, G., Khodagholy, D., & Gelinas, J. N. (2021). A transient postnatal quiescent period precedes emergence of mature cortical dynamics. *eLife*, *10*, e69011. https://doi.org/10.7554/eLife.69011

Dong, C., Ly, C., Dunlap, L. E., Vargas, M. V., Sun, J., Hwang, I.-W., Azinfar, A., Oh, W. C., Wetsel, W. C., Olson, D. E., & Tian, L. (2021). Psychedelic-inspired drug discovery using an engineered biosensor. *Cell*, *184*(10), 2779-2792.e18. https://doi.org/10.1016/j.cell.2021.03.043

Duan, Z. R. S., Che, A., Chu, P., Modol, L., Bollmann, Y., Babij, R., Fetcho, R. N., Otsuka, T., Fuccillo, M. V., Liston, C., Pisapia, D. J., Cossart, R., & García, N. V. D. M. (2020). GABAergic Restriction of Network Dynamics Regulates Interneuron Survival in the Developing Cortex. *Neuron*, *105*(1), 75-92.e5. https://doi.org/10.1016/j.neuron.2019.10.008

Dugué, G. P., Lörincz, M. L., Lottem, E., Audero, E., Matias, S., Correia, P. A., Léna, C., & Mainen, Z. F. (2014). Optogenetic Recruitment of Dorsal Raphe Serotonergic Neurons Acutely Decreases Mechanosensory Responsivity in Behaving Mice. *PLOS ONE*, *9*(8), e105941. https://doi.org/10.1371/journal.pone.0105941

Edden, R. A. E., Crocetti, D., Zhu, H., Gilbert, D. L., & Mostofsky, S. H. (2012). Reduced GABA Concentration in Attention-Deficit/Hyperactivity Disorder. *Archives of General Psychiatry*, *69*(7), 750–753. https://doi.org/10.1001/archgenpsychiatry.2011.2280

Engel, A., & Van den Broeck, C. (2001). *Statistical Mechanics of Learning*. Cambridge University Press. https://doi.org/10.1017/CBO9781139164542

Erzurumlu, R. S., & Gaspar, P. (2012). Development and critical period plasticity of the barrel cortex. *The European Journal of Neuroscience*, *35*(10), 1540–1553. https://doi.org/10.1111/j.1460-9568.2012.08075.x

Faulkner, P., & Deakin, J. F. W. (2014). The role of serotonin in reward, punishment and behavioural inhibition in humans: Insights from studies with acute tryptophan depletion. *Neuroscience & Biobehavioral Reviews*, *46*, 365–378. https://doi.org/10.1016/j.neubiorev.2014.07.024

Feinn, R., Nellissery, M., & Kranzler, H. R. (2005). Meta-analysis of the association of a functional serotonin transporter promoter polymorphism with alcohol dependence. *American Journal of Medical Genetics. Part B, Neuropsychiatric Genetics: The Official Publication of the International Society of Psychiatric Genetics*, *133B*(1), 79–84. https://doi.org/10.1002/ajmg.b.30132

Feng, Y.-Y., Bromberg-Martin, E. S., & Monosov, I. E. (2024). Dorsal raphe neurons integrate the values of reward amount, delay, and uncertainty in multi-attribute decision-making. *Cell Reports*, *43*(6), 114341. https://doi.org/10.1016/j.celrep.2024.114341

Férézou, I., Cauli, B., Hill, E. L., Rossier, J., Hamel, E., & Lambolez, B. (2002). 5-HT3 Receptors Mediate Serotonergic Fast Synaptic Excitation of Neocortical Vasoactive Intestinal

Peptide/Cholecystokinin Interneurons. *The Journal of Neuroscience*, *22*(17), 7389–7397. https://doi.org/10.1523/JNEUROSCI.22-17-07389.2002

Fogaça, M. V., & Duman, R. S. (2019). Cortical GABAergic Dysfunction in Stress and Depression: New Insights for Therapeutic Interventions. *Frontiers in Cellular Neuroscience*, *13*. https://www.frontiersin.org/articles/10.3389/fncel.2019.00087

Fonseca, M. S., Murakami, M., & Mainen, Z. F. (2015). Activation of Dorsal Raphe Serotonergic Neurons Promotes Waiting but Is Not Reinforcing. *Current Biology*, *25*(3), 306–315. https://doi.org/10.1016/j.cub.2014.12.002

Foote, W. E., Sheard, M. H., & Aghajanian, G. K. (1969). Comparison of Effects of LSD and Amphetamine on Midbrain Raphe Units. *Nature*, *222*(5193), 567–569. https://doi.org/10.1038/222567a0

Frazer, S., Otomo, K., & Dayer, A. (2015). Early-life serotonin dysregulation affects the migration and positioning of cortical interneuron subtypes. *Translational Psychiatry*, *5*(9), Article 9. https://doi.org/10.1038/tp.2015.147

Fritze, S., Spanagel, R., & Noori, H. R. (2017). Adaptive dynamics of the 5-HT systems following chronic administration of selective serotonin reuptake inhibitors: A meta-analysis. *Journal of Neurochemistry*, *142*(5), 747–755. https://doi.org/10.1111/jnc.14114

Fu, Y., Tucciarone, J. M., Espinosa, J. S., Sheng, N., Darcy, D. P., Nicoll, R. A., Huang, Z. J., & Stryker, M. P. (2014). A cortical circuit for gain control by behavioral state. *Cell*, *156*(6), 1139–1152. https://doi.org/10.1016/j.cell.2014.01.050

Furutachi, S., Franklin, A. D., Aldea, A. M., Mrsic-Flogel, T. D., & Hofer, S. B. (2024). Cooperative thalamocortical circuit mechanism for sensory prediction errors. *Nature*, 1–9. https://doi.org/10.1038/s41586-024-07851-w

Galvin, V. C., & Disney, A. A. (2023). Neuromodulation in Cortical Circuits. In A. D. Reyes, W. M. Usrey, & S. M. Sherman (Eds.), *The Cerebral Cortex and Thalamus* (p. 0). Oxford University Press. https://doi.org/10.1093/med/9780197676158.003.0010

Garcia, S. L., Laffere, A., Toschi, C., Schilling, L., Podlaski, J., Fritsche, M., Zatka-Haas, P., Li, Y., Bogacz, R., Saxe, A., & Lak, A. (2023). *Striatal dopamine reflects individual long-term learning trajectories* (p. 2023.12.14.571653). bioRxiv. https://doi.org/10.1101/2023.12.14.571653

Garcia-Garcia, A. L., Meng, Q., Canetta, S., Gardier, A. M., Guiard, B. P., Kellendonk, C., Dranovsky, A., & Leonardo, E. D. (2017). Serotonin Signaling through Prefrontal Cortex 5-HT1A Receptors during Adolescence Can Determine Baseline Mood-Related Behaviors. *Cell Reports*, *18*(5), 1144–1156. https://doi.org/10.1016/j.celrep.2017.01.021

Ghezzi, F., Baruchin, L. J., Ha, N. T., Shah-Ostrowski, M. J., Chama, A. G. C., Stacey, J. A., & Butt, S. J. B. (2023). *GABAergic circuits reflect different requirements for emergent perception in postnatal mouse neocortex* (p. 2023.11.21.568139). bioRxiv. https://doi.org/10.1101/2023.11.21.568139

Girgenti, M. J., Wang, J., Ji, D., Cruz, D. A., Stein, M. B., Gelernter, J., Young, K. A., Huber, B. R., Williamson, D. E., Friedman, M. J., Krystal, J. H., Zhao, H., & Duman, R. S. (2021). Transcriptomic organization of the human brain in post-traumatic stress disorder. *Nature Neuroscience*, *24*(1), Article 1. https://doi.org/10.1038/s41593-020-00748-7

Goldt, S., Advani, M. S., Saxe, A. M., Krzakala, F., & Zdeborová, L. (2019). *Generalisation dynamics of online learning in over-parameterised neural networks* (arXiv:1901.09085). arXiv. https://doi.org/10.48550/arXiv.1901.09085

Golebiowska, J., Hołuj, M., Potasiewicz, A., Piotrowska, D., Kuziak, A., Popik, P., Homberg, J. R., & Nikiforuk, A. (2019). Serotonin transporter deficiency alters socioemotional ultrasonic communication in rats. *Scientific Reports*, *9*(1), 20283. https://doi.org/10.1038/s41598-019-56629-y

Golshani, P., Gonçalves, J. T., Khoshkhoo, S., Mostany, R., Smirnakis, S., & Portera-Cailliau, C. (2009). Internally Mediated Developmental Desynchronization of Neocortical Network Activity. *Journal of Neuroscience*, *29*(35), 10890–10899.

https://doi.org/10.1523/JNEUROSCI.2012-09.2009

Gómez, L. J., Dooley, J. C., Sokoloff, G., & Blumberg, M. S. (2021). Parallel and Serial Sensory Processing in Developing Primary Somatosensory and Motor Cortex. *Journal of Neuroscience*, *41*(15), 3418–3431. https://doi.org/10.1523/JNEUROSCI.2614-20.2021

González-Maeso, J., Yuen, T., Ebersole, B. J., Wurmbach, E., Lira, A., Zhou, M., Weisstaub, N., Hen, R., Gingrich, J. A., & Sealfon, S. C. (2003). Transcriptome fingerprints distinguish hallucinogenic and nonhallucinogenic 5-hydroxytryptamine 2A receptor agonist effects in mouse somatosensory cortex. *The Journal of Neuroscience: The Official Journal of the Society for Neuroscience*, *23*(26), 8836–8843. https://doi.org/10.1523/JNEUROSCI.23-26-08836.2003

Green, S. A., Hernandez, L., Tottenham, N., Krasileva, K., Bookheimer, S. Y., & Dapretto, M. (2015). Neurobiology of Sensory Overresponsivity in Youth With Autism Spectrum Disorders. *JAMA Psychiatry*, *72*(8), 778–786. https://doi.org/10.1001/jamapsychiatry.2015.0737

Grinvald, A., Lieke, E., Frostig, R. D., Gilbert, C. D., & Wiesel, T. N. (1986). Functional architecture of cortex revealed by optical imaging of intrinsic signals. *Nature*, *324*(6095), Article 6095. https://doi.org/10.1038/324361a0

Grinvald, A., Manker, A., & Segal, M. (1982). Visualization of the spread of electrical activity in rat hippocampal slices by voltage-sensitive optical probes. *The Journal of Physiology*, *333*(1), 269–291. https://doi.org/10.1113/jphysiol.1982.sp014453

Grossman, C. D., Bari, B. A., & Cohen, J. Y. (2022). Serotonin neurons modulate learning rate through uncertainty. *Current Biology*, *32*(3), 586-599.e7. https://doi.org/10.1016/j.cub.2021.12.006

Gullino, L. S., Fuller, C., Dunn, P., Collins, H. M., El Mestikawy, S., & Sharp, T. (2024). Evidence for a Role of 5-HT-glutamate Co-releasing Neurons in Acute Stress Mechanisms. *ACS Chemical Neuroscience*, *15*(6), 1185–1196.

https://doi.org/10.1021/acschemneuro.3c00758

Guo, C. C.-G., He, T., Grandjean, J., & Homberg, J. (2021). Knockout serotonin transporter in rats moderates outcome and stimulus generalization. *Translational Psychiatry*, *11*(1), Article 1. https://doi.org/10.1038/s41398-020-01162-0

Guo, J.-D., O'Flaherty, B. M., & Rainnie, D. G. (2017). Serotonin gating of cortical and thalamic glutamate inputs onto principal neurons of the basolateral amygdala. *Neuropharmacology*, *126*, 224–232. https://doi.org/10.1016/j.neuropharm.2017.09.013

Hajós, M., Gartside, S. E., Villa, A. E., & Sharp, T. (1995). Evidence for a repetitive (burst) firing pattern in a sub-population of 5-hydroxytryptamine neurons in the dorsal and median raphe nuclei of the rat. *Neuroscience*, *69*(1), 189–197. https://doi.org/10.1016/0306-4522(95)00227-a

Halvorsen, A., Hesel, B., Østergaard, S. D., & Danielsen, A. A. (2019). In utero exposure to selective serotonin reuptake inhibitors and development of mental disorders: A systematic review and meta-analysis. *Acta Psychiatrica Scandinavica*, *139*(6), 493–507. https://doi.org/10.1111/acps.13030

Hamada, H. T., Abe, Y., Takata, N., Taira, M., Tanaka, K. F., & Doya, K. (2022). *Optogenetic activation of dorsal raphe serotonin neurons induces a brain-wide response in reward network* (p. 2022.08.07.503074). bioRxiv. https://doi.org/10.1101/2022.08.07.503074

Hamada, H. T., Abe, Y., Takata, N., Taira, M., Tanaka, K. F., & Doya, K. (2024). Optogenetic activation of dorsal raphe serotonin neurons induces brain-wide activation. *Nature Communications*, *15*(1), 4152. https://doi.org/10.1038/s41467-024-48489-6

Hansen, H. D., Lindberg, U., Ozenne, B., Fisher, P. M., Johansen, A., Svarer, C., Keller, S. H., Hansen, A. E., & Knudsen, G. M. (2020). Visual stimuli induce serotonin release in occipital cortex: A simultaneous positron emission tomography/magnetic resonance imaging study. *Human Brain Mapping*, *41*(16), 4753–4763. https://doi.org/10.1002/hbm.25156

Harkin, E. F., Grossman, C. D., Cohen, J. Y., Béïque, J.-C., & Naud, R. (2023). *Serotonin predictively encodes value* (p. 2023.09.19.558526). bioRxiv. https://doi.org/10.1101/2023.09.19.558526

Haroush, N., & Marom, S. (2019). Inhibition increases response variability and reduces stimulus discrimination in random networks of cortical neurons. *Scientific Reports*, *9*(1), Article 1. https://doi.org/10.1038/s41598-019-41220-2

He, C. X., Arroyo, E. D., Cantu, D. A., Goel, A., & Portera-Cailliau, C. (2018). A Versatile Method for Viral Transfection of Calcium Indicators in the Neonatal Mouse Brain. *Frontiers in Neural Circuits*, *12*, 56. https://doi.org/10.3389/fncir.2018.00056

Hecht, P. M., Hudson, M., Connors, S. L., Tilley, M. R., Liu, X., & Beversdorf, D. Q. (2016). Maternal serotonin transporter genotype affects risk for ASD with exposure to prenatal stress. *Autism Research: Official Journal of the International Society for Autism Research*, *9*(11), 1151–1160. https://doi.org/10.1002/aur.1629

Heinz, A., Jones, D. W., Mazzanti, C., Goldman, D., Ragan, P., Hommer, D., Linnoila, M., & Weinberger, D. R. (2000). A relationship between serotonin transporter genotype and in vivo protein expression and alcohol neurotoxicity. *Biological Psychiatry*, *47*(7), 643–649. https://doi.org/10.1016/s0006-3223(99)00171-7

Hesse, S., Stengler, K., Regenthal, R., Patt, M., Becker, G.-A., Franke, A., Knüpfer, H., Meyer, P. M., Luthardt, J., Jahn, I., Lobsien, D., Heinke, W., Brust, P., Hegerl, U., & Sabri, O. (2011). The serotonin transporter availability in untreated early-onset and late-onset patients with obsessive–compulsive disorder. *International Journal of Neuropsychopharmacology*, *14*(5), 606–617. https://doi.org/10.1017/S1461145710001604

Hidalgo, R. B., & Davidson, J. R. (2000). Selective serotonin reuptake inhibitors in post-traumatic stress disorder. *Journal of Psychopharmacology (Oxford, England)*, *14*(1), 70–76. https://doi.org/10.1177/026988110001400110

Hill, D. K., & Keynes, R. D. (1949). Opacity changes in stimulated nerve. *The Journal of Physiology*, *108*(3), 278–281. https://doi.org/10.1113/jphysiol.1949.sp004331

Ho, H., Fowle, A., Coetzee, M., Greger, I. H., & Watson, J. F. (2020). An inhalation anaesthesia approach for neonatal mice allowing streamlined stereotactic injection in the brain. *Journal of Neuroscience Methods*, *342*, 108824. https://doi.org/10.1016/j.jneumeth.2020.108824

Hoerder-Suabedissen, A., Ocana-Santero, G., Draper, T. H., Scott, S. A., Kimani, J. G., Shelton, A. M., Butt, S. J. B., Molnár, Z., & Packer, A. M. (2022). Temporal origin of mouse claustrum and development of its cortical projections. *Cerebral Cortex*, bhac318. https://doi.org/10.1093/cercor/bhac318

Holtmaat, A., Bonhoeffer, T., Chow, D. K., Chuckowree, J., De Paola, V., Hofer, S. B., Hübener, M., Keck, T., Knott, G., Lee, W.-C. A., Mostany, R., Mrsic-Flogel, T. D., Nedivi, E., Portera-Cailliau, C., Svoboda, K., Trachtenberg, J. T., & Wilbrecht, L. (2009). Long-term, high-resolution imaging in the mouse neocortex through a chronic cranial window. *Nature Protocols*, *4*(8), 1128–1144. https://doi.org/10.1038/nprot.2009.89

Holze, F., Singh, N., Liechti, M. E., & D'Souza, D. C. (2024). Serotonergic Psychedelics: A Comparative Review of Efficacy, Safety, Pharmacokinetics, and Binding Profile. *Biological Psychiatry: Cognitive Neuroscience and Neuroimaging*, *9*(5), 472–489. https://doi.org/10.1016/j.bpsc.2024.01.007

Huang, S., Wu, S. J., Sansone, G., Ibrahim, L. A., & Fishell, G. (2024). Layer 1 neocortex: Gating and integrating multidimensional signals. *Neuron*, *112*(2), 184–200. https://doi.org/10.1016/j.neuron.2023.09.041

Iigaya, K., Fonseca, M. S., Murakami, M., Mainen, Z. F., & Dayan, P. (2018). An effect of serotonergic stimulation on learning rates for rewards apparent after long intertrial intervals. *Nature Communications*, *9*(1), Article 1. https://doi.org/10.1038/s41467-018-04840-2

Jacobs, B. L., & Fornal, C. A. (1997). Serotonin and motor activity. *Current Opinion in Neurobiology*, *7*(6), 820–825. https://doi.org/10.1016/s0959-4388(97)80141-9

Jauhar, S., Arnone, D., Baldwin, D. S., Bloomfield, M., Browning, M., Cleare, A. J., Corlett, P., Deakin, J. F. W., Erritzoe, D., Fu, C., Fusar-Poli, P., Goodwin, G. M., Hayes, J., Howard, R., Howes, O. D., Juruena, M. F., Lam, R. W., Lawrie, S. M., McAllister-Williams, H., … Cowen, P. J. (2023). A leaky umbrella has little value: Evidence clearly indicates the serotonin system is implicated in depression. *Molecular Psychiatry*, *28*(8), 3149–3152. https://doi.org/10.1038/s41380-023-02095-y

Jauhar, S., Cowen, P. J., & Browning, M. (2023). Fifty years on: Serotonin and depression. *Journal of Psychopharmacology (Oxford, England)*, *37*(3), 237–241. https://doi.org/10.1177/02698811231161813

Jennings, K. A., Lesch, K.-P., Sharp, T., & Cragg, S. J. (2010). Non-linear relationship between 5-HT transporter gene expression and frequency sensitivity of 5-HT signals. *Journal of Neurochemistry*, *115*(4), 965–973. https://doi.org/10.1111/j.1471-4159.2010.07001.x

Ji, S., Zhang, Y., Chen, N., Liu, X., Li, Y., Shao, X., Yang, Z., Yao, Z., & Hu, B. (2022). Shared increased entropy of brain signals across patients with different mental illnesses: A coordinate-based activation likelihood estimation meta-analysis. *Brain Imaging and Behavior*, *16*(1), 336–343. https://doi.org/10.1007/s11682-021-00507-7

Jiang, X., Li, X., Xing, H., Huang, X., Xu, X., & Li, J. (2021). Brain Entropy Study on Obsessive-Compulsive Disorder Using Resting-State fMRI. *Frontiers in Psychiatry*, *12*, 764328. https://doi.org/10.3389/fpsyt.2021.764328

Johnson, P. L., Molosh, A. I., Federici, L. M., Bernabe, C., Haggerty, D., Fitz, S. D., Nalivaiko, E., Truitt, W., & Shekhar, A. (2019). Assessment of fear and anxiety associated behaviors, physiology and neural circuits in rats with reduced serotonin transporter (SERT) levels. *Translational Psychiatry*, *9*(1), 33. https://doi.org/10.1038/s41398-019-0368-y

Jones, K. L., Smith, R. M., Edwards, K. S., Givens, B., Tilley, M. R., & Beversdorf, D. Q. (2010). Combined effect of maternal serotonin transporter genotype and prenatal stress in modulating offspring social interaction in mice. *International Journal of Developmental Neuroscience: The Official Journal of the International Society for Developmental Neuroscience*, *28*(6), 529–536. https://doi.org/10.1016/j.ijdevneu.2010.05.002

Kalueff, A. V., Olivier, J. D. A., Nonkes, L. J. P., & Homberg, J. R. (2010). Conserved role for the serotonin transporter gene in rat and mouse neurobehavioral endophenotypes. *Neuroscience and Biobehavioral Reviews*, *34*(3), 373–386. https://doi.org/10.1016/j.neubiorev.2009.08.003

Kanen, J. W., Apergis-Schoute, A. M., Yellowlees, R., Arntz, F. E., van der Flier, F. E., Price, A., Cardinal, R. N., Christmas, D. M., Clark, L., Sahakian, B. J., Crockett, M. J., & Robbins, T. W. (2021). Serotonin depletion impairs both Pavlovian and instrumental reversal learning in healthy humans. *Molecular Psychiatry*, *26*(12), 7200–7210. https://doi.org/10.1038/s41380-021-01240-9

Kanwisher, N., Khosla, M., & Dobs, K. (2023). Using artificial neural networks to ask 'why' questions of minds and brains. *Trends in Neurosciences*, *46*(3), 240–254. https://doi.org/10.1016/j.tins.2022.12.008

Kato, T., Mitsukura, Y., Yoshida, K., Mimura, M., Takata, N., & Tanaka, K. F. (2022). Oscillatory Population-Level Activity of Dorsal Raphe Serotonergic Neurons Is Inscribed in Sleep Structure. *Journal of Neuroscience*, *42*(38), 7244–7255. https://doi.org/10.1523/JNEUROSCI.2288-21.2022

Kawai, R., Markman, T., Poddar, R., Ko, R., Fantana, A., Dhawale, A., Kampff, A. R., & Ölveczky, B. P. (2015). Motor cortex is required for learning but not executing a motor skill. *Neuron*, *86*(3), 800–812. https://doi.org/10.1016/j.neuron.2015.03.024

Keller, G. B., & Mrsic-Flogel, T. D. (2018). Predictive Processing: A Canonical Cortical Computation. *Neuron*, *100*(2), 424–435. https://doi.org/10.1016/j.neuron.2018.10.003

Kellner, M. (2010). Drug treatment of obsessive-compulsive disorder. *Dialogues in Clinical Neuroscience*, *12*(2), 187–197.

Kendler, K. S., Kuhn, J. W., Vittum, J., Prescott, C. A., & Riley, B. (2005). The interaction of stressful life events and a serotonin transporter polymorphism in the prediction of episodes of major depression: A replication. *Archives of General Psychiatry*, *62*(5), 529–535. https://doi.org/10.1001/archpsyc.62.5.529

Kepser, L.-J., & Homberg, J. R. (2015). The neurodevelopmental effects of serotonin: A behavioural perspective. *Behavioural Brain Research*, *277*, 3–13. https://doi.org/10.1016/j.bbr.2014.05.022

Keshmiri, S. (2020). Entropy and the Brain: An Overview. *Entropy*, *22*(9), 917. https://doi.org/10.3390/e22090917

Kirmse, K., & Zhang, C. (2022). Principles of GABAergic signaling in developing cortical network dynamics. *Cell Reports*, *38*(13), 110568. https://doi.org/10.1016/j.celrep.2022.110568

Kjaerby, C., Athilingam, J., Robinson, S. E., Iafrati, J., & Sohal, V. S. (2016). Serotonin 1B Receptors Regulate Prefrontal Function by Gating Callosal and Hippocampal Inputs. *Cell Reports*, *17*(11), 2882–2890. https://doi.org/10.1016/j.celrep.2016.11.036

Klempin, F., Babu, H., De Pietri Tonel, D., Alarcon, E., Fabel, K., & Kempermann, G. (2010). Oppositional Effects of Serotonin Receptors 5-HT1a, 2, and 2c in the Regulation of Adult Hippocampal Neurogenesis. *Frontiers in Molecular Neuroscience*, *3*. https://doi.org/10.3389/fnmol.2010.00014

Koc, D., Tiemeier, H., Stricker, B. H., Muetzel, R. L., Hillegers, M., & El Marroun, H. (2023). Prenatal Antidepressant Exposure and Offspring Brain Morphologic Trajectory. *JAMA Psychiatry*, *80*(12), 1208–1217. https://doi.org/10.1001/jamapsychiatry.2023.3161

Korkmaz, N. D., Cikrikcili, U., Akan, M., & Yucesan, E. (2024). Psychedelic therapy in depression and substance use disorders. *European Journal of Neuroscience*, *60*(2), 4063–4077. https://doi.org/10.1111/ejn.16421

Kourdougli, N., Suresh, A., Liu, B., Juarez, P., Lin, A., Chung, D. T., Graven Sams, A., Gandal, M. J., Martínez-Cerdeño, V., Buonomano, D. V., Hall, B. J., Mombereau, C., & Portera-Cailliau, C. (2023). Improvement of sensory deficits in fragile X mice by increasing cortical interneuron activity after the critical period. *Neuron*, *111*(18), 2863-2880.e6. https://doi.org/10.1016/j.neuron.2023.06.009

Kriegeskorte, N., & Golan, T. (2019). Neural network models and deep learning—A primer for biologists. *Current Biology*, *29*(7), R231–R236. https://doi.org/10.1016/j.cub.2019.02.034

Kriegeskorte, N., Mur, M., & Bandettini, P. A. (2008). Representational similarity analysis—Connecting the branches of systems neuroscience. *Frontiers in Systems Neuroscience*, *2*. https://doi.org/10.3389/neuro.06.004.2008

Krystal, J. H., & Neumeister, A. (2009). Noradrenergic and Serotonergic Mechanisms in the Neurobiology of Posttraumatic Stress Disorder and Resilience. *Brain Research*, *1293*, 13–23. https://doi.org/10.1016/j.brainres.2009.03.044

Kubitschke, M., Müller, M., Wallhorn, L., Pulin, M., Mittag, M., Pollok, S., Ziebarth, T., Bremshey, S., Gerdey, J., Claussen, K. C., Renken, K., Groß, J., Gneiße, P., Meyer, N., Wiegert, J. S., Reiner, A., Fuhrmann, M., & Masseck, O. A. (2022). Next generation genetically encoded fluorescent sensors for serotonin. *Nature Communications*, *13*(1), Article 1. https://doi.org/10.1038/s41467-022-35200-w

Kullander, K., & Topolnik, L. (2021). Cortical disinhibitory circuits: Cell types, connectivity and function. *Trends in Neurosciences*, *44*(8), 643–657. https://doi.org/10.1016/j.tins.2021.04.009

Lambert, T. J. (2019). FPbase: A community-editable fluorescent protein database. *Nature Methods*, *16*(4), Article 4. https://doi.org/10.1038/s41592-019-0352-8

Larsen, B., & Luna, B. (2018). Adolescence as a neurobiological critical period for the development of higher-order cognition. *Neuroscience and Biobehavioral Reviews*, *94*, 179–195. https://doi.org/10.1016/j.neubiorev.2018.09.005

Laurent, A., Goaillard, J.-M., Cases, O., Lebrand, C., Gaspar, P., & Ropert, N. (2002). Activity-dependent presynaptic effect of serotonin 1B receptors on the somatosensory thalamocortical transmission in neonatal mice. *The Journal of Neuroscience: The Official Journal of the Society for Neuroscience*, *22*(3), 886–900. https://doi.org/10.1523/JNEUROSCI.22-03-00886.2002

Lebrand, C., Cases, O., Adelbrecht, C., Doye, A., Alvarez, C., El Mestikawy, S., Seif, I., & Gaspar, P. (1996). Transient Uptake and Storage of Serotonin in Developing Thalamic Neurons. *Neuron*, *17*(5), 823–835. https://doi.org/10.1016/S0896-6273(00)80215-9

LeDuke, D. O., Borio, M., Miranda, R., & Tye, K. M. (2023). Anxiety and depression: A top-down, bottom-up model of circuit function. *Annals of the New York Academy of Sciences*, *1525*(1), 70–87. https://doi.org/10.1111/nyas.14997

Lee, H.-J., Lee, M.-S., Kang, R.-H., Kim, H., Kim, S.-D., Kee, B.-S., Kim, Y. H., Kim, Y.-K., Kim, J. B., Yeon, B. K., Oh, K. S., Oh, B.-H., Yoon, J.-S., Lee, C., Jung, H. Y., Chee, I.-S., & Paik, I. H. (2005). Influence of the serotonin transporter promoter gene polymorphism on susceptibility to posttraumatic stress disorder. *Depression and Anxiety*, *21*(3), 135–139. https://doi.org/10.1002/da.20064

Lee, S., Hjerling-Leffler, J., Zagha, E., Fishell, G., & Rudy, B. (2010). The Largest Group of Superficial Neocortical GABAergic Interneurons Expresses Ionotropic Serotonin Receptors. *The Journal of Neuroscience*, *30*(50), 16796–16808. https://doi.org/10.1523/JNEUROSCI.1869-10.2010

Lee, S., Kruglikov, I., Huang, Z. J., Fishell, G., & Rudy, B. (2013). A disinhibitory circuit mediates motor integration in the somatosensory cortex. *Nature Neuroscience*, *16*(11), 1662–1670. https://doi.org/10.1038/nn.3544

Leighton, A. H., Cheyne, J. E., Houwen, G. J., Maldonado, P. P., De Winter, F., Levelt, C. N., & Lohmann, C. (2021). Somatostatin interneurons restrict cell recruitment to retinally driven spontaneous activity in the developing cortex. *Cell Reports*, *36*(1), 109316.

https://doi.org/10.1016/j.celrep.2021.109316

Lerner, T. N., Shilyansky, C., Davidson, T. J., Evans, K. E., Beier, K. T., Zalocusky, K. A., Crow, A. K., Malenka, R. C., Luo, L., Tomer, R., & Deisseroth, K. (2015). Intact-Brain Analyses Reveal Distinct Information Carried by SNc Dopamine Subcircuits. *Cell*, *162*(3), 635–647. https://doi.org/10.1016/j.cell.2015.07.014

Lesch, K.-P., Bengel, D., Heils, A., Sabol, S. Z., Greenberg, B. D., Petri, S., Benjamin, J., Müller, C. R., Hamer, D. H., & Murphy, D. L. (1996). Association of Anxiety-Related Traits with a Polymorphism in the Serotonin Transporter Gene Regulatory Region. *Science*, *274*(5292), 1527–1531. https://doi.org/10.1126/science.274.5292.1527

Lesch, K.-P., & Waider, J. (2012). Serotonin in the Modulation of Neural Plasticity and Networks: Implications for Neurodevelopmental Disorders. *Neuron*, *76*(1), 175–191. https://doi.org/10.1016/j.neuron.2012.09.013

Leslie, M. J., Bennett-Clarke, C. A., & Rhoades, R. W. (1992). Serotonin 1B receptors form a transient vibrissa-related pattern in the primary somatosensory cortex of the developing rat. *Brain Research. Developmental Brain Research*, *69*(1), 143–148. https://doi.org/10.1016/0165-3806(92)90132-g

Li, H., Jiang, W., Ling, L., Pratelli, M., Chen, C., Gupta, V., Godavarthi, S. K., & Spitzer, N. C. (2024). Generalized fear after acute stress is caused by change in neuronal cotransmitter identity. *Science*, *383*(6688), 1252–1259. https://doi.org/10.1126/science.adj5996

Li, H., Pratelli, M., Godavarthi, S., Zambetti, S., & Spitzer, N. C. (2020). Decoding Neurotransmitter Switching: The Road Forward. *Journal of Neuroscience*, *40*(21), 4078–4089. https://doi.org/10.1523/JNEUROSCI.0005-20.2020

Li, L., Zhang, L.-Z., He, Z.-X., Ma, H., Zhang, Y.-T., Xun, Y.-F., Yuan, W., Hou, W.-J., Li, Y.-T., Lv, Z.-J., Jia, R., & Tai, F.-D. (2021). Dorsal raphe nucleus to anterior cingulate cortex 5-HTergic neural circuit modulates consolation and sociability. *eLife*, *10*, e67638.

https://doi.org/10.7554/eLife.67638

Li, Y., Simmler, L. D., Van Zessen, R., Flakowski, J., Wan, J.-X., Deng, F., Li, Y.-L., Nautiyal, K. M., Pascoli, V., & Lüscher, C. (2021). Synaptic mechanism underlying serotonin modulation of transition to cocaine addiction. *Science*, *373*(6560), 1252–1256. https://doi.org/10.1126/science.abi9086

Li, Y., Zhong, W., Wang, D., Feng, Q., Liu, Z., Zhou, J., Jia, C., Hu, F., Zeng, J., Guo, Q., Fu, L., & Luo, M. (2016). Serotonin neurons in the dorsal raphe nucleus encode reward signals. *Nature Communications*, *7*(1), Article 1. https://doi.org/10.1038/ncomms10503

Lim, L., Mi, D., Llorca, A., & Marín, O. (2018). Development and functional diversification of cortical interneurons. *Neuron*, *100*(2), 294–313. https://doi.org/10.1016/j.neuron.2018.10.009

Lima, J., Sharp, T., Bannerman, D. M., & McHugh, S. B. (2019). Enhanced discriminative aversive learning and amygdala responsivity in 5-HT transporter mutant mice. *Translational Psychiatry*, *9*(1), 139. https://doi.org/10.1038/s41398-019-0476-8

Lin, S.-H., Lee, L.-T., & Yang, Y. K. (2014). Serotonin and mental disorders: A concise review on molecular neuroimaging evidence. *Clinical Psychopharmacology and Neuroscience: The Official Scientific Journal of the Korean College of Neuropsychopharmacology*, *12*(3), 196–202. https://doi.org/10.9758/cpn.2014.12.3.196

Lipton, P. (1973). Effects of membrane depolarization on light scattering by cerebral cortical slices. *The Journal of Physiology*, *231*(2), 365–383. https://doi.org/10.1113/jphysiol.1973.sp010238

Lira, A., Zhou, M., Castanon, N., Ansorge, M. S., Gordon, J. A., Francis, J. H., Bradley-Moore, M., Lira, J., Underwood, M. D., Arango, V., Kung, H. F., Hofer, M. A., Hen, R., & Gingrich, J. A. (2003). Altered depression-related behaviors and functional changes in the dorsal raphe nucleus of serotonin transporter-deficient mice. *Biological Psychiatry*, *54*(10), 960–971. https://doi.org/10.1016/S0006-3223(03)00696-6

Liu, X., Song, D., Yin, Y., Xie, C., Zhang, H., Zhang, H., Zhang, Z., Wang, Z., & Yuan, Y. (2020). Altered Brain Entropy as a predictor of antidepressant response in major depressive disorder. *Journal of Affective Disorders*, *260*, 716–721. https://doi.org/10.1016/j.jad.2019.09.067

Liu, Z., Zhou, J., Li, Y., Hu, F., Lu, Y., Ma, M., Feng, Q., Zhang, J., Wang, D., Zeng, J., Bao, J., Kim, J.-Y., Chen, Z.-F., El Mestikawy, S., & Luo, M. (2014). Dorsal Raphe Neurons Signal Reward through 5-HT and Glutamate. *Neuron*, *81*(6), 1360–1374. https://doi.org/10.1016/j.neuron.2014.02.010

Lottem, E., Lörincz, M. L., & Mainen, Z. F. (2016). Optogenetic Activation of Dorsal Raphe Serotonin Neurons Rapidly Inhibits Spontaneous But Not Odor-Evoked Activity in Olfactory Cortex. *Journal of Neuroscience*, *36*(1), 7–18. https://doi.org/10.1523/JNEUROSCI.3008-15.2016

Luo, Y., Kataoka, Y., Ostinelli, E. G., Cipriani, A., & Furukawa, T. A. (2020). National Prescription Patterns of Antidepressants in the Treatment of Adults With Major Depression in the US Between 1996 and 2015: A Population Representative Survey Based Analysis. *Frontiers in Psychiatry*, *11*, 35. https://doi.org/10.3389/fpsyt.2020.00035

Ly, C., Greb, A. C., Cameron, L. P., Wong, J. M., Barragan, E. V., Wilson, P. C., Burbach, K. F., Zarandi, S. S., Sood, A., Paddy, M. R., Duim, W. C., Dennis, M. Y., McAllister, A. K., Ori-McKenney, K. M., Gray, J. A., & Olson, D. E. (2018). Psychedelics Promote Structural and Functional Neural Plasticity. *Cell Reports*, *23*(11), 3170–3182. https://doi.org/10.1016/j.celrep.2018.05.022

Lynne E. Rueter, Casimir A. Fornal, & Barry L. Jacobs. (1997). A Critical Review of 5-HT Brain Microdialysis and Behavior. *Reviews in the Neurosciences*, *8*(2), 117–138. https://doi.org/10.1515/REVNEURO.1997.8.2.117

Ma, Y., Shaik, M. A., Kozberg, M. G., Kim, S. H., Portes, J. P., Timerman, D., & Hillman, E. M. C. (2016). Resting-state hemodynamics are spatiotemporally coupled to synchronized and

symmetric neural activity in excitatory neurons. *Proceedings of the National Academy of Sciences of the United States of America*, *113*(52), E8463–E8471. https://doi.org/10.1073/pnas.1525369113

Maddaloni, G., Bertero, A., Pratelli, M., Barsotti, N., Boonstra, A., Giorgi, A., Migliarini, S., & Pasqualetti, M. (2017). Development of Serotonergic Fibers in the Post-Natal Mouse Brain. *Frontiers in Cellular Neuroscience*, *11*, 202. https://doi.org/10.3389/fncel.2017.00202

Mahn, M., Saraf-Sinik, I., Patil, P., Pulin, M., Bitton, E., Karalis, N., Bruentgens, F., Palgi, S., Gat, A., Dine, J., Wietek, J., Davidi, I., Levy, R., Litvin, A., Zhou, F., Sauter, K., Soba, P., Schmitz, D., Luthi, A., … Yizhar, O. (2021). Efficient optogenetic silencing of neurotransmitter release with a mosquito rhodopsin. *Neuron*, *109*(10), 1621-1635.e8. https://doi.org/10.1016/j.neuron.2021.03.013

Mannelli, S. S., Ivashinka, Y., Saxe, A., & Saglietti, L. (2024). *Tilting the Odds at the Lottery: The Interplay of Overparameterisation and Curricula in Neural Networks* (arXiv:2406.01589). arXiv. https://doi.org/10.48550/arXiv.2406.01589

Marcinkiewcz, C. A., Mazzone, C. M., D'Agostino, G., Halladay, L. R., Hardaway, J. A., DiBerto, J. F., Navarro, M., Burnham, N., Cristiano, C., Dorrier, C. E., Tipton, G. J., Ramakrishnan, C., Kozicz, T., Deisseroth, K., Thiele, T. E., McElligott, Z. A., Holmes, A., Heisler, L. K., & Kash, T. L. (2016). Serotonin engages an anxiety and fear-promoting circuit in the extended amygdala. *Nature*, *537*(7618), 97–101. https://doi.org/10.1038/nature19318

Marco, E. J., Hinkley, L. B. N., Hill, S. S., & Nagarajan, S. S. (2011). Sensory processing in autism: A review of neurophysiologic findings. *Pediatric Research*, *69*(5 Pt 2), 48R-54R. https://doi.org/10.1203/PDR.0b013e3182130c54

Marques-Smith, A., Lyngholm, D., Kaufmann, A.-K., Stacey, J. A., Hoerder-Suabedissen, A., Becker, E. B. E., Wilson, M. C., Molnár, Z., & Butt, S. J. B. (2016). A Transient

Translaminar GABAergic Interneuron Circuit Connects Thalamocortical Recipient Layers in Neonatal Somatosensory Cortex. *Neuron*, *89*(3), 536–549. https://doi.org/10.1016/j.neuron.2016.01.015

Marquez, M. M., & Chacron, M. J. (2020). Chapter 25—Serotonin and sensory processing. In C. P. Müller & K. A. Cunningham (Eds.), *Handbook of Behavioral Neuroscience* (Vol. 31, pp. 449–459). Elsevier. https://doi.org/10.1016/B978-0-444-64125-0.00025-6

Martini, F. J., Guillamón-Vivancos, T., Moreno-Juan, V., Valdeolmillos, M., & López-Bendito, G. (2021). Spontaneous Activity in Developing Thalamic and Cortical Sensory Networks. *Neuron*, *109*(16), 2519–2534. https://doi.org/10.1016/j.neuron.2021.06.026

Maximo, J. O., Nelson, C. M., & Kana, R. K. (2021). 'Unrest while Resting'? Brain entropy in autism spectrum disorder. *Brain Research*, *1762*, 147435. https://doi.org/10.1016/j.brainres.2021.147435

May, L., & Gjorgjieva, J. (2024). *Pre-training artificial neural networks with spontaneous retinal activity improves motion prediction in natural scenes* (p. 2024.06.15.599143). bioRxiv. https://doi.org/10.1101/2024.06.15.599143

McHugh, S. B., Barkus, C., Lima, J., Glover, L. R., Sharp, T., & Bannerman, D. M. (2015). SERT and uncertainty: Serotonin transporter expression influences information processing biases for ambiguous aversive cues in mice. *Genes, Brain, and Behavior*, *14*(4), 330–336. https://doi.org/10.1111/gbb.12215

Melani, R., & Tritsch, N. X. (2022). Inhibitory co-transmission from midbrain dopamine neurons relies on presynaptic GABA uptake. *Cell Reports*, *39*(3), 110716. https://doi.org/10.1016/j.celrep.2022.110716

Meneses, A., & Liy-Salmeron, G. (2012). Serotonin and emotion, learning and memory. *Reviews in the Neurosciences*, *23*(5–6), 543–553. https://doi.org/10.1515/revneuro-2012-0060

Meng, X., Grandjean, J., Sbrini, G., Schipper, P., Hofwijks, N., Stoop, J., Calabrese, F., & Homberg, J. (2022). Tryptophan Hydroxylase 2 Knockout Male Rats Exhibit a

Strengthened Oxytocin System, Are Aggressive, and Are Less Anxious. *ACS Chemical Neuroscience*, *13*(20), 2974–2981. https://doi.org/10.1021/acschemneuro.2c00448

Miceli, S., Nadif Kasri, N., Joosten, J., Huang, C., Kepser, L., Proville, R., Selten, M. M., van Eijs, F., Azarfar, A., Homberg, J. R., Celikel, T., & Schubert, D. (2017). Reduced Inhibition within Layer IV of Sert Knockout Rat Barrel Cortex is Associated with Faster Sensory Integration. *Cerebral Cortex (New York, NY)*, *27*(2), 933–949. https://doi.org/10.1093/cercor/bhx016

Michely, J., Eldar, E., Erdman, A., Martin, I. M., & Dolan, R. J. (2022). Serotonin modulates asymmetric learning from reward and punishment in healthy human volunteers. *Communications Biology*, *5*(1), 1–9. https://doi.org/10.1038/s42003-022-03690-5

Miller, K. D. (2003). Understanding Layer 4 of the Cortical Circuit: A Model Based on Cat V1. *Cerebral Cortex*, *13*(1), 73–82. https://doi.org/10.1093/cercor/13.1.73

Miller, K. D. (2016). Canonical computations of cerebral cortex. *Current Opinion in Neurobiology*, *37*, 75–84. https://doi.org/10.1016/j.conb.2016.01.008

Miyazaki, K., Miyazaki, K. W., & Doya, K. (2011). Activation of Dorsal Raphe Serotonin Neurons Underlies Waiting for Delayed Rewards. *Journal of Neuroscience*, *31*(2), 469–479. https://doi.org/10.1523/JNEUROSCI.3714-10.2011

Miyazaki, K., Miyazaki, K. W., Yamanaka, A., Tokuda, T., Tanaka, K. F., & Doya, K. (2018). Reward probability and timing uncertainty alter the effect of dorsal raphe serotonin neurons on patience. *Nature Communications*, *9*(1), 2048. https://doi.org/10.1038/s41467-018-04496-y

Miyazaki, K. W., Miyazaki, K., Tanaka, K. F., Yamanaka, A., Takahashi, A., Tabuchi, S., & Doya, K. (2014). Optogenetic Activation of Dorsal Raphe Serotonin Neurons Enhances Patience for Future Rewards. *Current Biology*, *24*(17), 2033–2040. https://doi.org/10.1016/j.cub.2014.07.041

Moberg, S., & Takahashi, N. (2022). Neocortical layer 5 subclasses: From cellular properties to

roles in behavior. *Frontiers in Synaptic Neuroscience*, *14*, 1006773. https://doi.org/10.3389/fnsyn.2022.1006773

Modol, L., Bollmann, Y., Tressard, T., Baude, A., Che, A., Duan, Z. R. S., Babij, R., García, N. V. D. M., & Cossart, R. (2020). Assemblies of Perisomatic GABAergic Neurons in the Developing Barrel Cortex. *Neuron*, *105*(1), 93-105.e4. https://doi.org/10.1016/j.neuron.2019.10.007

Mòdol, L., Moissidis, M., & Marín, O. (2023). *Somatostatin interneurons control the timing of developmental desynchronization in cortical networks* (p. 2023.12.21.572767). bioRxiv. https://doi.org/10.1101/2023.12.21.572767

Mòdol, L., Moissidis, M., Selten, M., Oozeer, F., & Marín, O. (2024). Somatostatin interneurons control the timing of developmental desynchronization in cortical networks. *Neuron*, *0*(0). https://doi.org/10.1016/j.neuron.2024.03.014

Moliner, R., Girych, M., Brunello, C. A., Kovaleva, V., Biojone, C., Enkavi, G., Antenucci, L., Kot, E. F., Goncharuk, S. A., Kaurinkoski, K., Kuutti, M., Fred, S. M., Elsilä, L. V., Sakson, S., Cannarozzo, C., Diniz, C. R. A. F., Seiffert, N., Rubiolo, A., Haapaniemi, H., … Castrén, E. (2023). Psychedelics promote plasticity by directly binding to BDNF receptor TrkB. *Nature Neuroscience*, *26*(6), 1032–1041. https://doi.org/10.1038/s41593-023-01316-5

Moncrieff, J., Cooper, R. E., Stockmann, T., Amendola, S., Hengartner, M. P., & Horowitz, M. A. (2022). The serotonin theory of depression: A systematic umbrella review of the evidence. *Molecular Psychiatry*, 1–14. https://doi.org/10.1038/s41380-022-01661-0

Montgomery, A. K., Shuffrey, L. C., Guter, S. J., Anderson, G. M., Jacob, S., Mosconi, M. W., Sweeney, J. A., Turner, J. B., Sutcliffe, J. S., Cook, E. H., & Veenstra-VanderWeele, J. (2018). Maternal Serotonin Levels Are Associated With Cognitive Ability and Core Symptoms in Autism Spectrum Disorder. *Journal of the American Academy of Child and Adolescent Psychiatry*, *57*(11), 867–875. https://doi.org/10.1016/j.jaac.2018.06.025

Morales, D. R., Slattery, J., Evans, S., & Kurz, X. (2018). Antidepressant use during pregnancy

and risk of autism spectrum disorder and attention deficit hyperactivity disorder: Systematic review of observational studies and methodological considerations. *BMC Medicine*, *16*(1), 6. https://doi.org/10.1186/s12916-017-0993-3

Morone, K. A., Neimat, J. S., Roe, A. W., & Friedman, R. M. (2017). Review of functional and clinical relevance of intrinsic signal optical imaging in human brain mapping. *Neurophotonics*, *4*(3), 031220. https://doi.org/10.1117/1.NPh.4.3.031220

Morton, R. A., Yanagawa, Y., & Valenzuela, C. F. (2015). Electrophysiological Assessment of Serotonin and GABA Neuron Function in the Dorsal Raphe during the Third Trimester Equivalent Developmental Period in Mice. *eNeuro*, *2*(6). https://doi.org/10.1523/ENEURO.0079-15.2015

Mosienko, V., Bert, B., Beis, D., Matthes, S., Fink, H., Bader, M., & Alenina, N. (2012). Exaggerated aggression and decreased anxiety in mice deficient in brain serotonin. *Translational Psychiatry*, *2*(5), e122–e122. https://doi.org/10.1038/tp.2012.44

Muller, C. L., Anacker, A. M. J., & Veenstra-VanderWeele, J. (2016). The serotonin system in autism spectrum disorder: From biomarker to animal models. *Neuroscience*, *321*, 24–41. https://doi.org/10.1016/j.neuroscience.2015.11.010

Munz, M., Bharioke, A., Kosche, G., Moreno-Juan, V., Brignall, A., Rodrigues, T. M., Graff-Meyer, A., Ulmer, T., Haeuselmann, S., Pavlinic, D., Ledergerber, N., Gross-Scherf, B., Rózsa, B., Krol, J., Picelli, S., Cowan, C. S., & Roska, B. (2023). Pyramidal neurons form active, transient, multilayered circuits perturbed by autism-associated mutations at the inception of neocortex. *Cell*, *186*(9), 1930-1949.e31. https://doi.org/10.1016/j.cell.2023.03.025

Murphy, D. L., & Lesch, K.-P. (2008). Targeting the murine serotonin transporter: Insights into human neurobiology. *Nature Reviews Neuroscience*, *9*(2), Article 2. https://doi.org/10.1038/nrn2284

Murthy, S., Niquille, M., Hurni, N., Limoni, G., Frazer, S., Chameau, P., van Hooft, J. A., Vitalis,

T., & Dayer, A. (2014). Serotonin receptor 3A controls interneuron migration into the neocortex. *Nature Communications*, *5*(1), Article 1. https://doi.org/10.1038/ncomms6524

Narboux-Nême, N., Pavone, L. M., Avallone, L., Zhuang, X., & Gaspar, P. (2008). Serotonin transporter transgenic (SERTcre) mouse line reveals developmental targets of serotonin specific reuptake inhibitors (SSRIs). *Neuropharmacology*, *55*(6), 994–1005. https://doi.org/10.1016/j.neuropharm.2008.08.020

Nath, T., Mathis, A., Chen, A. C., Patel, A., Bethge, M., & Mathis, M. W. (2019). Using DeepLabCut for 3D markerless pose estimation across species and behaviors. *Nature Protocols*, *14*(7), Article 7. https://doi.org/10.1038/s41596-019-0176-0

Nicolini, H. (2010). Serotonin transporter gene polymorphisms & obsessive-compulsive disorder. *The Indian Journal of Medical Research*, *132*(6), 663–665.

Ocana-Santero, G., Packer, A. M., Sharp, T., & Butt, S. J. B. (2024). In Vivo Two-Photon Microscopy Reveals Sensory-Evoked Serotonin (5-HT) Release in Adult Mammalian Neocortex. *ACS Chemical Neuroscience*, *15*(3), 456–461. https://doi.org/10.1021/acschemneuro.3c00725

Ogelman, R., Gomez Wulschner, L. E., Hoelscher, V. M., Hwang, I.-W., Chang, V. N., & Oh, W. C. (2024). Serotonin modulates excitatory synapse maturation in the developing prefrontal cortex. *Nature Communications*, *15*(1), 1368. https://doi.org/10.1038/s41467-024-45734-w

Okaty, B. W., Commons, K. G., & Dymecki, S. M. (2019). Embracing diversity in the 5-HT neuronal system. *Nature Reviews Neuroscience*, *20*(7), 397–424. https://doi.org/10.1038/s41583-019-0151-3

Ostlund, S. B., & Balleine, B. W. (2005). Lesions of Medial Prefrontal Cortex Disrupt the Acquisition But Not the Expression of Goal-Directed Learning. *Journal of Neuroscience*, *25*(34), 7763–7770. https://doi.org/10.1523/JNEUROSCI.1921-05.2005

Owens, M. J., Morgan, W. N., Plott, S. J., & Nemeroff, C. B. (1997). Neurotransmitter receptor

and transporter binding profile of antidepressants and their metabolites. *The Journal of Pharmacology and Experimental Therapeutics*, *283*(3), 1305–1322.

Pachitariu, M., Stringer, C., Dipoppa, M., Schröder, S., Rossi, L. F., Dalgleish, H., Carandini, M., & Harris, K. D. (2017). *Suite2p: Beyond 10,000 neurons with standard two-photon microscopy* (p. 061507). bioRxiv. https://doi.org/10.1101/061507

Packer, A. M., Russell, L. E., Dalgleish, H. W. P., & Häusser, M. (2015). Simultaneous all-optical manipulation and recording of neural circuit activity with cellular resolution in vivo. *Nature Methods*, *12*(2), 140–146. https://doi.org/10.1038/nmeth.3217

Pan, W., Pan, J., Zhao, Y., Zhang, H., & Tang, J. (2021). Serotonin Transporter Defect Disturbs Structure and Function of the Auditory Cortex in Mice. *Frontiers in Neuroscience*, *15*. https://www.frontiersin.org/articles/10.3389/fnins.2021.749923

Pan, Y., & Monje, M. (2020). Activity Shapes Neural Circuit Form and Function: A Historical Perspective. *The Journal of Neuroscience*, *40*(5), 944–954. https://doi.org/10.1523/JNEUROSCI.0740-19.2019

Paquelet, G. E., Carrion, K., Lacefield, C. O., Zhou, P., Hen, R., & Miller, B. R. (2022). Single-cell activity and network properties of dorsal raphe nucleus serotonin neurons during emotionally salient behaviors. *Neuron*. https://doi.org/10.1016/j.neuron.2022.05.015

Pedregosa, F., Varoquaux, G., Gramfort, A., Michel, V., Thirion, B., Grisel, O., Blondel, M., Prettenhofer, P., Weiss, R., Dubourg, V., Vanderplas, J., Passos, A., Cournapeau, D., Brucher, M., Perrot, M., & Duchesnay, É. (2011). Scikit-learn: Machine Learning in Python. *The Journal of Machine Learning Research*, *12*(null), 2825–2830.

Pezawas, L., Meyer-Lindenberg, A., Drabant, E. M., Verchinski, B. A., Munoz, K. E., Kolachana, B. S., Egan, M. F., Mattay, V. S., Hariri, A. R., & Weinberger, D. R. (2005). 5-HTTLPR polymorphism impacts human cingulate-amygdala interactions: A genetic susceptibility mechanism for depression. *Nature Neuroscience*, *8*(6), Article 6.

https://doi.org/10.1038/nn1463

Piet, A., Ponvert, N., Ollerenshaw, D., Garrett, M., Groblewski, P. A., Olsen, S., Koch, C., & Arkhipov, A. (2024). Behavioral strategy shapes activation of the Vip-Sst disinhibitory circuit in visual cortex. *Neuron*, *112*(11), 1876-1890.e4. https://doi.org/10.1016/j.neuron.2024.02.008

Pourhamzeh, M., Moravej, F. G., Arabi, M., Shahriari, E., Mehrabi, S., Ward, R., Ahadi, R., & Joghataei, M. T. (2022). The Roles of Serotonin in Neuropsychiatric Disorders. *Cellular and Molecular Neurobiology*, *42*(6), 1671–1692. https://doi.org/10.1007/s10571-021-01064-9

Prönneke, A., Scheuer, B., Wagener, R. J., Möck, M., Witte, M., & Staiger, J. F. (2015). Characterizing VIP Neurons in the Barrel Cortex of VIPcre/tdTomato Mice Reveals Layer-Specific Differences. *Cerebral Cortex (New York, NY)*, *25*(12), 4854–4868. https://doi.org/10.1093/cercor/bhv202

Pudovkina, O. L., Cremers, T. I. F. H., & Westerink, B. H. C. (2002). The interaction between the locus coeruleus and dorsal raphe nucleus studied with dual-probe microdialysis. *European Journal of Pharmacology*, *445*(1–2), 37–42. https://doi.org/10.1016/s0014-2999(02)01663-1

Puig, M. V., & Gener, T. (2015). Serotonin Modulation of Prefronto-Hippocampal Rhythms in Health and Disease. *ACS Chemical Neuroscience*, *6*(7), 1017–1025. https://doi.org/10.1021/cn500350e

Qu, Y., Chang, L., Ma, L., Wan, X., & Hashimoto, K. (2023). Rapid antidepressant-like effect of non-hallucinogenic psychedelic analog lisuride, but not hallucinogenic psychedelic DOI, in lipopolysaccharide-treated mice. *Pharmacology Biochemistry and Behavior*, *222*, 173500. https://doi.org/10.1016/j.pbb.2022.173500

Ramamoorthy, S., Bauman, A. L., Moore, K. R., Han, H., Yang-Feng, T., Chang, A. S., Ganapathy, V., & Blakely, R. D. (1993). Antidepressant- and cocaine-sensitive human

serotonin transporter: Molecular cloning, expression, and chromosomal localization. *Proceedings of the National Academy of Sciences of the United States of America*, *90*(6), 2542–2546. https://doi.org/10.1073/pnas.90.6.2542

Ranade, S. P., & Mainen, Z. F. (2009). Transient Firing of Dorsal Raphe Neurons Encodes Diverse and Specific Sensory, Motor, and Reward Events. *Journal of Neurophysiology*, *102*(5), 3026–3037. https://doi.org/10.1152/jn.00507.2009

Rebello, T. J., Yu, Q., Goodfellow, N. M., Caffrey Cagliostro, M. K., Teissier, A., Morelli, E., Demireva, E. Y., Chemiakine, A., Rosoklija, G. B., Dwork, A. J., Lambe, E. K., Gingrich, J. A., & Ansorge, M. S. (2014). Postnatal day 2 to 11 constitutes a 5-HT-sensitive period impacting adult mPFC function. *The Journal of Neuroscience: The Official Journal of the Society for Neuroscience*, *34*(37), 12379–12393. https://doi.org/10.1523/JNEUROSCI.1020-13.2014

Reggiani, J. D. S., Jiang, Q., Barbini, M., Lutas, A., Liang, L., Fernando, J., Deng, F., Wan, J., Li, Y., Chen, C., & Andermann, M. L. (2023). Brainstem serotonin neurons selectively gate retinal information flow to thalamus. *Neuron*, *111*(5), 711-726.e11. https://doi.org/10.1016/j.neuron.2022.12.006

Ren, J., Friedmann, D., Xiong, J., Liu, C. D., Ferguson, B. R., Weerakkody, T., DeLoach, K. E., Ran, C., Pun, A., Sun, Y., Weissbourd, B., Neve, R. L., Huguenard, J., Horowitz, M. A., & Luo, L. (2018). Anatomically Defined and Functionally Distinct Dorsal Raphe Serotonin Sub-systems. *Cell*, *175*(2), 472-487.e20. https://doi.org/10.1016/j.cell.2018.07.043

Ren, J., Isakova, A., Friedmann, D., Zeng, J., Grutzner, S. M., Pun, A., Zhao, G. Q., Kolluru, S. S., Wang, R., Lin, R., Li, P., Li, A., Raymond, J. L., Luo, Q., Luo, M., Quake, S. R., & Luo, L. (2019). Single-cell transcriptomes and whole-brain projections of serotonin neurons in the mouse dorsal and median raphe nuclei. *eLife*, *8*, e49424. https://doi.org/10.7554/eLife.49424

Riccio, O., Jacobshagen, M., Golding, B., Vutskits, L., Jabaudon, D., Hornung, J. P., & Dayer, A.

G. (2011). Excess of serotonin affects neocortical pyramidal neuron migration. *Translational Psychiatry*, *1*(10), e47. https://doi.org/10.1038/tp.2011.49

Rogawski, M. A., & Aghajanian, G. K. (1979). Response of central monoaminergic neurons to lisuride: Comparison with LSD. *Life Sciences*, *24*(14), 1289–1297. https://doi.org/10.1016/0024-3205(79)90148-6

Rowland, J. M., van der Plas, T. L., Loidolt, M., Lees, R. M., Keeling, J., Dehning, J., Akam, T., Priesemann, V., & Packer, A. M. (2023). Propagation of activity through the cortical hierarchy and perception are determined by neural variability. *Nature Neuroscience*, *26*(9), Article 9. https://doi.org/10.1038/s41593-023-01413-5

Russell, L. (2024). *Llerussell/Naparm* [MATLAB]. https://github.com/llerussell/Naparm (Original work published 2019)

Saad, D., & Solla, S. A. (1995). On-line learning in soft committee machines. *Physical Review E*, *52*(4), 4225–4243. https://doi.org/10.1103/PhysRevE.52.4225

Saeb, S., Lonini, L., Jayaraman, A., Mohr, D. C., & Kording, K. P. (2017). The need to approximate the use-case in clinical machine learning. *GigaScience*, *6*(5), gix019. https://doi.org/10.1093/gigascience/gix019

Sahu, A., Gopalakrishnan, L., Gaur, N., Chatterjee, O., Mol, P., Modi, P. K., Dagamajalu, S., Advani, J., Jain, S., & Keshava Prasad, T. S. (2018). The 5-Hydroxytryptamine signaling map: An overview of serotonin-serotonin receptor mediated signaling network. *Journal of Cell Communication and Signaling*, *12*(4), 731–735. https://doi.org/10.1007/s12079-018-0482-2

Saitow, F., Takumi, T., & Suzuki, H. (2020). Upregulated 5-HT1A receptor-mediated currents in the prefrontal cortex layer 5 neurons in the 15q11–13 duplication mouse model of autism. *Molecular Brain*, *13*, 115. https://doi.org/10.1186/s13041-020-00655-9

Sakai, K. (2011). Sleep-waking discharge profiles of dorsal raphe nucleus neurons in mice. *Neuroscience*, *197*, 200–224. https://doi.org/10.1016/j.neuroscience.2011.09.024

Salichon, N., Gaspar, P., Upton, A. L., Picaud, S., Hanoun, N., Hamon, M., Maeyer, E. D., Murphy, D. L., Mössner, R., Lesch, K. P., Hen, R., & Seif, I. (2001). Excessive Activation of Serotonin (5-HT) 1B Receptors Disrupts the Formation of Sensory Maps in Monoamine Oxidase A and 5-HT Transporter Knock-Out Mice. *Journal of Neuroscience*, *21*(3), 884–896. https://doi.org/10.1523/JNEUROSCI.21-03-00884.2001

Salvan, P., Fonseca, M., Winkler, A. M., Beauchamp, A., Lerch, J. P., & Johansen-Berg, H. (2023). Serotonin regulation of behavior via large-scale neuromodulation of serotonin receptor networks. *Nature Neuroscience*, *26*(1), 53–63. https://doi.org/10.1038/s41593-022-01213-3

Salzberg, B. M., Obaid, A. L., & Gainer, H. (1985). Large and rapid changes in light scattering accompany secretion by nerve terminals in the mammalian neurohypophysis. *Journal of General Physiology*, *86*(3), 395–411. https://doi.org/10.1085/jgp.86.3.395

Sapey-Triomphe, L.-A., Lamberton, F., Sonié, S., Mattout, J., & Schmitz, C. (2019). Tactile hypersensitivity and GABA concentration in the sensorimotor cortex of adults with autism. *Autism Research*, *12*(4), 562–575. https://doi.org/10.1002/aur.2073

Sargin, D., Jeoung, H.-S., Goodfellow, N. M., & Lambe, E. K. (2019). Serotonin Regulation of the Prefrontal Cortex: Cognitive Relevance and the Impact of Developmental Perturbation. *ACS Chemical Neuroscience*, *10*(7), 3078–3093. https://doi.org/10.1021/acschemneuro.9b00073

Sato, J. R., Takahashi, D. Y., Hoexter, M. Q., Massirer, K. B., & Fujita, A. (2013). Measuring network's entropy in ADHD: A new approach to investigate neuropsychiatric disorders. *NeuroImage*, *77*, 44–51. https://doi.org/10.1016/j.neuroimage.2013.03.035

Saxe, A. M., Sodhani, S., & Lewallen, S. (2022). *The Neural Race Reduction: Dynamics of Abstraction in Gated Networks* (arXiv:2207.10430). arXiv. https://doi.org/10.48550/arXiv.2207.10430

Schindelin, J., Arganda-Carreras, I., Frise, E., Kaynig, V., Longair, M., Pietzsch, T., Preibisch, S.,

Rueden, C., Saalfeld, S., Schmid, B., Tinevez, J.-Y., White, D. J., Hartenstein, V., Eliceiri, K., Tomancak, P., & Cardona, A. (2012). Fiji: An open-source platform for biological-image analysis. *Nature Methods*, *9*(7), Article 7. https://doi.org/10.1038/nmeth.2019

Schmitz, D., Gloveli, T., Empson, R. M., Draguhn, A., & Heinemann, U. (1998). Serotonin reduces synaptic excitation in the superficial medial entorhinal cortex of the rat via a presynaptic mechanism. *The Journal of Physiology*, *508*(Pt 1), 119–129. https://doi.org/10.1111/j.1469-7793.1998.119br.x

Schultz, W. (2016). Dopamine reward prediction error coding. *Dialogues in Clinical Neuroscience*, *18*(1), 23–32.

Schuman, B., Dellal, S., Prönneke, A., Machold, R., & Rudy, B. (2021). Neocortical Layer 1: An Elegant Solution to Top-Down and Bottom-Up Integration. *Annual Review of Neuroscience*, *44*, 221–252. https://doi.org/10.1146/annurev-neuro-100520-012117

Seillier, L., Lorenz, C., Kawaguchi, K., Ott, T., Nieder, A., Pourriahi, P., & Nienborg, H. (2017). Serotonin Decreases the Gain of Visual Responses in Awake Macaque V1. *Journal of Neuroscience*, *37*(47), 11390–11405. https://doi.org/10.1523/JNEUROSCI.1339-17.2017

Sekssaoui, M., Bockaert, J., Marin, P., & Bécamel, C. (2024). Antidepressant-like effects of psychedelics in a chronic despair mouse model: Is the 5-HT2A receptor the unique player? *Neuropsychopharmacology*, *49*(4), 747–756. https://doi.org/10.1038/s41386-024-01794-6

Sengupta, A., Bocchio, M., Bannerman, D. M., Sharp, T., & Capogna, M. (2017). Control of Amygdala Circuits by 5-HT Neurons via 5-HT and Glutamate Cotransmission. *The Journal of Neuroscience: The Official Journal of the Society for Neuroscience*, *37*(7), 1785–1796. https://doi.org/10.1523/JNEUROSCI.2238-16.2016

Shang, J., Shea-Brown, E., & Mihalas, S. (2021). *Cortical representation variability aligns with in-class variances and can help one-shot learning* (p. 2021.01.27.428518). bioRxiv.

https://doi.org/10.1101/2021.01.27.428518

Shine, J. M., O'Callaghan, C., Walpola, I. C., Wainstein, G., Taylor, N., Aru, J., Huebner, B., & John, Y. J. (2022). Understanding the effects of serotonin in the brain through its role in the gastrointestinal tract. *Brain*, *145*(9), 2967–2981. https://doi.org/10.1093/brain/awac256

Shoji, H., Ikeda, K., & Miyakawa, T. (2023). Behavioral phenotype, intestinal microbiome, and brain neuronal activity of male serotonin transporter knockout mice. *Molecular Brain*, *16*(1), 32. https://doi.org/10.1186/s13041-023-01020-2

Siegel, F., Heimel, J. A., Peters, J., & Lohmann, C. (2012). Peripheral and Central Inputs Shape Network Dynamics in the Developing Visual Cortex In Vivo. *Current Biology*, *22*(3), 253–258. https://doi.org/10.1016/j.cub.2011.12.026

Sinclair-Wilson, A., Lawrence, A., Ferezou, I., Cartonnet, H., Mailhes, C., Garel, S., & Lokmane, L. (2023). Plasticity of thalamocortical axons is regulated by serotonin levels modulated by preterm birth. *Proceedings of the National Academy of Sciences*, *120*(33), e2301644120. https://doi.org/10.1073/pnas.2301644120

Sjaarda, C. P., Hecht, P., McNaughton, A. J. M., Zhou, A., Hudson, M. L., Will, M. J., Smith, G., Ayub, M., Liang, P., Chen, N., Beversdorf, D., & Liu, X. (2017). Interplay between maternal Slc6a4 mutation and prenatal stress: A possible mechanism for autistic behavior development. *Scientific Reports*, *7*(1), 8735. https://doi.org/10.1038/s41598-017-07405-3

Soiza-Reilly, M., Meye, F. J., Olusakin, J., Telley, L., Petit, E., Chen, X., Mameli, M., Jabaudon, D., Sze, J.-Y., & Gaspar, P. (2019). SSRIs target prefrontal to raphe circuits during development modulating synaptic connectivity and emotional behavior. *Molecular Psychiatry*, *24*(5), 726–745. https://doi.org/10.1038/s41380-018-0260-9

Spitzer, N. C. (2017). Neurotransmitter Switching in the Developing and Adult Brain. *Annual Review of Neuroscience*, *40*, 1–19.

https://doi.org/10.1146/annurev-neuro-072116-031204

Stein, A., Pearson, R. M., Goodman, S. H., Rapa, E., Rahman, A., McCallum, M., Howard, L. M., & Pariante, C. M. (2014). Effects of perinatal mental disorders on the fetus and child. *The Lancet*, *384*(9956), 1800–1819. https://doi.org/10.1016/S0140-6736(14)61277-0

Suarez, E. A., Bateman, B. T., Hernández-Díaz, S., Straub, L., Wisner, K. L., Gray, K. J., Pennell, P. B., Lester, B., McDougle, C. J., Zhu, Y., Mogun, H., & Huybrechts, K. F. (2022). Association of Antidepressant Use During Pregnancy With Risk of Neurodevelopmental Disorders in Children. *JAMA Internal Medicine*, *182*(11), 1149–1160. https://doi.org/10.1001/jamainternmed.2022.4268

Szadai, Z., Pi, H.-J., Chevy, Q., Ócsai, K., Albeanu, D. F., Chiovini, B., Szalay, G., Katona, G., Kepecs, A., & Rózsa, B. (2022). Cortex-wide response mode of VIP-expressing inhibitory neurons by reward and punishment. *eLife*, *11*, e78815. https://doi.org/10.7554/eLife.78815

Tamboli, S., Singh, S., Topolnik, D., El Amine Barkat, M., Radhakrishnan, R., Guet-McCreight, A., & Topolnik, L. (2024). Mouse hippocampal CA1 VIP interneurons detect novelty in the environment and support recognition memory. *Cell Reports*, *43*(4), 114115. https://doi.org/10.1016/j.celrep.2024.114115

Tanaka, M., Sato, A., Kasai, S., Hagino, Y., Kotajima-Murakami, H., Kashii, H., Takamatsu, Y., Nishito, Y., Inagaki, M., Mizuguchi, M., Hall, F. S., Uhl, G. R., Murphy, D., Sora, I., & Ikeda, K. (2018). Brain hyperserotonemia causes autism-relevant social deficits in mice. *Molecular Autism*, *9*(1), 60. https://doi.org/10.1186/s13229-018-0243-3

Tapper, A. R., & Molas, S. (2020). Midbrain circuits of novelty processing. *Neurobiology of Learning and Memory*, *176*, 107323. https://doi.org/10.1016/j.nlm.2020.107323

Tasaki, I., Watanabe, A., Sandlin, R., & Carnay, L. (1968). Changes in fluorescence, turbidity, and birefringence associated with nerve excitation. *Proceedings of the National Academy of Sciences*, *61*(3), 883–888. https://doi.org/10.1073/pnas.61.3.883

Teissier, A., Soiza-Reilly, M., & Gaspar, P. (2017). Refining the Role of 5-HT in Postnatal Development of Brain Circuits. *Frontiers in Cellular Neuroscience*, *11*. https://doi.org/10.3389/fncel.2017.00139

Thevenaz, P., Ruttimann, U. E., & Unser, M. (1998). A pyramid approach to subpixel registration based on intensity. *IEEE Transactions on Image Processing*, *7*(1), 27–41. https://doi.org/10.1109/83.650848

Tian, Z., Yamanaka, M., Bernabucci, M., Zhao, M., & Zhuo, M. (2017). Characterization of serotonin-induced inhibition of excitatory synaptic transmission in the anterior cingulate cortex. *Molecular Brain*, *10*(1), 21. https://doi.org/10.1186/s13041-017-0303-1

Tibrewal, P., Kiran, K. H. B., Shubha, G. N., Subhashree, D., Purushottam, M., Thennarasu, K., Reddy, Y. C. J., & Jain, S. (2010). Association of serotonin transporter gene polymorphisms with obsessive-compulsive disorder (OCD) in a south Indian population. *The Indian Journal of Medical Research*, *132*(6), 690–695.

Toda, T., Homma, D., Tokuoka, H., Hayakawa, I., Sugimoto, Y., Ichinose, H., & Kawasaki, H. (2013). Birth Regulates the Initiation of Sensory Map Formation through Serotonin Signaling. *Developmental Cell*, *27*(1), 32–46. https://doi.org/10.1016/j.devcel.2013.09.002

Torrens, M., Fonseca, F., Mateu, G., & Farré, M. (2005). Efficacy of antidepressants in substance use disorders with and without comorbid depression. A systematic review and meta-analysis. *Drug and Alcohol Dependence*, *78*(1), 1–22. https://doi.org/10.1016/j.drugalcdep.2004.09.004

Trulson, M. E., Heym, J., & Jacobs, B. L. (1981). Dissociations between the effects of hallucinogenic drugs on behavior and raphe unit activity in freely moving cats. *Brain Research*, *215*(1–2), 275–293. https://doi.org/10.1016/0006-8993(81)90507-2

Trulson, M. E., & Jacobs, B. L. (1979). Dissociations Between the Effects of LSD on Behavior and Raphe Unit Activity in Freely Moving Cats. *Science*, *205*(4405), 515–518.

https://doi.org/10.1126/science.451617

Tupper, K. W., Wood, E., Yensen, R., & Johnson, M. W. (2015). Psychedelic medicine: A re-emerging therapeutic paradigm. *CMAJ : Canadian Medical Association Journal*, *187*(14), 1054–1059. https://doi.org/10.1503/cmaj.141124

Unger, E. K., Keller, J. P., Altermatt, M., Liang, R., Matsui, A., Dong, C., Hon, O. J., Yao, Z., Sun, J., Banala, S., Flanigan, M. E., Jaffe, D. A., Hartanto, S., Carlen, J., Mizuno, G. O., Borden, P. M., Shivange, A. V., Cameron, L. P., Sinning, S., … Tian, L. (2020). Directed Evolution of a Selective and Sensitive Serotonin Sensor via Machine Learning. *Cell*, *183*(7), 1986-2002.e26. https://doi.org/10.1016/j.cell.2020.11.040

Ursino, M., Serra, M., Tarasi, L., Ricci, G., Magosso, E., & Romei, V. (2022). Bottom-up vs. top-down connectivity imbalance in individuals with high-autistic traits: An electroencephalographic study. *Frontiers in Systems Neuroscience*, *16*. https://doi.org/10.3389/fnsys.2022.932128

Valley, M. T., Moore, M. G., Zhuang, J., Mesa, N., Castelli, D., Sullivan, D., Reimers, M., & Waters, J. (2020). Separation of hemodynamic signals from GCaMP fluorescence measured with wide-field imaging. *Journal of Neurophysiology*, *123*(1), 356–366. https://doi.org/10.1152/jn.00304.2019

van Dyck, C. H., Malison, R. T., Staley, J. K., Jacobsen, L. K., Seibyl, J. P., Laruelle, M., Baldwin, R. M., Innis, R. B., & Gelernter, J. (2004). Central serotonin transporter availability measured with [123I]beta-CIT SPECT in relation to serotonin transporter genotype. *The American Journal of Psychiatry*, *161*(3), 525–531. https://doi.org/10.1176/appi.ajp.161.3.525

Vargas, M. V., Dunlap, L. E., Dong, C., Carter, S. J., Tombari, R. J., Jami, S. A., Cameron, L. P., Patel, S. D., Hennessey, J. J., Saeger, H. N., McCorvy, J. D., Gray, J. A., Tian, L., & Olson, D. E. (2023). Psychedelics promote neuroplasticity through the activation of intracellular 5-HT2A receptors. *Science*, *379*(6633), 700–706.

https://doi.org/10.1126/science.adf0435

Vasquez, B., Campos, B., Cao, A., Theint, A. T., & Zeiger, W. (2023). High-Sensitivity Intrinsic Optical Signal Imaging Through Flexible, Low-Cost Adaptations of an Upright Microscope. *eNeuro*, *10*(8). https://doi.org/10.1523/ENEURO.0046-23.2023

Veasey, S., Fornal, C., Metzler, C., & Jacobs, B. (1995). Response of serotonergic caudal raphe neurons in relation to specific motor activities in freely moving cats. *The Journal of Neuroscience*, *15*(7), 5346–5359. https://doi.org/10.1523/JNEUROSCI.15-07-05346.1995

Veenstra-VanderWeele, J., Muller, C. L., Iwamoto, H., Sauer, J. E., Owens, W. A., Shah, C. R., Cohen, J., Mannangatti, P., Jessen, T., Thompson, B. J., Ye, R., Kerr, T. M., Carneiro, A. M., Crawley, J. N., Sanders-Bush, E., McMahon, D. G., Ramamoorthy, S., Daws, L. C., Sutcliffe, J. S., & Blakely, R. D. (2012). Autism gene variant causes hyperserotonemia, serotonin receptor hypersensitivity, social impairment and repetitive behavior. *Proceedings of the National Academy of Sciences*, *109*(14), 5469–5474. https://doi.org/10.1073/pnas.1112345109

Verney, C., Lebrand, C., & Gaspar, P. (2002). Changing distribution of monoaminergic markers in the developing human cerebral cortex with special emphasis on the serotonin transporter. *The Anatomical Record*, *267*(2), 87–93. https://doi.org/10.1002/ar.10089

Virtanen, P., Gommers, R., Oliphant, T. E., Haberland, M., Reddy, T., Cournapeau, D., Burovski, E., Peterson, P., Weckesser, W., Bright, J., van der Walt, S. J., Brett, M., Wilson, J., Millman, K. J., Mayorov, N., Nelson, A. R. J., Jones, E., Kern, R., Larson, E., … van Mulbregt, P. (2020). SciPy 1.0: Fundamental algorithms for scientific computing in Python. *Nature Methods*, *17*(3), 261–272. https://doi.org/10.1038/s41592-019-0686-2

Vogel, C., Mössner, R., Gerlach, M., Heinemann, T., Murphy, D. L., Riederer, P., Lesch, K.-P., & Sommer, C. (2003). Absence of thermal hyperalgesia in serotonin transporter-deficient mice. *The Journal of Neuroscience: The Official Journal of the Society for Neuroscience*,

23(2), 708–715. https://doi.org/10.1523/JNEUROSCI.23-02-00708.2003

Wallach, J., Cao, A. B., Calkins, M. M., Heim, A. J., Lanham, J. K., Bonniwell, E. M., Hennessey, J. J., Bock, H. A., Anderson, E. I., Sherwood, A. M., Morris, H., de Klein, R., Klein, A. K., Cuccurazzu, B., Gamrat, J., Fannana, T., Zauhar, R., Halberstadt, A. L., & McCorvy, J. D. (2023). Identification of 5-HT2A receptor signaling pathways associated with psychedelic potential. *Nature Communications*, *14*(1), 8221. https://doi.org/10.1038/s41467-023-44016-1

Wan, J., Peng, W., Li, X., Qian, T., Song, K., Zeng, J., Deng, F., Hao, S., Feng, J., Zhang, P., Zhang, Y., Zou, J., Pan, S., Shin, M., Venton, B. J., Zhu, J. J., Jing, M., Xu, M., & Li, Y. (2021). A genetically encoded sensor for measuring serotonin dynamics. *Nature Neuroscience*, *24*(5), Article 5. https://doi.org/10.1038/s41593-021-00823-7

Wang, H.-L., Zhang, S., Qi, J., Wang, H., Cachope, R., Mejias-Aponte, C. A., Gomez, J. A., Mateo-Semidey, G. E., Beaudoin, G. M. J., Paladini, C. A., Cheer, J. F., & Morales, M. (2019). Dorsal Raphe Dual Serotonin-Glutamate Neurons Drive Reward by Establishing Excitatory Synapses on VTA Mesoaccumbens Dopamine Neurons. *Cell Reports*, *26*(5), 1128-1142.e7. https://doi.org/10.1016/j.celrep.2019.01.014

Wang, S.-K., Feng, M., Fang, Y., Lv, L., Sun, G.-L., Yang, S.-L., Guo, P., Cheng, S.-F., Qian, M.-C., & Chen, H.-X. (2023). Psychological trauma, posttraumatic stress disorder and trauma-related depression: A mini-review. *World Journal of Psychiatry*, *13*(6), 331–339. https://doi.org/10.5498/wjp.v13.i6.331

Wang, Y., Lin, W., Wu, N., Wang, S., Chen, M., Lin, Z., Xie, X.-Q., & Feng, Z. (2019). Structural insight into the serotonin (5-HT) receptor family by molecular docking, molecular dynamics simulation and systems pharmacology analysis. *Acta Pharmacologica Sinica*, *40*(9), 1138–1156. https://doi.org/10.1038/s41401-019-0217-9

Waterhouse, B. D., Moises, H. C., & Woodward, D. J. (1986). Interaction of serotonin with somatosensory cortical neuronal responses to afferent synaptic inputs and putative

neurotransmitters. *Brain Research Bulletin*, *17*(4), 507–518. https://doi.org/10.1016/0361-9230(86)90218-2

Watson, B. O., Yuste, R., & Packer, A. M. (2016). *PackIO and EphysViewer: Software tools for acquisition and analysis of neuroscience data* (p. 054080). bioRxiv. https://doi.org/10.1101/054080

Wert-Carvajal, C., Reneaux, M., Tchumatchenko, T., & Clopath, C. (2022). Dopamine and serotonin interplay for valence-based spatial learning. *Cell Reports*, *39*(2), 110645. https://doi.org/10.1016/j.celrep.2022.110645

Williams, T., Phillips, N. J., Stein, D. J., & Ipser, J. C. (2022). Pharmacotherapy for post traumatic stress disorder (PTSD). *The Cochrane Database of Systematic Reviews*, *3*, CD002795. https://doi.org/10.1002/14651858.CD002795.pub3

Wilmes, K. A., & Clopath, C. (2019). Inhibitory microcircuits for top-down plasticity of sensory representations. *Nature Communications*, *10*(1), 5055. https://doi.org/10.1038/s41467-019-12972-2

Wilson, S., & Argyropoulos, S. (2005). Antidepressants and sleep: A qualitative review of the literature. *Drugs*, *65*(7), 927–947. https://doi.org/10.2165/00003495-200565070-00003

Wisor, J. P., Wurts, S. W., Hall, F. S., Lesch, K. P., Murphy, D. L., Uhl, G. R., & Edgar, D. M. (2003). Altered rapid eye movement sleep timing in serotonin transporter knockout mice. *Neuroreport*, *14*(2), 233–238. https://doi.org/10.1097/00001756-200302100-00015

Wong, F. K., Bercsenyi, K., Sreenivasan, V., Portalés, A., Fernández-Otero, M., & Marín, O. (2018). Pyramidal cell regulation of interneuron survival sculpts cortical networks. *Nature*, *557*(7707), 668–673. https://doi.org/10.1038/s41586-018-0139-6

Wong, F. K., Selten, M., Rosés-Novella, C., Sreenivasan, V., Pallas-Bazarra, N., Serafeimidou-Pouliou, E., Hanusz-Godoy, A., Oozeer, F., Edwards, R., & Marín, O. (2022). Serotonergic regulation of bipolar cell survival in the developing cerebral cortex. *Cell Reports*, *40*(1), 111037. https://doi.org/10.1016/j.celrep.2022.111037

Woodburn, S. C., Levitt, C. M., Koester, A. M., & Kwan, A. C. (2024). Psilocybin Facilitates Fear Extinction: Importance of Dose, Context, and Serotonin Receptors. *ACS Chemical Neuroscience*. https://doi.org/10.1021/acschemneuro.4c00279

Wosniack, M. E., Kirchner, J. H., Chao, L.-Y., Zabouri, N., Lohmann, C., & Gjorgjieva, J. (2021). Adaptation of spontaneous activity in the developing visual cortex. *eLife*, *10*, e61619. https://doi.org/10.7554/eLife.61619

Wu, M. W., Kourdougli, N., & Portera-Cailliau, C. (2024). Network state transitions during cortical development. *Nature Reviews Neuroscience*, *25*(8), 535–552. https://doi.org/10.1038/s41583-024-00824-y

Yu, A. J., & Dayan, P. (2005). Uncertainty, Neuromodulation, and Attention. *Neuron*, *46*(4), 681–692. https://doi.org/10.1016/j.neuron.2005.04.026

Zhang, S., Xu, M., Kamigaki, T., Hoang Do, J. P., Chang, W.-C., Jenvay, S., Miyamichi, K., Luo, L., & Dan, Y. (2014). Long-range and local circuits for top-down modulation of visual cortex processing. *Science*, *345*(6197), 660–665. https://doi.org/10.1126/science.1254126

Zhang, W.-T., Chao, T.-H. H., Yang, Y., Wang, T.-W., Lee, S.-H., Oyarzabal, E. A., Zhou, J., Nonneman, R., Pegard, N. C., Zhu, H., Cui, G., & Shih, Y.-Y. I. (2022). Spectral fiber photometry derives hemoglobin concentration changes for accurate measurement of fluorescent sensor activity. *Cell Reports Methods*, *2*(7), 100243. https://doi.org/10.1016/j.crmeth.2022.100243

Zou, W.-J., Song, Y.-L., Wu, M.-Y., Chen, X.-T., You, Q.-L., Yang, Q., Luo, Z.-Y., Huang, L., Kong, Y., Feng, J., Fang, D.-X., Li, X.-W., Yang, J.-M., Mei, L., & Gao, T.-M. (2020). A discrete serotonergic circuit regulates vulnerability to social stress. *Nature Communications*, *11*(1), 4218. https://doi.org/10.1038/s41467-020-18010-w